

**School of Civil and Mechanical Engineering
Department of Civil Engineering**

**Investigations into Effect of By-product Binders in
Improvement of Cyclic Behaviour of Soil**

Mahdi Keramatikerman

**This thesis is presented for the Degree of
Doctor of Philosophy
of
Curtin University**

April 2018

Declaration

To the best of my knowledge and belief this thesis contains no material previously published by any other person except where due acknowledgment has been made. This thesis contains no material which has been accepted for the award of any other degree or diploma in any university.

Signature: 

Date: 09 April 2018.....

Abstract

This thesis investigates the effect of two by-product binders consisted of ground granulated blast furnace slag (GGBFS), and fly ash (FA) on liquefaction resistance of soil by performing a comprehensive series of preliminary and core experimental studies. Furthermore, a series of constitutive analysis have been performed based on the experimental studies to approximate the correlations of soil's particle shape and binder contents with monotonic liquefaction behaviour of soil.

In the preliminary experimental study stage, a series of direct shear tests, unconfined compressive strength (UCS) tests, ring shear tests, 1-D consolidation tests, and rigid-wall hydraulic conductivity tests conducted to investigate the effect of different types of additives (i.e., lime as a traditional, GGBFS as a by-product, and sawdust and tyre chips as reinforcement agents) on mechanical behaviour of soil. The results in this stage showed that the application of reinforcement additives (i.e., sawdust and tyre chips) is not fully efficient, and application of lime (i.e., traditional agent) is accompany with some deficiencies and environmental hazards. The experimental analysis on GGBFS showed that this by-product binder is the most effective additive to improve the mechanical behaviour of soil. Hence this additive was selected along with another by-product agent (i.e., FA) to complete the investigations.

In the next stage of the study, a series of undrained triaxial compression tests were conducted to investigate the effect of GGBFS (i.e., 0, 3, 5, and 7% by dry weight) and FA (i.e., 0, 2, 4, and 6% by dry weight) on monotonic, cyclic, and post cyclic behaviour of soil. All specimens were prepared using wet tamping method. The mixtures were compacted in five layers until a height of 125-mm was obtained. A diameter of 65-mm which provided an (aspect ratio of 2). The samples were saturated until the coefficient

of Skempton (i.e., B -value) was equal or greater than 0.95. The specimens were isotropically consolidated under the initial mean effective stresses (p_0') of 100, 200, or 400 kPa for GGBFS tests and 50, 70, and 90 kPa for FA tests. The specimens were prepared with an initial relative density (D_r) of 20%, 40%, and/or 60%.

The effect of different parameters such as binder contents, initial relative density, effective confining pressure, and curing time on strength characteristics of soil were investigated and the results were presented and analysed. The analysis on the effect of binder contents showed that increasing the binder content is effective to increase the ultimate deviatoric strength of sand in monotonic, cyclic and post-cyclic testing condition. The investigation of the effect of initial relative density showed that increasing the relative density is effective to increase the strength of the soil and increase in ultimate deviatoric strength of the soil was more apparent in binder added specimens in monotonic, cyclic, and post-cyclic testing conditions. The investigation of the effect of initial mean effective stress on GGBFS and FA amended specimens showed that the specimens tested under a greater initial mean effective stress have a lower ultimate deviatoric strength values due to suppression of dilatancy of soil. This behaviour was similar in all monotonic, cyclic, and post cyclic tests. As expected, the results also showed that increasing the curing time in FA or GGBFS amended specimens is effective to increase its ultimate deviatoric strength. In addition, the constitutive analysis based on the critical state of soil mechanics (CSSM) showed the correlations exist amongst monotonic liquefaction behaviour of soil and the soil particle shape and the FA contents.

Publications

The following publications have been resulted from my research period at Curtin University (*Asterisk= denotes the papers outputs of this thesis only)

Referred published authored Book:

1. Chegenizadeh, A. and **Keramatikerman, M.**, *Mitigating Sulphate Attacks in Geotechnical Engineering*. Nova Science Pub Inc. 2017.

Referred published journal papers:

- *1. **Keramatikerman, M.**, Chegenizadeh, A., & Nikraz, H. 2018. "Effect of Flyash on Post-Cyclic Behavior of Sand." *Journal of Earthquake Engineering*, 1-13.
- *2. **Keramatikerman, M.**, Chegenizadeh, A., Nikraz, H., & Sabbar, A. S. 2018. Effect of flyash on liquefaction behaviour of sand-bentonite mixture. *Soils and Foundations*. (In Press, Corrected Proof)
3. Chegenizadeh, A., **M. Keramatikerman**, and Nikraz, H., 2018. "Liquefaction resistance of fibre reinforced low-plasticity silt." *Soil Dynamics and Earthquake Engineering*, 104, pp.372-377.
- *4. **Keramatikerman, M.**, Chegenizadeh, A., Yilmaz, Y., & Nikraz, H. 2018. "Effect of Lime Treatment on Static Liquefaction Behavior of Sand–Bentonite Mixtures." *Journal of Materials in Civil Engineering*, 30(11), 06018017.
- *5. Chegenizadeh, A., **M. Keramatikerman**, G., Dalla Santa, and H. Nikraz. 2018. "Influence of Recycled Tyre Amendment on Mechanical Behaviour of Cut-off Walls." *Journal of Cleaner Production*. 177: 507-515.
6. **Keramatikerman, M.**, Chegenizadeh, A., & Nikraz, H. 2018. "Effect of Slag on Restoration Mechanical Characteristics of Ethanol Gasoline–Contaminated Clay." *Journal of Environmental Engineering*, 144(7), 06018001.
- *7. **Keramatikerman, M.**, A. Chegenizadeh, and H. Nikraz. 2018. "Shear Strength Characteristics of Over-consolidated Clay Treated with GGBFS." *Australian Geomechanics Journal (AGJ)* 53 (2): pp. 141-149.

- *8. **Keramatikerman, M.**, A. Chegenizadeh, and H. Nikraz. 2017. "Experimental study on effect of fly ash on liquefaction resistance of sand." *Soil Dynamics and Earthquake Engineering* 93: 1-6.
9. **Keramatikerman, M.**, A. Chegenizadeh, Pu, H. 2017. "Effect of Atrazine Contamination on Compressibility and Permeability Characteristics of Clay." *ASTM Geotechnical Testing Journal*, DOI: 10.1520/GTJ20160138. ISSN 0149-6115.
- *10. **Keramatikerman, M.**, and A. Chegenizadeh. 2017. "Effect of Particle Shape on Monotonic Liquefaction: Natural and Crushed Sand." *Experimental Mechanics* 57 (8): 1341-1348.
- *11. **Keramatikerman, M.**, A. Chegenizadeh, and H. Nikraz. 2017. "An investigation into effect of sawdust treatment on permeability and compressibility of soil-bentonite slurry cut-off wall." *Journal of Cleaner Production*. 162: 1-6.
- *12. **Keramatikerman, M.**, A. Chegenizadeh, and H. Nikraz. 2016. "Effect of GGBFS and lime binders on the engineering properties of clay." *Applied Clay Science* 132-133: 722-730.
13. Chegenizadeh, A., **M. Keramatikerman**, S. Panizza, and H. Nikraz. 2017. "Effect of powdered recycled tire on sulfate resistance of cemented clay." *Journal of Materials in Civil Engineering* 29 (10).
14. Vakili, M., A. Chegenizadeh, H. Nikraz, and **M. Keramatikerman**. 2016. "Investigation on shear strength of stabilised clay using cement, sodium silicate and slag." *Applied Clay Science* 124-125: 243-251.
15. Chegenizadeh, A., **M. Keramatikerman**, and H. Nikraz. 2016. "Flexible Pavement Modelling using Kenlayer." *Electronics Journal of Geotechnical Engineering (EJGE)*, Vol. 21, Bund. 07: 2467-2479.
16. **Keramatikerman, M.**, A. Chegenizadeh, and H. Nikraz. 2016. "Behavior of the Unbound Granular Materials in Pavement." *Australian. Journal of Basic and Applied Sciences*, 10(13): 155-163, 2016




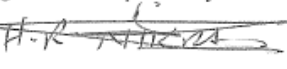
17. Chegenizadeh, A., **M., Keramatikerman**, and H. Nikraz. 2016. "Effect of Elastic Moduli of Asphalt Layer on Flexible Pavement: A Numerical Study." *Australian. Journal of Basic and Applied Sciences*, 10(12): 374-382, 2016.

Referred Published Conference paper

1. Chegenizadeh. A., **M., Keramatikerman**, and H. Nikraz. 2016. "A Study on Numerical Modelling of Rigid Pavement: Temperature and Thickness Effect" World Academy of Science, Engineering and Technology (WASET), 18th International Conference on Civil, Structural and Environmental Engineering, ICCSEE 2016, Zurich, Switzerland, January 12-13, 2016.
2. **Keramatikerman, M.**, and A. Chegenizadeh. 2015. "A Review of Soil Stabilization Techniques." World Academy of Science, Engineering and Technology (WASET), 17th International Conference on Civil and Geological Engineering ICCGE 2015, Chicago, USA, October 08-09, 2015.




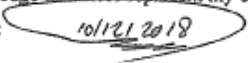
Mahdi Keramatikerman Attribution of Research Outputs

Chegenizadeh, A., M., Keramatikerman, G., Dalla Santa, and H. Nikraz. 2018. "Influence of Recycled Tyre Amendment on Mechanical Behaviour of Cut-off Walls." *Journal of Cleaner Production*. 177: 507-515.

	Conception and tests design	Performing experimental tests	Literature Review	Analysis	Interpretation & discussion	Critical review
Dr Amin Chegenizadeh	×		×	×	×	×
I acknowledge that these represent my contribution to the above research output. Signature: 						
Mahdi Keramatikerman	×	×	×	×	×	
I acknowledge that these represent my contribution to the above research output. Signature: 						
Dr Giorgia Dalla Santa	× (minor)		×		× (minor)	× (minor)
I acknowledge that these represent my contribution to the above research output. Signature: 						
Professor Hamid Nikraz	×		×			× (minor)
I acknowledge that these represent my contribution to the above research output. Signature: 						




Mahdi Keramatikerman Attribution of Research Outputs

Keramatikerman, M., Chegenizadeh, A., Nikraz, H., & Sabbar, A. S. 2018. Effect of flyash on liquefaction behaviour of sand-bentonite mixture. *Soils and Foundations*. (In Press, Corrected Proof)

	Conception and tests design	Performing experimental tests	Literature Review	Analysis	Interpretation & discussion	Critical review
Mahdi Keramatikerman	×	×	×	×	×	×
I acknowledge that these represent my contribution to the above research output. Signature: 						
Dr Amin Chegenizadeh	×		×	×	×	×
I acknowledge that these represent my contribution to the above research output. Signature: 						
Professor Hamid Nikraz	×		×			×
I acknowledge that these represent my contribution to the above research output. Signature: 						
Dr Ayad Salih Sabbar			×			× (minor)
I acknowledge that these represent my contribution to the above research output. Signature: 						



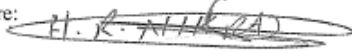
Mahdi Keramatikerman Attribution of Research Outputs

Chegenizadeh. A., M., Keramatikerman, and H. Nikraz. 2016. "A Study on Numerical Modelling of Rigid Pavement: Temperature and Thickness Effect" World Academy of Science, Engineering and Technology (WASET), 18th International Conference on Civil, Structural and Environmental Engineering, ICCSEE 2016, Zurich, Switzerland, January 12-13, 2016.

	Conception and tests design	Performing experimental tests	Literature Review	Analysis	Interpretation & discussion	Critical review
Dr Amin Chegenizadeh	×		×	×	×	×
I acknowledge that these represent my contribution to the above research output. Signature: 						
Mahdi Keramatikerman	×	×	×	×	×	
I acknowledge that these represent my contribution to the above research output. Signature: 						
Professor Hamid Nikraz	×		×			×
I acknowledge that these represent my contribution to the above research output. Signature: 						




Mahdi Keramatikerman Attribution of Research Outputs

Chegenizadeh, A., M., Keramatikerman, and H. Nikraz. 2016. "Effect of Elastic Moduli of Asphalt Layer on Flexible Pavement: A Numerical Study." *Australian Journal of Basic and Applied Sciences*, 10(12): 374-382, 2016.

	Conception and tests design	Performing experimental tests	Literature Review	Analysis	Interpretation & discussion	Critical review
Dr. Amin Chegenizadeh	×		×	×	×	×
I acknowledge that these represent my contribution to the above research output. Signature: 						
Mahdi Keramatikerman		×	×	×	×	
I acknowledge that these represent my contribution to the above research output. Signature: 						
Professor Hamid Nikraz	×					×
I acknowledge that these represent my contribution to the above research output. Signature: 						




Mahdi Keramatikerman Attribution of Research Outputs

Keramatikerman, M., A. Chegenizadeh, and H. Nikraz. 2016. "Behavior of the Unbound Granular Materials in Pavement." *Australian Journal of Basic and Applied Sciences*, 10(13): 155-163, 2016

	Conception and tests design	Performing experimental tests	Literature Review	Analysis	Interpretation & discussion	Critical review
Mahdi Keramatikerman	x	x	x	x	x	
I acknowledge that these represent my contribution to the above research output. Signature: 						
Dr. Amin Chegenizadeh	x		x		x	x
I acknowledge that these represent my contribution to the above research output. Signature: 						
Professor Hamid Nikraz	x		x			x
I acknowledge that these represent my contribution to the above research output. Signature: 						



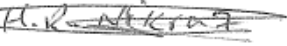

Mahdi Keramatikerman Attribution of Research Outputs

Chegenizadeh, A., M. Keramatikerman, and H. Nikraz. 2016. "Flexible Pavement Modelling using Kenlayer." *Electronics Journal of Geotechnical Engineering (EJGE)*, Vol. 21, Bund. 07: 2467-2479.

	Conception and tests design	Performing experimental tests	Literature Review	Analysis	Interpretation & discussion	Critical review
Dr Amin Chegenizadeh	×		×	×	×	×
I acknowledge that these represent my contribution to the above research output. Signature: 						
Mahdi Keramatikerman	×	×	×		×	
I acknowledge that these represent my contribution to the above research output. Signature: 						
Professor Hamid Nikraz	×					×
I acknowledge that these represent my contribution to the above research output. Signature: 						

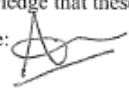
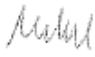


Mahdi Keramatikerman Attribution of Research Outputs

Vakili, M., A. Chegenizadeh, H. Nikraz, and M. Keramatikerman. 2016. "Investigation on shear strength of stabilised clay using cement, sodium silicate and slag." *Applied Clay Science* 124-125: 243-251.

	Conception and tests design	Performing experimental tests	Literature Review	Analysis	Interpretation & discussion	Critical review
Mohamad Vali Vakili		x	x	x	x	x
I acknowledge that these represent my contribution to the above research output. Signature: <i>on behalf</i>  (Non Contactable)						
Dr Amin Chegenizadeh	x		x		x	x
I acknowledge that these represent my contribution to the above research output. Signature: 						
Professor Hamid Nikraz	x		x			x
I acknowledge that these represent my contribution to the above research output. Signature: 						
Mahdi Keramatikerman	x		x	x		
I acknowledge that these represent my contribution to the above research output. Signature: 						



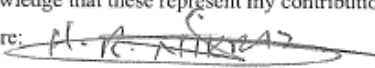
Mahdi Keramatikerman Attribution of Research Outputs

Chegenizadeh, A., M. Keramatikerman, S. Panizza, and H. Nikraz. 2017. "Effect of powdered recycled tire on sulfate resistance of cemented clay." *Journal of Materials in Civil Engineering* 29 (10).

	Conception and tests design	Performing experimental tests	Literature Review	Analysis	Interpretation & discussion	Critical review
Dr. Amin Chegenizadeh	×	×	×	×	×	×
I acknowledge that these represent my contribution to the above research output. Signature: 						
Mahdi Keramatikerman	×	×	×	×	×	×
I acknowledge that these represent my contribution to the above research output. Signature: 						
Samuel Panizza	×	×	×			
I acknowledge that these represent my contribution to the above research output. Signature: <i>on his behalf non contactable.</i> 						
Professor Hamid Nikraz	×		×			×
I acknowledge that these represent my contribution to the above research output. Signature: 						




Mahdi Keramatikerman Attribution of Research Outputs

Keramatikerman, M., A. Chegenizadeh, and H. Nikraz. 2016. "Effect of GGBFS and lime binders on the engineering properties of clay." *Applied Clay Science* 132-133: 722-730.

	Conception and tests design	Performing experimental tests	Literature Review	Analysis	Interpretation & discussion	Critical review
Mahdi Keramatikerman	×	×	×	×	×	×
I acknowledge that these represent my contribution to the above research output. Signature: 						
Dr Amin Chegenizadeh	×		×		×	×
I acknowledge that these represent my contribution to the above research output. Signature: 						
Professor Hamid Nikraz	×				×	×
I acknowledge that these represent my contribution to the above research output. Signature: 						

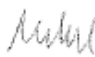
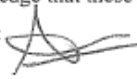

Mahdi Keramatikerman Attribution of Research Outputs

Keramatikerman, M., A. Chegenizadeh, and H. Nikraz. 2017. "An investigation into effect of sawdust treatment on permeability and compressibility of soil-bentonite slurry cut-off wall." *Journal of Cleaner Production*. 162: 1-6.

	Conception and tests design	Performing experimental tests	Literature Review	Analysis	Interpretation & discussion	Critical review
Mahdi Keramatikerman	×	×	×	×	×	×
I acknowledge that these represent my contribution to the above research output. Signature: 						
Dr Amin Chegenizadeh	×		×		×	×
I acknowledge that these represent my contribution to the above research output. Signature: 						
Professor Hamid Nikraz	×					×
I acknowledge that these represent my contribution to the above research output. Signature: 						




Mahdi Keramatikerman Attribution of Research Outputs

Keramatikerman, M., A. Chegenizadeh, and H. Nikraz. 2017. "Experimental study on effect of fly ash on liquefaction resistance of sand." *Soil Dynamics and Earthquake Engineering* 93: 1-6.

	Conception and tests design	Performing experimental tests	Literature Review	Analysis	Interpretation & discussion	Critical review
Mahdi Keramatikerman	×	×	×	×	×	×
I acknowledge that these represent my contribution to the above research output. Signature: 						
Dr Amin Chegenizadeh	×				×	×
I acknowledge that these represent my contribution to the above research output. Signature: 						
Professor Hamid Nikraz	×				×	×
I acknowledge that these represent my contribution to the above research output. Signature: 						


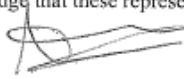

Mahdi Keramatikerman Attribution of Research Outputs

Keramatikerman, M., A. Chegenizadeh, and H. Nikraz. 2018. "Shear Strength Characteristics of Over-consolidated Clay Treated with GGBFS." *Australian Geomechanics Journal (AGJ)* 53 (2): pp. 141-149.

	Conception and tests design	Performing experimental tests	Literature Review	Analysis	Interpretation & discussion	Critical review
Mahdi Keramatikerman	×	×	×	×	×	×
I acknowledge that these represent my contribution to the above research output. Signature: 						
Dr Amin Chegenizadeh	×		×		×	×
I acknowledge that these represent my contribution to the above research output. Signature: 						
Professor Hamid Nikraz	×		×			×
I acknowledge that these represent my contribution to the above research output. Signature: 						




Mahdi Keramatikerman Attribution of Research Outputs

Keramatikerman, M., Chegenizadeh, A., & Nikraz, H. 2018. "Effect of Slag on Restoration Mechanical Characteristics of Ethanol Gasoline-Contaminated Clay." *Journal of Environmental Engineering*, 144(7), 06018001.

	Conception and tests design	Performing experimental tests	Literature Review	Analysis	Interpretation & discussion	Critical review
Mahdi Keramatikerman	×	×	×	×	×	×
I acknowledge that these represent my contribution to the above research output. Signature: 						
Dr Amin Chegenizadeh	×		×		×	×
I acknowledge that these represent my contribution to the above research output. Signature: 						
Professor Hamid Nikraz	×				×	×
I acknowledge that these represent my contribution to the above research output. Signature: 						




Mahdi Keramatikerman Attribution of Research Outputs

Chegenizadeh, A., M. Keramatikerman, and Nikraz, H., 2018. "Liquefaction resistance of fibre reinforced low-plasticity silt." *Soil Dynamics and Earthquake Engineering*, 104, pp.372-377.

	Conception and tests design	Performing experimental tests	Literature Review	Analysis	Interpretation & discussion	Critical review
Dr Amin Chegenizadeh	×		×	×	×	×
I acknowledge that these represent my contribution to the above research output. Signature: 						
Mahdi Keramatikerman	×	×	×	×	×	
I acknowledge that these represent my contribution to the above research output. Signature: 						
Professor Hamid Nikraz	×					×
I acknowledge that these represent my contribution to the above research output. Signature: 						

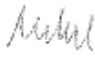

Mahdi Keramatikerman Attribution of Research Outputs

Keramatikerman, M., Chegenizadeh, A., & Nikraz, H. 2018. "Effect of Flyash on Post-Cyclic Behavior of Sand." *Journal of Earthquake Engineering*, 1-13.

	Conception and tests design	Performing experimental tests	Literature Review	Analysis	Interpretation & discussion	Critical review
Mahdi Keramatikerman	×	×	×	×	×	×
I acknowledge that these represent my contribution to the above research output. Signature: 						
Dr Amin Chegenizadeh	×				×	×
I acknowledge that these represent my contribution to the above research output. Signature: 						
Professor Hamid Nikraz	×					×
I acknowledge that these represent my contribution to the above research output. Signature: 						

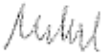

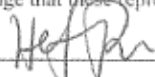
Mahdi Keramatikerman Attribution of Research Outputs

Keramatikerman, M., and A. Chegenizadeh. 2017. "Effect of Particle Shape on Monotonic Liquefaction: Natural and Crushed Sand." *Experimental Mechanics* 57 (8): 1341-1348.

	Conception and tests design	Performing experimental tests	Literature Review	Analysis	Interpretation & discussion	Critical review
Mahdi Keramatikerman	×	×	×	×	×	×
I acknowledge that these represent my contribution to the above research output. Signature: 						
Dr Amin Chegenizadeh	×				×	×
I acknowledge that these represent my contribution to the above research output. Signature: 						


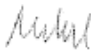
Mahdi Keramatikerman Attribution of Research Outputs

Keramatikerman, M., A. Chegenizadeh, Pu, H. 2017. "Effect of Atrazine Contamination on Compressibility and Permeability Characteristics of Clay." *ASTM Geotechnical Testing Journal*. DOI: 10.1520/GTJ20160138. ISSN 0149-6115.

	Conception and tests design	Performing experimental tests	Literature Review	Analysis	Interpretation & discussion	Critical review
Mahdi Keramatikerman	x	x	x	x	x	x
I acknowledge that these represent my contribution to the above research output. Signature: 						
Dr Amin Chegenizadeh	x		x		x	x
I acknowledge that these represent my contribution to the above research output. Signature: 						
Professor Hefu Pu			x		x	x
I acknowledge that these represent my contribution to the above research output. Signature: 						

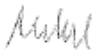

Mahdi Keramatikerman Attribution of Research Outputs

Chegenizadeh, A. and Keramatikerman, M., *Mitigating Sulphate Attacks in Geotechnical Engineering*. Nova Science Pub Inc. 2017.

	Conception and tests design	Performing experimental tests	Literature Review	Analysis	Interpretation & discussion	Critical review
Dr Amin Chegenizadeh	x		x	x	x	x
I acknowledge that these represent my contribution to the above research output. Signature: 						
Mahdi Keramatikerman	x	x	x	x	x	
I acknowledge that these represent my contribution to the above research output. Signature: 						

Mahdi Keramatikerman Attribution of Research Outputs

Keramatikerman, M., and A. Chegenizadeh. 2015. "A Review of Soil Stabilization Techniques." World Academy of Science, Engineering and Technology (WASET), 17th International Conference on Civil and Geological Engineering ICCGE 2015, Chicago, USA, October 08-09, 2015.

	Conception and tests design	Performing experimental tests	Literature Review	Analysis	Interpretation & discussion	Critical review
Mahdi Keramatikerman	×	×	×	×	×	
I acknowledge that these represent my contribution to the above research output. Signature: 						
Dr Amin Chegenizadeh	×		×	×	×	×
I acknowledge that these represent my contribution to the above research output. Signature: 						

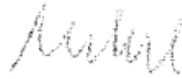
Mahdi Keramatikerman Attribution of Research Outputs

Keramatikerman, M., Chegenizadeh, A., Yilmaz, Y., & Nikraz, H. 2018. "Effect of Lime Treatment on Static Liquefaction Behavior of Sand-Bentonite Mixtures." *Journal of Materials in Civil Engineering*, 30(11), 06018017.

	Conception and tests design	Performing experimental tests	Literature Review	Analysis	Interpretation & discussion	Critical review
Mahdi Keramatikerman	×	×	×	×	×	

I acknowledge that these represent my contribution to the above research output.

Signature:



Dr Amin Chegenizadeh	×		×		×	×
----------------------	---	--	---	--	---	---

I acknowledge that these represent my contribution to the above research output.

Signature:



Dr Yuksel Yilmaz	×		×	× (minor)		× (minor)
------------------	---	--	---	-----------	--	-----------

I acknowledge that these represent my contribution to the above research output.

Signature:

 - 12/10/2018

Professor Hamid Nikraz	×		×			× (minor)
------------------------	---	--	---	--	--	-----------

I acknowledge that these represent my contribution to the above research output.

Signature:



Acknowledgements

I would like to take this opportunity to acknowledge all the persons contributed in the accomplishment of this work and without whom this PhD experience wouldn't been one of the best experiences in my life.

I would start by thanking my advisor Dr. Amin Chegenizadeh who trusted my capacity to carry this PhD and offered me all the scientific directions and human support that I needed. I would also like to appreciate the Professor Hamid Nikraz for his technical advices and encouraging attitude. I also, acknowledge the help of A/Professor Prabir Sarker for providing technical and human supports throughout my PhD studies.

I sincerely appreciate the Curtin University for financial support of my PhD studies by granting two major scholarships, the Australian Postgraduate Award (APA) and Curtin University Postgraduate Scholarship (CUPS), and for providing a productive research environment for me.

The technical comments on my research results received from Professor Hefu Pu, A/Professor Yuksel Yilmaz, Dr. Giorgio Dalla Santa, and Dr. Hamid Karimpour are highly appreciable.

The experimental tests executed in Geotechnical laboratory of Curtin University during this PhD studies could not have been possible without the great help of Mr. Mark Whittaker and his technical team including Mirzet Sehic and Darren Issac. I also extend my gratitude to the technical members of Microscopy and Microanalysis Facility (MMF) of John de Laeter Centre in Curtin University in particular Ms. Elaine Miller and Ms. Veronica Avery for their assistance in microstructural section.

I am wholeheartedly grateful to the endless support, sacrifice, and love of my mother and father, Zohreh and Ahmad throughout this PhD studies and my life. I would also

like to express my sincere gratitude to my brother and sisters, Bahman, Mahtab, and Mehrnaz, for their mateship, support and encouraging attitude throughout this PhD studies and my life.

Finally, I wish to express my deepest thanks and gratitude to my beloved wife, Ghazaleh, who joined me in a difficult time and support me in ups and downs of life with an unfailing love. I also, appreciate the help and support of my parents-in-law during my PhD studies.

Table of Contents

Declaration	ii
Abstract	iii
Publications	v
Attribution of Research Outputs	viii
Acknowledgements	xxv
Table of Contents	xxvii
List of Figures	xxxvi
List of Tables	xliv
Chapter 1. Introduction	1
1. Introduction	2
1.1. Problem Statement	2
1.2. Significance of Research	3
1.3. Research Scopes and Objective	4
1.4. Thesis Organisation	5
Chapter 2. Background and Literature Review	7
2. Background and Literature Review	8
2.1. Abstract	8
2.2. Applicable Ground Improvement Techniques in Liquefaction Mitigation	9
2.2.1. Physical Techniques	10
2.2.1.1. Vibro-compaction Technique	11
2.2.1.2. Stone-columns Technique	12
2.2.1.3. Compaction Grouting Technique	13
2.2.1.4. Dynamic Compaction Technique	13
2.2.2. Soil Reinforcement	14
2.2.2.1. Geo-synthetics	15
2.2.2.2. Scrap Tyre	17

2.2.2.2.1.	Scrap Tyre in Australia	18
2.2.2.2.2.	Review on Application of Recycled Tyres	19
2.2.3.	Chemical Additives	22
2.2.3.1.	Traditional Additives	23
2.2.3.1.1.	Lime	23
2.2.3.2.	Non-traditional Additives	28
2.2.3.2.1.	Ground Granular Blast Furnace Slag (GGBFS)	28
2.2.3.2.2.	Fly ash (FA)	31
2.3.	Critical Review on Previous Research	33
2.4.	Conclusions	39
Chapter 3.	Applied Experimental Devices	41
3.	Applied Experimental Devices	42
3.1.	Introduction	42
3.2.	Geotechnical Experimental Devices	42
3.2.1.	Direct Shear Device	43
3.2.2.	Ring Shear Device	45
3.2.3.	Oedometer Apparatus	46
3.2.4.	Unconfined Compressive Strength (UCS) Test	48
3.2.5.	Triaxial Testing Device	48
3.2.5.1.	Stress State in Triaxial Testing	50
3.2.5.2.	Sample Preparation	51
3.2.5.3.	Triaxial Testing Phases	53
3.2.5.4.	Triaxial Testing Types	54
3.3.	Micro-structural Analysis Devices	55
3.3.1.	Scanning Electron Microscopy (SEM) Imaging	55
3.3.2.	X-ray Powder Diffraction (XRD) Analysis	57
Chapter 4.	Preliminary Tests and Materials Selection	58
	CHAPTER INTRODUCTION	59

Part 1	Effect of Sawdust on Permeability and Compressibility of Sand-Bentonite	61
	4.1 Effect of Sawdust on Permeability and Compressibility of Sand-Bentonite	62
	4.1.1. Abstract	62
	4.1.2. Introduction	62
	4.1.3. Materials and Methods	64
	4.1.3.1. Constituent Materials	64
	4.1.3.2. Sample Preparation	65
	4.1.3.3. Methodology	66
	4.1.4. Results and Discussion	67
	4.1.4.1. Hydraulic Conductivity Tests (k_f)	67
	4.1.4.2. Consolidation Tests	68
	4.1.4.2.1. Compression Index (C_I) and Swelling Index (C_s)	68
	4.1.4.2.2. Coefficient of Consolidation (c_v)	69
	4.1.4.2.3. Coefficient of Volume Compressibility (m_v) and Coefficient of Compressibility (a_v)	73
	4.1.4.2.4. Computed Hydraulic Conductivity (k_{theory})	75
	4.1.5. Conclusions	77
Part 2	Effect of Recycled Tyre on Mechanical Behaviour of Sand-bentonite	78
	4.2. Effect of Recycled Tyre on Mechanical Behaviour of Sand-bentonite	79
	4.2.1. Abstract	79
	4.2.2. Introduction	79
	4.2.3. Materials and Methods	82
	4.2.4. Laboratory Test Setup	85
	4.2.5. Results and Discussion	86
	4.2.5.1. Consolidation Tests	86
	4.2.5.1.1. Deformation vs Time Relations	86
	4.2.5.2. Compression Index and Swelling Index	90

4.2.5.3.	Coefficient of Consolidation	94
4.02.5.4.	Terzaghi Hydraulic Conductivity (k_{theory})	99
4.2.5.5.	Rigid-Wall Hydraulic Conductivity Tests (k_f)	103
4.2.6.	Conclusions	105
Part 3	Effect of Lime and GGBFS on Engineering Properties of Clay	106
4.3.	Effect of Lime and GGBFS on Engineering Properties of Clay	107
4.3.1.	Abstract	107
4.3.2.	Introduction	108
4.3.3.	Material Used	112
4.3.4.	Methodology	114
4.3.4.1.	Volumetric Shrinkage Strain Tests	115
4.3.4.2.	Unconfined Compressive Strength Tests	118
4.3.4.3.	Ring Shear Tests	119
4.3.5.	Results and Discussion	120
4.3.5.1.	Volumetric Shrinkage Strain Tests	120
4.3.5.1.1.	Effect of Lime Addition	120
4.3.5.1.2.	Effect of GGBFS on Shrinkage	122
4.3.5.1.3.	Effect of Partial Replacement of Lime with GGBFS	124
4.3.5.2.	Effect of GGBFS-Lime Ratios on Compressive Strength	126
4.3.5.3.	Effect of GGBFS-Lime Ratios on Shear Strength	127
4.3.5.4.	Microstructural Study	129
4.3.5.4.1.	SEM/EDS Characterisation	129
4.3.5.4.2.	XRD Analysis	132
4.3.6.	Conclusions	133
Part 4	Shear Strength Characteristics of Over-consolidated Clay Treated with GGBFS	136
4.4.	Shear Strength Characteristics of Over-consolidated clay Treated with GGBFS	137
4.4.1.	Abstract	137

4.4.2.	Introduction	137
4.4.3.	Materials Used	139
4.4.4.	Methodology	141
4.4.5.	Results and Discussion	143
4.4.5.1.	Effect of GGBFS Contents	143
4.4.5.2.	Effect of Effective Normal Stress (σ'_n)	146
4.4.5.3.	Effect of Curing Time	150
4.4.6.	Conclusions	151
4.5.	CHAPTER CONCLUSIONS	153
Chapter 5.	Monotonic Behaviour of Sand-FA Mixture	158
	CHAPTER INTRODUCTION	159
5.	Monotonic Behaviour of Sand-FA Mixture	160
5.1.	Abstract	160
5.2.	Introduction	161
5.3.	Materials Used	162
5.4.	Specimen Preparation and Triaxial Testing	165
5.5.	Triaxial Test Results	166
5.5.1.	Effect of FA Contents	166
5.5.2.	Effect of Initial Mean Effective Stress	169
5.5.3.	Effect of Relative Density	172
5.5.4.	Effect of Curing Time	175
5.6.	Conclusions	176
Chapter 6.	Effect of Binders on Cyclic Behaviour of Sand	178
	CHAPTER INTRODUCTION	179
Part 1	Effect of FA on Cyclic Behaviour of Sand	180
6.1.	Effect of FA on Cyclic Behaviour of Sand	181
6.1.1.	Abstract	181
6.1.2.	Introduction	182

6.1.3.	Testing Materials	184
6.1.3.1.	Sand	184
6.1.3.2.	Fly Ash (FA)	185
6.1.4.	Methodology	186
6.1.5.	Results and Discussion	188
6.1.5.1.	Effect of Relative Density on Liquefaction Resistance	188
6.1.5.2.	Effect of FA Content on Liquefaction of Soil	191
6.1.5.3.	Effect of Effective Confining Pressure and Curing Time on Liquefaction Resistance	193
6.1.6.	Conclusion	196
Part 2	Effect of GGBFS on Cyclic Behaviour of Sand	197
6.2.	Effect of GGBFS on Cyclic Behaviour of Sand	198
6.2.1.	Abstract	198
6.2.2.	Introduction	199
6.2.3.	Materials Used	200
6.2.4.	Sample Preparation and Laboratory Test Setup	204
6.2.5.	Results and Discussions	208
6.2.5.1.	Effect of GGBFS Contents	208
6.1.1.1.	Effect of Effective Confining Pressure (σ'_3)	213
6.2.5.3.	Effect of Relative Density (D_r)	215
6.2.5.4.	Effect of Curing Time	218
6.2.6.	Conclusion	222
6.3.	CHAPTER CONCLUSIONS	224
Chapter 7.	Effect of Binders on Post-Cyclic Behaviour of Sand	226
	CHAPTER INTRODUCTION	227
Part 1	Effect of FA on Post-cyclic Behaviour of Sand	228
7.1.	Effect of FA on Post-cyclic Behaviour of Sand	229
7.1.1.	Abstract	229

7.1.2.	Introduction	229
7.1.2.1.	Post-cyclic Behaviour of Soil	229
7.1.2.2.	Ground Improvement	231
7.1.3.	Materials and Methods	233
7.1.3.1.	Materials Used	233
7.1.3.2.	Specimen Preparation	235
7.1.3.3.	Testing Procedure	236
7.1.4.	Results and Discussion	240
7.1.4.1.	Typical Monotonic Triaxial Tests	240
7.1.4.2.	Post-cyclic Triaxial Tests	242
7.1.4.2.1.	Effect of FA Contents	242
7.1.4.2.2.	Effect of Relative Density	245
7.1.4.2.3.	Effect of Initial Mean Effective Stress	249
7.1.5.	Conclusions	250
Part 2	Effect of GGBFS on Post-cyclic Behaviour of Sand	252
7.2.	Effect of GGBFS on Post-Cyclic Behaviour of sand	253
7.2.1.	Abstract	253
7.2.2.	Introduction	254
7.2.3.	Materials Used	257
7.2.4.	Sample Preparations and Testing Setup	260
7.2.5.	Results and Discussion	250
7.2.5.1.	Effect of GGBFS Contents on Post-cyclic	263
7.2.5.2.	Effect of Initial Mean Effective Stress	267
7.2.5.3.	Effect of Initial Relative Density	271
7.2.6.	Conclusions	275
7.3.	CHAPTER CONCLUSIONS	278
Chapter 8.	Constitutive Modelling of Sand-FA Mixture	280
	CHAPTER INTRODUCTION	281

Part 1	Effect of Particle Shape on Monotonic Liquefaction	282
	8.1. Effect of Particle Shape on Monotonic Liquefaction	283
	8.1.1. Abstract	283
	8.1.2. Introduction	283
	8.1.3. Test Materials and Methods	286
	8.1.4. Results and Discussions	291
	8.1.4.1. Stress-strain Relation	292
	8.1.4.2. Critical State Locus in $e-p'$ Plane	293
	8.1.4.3. Critical State Locus in $q-p'$ Plane	299
	8.1.4.4. Liquefaction Inception	302
	8.1.5. Conclusions	304
Part 2	Constitutive Modelling of Sand-FA Mixture	306
	8.2. Constitutive Modelling of Sand-FA Mixture	307
	8.2.1. Abstract	307
	8.2.2. Introduction	307
	8.2.3. Materials Used	310
	8.2.4. Specimen Preparation and Triaxial Tests	311
	8.2.5. Triaxial Test Results	312
	8.2.5.1. Typical Stress-Strain Relation	312
	8.2.5.2. Critical State Locus in e_p - $\log p'$ Plane	315
	8.2.5.3. Critical State Locus in $q-p'$ Plane	318
	8.2.5.4. Flow Liquefaction	320
	8.2.6. Conclusions	322
	8.3. CHAPTER CONCLUSIONS	324
Chapter 9.	Conclusions and Recommendations	326
	9. Conclusions	327
	9.1. Monotonic Behaviour	328
	9.2. Cyclic Behaviour	330

9.2.1. Effect of FA on Cyclic Liquefaction	330
9.2.2. Effect of GGBFS on Cyclic Liquefaction	331
9.3. Post-cyclic Behaviour	332
9.3.1. Effect of FA on Post-cyclic Behaviour	333
9.3.2. Effect of GGBFS on Post-cyclic Behaviour	334
9.4. Constitutive Modelling	336
9.4.1. Effect of Particle Shape on Monotonic Behaviour	336
9.4.2. Effect of FA on Monotonic Behaviour	338
9.5. Recommendations for Future Studies	339
References	341
Appendixes	376

List of Figures

Fig. 2.1. An example of liquefaction disastrous effects at the Saaiplaas tailings dam (Fourie et al. 2001).	9
Fig. 2.2. Classification of applicable ground improvement methods to reduce the liquefaction hazard	10
Fig. 2.3. Classification of soil reinforcement methods in liquefaction mitigation	15
Fig. 2.4. Bulk continuous filament (BCF) as a typical geo-synthesis used in soil reinforcement (Chegenizadeh et al. 2018a)	17
Fig. 2.5. powdered and crumbed recycled tyres produced from scrap tyre in different industries	18
Fig. 2.6. Classification of chemical additives application in liquefaction mitigation	23
Fig. 2.7. A typical scanning electron microscopy (SEM) of the lime	27
Fig. 2.8. A typical scanning electron microscopy (SEM) of the ordinary Portland cement (OPC)	27
Fig. 2.9. Scanning electron microscopy (SEM) of the ground granulated blast furnace slag (GGBFS)	30
Fig. 2.10. A typical scanning electron microscopy (SEM) of the fly ash (FA) class C.	33
Fig. 2.11. A schematic overview of a triaxial monotonic, cyclic, and post cyclic triaxial tests.	34
Fig. 3.1. The sample container in direct shear test	44
Fig. 3.2. A direct shear testing apparatus used to conduct the tests in this study	44
Fig. 3.3. A Bromhead ring shear device used to conduct the tests	45
Fig. 3.4. A prepared sample in the container in the ring shear device	46
Fig. 3.5. A prepared sample in the container in the ring shear device	47
Fig. 3.6. An oedometer device to measure the consolidation of the sample	47
Fig. 3.7. A cylindrical sample in a UCS testing device	48
Fig. 3.8. Gecomp cyclic triaxial device used to perform the tests in this study	50
Fig. 3.9. Schematic overview for stress-strain ($q-p'$) and pore water pressure ratio ($r_u-\varepsilon_a$) phases in triaxial tests	51

Fig. 3.10. Sample preparation in a triaxial device using moist tamping method (a) Sample preparation in a steel split mould; and (b) prepared sample on pedestal and ready for the tests.	52
Fig. 3.11. A typical scanning electron microscopy (SEM) image used to conduct the microstructural analysis of the study	56
Fig. 3.12. Prepared specimens for SEM testing in sample holder of the SEM device	56
Fig. 4.1. Particle size distribution (PSD) of the used materials.	65
Fig. 4.2. (a) Variation of void ratio (e) versus logarithm of effective overburden pressure ($e - \log \sigma'_n$) for control SB backfill mixture and sawdust amended specimens; (b) Variation of compression index (C_i) and swelling index (C_s) versus sawdust contents	69
Fig. 4.3. Computed c_v values versus effective overburden pressure (σ'_n) for SB backfill mixture and sawdust amended mixtures based on (a) Casagrande method; (b) Taylor method	71
Fig. 4.4. Computed c_v values versus sawdust content for SB backfill mixture and sawdust amended mixtures based on (a) Casagrande method; (b) Taylor method	72
Fig. 4.5. Computed c_v values based on the Taylor method relative to c_v values computed based on the Casagrande method versus σ'_n for sawdust amended specimens	73
Fig. 4.6. (a) Coefficients of volume compressibility (m_v) versus effective overburden pressure (σ'_n) for SB backfill and sawdust amended mixtures; (b) coefficient of compressibility (a_v) versus effective overburden pressure (σ'_n) for SB backfill and sawdust amended mixtures	74
Fig. 4.7. Hydraulic conductivity (k_{theory}) as a function of effective overburden pressure ($\log \sigma'_n$) for control SB backfill mixture and sawdust amended specimens	75
Fig. 4.8. Hydraulic conductivity (k_{theory}) as a function of void ratio (e) for control backfill mixture and sawdust amended specimens	76
Fig. 4.9. Comparison between the computed and measured hydraulic conductivity (i.e., k_f and k_{theory}) as a function of sawdust content for SB control mixture and sawdust amended specimens	76
Fig. 4.10. Particle grading of the used materials.	84
Fig. 4.11. A typical slump test performed on SB backfill.	85
Fig. 4.12. Typical settlement behaviour for control SB and PRT amended backfills as a function of the vertical strain (ϵ_v): (a) $\log t$; (b) $t^{1/2}$ under 1280 kPa (185.65 psi) effective overburden stress (σ'_n).	89
Fig. 4.13. Typical settlement behaviour for control SB and CRT amended backfills as a function of the vertical strain (ϵ_v): (a) $\log t$; (b) $t^{1/2}$ under 1280 kPa (185.65 psi) effective overburden stress (σ'_n).	90

Fig. 4.14. Void ratio (e) versus logarithm of effective overburden stress ($\log \sigma'_n$) for control SB backfill mixture and (a) PRT amended specimens and; (b) CRT amended specimens	93
Fig. 4.15. Variation of the compression index (C_c) and swelling index (C_s) versus recycled tyre content	93
Fig. 4.16. Computed c_v values based on Casagrande method versus logarithm effective overburden stress (σ'_n) for SB backfill mixture and (a) PRT amended specimens; (b) CRT amended specimens	96
Fig. 4.17. Computed c_v values based on Taylor method versus logarithm effective overburden stress (σ'_n) for SB backfill mixture and (a) PRT amended specimens and; (b) CRT amended specimens	97
Fig. 4.18. Computed c_v values based on the Taylor method relative to c_v values computed based on the Casagrande method versus σ'_n for (a) PRT amended specimens and; (b) CRT amended specimens	98
Fig. 4.19. Hydraulic conductivity (k_{theory}) as a function of effective overburden stress (σ'_n) for control SB backfill mixture and (a) PRT amended specimens; (b) CRT amended specimens	101
Fig. 4.20. Hydraulic conductivity (k_{theory}) as a function of void ratio (e) for control backfill mixture and (a) PRT amended specimens; (b) CRT amended specimens	102
Fig. 4.21. The computed hydraulic conductivity based on Terzaghi consolidation theory (i.e., k_{theory}) as a function of tyre content for SB control mixture and (a) PRT amended specimens; (b) CRT amended specimens	103
Fig. 4.22. Particle size distribution of kaolinite.	113
Fig. 4.23. SEM micrograph of the used kaolinite	113
Fig. 4.24. SEM micrograph of the used GGBFS	113
Fig. 4.25. (a) Typical relationship between volumetric shrinkage and curing time for different percentages of lime. (b) Typical relationship between volumetric shrinkage and different percentages of lime after different curing times.	122
Fig. 4.26. (a) Typical relationship between volumetric shrinkage and curing time for different percentages of GGBFS (b) Typical relationship between volumetric shrinkage and different percentages of GGBFS after different curing periods	123
Fig. 4.27. (a) The cracks that developed due to shrinkage in an untreated specimen after 28 days curing (b) Samples (1) 10PC-6G, (2) 10PC-4G and (3) 10PC-2G after 28 days curing, showing the effect of the GGBFS in reducing cracking due to shrinkage	124
Fig. 4.28. (a) The relationship between volumetric shrinkage and different percentages of GGBFS content and 2% lime for different curing times.	125

	(b) The relationship between volumetric shrinkage and different percentages of lime content and 2% GGBFS for different curing times	
Fig. 4.29.	(a) Results for unconfined compressive strength (UCS) in mixtures of clay with different ratios of lime. (b) Results for unconfined compressive strength (UCS) in mixtures of clay with different ratios of GGBFS-lime	127
Fig. 4.30.	(a) Results of shear strength tests on mixtures of clay and cement with different S/L ratios under 50 kPa normal stress. (b) Results of shear strength tests on mixtures of clay and cement with different S/L ratios under 100 kPa normal stress	128
Fig. 4.31.	(a) Scanning electron micrograph of a 28 day cured GGBFS mixed with lime at a ratio of (6:2) at a micrograph of 100 μm and (b) scanning electron micrograph of a 28 day cured GGBFS mixed with lime at a ratio of (6:2) showing the formation of cementitious crystalline products after pozzolanic reactions, (c) showing the presence of a small amount of needle-like ettringite, and (d) showing other forms of cementitious material (amorphous and fibrous).	131
Fig. 4.32.	XRD crystalline phase analysis of untreated clay, 28 day cured clay treated with 6% GGBFS, 6% lime and GGBFS-lime at a ratio of (6:2). The abbreviations are: Q-quartz, K-kaolinite, CSH-calcium silicate hydrate, CAH-calcium aluminate hydrate, P-portlandite, E-ettringite. H-halloysite	134
Fig. 4.33.	Scanning electron microscopic (SEM) image of the used Rockingham clay.	140
Fig. 4.34.	Scanning electron microscopic (SEM) image of the used GGBFS.	141
Fig. 4.35.	Typical discontinued graphs for variation of shear stress versus displacement (τ - ϵ) under 100 kPa effective normal stress for (a) untreated clay; (b) clay treated with 3% GGBFS; (c) clay treated with 5% GGBFS; (d) clay treated with 7% GGBFS.	145
Fig. 4.36.	A typical graph for variation of shear stress versus displacement (τ - ϵ) under 100 kPa effective normal stress acquired from discontinued graphs	145
Fig. 4.37.	Failure envelope for untreated and GGBFS treated clay specimens (a) fully softened; (b) residual.	147
Fig. 4.38.	Failure envelope shows drained shear strength characteristics in fully softened condition for (a) 7% GGBFS treated specimens; (b) 5% GGBFS treated specimens; (c) 3% GGBFS treated specimens; (d) untreated specimens.	149
Fig. 5.1.	Particle size distribution of used materials	163
Fig. 5.2.	X-ray powder diffraction (XRD) analysis of used sand and FA	163
Fig. 5.3.	Scanning electron microscopic (SEM) of used sand	164

Fig. 5.4. Scanning electron microscopic (SEM) of used FA	164
Fig. 5.5. Undrained shear response for untreated soil and FA treated specimens with an initial relative density of 20% under 50 kPa initial mean effective stress acquired from monotonic triaxial tests (a) stress path ($q-p'$); (b) stress-strain relation; and (c) excess pore water pressure versus axial strain.	169
Fig. 5.6. Effect of FA contents on stress path ($q-p'$) in post-cyclic tests (a) untreated soil; (b) FA=2%; (c) FA=4%; and (d) FA=6%.	172
Fig. 5.7. Variations of the ultimate deviatoric stress acquired from post-cyclic tests for untreated and FA treated specimens	172
Fig. 5.8. Typical stress path ($q-p'$) and stress-strain ($q-\epsilon_a$) acquired from post-cyclic tests for (a) untreated soil; and (b) FA=2%	174
Fig. 5.9. Variations of the ultimate deviatoric stress acquired from monotonic tests for untreated and 2% FA treated specimens	175
Fig. 5.10. Effect of curing time in variations of ultimate deviatoric stress acquired from monotonic tests for FA treated specimens.	176
Fig. 6.1. (a) Particle size distribution (PSD) of the employed Baldvis yellow sand and ;(b) Scanning electron microscopy (SEM) of the used sand in this study	185
Fig. 6.2. Scanning electron microscopic (SEM) image of the employed FA	186
Fig. 6.3. (a) Effect of relative density on liquefaction behaviour of the untreated soil under 50 kPa CP and 0.2 CSR. (b) Effect of relative density on liquefaction resistance of the sand mixed with 2% FA under 50 kPa CP and 0.2 CSR. (c) Comparison of the cyclic behaviour of the untreated soil and sand mixed with 2% FA with 20%, 40%, 60% and 80% relative density and 0.2 CSR under 50 kPa CP.	190
Fig. 6.4. (a) Effect of 4% FA addition on liquefaction resistance of the sand with a 20% relative density and 0.2 CSR under 90, 70 and 50 kPa effective confining pressure (b) Effect of 6% FA addition on liquefaction resistance of the sand with a 20% relative density and 0.2 CSR under 90, 70 and 50 kPa effective confining pressure.	192
Fig. 6.5. (a) Variation of CSR with cycle number to liquefaction at different effective confining pressure for sand mixed with 2% FA and 20% relative density. (b) Variation of CSR with cycle number to liquefaction for different curing times for sand mixed with 2% FA and 20% relative density under 50 kPa effective confining pressure.	194
Fig. 6.6. Particle size distribution of used sand and GGBFS.	203
Fig. 6.7. A typical SEM image shows geometry of the used sand in this study	203
Fig. 6.8. A typical specimen during preparation in split mould	206
Fig. 6.9. An overview of structure of the study	206

Fig. 6.10. Typical results of cyclic triaxial tests for GGBFS treated specimen (a) Effective stress path; (b) stress-strain relationship (hysteresis loop).	209
Fig. 6.11. Effect of GGBFS contents on liquefaction resistance of the soil for specimens under effective confining pressure of 200 kPa and an initial relative density of 60% (a) variations of the cyclic stress ratio (CSR) versus number of cycles to liquefaction (N_L); (b) variation of the cycle numbers (N_L) versus GGBFS contents	212
Fig. 6.12. Effect of GGBFS contents on pore water pressure ratio of the specimens under 200 kPa effective confining pressure, CSR value of 0.20, and an initial relative density of 60%	212
Fig. 6.13. Effect of effective confining pressure on liquefaction resistance of the 5% GGBFS treated specimens at a pre-consolidation relative density of 60% (a) variations of the cyclic stress ratio (CSR) versus number of cycles to liquefaction (N_L); (b) variation of the cycle numbers (N_L) versus effective confining pressures.	214
Fig. 6.14. Effect of effective confining pressure on pore water pressure ratio of the GGBFS treated specimens for a CSR value of 0.20, a pre-consolidation relative density of 60%, GGBFS= 5%.	215
Fig. 6.15. Effect of initial relative density on liquefaction resistance of the GGBFS treated soil for specimens under effective confining pressure of 200 kPa (a) variations of the cyclic stress ratio (CSR) versus number of cycles to liquefaction (N_L); (b) variation of the cycle numbers (N_L) versus initial relative densities.	217
Fig. 6.16. Effect of relative density on liquefaction resistance of the untreated and GGBFS treated specimens for a pre-consolidation relative density of 60%, a GGBFS content of 5%, and a CSR value of 0.20.	218
Fig. 6.17. Effect of curing time on liquefaction resistance of the GGBFS treated soil for specimens under effective confining pressure of 200 kPa and a pre-consolidation relative density of 60% (a) variations of the cyclic stress ratio (CSR) versus number of cycles to liquefaction (N_L); (b) variation of the cycle numbers (N_L) versus curing time.	221
Fig. 6.18. Effect of curing time on pore water pressure ratio of the specimens at 200 kPa effective confining pressure, CSR value of 0.20, and a pre-consolidation relative density of 60%	221
Fig. 7.1. Schematic overview for stress-strain ($q-p'$) and pore water pressure ratio ($r_u-\varepsilon_a$) phases in monotonic and two post-cyclic tests	231
Fig. 7.2. Particle size distribution of used materials	234
Fig. 7.3. Scanning electron microscopy (SEM) image of used sand	234
Fig. 7.4. Scanning electron microscopy (SEM) image of used fly ash (FA)	235
Fig. 7.5. Typical effective stress paths ($q-p'$) recorded in cyclic stage and before initiation of the post-cyclic phase for (a) $r_u= 0.25$; (b) $r_u= 0.50$; and (c) $r_u= 0.75$	238

Fig. 7.6. Typical undrained shear response for untreated soil and FA treated specimens with an initial relative density of 20% under 50 kPa initial mean effective stress acquired from monotonic triaxial tests (a) stress path ($q-p'$); (b) stress-strain relation; and (c) excess pore water pressure versus axial strain.	242
Fig. 7.7. Effect of FA contents on stress path ($q-p'$) in post-cyclic tests (a) untreated soil; (b) FA=2%; (c) FA=4%; and (d) FA=6%.	244
Fig. 7.8. Variations of the ultimate deviatoric stress acquired from post-cyclic tests for untreated and FA treated specimens	245
Fig. 7.9. Typical stress path ($q-p'$) acquired from post-cyclic tests on (a) untreated soil; (b) FA=2%; (c) FA=4%; and (d) FA=6%.	247
Fig. 7.10. Effect of relative density in variations of ultimate deviatoric stress in post-cyclic phase for untreated and 2% FA treated specimens for (a) $D_r=20\%$; (b) $D_r=40\%$; and (c) $D_r=60\%$.	249
Fig. 7.11. Effect of initial mean effective stress in variations of ultimate deviatoric stress acquired from monotonic and post-cyclic tests for 2% FA treated specimens.	250
Fig. 7.12. Schematic overview for stress-strain ($q-p'$) and pore water pressure ratio ($r_u-\varepsilon_a$) phases in monotonic and two post-cyclic tests	256
Fig. 7.13. Particle size distribution of used materials	258
Fig. 7.14. Scanning electron microscopy (SEM) image of used sand	259
Fig. 7.15. Scanning electron microscopy (SEM) image of used GGBFS	259
Fig. 7.16. Typical effective stress paths ($q-p'$) recorded in cyclic stage and before initiation of the post-cyclic phase for (a) $r_u=0.25$; (b) $r_u=0.50$; and (c) $r_u=0.75$	262
Fig. 7.17. Effect of GGBFS contents on shearing response of sand in post-cyclic phase (a) $r_u=0.25$; (b) $r_u=0.50$; and (c) $r_u=0.75$.	266
Fig. 7.18. The ultimate deviatoric stress acquired from post-cyclic tests for untreated and GGBFS treated specimens	267
Fig. 7.19. Effect of initial mean effective stress on shearing response of GGBFS treated specimens in post-cyclic phase (a) $r_u=0.25$; (b) $r_u=0.50$; and (c) $r_u=0.75$.	270
Fig. 7.20. The ultimate deviatoric stress acquired from post-cyclic tests for GGBFS treated specimens tested at different initial mean effective stress	271
Fig. 7.21. Effect of initial relative density on shearing response of the untreated and 5% GGBFS treated specimens in post-cyclic phase (a) $r_u=0.25$; (b) $r_u=0.50$; and (c) $r_u=0.75$.	274
Fig. 7.22. Summary of the ultimate deviatoric stresses for untreated and 5% GGBFS treated specimens in post-cyclic phase for (a) $D_r=40\%$; and (b) $D_r=60\%$	275

Fig. 8.1. Scanning electron microscopic (SEM) images for (a) natural sand; (b) crushed sand; (c) mixed sand	287
Fig. 8.2. Particle size distribution for tested sands	288
Fig. 8.3. Procedure for calculation of particle shape descriptors (Principles from Krumbein and Sloss, 1963 ; Cho et al, 2006).	289
Fig. 8.4. Undrained shear behaviour of NS, MS, and CS specimens under 500 kPa initial mean effective stress (a) stress path ($q-p'$); (b) stress-strain relation.	292
Fig. 8.5. Critical state locus in $e-p'$ plane for CS, MS, and NS specimens.	295
Fig. 8.6. Slope of critical state locus (λ_{cs}) in $e-p'$ plane versus (a) roundness; (b) sphericity; and (c) regularity.	297
Fig. 8.7. Critical state locus intercept (e_I) in $e-p'$ plane versus (a) roundness; (b) sphericity; and (c) regularity.	298
Fig. 8.8. Critical state locus in $q-p'$ plane for CS, MS, and NS specimens.	300
Fig. 8.9. Variation of the Critical state slope in $q-p'$ plane versus (a) roundness; (b) sphericity; and (c) regularity	302
Fig. 8.10. Variation of the stress ratio (q/p') versus void ratio for CS, MS, and NS.	304
Fig. 8.11. Typical critical state parameters of the soil in a monotonic triaxial test in (a) $q-p'$ plane; (b) $v-\log p'$ plane.	308
Fig. 8.12. Particle size distribution of the used materials	311
Fig. 8.13. Undrained shear behaviour of untreated and FA treated specimens under 500 kPa initial mean effective stress (a) stress path ($q-p'$); (b) stress-strain relation.	314
Fig. 14. Critical state locus in $e-\log p'$ plane for untreated and FA treated soil	316
Fig. 8.15. Effect of FA contents on (a) critical state slope (λ_{cs}) in $e_p-\log p'$ plane; (b) critical state intercept (Γ_{cs}) in $e_p-\log p'$ plane.	317
Fig. 8.16. Critical state locus in $q-p'$ plane for untreated and FA treated specimens	319
Fig. 8.17. Variation of the critical state frictional angle (ϕ_{cs}) versus FA contents	320
Fig. 8.18. Variation of the stress ratio (q/p') versus void ratio for untreated and FA treated specimens	321
Fig. 8.19. Typical brittleness index (I_B) for untreated and FA treated specimens.	322

List of Tables

Table 2.1. main studies conducted on improvement of the liquefaction resistance of soil using different agents	39
Table 4.1. Characteristics of each backfill mixture	66
Table 4.2. A summary of hydraulic conductivity test results.	68
Table 4.3. Characteristics of each backfill mixture	84
Table 4.4. A summary of hydraulic conductivity test results.	104
Table 4.5. The chemical properties of the lime (Cockburn Cement 2012)	114
Table 4.6. The chemical properties of the GGBFS used in this study (BGC Cement 2013).	114
Table 4.7. A summary of the mix design for the volumetric shrinkage strain tests	117
Table 4.8. A summary of the mix design for the unconfined compressive strength (UCS)	118
Table 4.9. A summary of the mix design for the ring shear tests	120
Table 4.10. Particle size distribution (PSD) and index properties of the Rockingham clay used to perform the tests	140
Table 4.11. Experimental program to perform the tests in this study	143
Table 4.12. A summary of drained fully softened and residual shear strength characteristics of untreated clay and clay treated with different GGBFS contents.	150
Table 4.13. A summary of drained fully softened and residual shear strength characteristics of untreated clay and clay treated with 7% GGBFS at 7, 14, and 28 days curing time	151
Table 5.1. Experimental program and mixtures characteristics	166
Table 6.1. Chemical compositions of the employed Collie Fly ash (Flyash Australia 2016)	185
Table 6.2. Experimental program designed to investigate effect of the relative density (D_r), FA content, effective confining pressure (CP) and curing time (CT) on cyclic behaviour of the fly ash (FA) treated soil.	187
Table 6.3. Effect of relative density on liquefaction resistance of the untreated soil and sand mixed with 2% FA under 50 kPa CP and 0.2 CSR and 1 HZ frequency.	190

Table 6.4. A summary of the results to investigate effect of the 4% and 6% FA addition on liquefaction resistance of the sand with 20% relative density and under 50, 70 and 90 kPa effective confining pressure.	193
Table 6.5. A summary of the results to investigate effect of the 50, 70 and 90 kPa effective confining pressure on liquefaction resistance of the sand mixed with 2% FA and 20% relative density.	195
Table 6.6. A summary of the results to investigate effect of the 14 and 28 days curing time on liquefaction resistance of the sand mixed with 2% FA and 20% relative density under 50 kPa effective confining pressure.	195
Table 6.7. Chemical composition of used GGBFS (BGC Cement 2013a).	202
Table 6.8. Physical characteristics of used GGBFS (BGC Cement 2013a).	202
Table 6.9. Experimental program to investigate cyclic behaviour of the GGBFS treated soil.	207
Table 6.10. Effect of GGBFS contents on improvement of the liquefaction resistance of the specimens under 200 kPa effective confining pressure and a pre-consolidation relative density of 60%.	211
Table 6.11. Effect of curing time on improvement of the liquefaction resistance of the specimens at a pre-consolidation void ratio of 60% and a GGBFS content of 5%.	220
Table 7.1. Experimental program and key results for tests	239
Table 7.2. Chemical composition of the used GGBFS (BGC Cement 2013a).	258
Table 7.3. Experimental program and key results for tests	263
Table 8.1. Properties of the tested sands in this study	288
Table 8.2. Experimental program conducted in this study and recorded results	293
Table 8.3. Experimental program conducted in this study and recorded results	312
Table 8.4. Effect of FA on critical frictional angle and slope factor	319

List of Notations, Symbols and Acronyms

λ_{cs}	Critical state locus slopes
Γ	Void ratio intercept at $p'=1$
Γ_{cs}	Critical state intercept
ε_v	Vertical strain
γ_d	Dry unit weight
$\Delta\sigma_3$	Cell pressure
ϕ	Friction angle
ϕ_{fs}	Fully softened friction angle
ϕ_r	Residual softened friction angle
ϕ_{cs}	Critical state friction angle
τ	Shear strength
τ_{fs}	Fully softened shear strength
τ_r	Residual shear strength
τ_p	Intact mobilised shear strength
ε	Displacement
ψ	State parameter
σ'_n	effective overburden pressure / effective normal stress
σ'_1	Effective major principal stress
σ'_3	Effective minor principal stress.
a_v	Coefficient of compressibility
c_v	coefficient of consolidation
C_i	compression index
C_s	swelling index
CSR	Cyclic stress ratio
CSL	Critical state line

C_c	coefficient of curvature
C_u	uniformity coefficient
c_{fs}	Fully softened cohesion
D_r	Relative density
D_{rp}	Post-consolidation relative density
e	void ratio
e_p	Post-consolidation void ratio
e_r	Void ratio intercept at $p=0$
e_0	Pre-consolidation void ratio
e_{max}	Maximum void ratio
e_{min}	Minimum void ratio
e	global void ratio
e_{cs}	Critical state void ratio
EC	electric conductivity (EC)
n	Porosity
m_v	Coefficient of volume compressibility
m	Slope factor
m_{fs}	Fully softened slope factor
m_r	Residual softened slope factor
k_f	final hydraulic conductivity
k_{theor}	hydraulic conductivity values using consolidation theory
G_s	Specific gravity
m	Slope factor
m_{fs}	Fully softened slope factor
m_r	Residual softened slope factor
OCR	Over-consolidation ratio
q_u	Ultimate deviatoric stress

q	Deviator stress
p'	Mean effective normal stress
p_0'	Initial mean effective confining pressure
u/σ	Pore water pressure ratio
N_L	Number of cycles to liquefaction
S	Sphericity
SEM	Scanning electron microscopic
ρ	Regularity
p_a	Atmospheric pressure (=101 kPa)
q/p'	Critical stress ratio
I_B	Brittleness index
v	Specific volume
V	Total volumetric shrinkage
V_w	Wet volumetric shrinkage
V_d	Dry volumetric shrinkage

Chapter 1

Introduction

1. Introduction

1.1. Problem Statement

Liquefaction is one of the most catastrophic phenomena in the world that happens due to soil loss of strength and stiffness during seismic events in a saturated soil, and its mitigation is of great importance. From the geotechnical engineering viewpoint, the liquefaction hazard can be mitigated by application of the ground improvement techniques. The ground improvement is a subcategory of the geotechnical engineering that offers different techniques to improve or to restore the strength of the soil against external stimuli. However, there are different ground improvement methods and techniques to improve the strength of soils, application of some of these techniques are not recommended due to the costly or their hazardous nature for the environment. For instance, there are a variety of soil modification (densification) techniques to improve the mechanical behaviour of soil and to mitigate the destructive effects of liquefaction, however they are highly dependent on application of the heavy construction machineries which impose a great amount of cost on the projects. The soil modification techniques such as vibro-compactions, stone coulomb, dynamic compaction, and compaction grouting are some of these techniques that are applied in soil improvement projects.

Improvement or restoration mechanical behaviour of soil by application of additives is one of the most popular methods in soil improvement projects. In comparison with the densification techniques, application of this method is not only time saving but also cost effective and can be implemented with conventional construction machineries. The additives improve the mechanical behaviour of soil by improving the bonds amongst soil particles. There are a wide variety of additives, which have been used since many years ago. For instance, Portland cement (PC) and lime are known as two

traditional agents that widely have been used since many years ago in ground improvement projects. They are known as the most applicable additives in ground improvement projects, however, they are expensive and non-environmental friendly admixtures in comparison with other additives. For instance, it has been indicated that production of one tonne Portland cement (PC) causes generation of 0.95 tonne CO₂ in the environment, 5000 MJ energy use, 1.5 tonne mineral extraction, and 0.02 waste disposal for the environment (Higgins 2007).

On the other hand, developments in knowledge have led to the production of new materials and consequently some new by-products. One of the by-products recently considered for use in geotechnical engineering is the ground granulated blast furnace slag (GGBFS), which remains after the steel manufacturing process. Application of GGBFS in civil engineering projects is not only cost effective and energy saving but also reduces the carbon emissions and is environmentally friendly (Higgins, 2007). For instance, it has been indicated that production of one tonne GGBFS causes generation of 0.07 tonne CO₂ in the environment (carbon emission), usage of 1300 MJ energy, no mineral extractions, and saving one tonne waste disposal (Higgins, 2007). The application of GGBFS has been encouraged by the ground improvement practitioners as it has a hydration and pozzolanic products that can improve the strength characteristics of soils. The fly ash (FA) also is known as another environmental-friendly by-product in ground improvement since it generates from fired coal process in electrical generation plants and has a hydration characteristic.

1.2. Significance of Research

Liquefaction is a common phenomenon in many parts of the world. This phenomenon puts on risk people's lives, destructs the structures, and imposes many costs. On the other hand, the geotechnical structures such as dams, embankments, and slopes are

counted as the most vulnerable systems during or after a liquefaction event. Hence, investigations into the liquefaction mitigation practices are of great importance since it can save the human's life and the millions of dollars cost of the projects. However, there are different techniques and methods to mitigate the destructive effects of the liquefaction for geotechnical structures, they are not cost effective or applicable due to their dangerous nature for the environment. On the other hand, thousands millions tonnes of by-products materials from different industry are generated each year which their stockpile can be costly and causes environmental hazards. Therefore, controlling the possibility of the application of these by-product materials in different industry is another urgent issue. The GGBFS and FA are two by-products from steel industry and power generation plants with a high production rate in Australia which have a characteristic like PC and lime, which evaluation of their application against liquefaction is topic of this study. Possibility of the application of GGBFS and FA against liquefaction not only can be effective to improve the strength of the geotechnical structures but also can be helpful to reduce the carbon footprint and the cost of the projects.

1.3. Research Scopes and Objective

There are different parameters which are effective in forming liquefaction strength of the soil. Beside of seismic strength and characteristics and from geotechnical point of view. The soil characteristics and applied stresses have the main role in forming liquefaction behaviour of a soil. The soil characteristics such as relative density and particle shape are the effective parameters of the soil in occurrence of the soil liquefaction. Beside of them, the behaviour of the soil after addition of binders and the effect of curing time, are the most effective parameters of the soil after improvement

which are required to be evaluated. In addition, the liquefaction is a phenomenon which can be occurred due to the fast monotonic, cyclic, or post-cyclic stresses in saturated soils. This phenomenon can also occur during a seismic event or up to a couple of hours after an actual seismic event.

1.4. Thesis Organisation

This thesis investigates the effect of the by-product binders on liquefaction behaviour of the soil by conducting a series of comprehensive experimental studies in nine chapters. A summary of the contents in each chapter listed below.

- Chapter 1 is the introduction chapter and provide a summary of the problem statement, significance of the research, research scopes and objectives;
- In Chapter 2 a background and literature review has been conducted on the relevant studies in this area;
- Chapter 3 is introduced the geotechnical experimental apparatus used to evaluate the soil characteristics in this study;
- In Chapter 4 the results of preliminary experimental studies on different binders have been presented and analysed and the selected materials have been introduced to conduct the main analysis in the next stage.
- In Chapter 5, the results of undrained monotonic triaxial compression tests on liquefaction behaviour of the FA amended soil have been presented and analysed;
- In Chapter 6, the results of undrained cyclic triaxial tests to investigate the effect of binders (i.e., FA and GGBFS) on liquefaction behaviour of the soil have been presented and analysed;

- In Chapter 7, the results of post-cyclic monotonic triaxial compression tests on liquefaction behaviour of the soil mixed with binders (i.e., FA and GGBFS) have been presented and evaluated.
- In Chapter 8, the constitutive analysis based on critical state of soil mechanics (CSSM) have been presented for the soil shape parameters and for the soil mixed with FA.
- In Chapter 9, the acquired results in previous chapters have been summarised, and the recommendations have been offered.

This thesis is a comprehensive study on effect of by-product binders on improvement of the cyclic behaviour of soil, and various test types have been employed in two main parts. The first part, is the preliminary section (i.e., Chapter 4), which contains performing various tests to achieve the most suitable binders and the percentage to step into the second part. For instance, by-product materials such as tyre chips, sawdust, fly ash and GGBFS were selected and the preliminary tests were conducted in an innovative method to select the most effective binders. Therefore, a clear goal has been targeted and achieved through various tests in the first part. The conclusions from the first stage of the experimental studies showed that the fly ash and GGBFS are the most effective binders amongst others, therefore, the studies continued two recent by-products, and in the second stage (i.e., Chapter 5, 6, 7, and 8), the strength characteristics of the mentioned mixtures were investigated by performing a series of triaxial testing (Monotonic, cyclic, & post-cyclic). Therefore, a full set of focused experimental studies have been designed and conducted through this research.

Chapter 2

Background and Literature Review

2. Background and Literature Review

2.1. Abstract

Liquefaction is one of the most catastrophic phenomena in the world that happens due to soil loss of strength and stiffness during seismic events in saturated soils. Recent investigations show that the main failures for the geo-structures such as embankments, dams, and slopes have occurred from 2 to 24 hours after an actual seismic event ([Wang et al. 2015a](#); [Soroush and Soltani-Jigheh 2009](#)). Hence, improving mechanical characteristics of the soil during and after a seismic event has been of great importance for the geotechnical practitioners. During a liquefaction event, the pore water pressure is generated due to the seismic loadings and application of techniques, which reduce the pores or produce a strong bonding characteristic amongst soil particles are effective methods to reduce the liquefaction hazards. The ground improvement is a branch in geotechnical engineering science that offers a variety of techniques that enhance the mechanical characteristics of soil. The techniques such as soil densification, reinforcement, and application of chemical additives are three categories of the ground improvement techniques. These techniques have been analysed and discussed in the following sections. Fig. [2.1](#) shows an example of the disastrous effects of the liquefaction in a tailing dam.



Fig. 2.1. An example of the liquefaction disastrous effects at the Saaiploas tailings dam (Fourie et al. 2001).

2.2. Applicable Ground Improvement Techniques in Liquefaction Mitigation

The effective ground improvement methods in reducing the liquefaction hazard can be divided into three main techniques as physical methods, reinforcement methods, and application of chemical additives methods (Keramatikerman and Chegenizadeh 2015). Fig. 2.2 shows a more detailed categorisation of the applicable methods to reduce the liquefaction. In continue each method has been expanded and discussed.



Fig. 2.2. Classification of applicable ground improvement methods to reduce the liquefaction hazard

2.2.1. Physical Techniques

The physical techniques refer to changing the physical nature of soil particles by increasing the soil density and interlocking forces using heavy machinery such as vibrator, or compactor (Makusa 2012). In these methods, the soil is compacted and densified by displacing the pores and voids by means of a heavy pressure from external

stimuli. Application of an appropriate level of pressure is an important issue in this method since applying a high level of pressure can cause a particle breakage and losing the engineering properties of the soil. The physical techniques are known as expensive techniques since is performed by means of mechanical machinery tools.

2.2.1.1. Vibro-compaction Technique

The vibro-compaction or vibro-flotation technique is applicable for loose to medium dense soil. The soil around the vibrator transforms into a quick condition by application of mechanical vibration and supply of water simultaneously and the soil reaches to the densest possible state by temporarily deactivating the effective stress. Due to compaction of the soil in an unstressed condition, a permanent densification is attained for the soil. This is very effective to increase the resistance of the soil against additional dynamic loadings induced by external shock stresses during an earthquake event. The vibro-compaction is a process which increases the internal friction and modulus of deformation and reduced the compressibility and initial void ratio of the soil ([Baumann and Bauer 1974](#)). Initially, the running vibrator which is suspended from the rig excavates the soil by means of its weight and the water jets. In fact, it produces a liquefied condition for the surrounded soil and helps the soil penetrates into the required depth of the soil. The jetting the water into the soil is stopped at this stage and the compaction is commenced. The ground in the surface forms a cone-shaped depression because of compaction at this stage. When the power consumption reaches its peak, the rig brings up the vibrator for 30-50 cm and repeats the compaction process. The excavated hole in vibro-compaction method has a diameter in the range of 1.5 to 3.0 m for a very fine sand to clean gravel ([Baumann and Bauer 1974](#)).

2.2.1.2. Stone-columns Technique

There is a large study on application of the stone column or gravel drain technique to reduce hazardous impacts of the liquefaction in the literature ([Seed and Booker 1977](#); [Ishihara and Yamazaki 1980](#); [Tokimatsu and Yoshimi 1980](#); [Baez and Martin 1995](#); [Boulanger et al. 1998](#); [Adalier and Elgamal 2004](#) amongst others). The stone column technique is performed by vibro-replacement of the stones. In this method, the density of the surrounding soil increases and increase the potential for carrying a greater stress level. The water can drain in stone columns and the pore water pressure built-up is controlled ([Adalier and Elgamal 2004](#)).

This method is a satisfactory technique to apply in urban areas since construction of the stone columns are not accompanied with noise or vibration unlike the other ground improvement techniques such as dynamic compaction and blasting. The stone columns constructs using two techniques of vibro-replacement and auger-casing. In the first technique, the running vibrator is inserted into the ground until the desired level by means of water jet and vibration power. Then, the columns are filled by stone backfills (i.e., gravel) and compacted by raising and lowering the running vibrator. This helps the gravels completely fill the column and provide a more densified condition for the hole and surrounding soil. The densification level in this method is a function of different parameters such as fine contents, soil initial density, column diameter, gravel shape etc. ([Adalier and Elgamal 2004](#)). A satisfactory level of densification is attained in construction of the stone-columns using auger-casing method since the filling and compacting the columns is performed using a compaction-rod system ([Saito et al. 1987](#); [Ono et al. 1991](#); [Oishi and Tanaka 1993](#)).

2.2.1.3. Compaction Grouting Technique

The compaction grouting technique consists of injection of a stiff slurry which is a combination of soil, PC, and water into the ground by means of a running vibrator. However, the prepared grout does not penetrate into an original soil, the injection of the grout causes generation of the slurry bulbs in a controlled manner, which displaces the surrounding soil (Boulanger and Hayden 1995). In this method, the grout pipes is inserted through the soil while the compaction grout is inserting into the grout pipes. However, the surface ground has the lowest disturbance in this method, there is little understanding about grouting mechanisms.

2.2.1.4. Dynamic Compaction Technique

In the dynamic compaction (DC) technique the cohesion-less soil is densified using a high-energy tamping by dropping a heavy mass of 10 to 40 tonnes from a height between 10 to 25 m onto the pre-designed point on the ground surface (Chow et al. 1992; Feng et al. 2015). The dynamic compaction designing is mainly an empirical method due to the high complexity of soil behaviour under a high-energy impact. This technique is mainly conducted based on the experience of the ground improvement designer. Generally, in this method a series of pilot tests are conducted to ensure the designer to achieve the required parameters such as tamping weight, number of droppings, height to minimize the cost (Chow et al. 1992).

The initial formula to design a DC testing was introduced by Menard and Broise (1975), which was a correlation between depth of improvement and impact energy per drop. The proposed equation was not an accurate method to estimate depth improvement of soil since the effect of soil type and tamping process was ignored in this method. This equation was modified by Lukas (1986) as follow:

$$d_{max} = n(WH)^{1/2} \quad (2.1)$$

Where, d_{max} = dynamic compaction improvement depth (m); W = mass of the tamper (tonnes); H = drop height (m); and n = empirical coefficient derived from statistical data which is a factor of soil type, efficiency of fall mechanism, and the impact energy.

2.2.2. Soil Reinforcement

The soil reinforcement technique has a concept similar to mechanical technique. In this method, the soil strength increases due to an increase in interlocking forces amongst soil particles and reinforcement agent. The soil reinforcement method can be categorised in two sub-categories of the geo-synthetics group and tyre products. As mentioned, the interlocking forces amongst soil particles are the main reason for increasing the shear strength of the soil. Fig. 2.3 shows a categorisation of the reinforcement method in liquefaction mitigation.

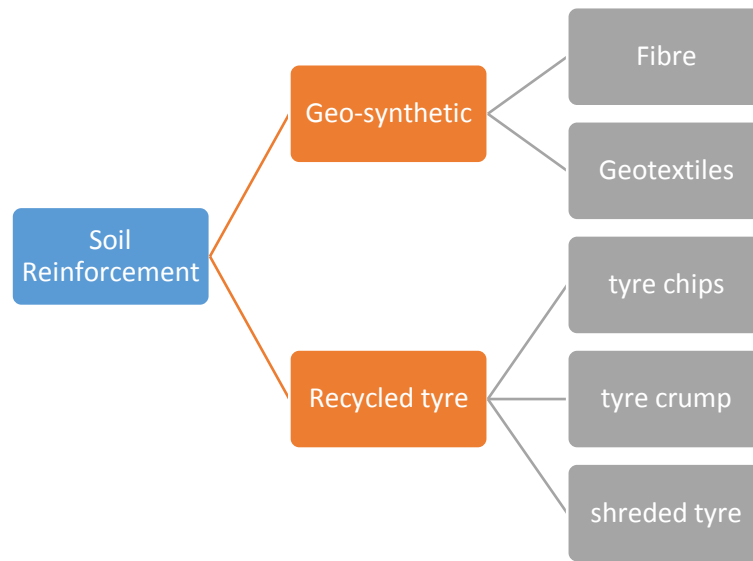


Fig. 2.3. Classification of soil reinforcement methods in liquefaction mitigation

2.2.2.1. Geo-synthetics

The soil reinforcement is an effective technique to improve the strength and bearing capacity of the soil. Application of geo-synthetics in ground improvement originated from the role of roots of trees in soil (Gray 1970; Waldron 1977; Wu et al. 1988). The geo-textiles, geo-grid, and fibres, are common types of soil reinforcement using geo-synthetics materials. Fig. 2.4 shows an example of a type of used fibre in improvement of liquefaction resistance of the soil. Chegenizadeh (2012) conducted a broad range of ground improvement study to investigate the effect of different types of natural and plastic fibres in ground improvement. In another example, Noorzad and Fardad Amini (2014) investigated the effect of randomly distributed fibre reinforced soil by performing a series of cyclic triaxial tests. They indicated that liquefaction resistance and shear

modulus of the sand increased by addition of randomly distributed fibre. They also investigated the effect of fibre content and fibre length in liquefaction resistance of the soil. In another example, Boominathan and Hari (2002) investigated the effect of fibre reinforcement on the liquefaction strength of FA. They indicated that the addition of fibre increased the liquefaction resistance of FA due to the provision of interlocking behaviour and dissipating excess pore water pressure amongst FA particles. In another study, Vercueil et al. (1997) investigated the effect of the addition of woven and non-woven geosynthetics with different mechanical characteristics to the sand and reported that the cyclic strength of the soil increased when geotextiles were included in the sand. Maher and Ho (1993) investigated the behaviour of fibre-reinforced cemented sand under cyclic loading. The results indicated that the addition of fibre improved the cyclic strength of the cemented sand. In another effort, Ibraim et al. (2010) investigated the effect of discrete flexible fibre (DFF) on monotonic undrained liquefaction of a loose sand susceptible to liquefaction. It was indicated that the reinforcement converted the soil behaviour from a strain softening into a strain hardening response and improved its liquefaction strength. Hamidi and Hooresfand (2013) in a similar study on a reinforced cemented sand indicated that the fibre reinforcement reduces the occurrence potential of liquefaction. Haeri et al. (2000) investigated the effect of geotextile reinforcement. In another case, the effect of cyclic loads on geotextile materials was investigated by Naeini and Gholampoor (2014). They studied the cyclic response of the silty sand reinforced with geotextile by performing a series of cyclic triaxle tests. The results indicated that geotextile inclusion led to an increase in axial modulus and a decrease in the ductility of the silty sand specimens.



Fig. 2.4. Bulk continuous filament (BCF) as a typical geo-synthesis used in soil reinforcement ([Chegenizadeh et al. 2018a](#))

2.2.2.2. Scrap Tyre

Nowadays, along with development and diversity of products manufactured by companies, there are a variety of by-product materials available that have a potential of application in ground improvement projects. The scrap tyre disposal has been indicated as a growing issue in different parts of the world, in particular in Australia. There are two main technologies to manufacture crumb tyres, which are known as ambient grinding and cryogenic procession. In the first method, the crumb tyre is produced after passing through three main steps to purify the tyre from metal and fabric components. In the first stage, the feedstock is shredded to the small particles, and then in the second stage, the machine purifies the rubber from metals and fabric by grinding the small particles, and in the final stage, a finishing mill grinds the products based on the requirements of design. In the cryogenic processing method, the tyre chips are freezing to the level of -80°C using a liquid nitrogen before downsizing. This process causes the tyre chips have a brittle characteristic, which is helpful in downsizing

process in the next stage ([Scrap Tire News 2017](#)). Fig. 2.5. shows two types of crumbed and powdered scrap tyres after the grinding process.

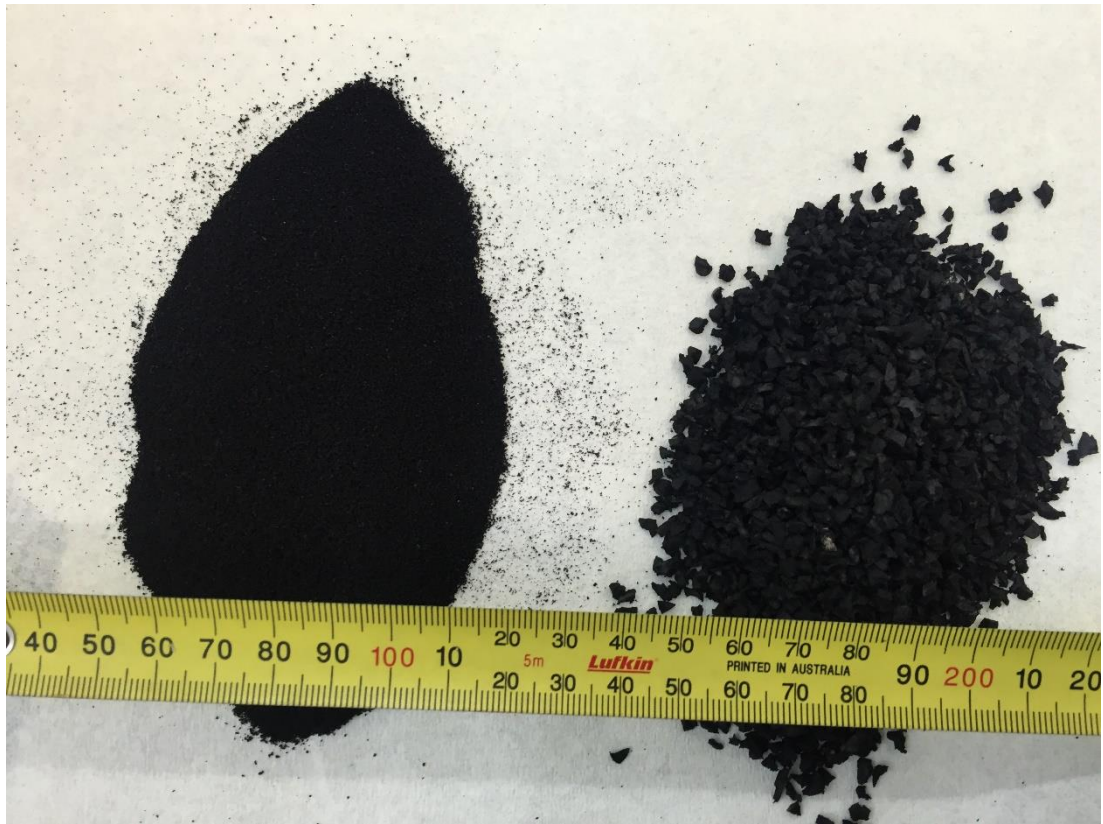


Fig. 2.5. powdered and crumbed recycled tyres produced from scrap tyre in different industries

2.2.2.2.1. Scrap Tyre in Australia

It has been estimated that over 285 million of tyres scrapped each year and about 300 million stockpiled until 2001 ([Vashisth et al., 1998](#); [Rubber Manufacturers Association, 2002](#); [Edil et al., 2004](#)). Some other studies indicate that approximately 52.5 million tyres are disposed in Australia each year, of which only 13% are being recycled ([SITA 2016](#)). The major portion of these tyres is stockpiled or deposited in landfill sites which can have a significant impact on the environment. The scrap tyre is obtained from three main sources of passenger tyres, truck tyres, and off-the-road

(OTR) tyres. The passenger tyres consisted of conventional cars, motorcycles and caravan. The truck tyres include the tyres of buses, commercial vehicles, trailers, and fire fighting vehicles, and the OTR tyres are the vehicles, which are used in the agricultural, construction and mining areas (Hyder 2012).

2.2.2.2.2. Review on Application of Recycled Tyres

While the majority of recycled tyres is used in the construction industry, there is still a substantial potential for application of tyres in geotechnical engineering projects. Several studies have investigated applications for recycled tyres in the construction and pavement industries (Bosscher et al. 1997; Raghavan et al. 1998; Hernández-Olivares et al. 2007; Huang et al. 2007). Recently, application of recycled tyre chips (RTC) has been considered by researchers in geotechnics science (Towhata, 2008; Kaneko et al., 2012; Hong et al., 2015; Mashiri et al., 2016). For instance, Mashiri et al. (2016) investigated effect of tyre chips on sand and indicated that addition of tyre chips in a range of 20% to 40% increased the cyclic strength of the sand. It was reported that addition of tyre chips up to 10% has no effect on liquefaction resistance of the sand and addition of the tyre chips in a range of 30% to 33% is very effective to improve the liquefaction resistance (Mashiri et al., 2016). In another example, Hong et al. (2015) investigated cyclic strength of the Christchurch sand by addition of the 40% (by volume) tyre chips. They observed that addition of the tyre chips decreased liquefaction resistance of the sand and argued that it is due to deformability property of the tyre and weakness in absorbing the energy of compaction (Towhata, 2008). The seismic characteristics of sand mixed with rubber was investigated by Kaneko et al. (2012). They reported that tyre chips either mixed with sand or as a separated layer of material reduced the generation of excess pore water pressure, leading to an increase

in liquefaction resistance ([Kaneko et al., 2012](#)). They recommended placing a layer of tyre chips at the bottom of the sand layer as a more effective means of preventing liquefaction than sand mixed with the same percentage of tyre chips ([Kaneko et al., 2012](#)). In another case, [Towhata \(2008\)](#) substituted shredded tyre chips with cement in a mixture with sand as a backfill material in a pipeline trench project and carried out a simulation using a shaking table model to investigate the liquefaction resistance of the new mixture. He recommended its application as it was cost effective and decreased susceptibility to liquefaction ([Towhata, 2008](#)). [Uchimura et al. \(2007\)](#) used a shaking table to study effect of the cyclic strength of the tyre treated sand. They reported that tyre chips increased the liquefaction strength of the sand. They validated the results by performing a series of cyclic triaxial tests. [Youwai and Bergado \(2003\)](#) reported that addition of the tyre chips increased the cyclic strength of the sand and reduced its vertical deformation. It was reported that this behaviour is more pronounced when the used tyre chips is more than 30% ([Youwai and Bergado, 2003](#)). [Neaz Sheikh et al. \(2012\)](#) reported that the addition of the tyre chips increased the vertical strain and reduced the shear strength of the soil. It was noted that increasing the size of tyre chips is effective to improve the shear strength of the sand. It was also reported that increasing the confining pressure increased the shear strength and vertical displacement of the soil ([Neaz Sheikh et al., 2012](#)). [Hazarika et al. \(2010\)](#) carried out a similar study using tyre chips and sand mixtures to investigate the liquefaction resistance of soil as a backfill material in pipelines, based on undrained cyclic shear tests and a model shaking table test, reported that the application of 50% tyre chips was very effective in reducing the liquefaction capacity of the sand.

Recycled tyres also have great potential for use in ground improvement projects (Lee et al. 1999; Consoli et al. 2001; Akbulut et al. 2007). For instance, Patil et al. (2011) studied the effect of adding crumbed recycled rubber to clay specimens to control swelling. They noted that crumbed recycled rubber was useful for controlling the swelling behaviour of the specimens. In another example, Özkul and Baykal (2007) investigated the effect of fibrous rubber on clay. The results showed an increase in peak shear strength up to a certain normal load (300 kPa), after which shear strength decreased. Neaz Sheikh et al. (2012) investigated the effect of tyre addition on shear strength and compressibility of the soil. They indicated that addition of tyre crumb to the soil caused a reduction in shear strength characteristics of the soil and remarkable axial strain was recorded for the mixture due to its ductility capacity. The results also indicated that the preloading can be effective to reduce the settlement. Li et al. (2016) investigated dynamic behaviour of two sizes of rubber crumb mixed with soil by performing a series of cyclic triaxial and resonant column tests. It was indicated that the liquefaction resistance of the soil increased by increasing the tyre content and size. Moreover, the damping ratio was slightly higher at low stress pressure. Guleria and Dutta (2011) investigated unconfined compressive strength of three types of the tyre chips in dry, sodium hydroxide, and carbon tetrachloride treated conditions mixed with FA, lime, and gypsum. The specimens were cured at four curing times (i.e. 7, 28, 90, 180 days) and three curing methods of desiccator, burlap, and water-filled container. Results showed that carbon tetrachloride and sodium hydroxide treatment are effective to increase the UCS strength of the benchmark mixture. It was also indicated that curing method using water-filled container and burlap desiccator is the most effective methods to increase UCS strength of the soil. The specimens showed the maximum UCS values after 90-day curing period. Priyadarshie et al. (2015) investigated shear

strength and compaction behaviour of the tyre crumble in combination with FA and kaolinite clay. Results indicated that addition of the tyre crumbles to clay and FA caused a reduction for the maximum dry density and increased the optimum moisture content (OMC) of the clay. However, no significant changes were recorded for the FA. It was also concluded that the mixture of tyre with FA has more resistance against applied load. The CBR behaviour of the tyre-clay mixture improved 5 times, whereas the tyre-FA mixture improvement was 3 times greater than its benchmark mixture. It should be considered that the cost of tyre is a function of its size, meaning that shredded and powdered recycled tyres are more expensive than the other types.

2.2.3. Chemical Additives

The third method in ground improvement is performed by application of chemical additives into the soil to improve its strength and durability properties. The applied additives usually have a hydration and pozzolanic characteristics, which provide bonds amongst soil particles and increase the soil strength characteristics. Portland cement (PC) and lime are two popular chemical agents which world widely apply in geotechnical engineering projects. The chemical agents are divided into two main groups of environmental friendly non-environmental friendly products. A schematic categorisation of the applicable ground improvement techniques have demonstrated in Fig. 2.6. As shown, the chemical agents are divided into two main categories of non-environmental friendly and environmental friendly agents. However, the traditional additives are effective agents and have been used since many years ago, they are expensive and not environmental friendly products. In contrast, the non-traditional additives, are by-product of other industries. Hence, they are cheap products and their

application can help to reduce their stockpile and accordingly reduce the carbon footprint. Following sections discuss more the traditional and non-traditional additives.

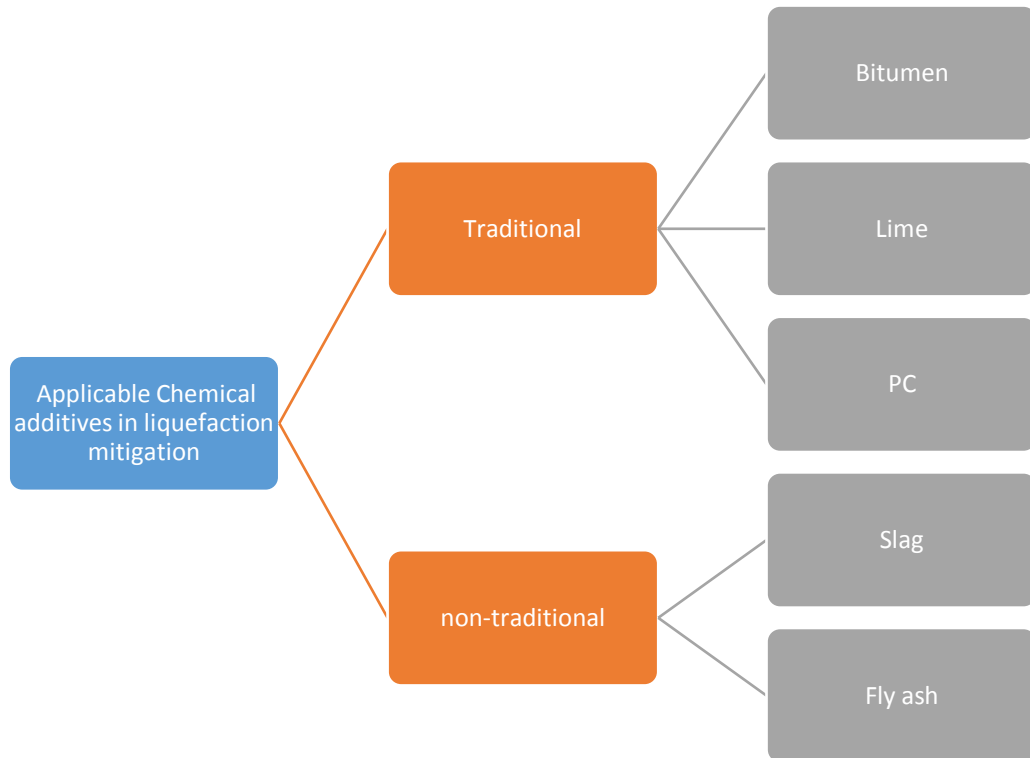


Fig. 2.6. Classification of chemical additives application in liquefaction mitigation

2.2.3.1. Traditional Additives

2.2.3.1.1. Lime

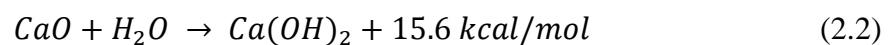
The use of lime for stabilisation has also been of interest to many researchers. Reference (Celauro et al. 2012) studied the design procedure for lime stabilisation in road and pavement engineering. From a geological perspective, relating to microstructure and the addition of lime, long-term stability of lime stabilised gypsums soils was studied by conducting wet and dry cycles on the mechanical treatment of a fine soil with different gypsum doses (Aldood et al. 2014a). Reference (Aldood et

al. 2014b) also studied performance of freeze and thaw cycles on gypsum soil stabilised by lime. A constant rate of 3% of lime and 28 days curing at 20°C were applied to mentioned studies. In another case, performance of tyre cord on mechanical properties of lime stabilised and unstabilised clayey soil were studied (Jafari and Esna-ashari 2012).

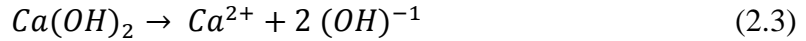
Vakili et al. (2015) investigated the effect of sodium silicate on the shear resistance of clay. They used the same method as previous researchers and observed that the addition of sodium silicate to soil is not an appropriate option.

However, lime (CaO) is known as the most applicable agent in pavement projects (Bell 1996; Prusinski and Bhattacharja 1999; Eades and Grim, 1960) especially in improvement of a clayey subgrade (Petry and Little, 2002).

Addition of lime to a clay soil system containing water results in hydration, cation exchange and pozzolanic reactions. The lime absorbs the moisture of the soil and becomes hydrated lime ($Ca(OH)_2$) through a rapid reaction that produces a large amount of heat through the hydration process. This reaction is illustrated in equation (1) (Kitazume and Terashi 2013).



The hydrated lime dissolves into the existing pore water and increases the concentration of calcium (Ca^{2+}) and hydroxyl (OH)⁻¹ ions (See equation (2)). Then cation exchange occurs between the ions of the clay grains and the calcium ions of the lime on the surface of the clay minerals (Bell 1996).



The Ca^{2+} and $(OH)^{-1}$ ions react with Al and Si minerals in the clay particles while they are in the pore water and undergo pozzolanic reactions and generate hydration products such as calcium aluminate hydrate (CAH), calcium silicate hydrate (CSH), and calcium aluminium silicate hydrate (CASH). These hydration products play the main role in soil stabilisation by lime. Equations (3), (4) and (5) show the generation of hydration products (Bell 1996; Al-Mukhtar et al. 2012).

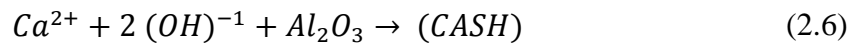
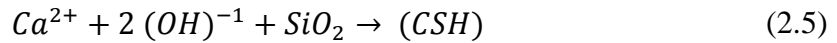
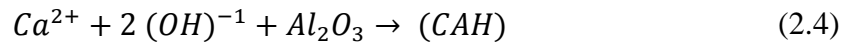


Fig. 2.7. and 2.8 show a typical scanning electron microscopic (SEM) view of the lime and ordinary Portland cement (OPC) respectively. Lime has hydration and pozzolanic characteristics similar to Portland cement (PC). In addition, the processes associated with production of this additive are hazardous for the environment in terms of carbon emissions and energy consumption (Higgins 2007, Yi et al. 2013). For instance, European commission (2013) reported that the major environmental concerns associated with lime manufacturing are consumption of a high amount of energy and major air pollutions. Another report raised same issues and indicated that lime production process accompanies with generation of toxic elements such as arsenic, lead, mercury, nickel, etc. These toxic elements put the public health at risk (EPA 2004).

In addition, although the application of lime enhances the engineering properties of soil to a certain extent, there are also some deficiencies. For instance, lime stabilisation has been shown to decrease the plasticity of the soil (Clare and Cruchley 1957) and

lead to fragile collapse characteristics in specimens that rapidly lost strength at the time of failure (Sabry et al. 1996). Therefore, the application of other additives such as fibre along with the lime to reduce its contribution or partial or full replacement of the lime with more environmentally friendly products has been encouraged by many researchers (Cai et al., 2006; Wild et al. 1998; 1999; James et al. 2008; Oti et al. 2014; Yi et al. 2015).

There is a huge body of literature by various researchers on soil stabilisation techniques using traditional chemical additives such as Portland cement (PC), lime, and bitumen. For instance, Celauro et al. (2012a) and (2012b) reviewed design methodology for lime stabilised soils, and proposed changes in Italian standards to be matched with European standards in terms of employing lime in soil stabilisation. Hashemi et al. (2015) investigated characteristics of lime on clayey soil stabilisation by considering the changes that happen in microstructures of the specimens during curing time. They observed that lime reinforced and distributed into the materials within the first week.



Fig. 2.7. A typical scanning electron microscopy (SEM) of the lime

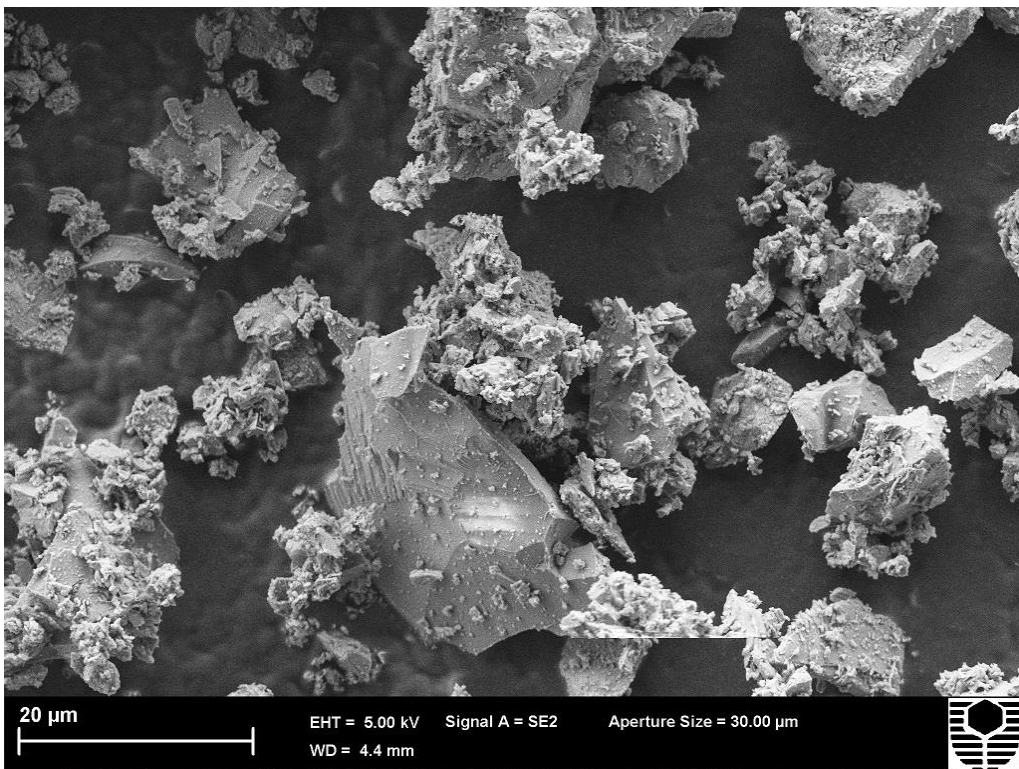


Fig. 2.8. A typical scanning electron microscopy (SEM) of the ordinary Portland cement (OPC)

2.2.3.2. Non-traditional Additives

However, application of traditional agents such as Portland cement (PC) and lime improves the engineering behaviour of soil, their application and production process accompanies with the hazards for the environment and human. As such, new studies conducted to reduce contribution of these harmful products and substitute them with eco-friendly products ([Keramatikerman et al. 2016](#); [Vakili et al. 2016](#)).

2.2.3.2.1. Ground Granular Blast Furnace Slag (GGBFS)

The ground granulated blast-furnace slag (GGBFS) is a by-product from the steel industry, and application of this material is a common practice in ground improvement projects as it improves the durability, sulphate and chloride resistance. The GGBFS also provides protection against alkali silica reaction. This product has a hydration phases very similar to the PC. For instance, generation of the ettringite, calcium silicate hydrate (C-S-H), calcium aluminium hydrate (C-A-H), and calcium aluminium silicate hydrate (C-A-S-H) are similar to PC. Fig. 2.9. shows a typical scanning electron microscopic (SEM) view of the GGBFS.

Higgins ([2007](#)) compared environmental impacts of the GGBFS and PC and indicated that production of 1 tone PC led to generation of 0.95 tone CO₂ in the environment, 5000 MJ energy use, 1.5 tone mineral extraction, and 0.02 waste disposal, whereas production of the 1 tone GGBFS led to generation of 0.07 tone CO₂ in the environment (carbon emission), usage of 1300 MJ energy, no mineral extractions and saving 1 tone waste disposal.

Developments in knowledge have led to the production of new materials and consequently some new by-products. One of the by-products recently considered for

use in geotechnical engineering is ground granulated blast furnace slag (GGBFS), which remains after the steel manufacturing process. Application of GGBFS in civil engineering projects is not only cost effective and energy saving but also reduces the carbon emissions and is environmentally friendly (Higgins 2007). Stabilisation clay using GGBFS has been subject of some recent studies (Vakili et al. 2016; Yi, et al. 2013). For instance, James et al. (2008) investigated effect of the GGBFS on a lime treated clay and concluded that addition of GGBFS for a fixed proportion of the lime caused an increase in production of the pozzolanic products and greater values of the unconfined compressive strength. In another study, Nidzam and Kinuthia (2010), indicated that application of the GGBFS, improves the engineering properties of the soil including strength, durability and its resistance to swelling. They also highlighted that application of the GGBFS has a lower environmental impact and is more cost effective in compare with other additives when applies as a soil stabiliser. Wild et al., (1999) indicated that the partial substitution of the lime with GGBFS to a certain amount, significantly reduced the sulphate expansion associated with sulphate bearing clay soil.

Some researchers have employed GGBFS along with lime in their studies. For instance, Yi et al. (2015) partially substituted quick lime and hydrated lime with GGBFS and compared the effect on mechanical and microstructural properties in the stabilisation of marine clay, reporting that the unconfined compressive strength (UCS) of the hydrated lime activated GGBFS was slightly better than for quick lime activated GGBFS.

In another study, Wild et al. (1998) investigated the effect of partial replacement of lime with GGBFS in a clay soil stabilisation including sulphate. They reported that with regard to long-term effects, the stabilisation of clay using more GGBFS and less

lime is very effective. When the percentage of GGBFS is lower and lime is higher, the addition of the gypsum is very effective for soil stabilisation. For short-term soil stabilisation, the addition of more GGBFS and less lime with gypsum was more effective due to acceleration of the hydration process.

The addition of some other by-product materials such as slags were used widely by many researchers. For instance, Vakili et al. (2015) in a comprehensive experimental study using a direct shear device investigated the effect of slag on clay stabilisation and reported that slag is an appropriate agent to stabilise clay.

Goodarzi and Salimi (2015), using a series of experimental tests, figured out the effect of granulated blast furnace slag to stabilise dispersive clayey soil. It was reported that employing slag is very effective to solve the depressiveness of the soil.

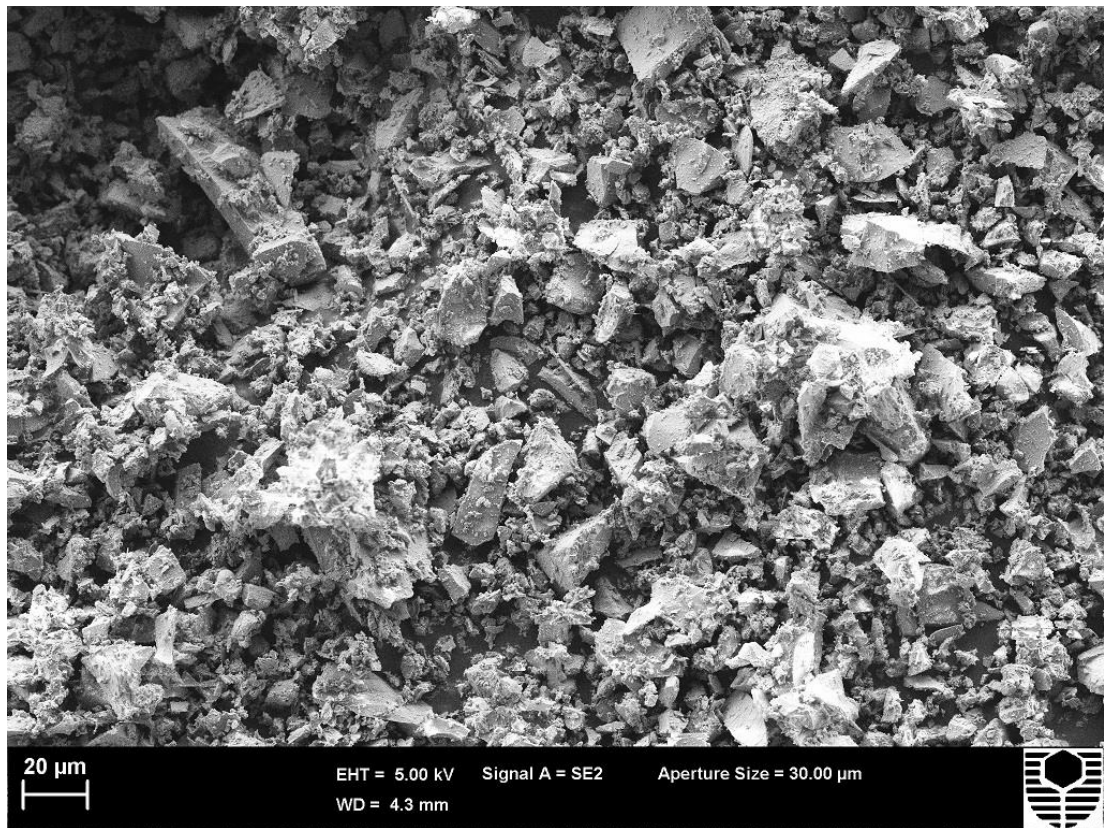


Fig. 2.9. Scanning electron microscopy (SEM) of the ground granulated blast furnace slag (GGBFS)

2.2.3.2.2. Fly Ash (FA)

Fly ash (FA) is a fine and grey by-product materials which is generated from fired coal in electricity power stations. It has a well-rounded shape and has some characteristics which encourage the practitioners to use it in ground improvement projects. There are two types of the fly ash in the market. Both fly ash class F and class C mainly contain silicone dioxide (SiO_2) and lime (CaO), however the amount of lime in fly ash class C is more abundant. Fly ash class F has a pozzolanic characteristics, generated from the burned old coals, and requires mixing with another cementitious agent such as cement. In contrast, the fly ash class C generated from the burned younger coals, and has a self-cementing characteristics as well as pozzolanic characteristics, and does not need an activator when for application ([Civil Engineering World Blogspot, 2018](#)). Fly ash type F has a more availability in Australia, and therefore is of interest to this study. Fig. 2.10. shows a typical scanning electron microscopic (SEM) view of the fly ash class C.

Previous studies investigated the effect of FA in ground improvement ([Horpibulsuk et al. 2011; 2009; Prabakar et al. 2004](#) amongst others). Recently, FA has been considered by many researchers as an effective ground improvement agent. For instance, Keramatikerman et al. ([2017](#)) investigated the effect of FA stabilisation in the liquefaction resistance of sand. They indicated that the FA is effective to increase the cyclic strength of soil. In fact, FA is a by-product material that increases the reactive surfaces of the soil particles and promotes hydration and pozzolanic reactions ([Horpibulsuk et al 2011](#)). Cokca ([2001](#)) investigated the effects of different percentages of FA on expansive soil and concluded that FA successfully stabilises this soil. He used the free swell testing method and reported the effect of stabilisation on swelling potential.

Dermatas and Meng (2003) investigated the effect of FA on the stabilisation of contaminated soil. They employed scanning electron microscopy (SEM) to analyse the microstructures and summarised that mechanical properties of the soil increased by applying FA.

Kolias et al. (2005) investigated the effect of FA and cement on clayey soil. They calculated the modulus of elasticity by applying various stresses after 90 days. They reported an increase in soil strength using FA and cement to stabilise clayey soil. Non-traditional additives is the second group in the chemical additive category as defined by Chegenizadeh and Keramatikerman (2015).

Yencho et al. (2013) studied the effect of preserved FA in liquefaction, and they performed a significant number of cyclic triaxle tests by considering the effects of confining stresses, density and cyclic ratio. They did not find a relation between dry density and the probability of liquefaction. All of the above-mentioned literatures have been performed in the laboratory and using cyclic triaxle and repeated loading triaxle tests. To date, very little is known about cyclic behaviour of soil once it becomes stabilised, and therefore this research intends to study this very important issue. To remedy this major deficiency in the soil stabilisation area, experimental studies according to the above-mentioned literature will be employed and will be verified by numerical modelling.

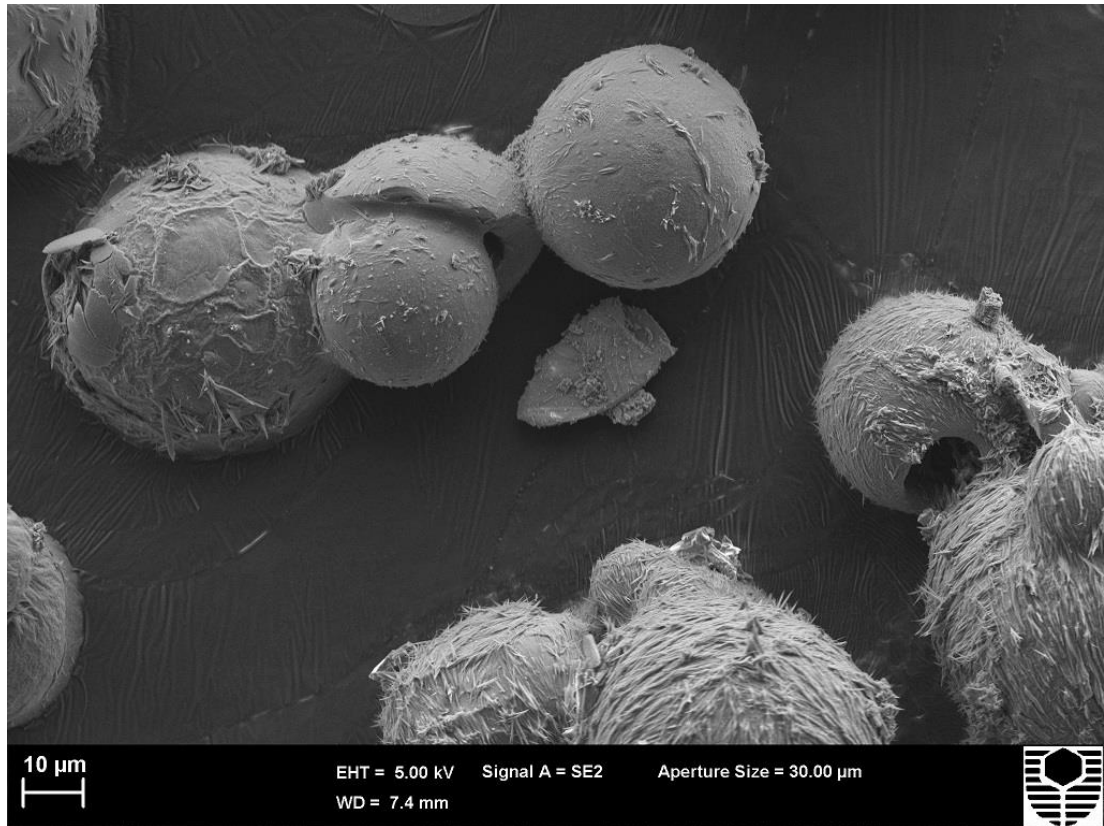


Fig. 2.10. A typical scanning electron microscopy (SEM) of the fly ash (FA) class C.

2.3. A Critical Review on Similar Studies

Liquefaction is a state that saturated soil loses the strength and stiffness during a seismic or static loading event. Application of a triaxial testing device is a common method to assess the liquefaction behaviour of the soil in laboratory. A pore water pressure ratio equal to the unity represents a full liquefaction state. In fact, this is a condition that the pore pressure is equal to the confining pressure. Fig. 2.11 illustrates a schematic overview of a monotonic and cyclic test using a triaxial device.

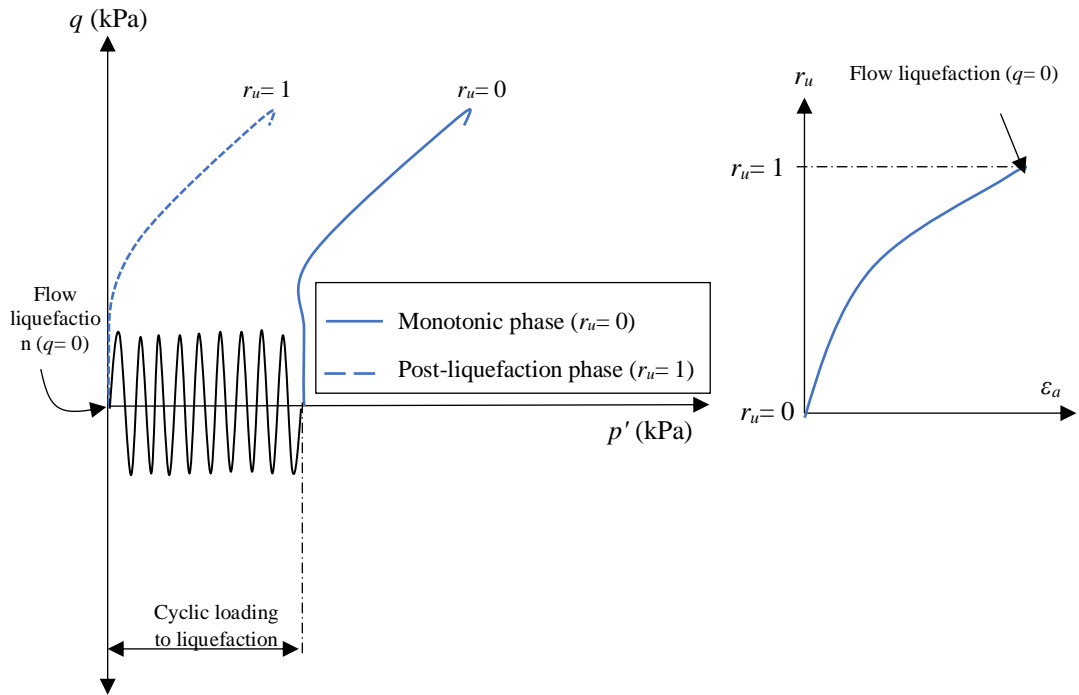


Fig. 2.11. A schematic overview of a triaxial monotonic, cyclic, and post cyclic triaxial tests.

Many studies have been conducted to investigate effect of various additives to improve liquefaction resistance of the soil using experimental devices. For instance, Clough et al. (1989) investigated the effect of cementation on liquefaction behavior of sand by performing a series of triaxial and cubical cyclic shear tests. To do so, they modified an originally monotonic cubical cyclic shear apparatus to a dynamic device model to model the seismic loadings.

They focused their studies on unit weight and the level of cementation and indicated that cemented sand has a liquefaction resistance greater than un-cemented sand. It was also mentioned that increasing both unit weight and percentage of cementation increase the liquefaction resistance, however, when the cementation content reaches to a specific percentage, it reduces the effectiveness of the unit weight. They also investigated the relation of the unconfined compressive Strength (UCS) of the

cemented sand with liquefaction and concluded that when the UCS value is greater than 10 t/m^2 , the soil does not liquefy.

In a similar study on liquefaction resistance of an artificially cemented sand using cyclic triaxial resonant column tests by Saxena et al. (1988), effect of cement content, curing time, relative density, and effective confining pressure were investigated. They indicated that the liquefaction resistance increased when a low percentage of cement was added into the specimens. It was also concluded that the liquefaction resistance of the cemented sand increased by increasing the curing period and relative density.

In another study, Maher et al. (1994) investigated the effect of grouting on liquefaction resistance of the sand by performing a series of consolidation drained (CD) and consolidation undrained (CU) cyclic and monotonic triaxial tests. They investigated the effect of parameters such as grouting types (i.e., sodium silicate, acrylate polymer gel, and micro-fine cement), curing periods, void ratios, and cyclic stress ratios (CSR). It was indicated that application of grouting gels is effective to improve liquefaction resistance of the sand. It was also indicated that increasing the liquefaction resistance due to curing time relates to the type of used grouting gel. For instance, for case of the sodium silicate or acrylate polymer, maximum resistance was recorded after first 14 days curing period, and no remarkable increase in liquefaction resistance was recorded after 60 days curing period. However, for the case of micro-fine cement the recorded maximum liquefaction resistance was up to 28 days curing period. The results showed that increase in confining pressure caused a greater strength and accordingly a higher liquefaction resistance. They added that increasing the grouting content improved the liquefaction resistance of the sand however, it increased the brittleness and fragility of the specimens from the other side.

In another study, Liao et al. (2003) investigated the effect of colloid silica grouting on

liquefaction resistance of the sand by performing a series of cyclic triaxial tests. They indicated that despite of low strength of the used grouting gel, grouted sand has a greater resistance against liquefaction in comparison with control specimen. It was also mentioned that in case of an un-grouted sand a sudden axial strain was recorded immediately after liquefaction, however this deformation was gradual in case of a grouted sand.

Only some limited studies investigated the effect of innovative materials on liquefaction behavior of soil. For instance, Boominathan and Hari (2002) investigated the effect of reinforcement (i.e., randomly distributed fibers) on fly ash by performing a series of stress-controlled triaxial tests. They investigated the effect of relative density, effective confining pressure, aspect ratio of the fiber, and cyclic stress ratio (CSR) on liquefaction resistance of fly ash. They concluded that the reinforced specimens have a greater resistance against liquefaction in lower confining pressure. They also indicated that increasing the reinforcement agent improved the liquefaction resistance when the specimens were prepared at a lower relative density. It is mentioned that 2% fiber is the most effective amount to reduce the effect of liquefaction (Boominathan and Hari 2002).

In another study, Maher and Ho (2014) investigated the effect of fiber reinforcement on monotonic and cyclic loadings by performing a series of triaxial and splitting tension tests. Results showed that addition of reinforcement agent increases both cyclic strength and tensile strength of the specimens.

In another study on reinforcement additives, Noorzad and Fardad Amini (2014) investigated the effect of randomly distributed soil on liquefaction strength of the sand. Similarly, they concluded that presence of the reinforcement agent is effective to improve liquefaction resistance of the Babolsar sand.

In another similar study, Maheshwari et al. (2012) investigated the liquefaction resistance of the sand reinforced by geogrid, and two types of fiber using shaking table tests. They recorded a reduction in the maximum pore water pressure ratio of the specimens when the fibers or geogrid were added into the soil. More reduction was recorded when more additives were added into the soil.

Uchimura et al. (2007) investigated the effect of tyre chips on liquefaction resistance of sand as a backfill material in case of a buried pipe by performing a series of cyclic triaxial and shaking table tests. They concluded that addition of tyre chips in sand is effective to improve liquefaction resistance of a buried pipe and reduces the uplifting problem. Similarly, it was mentioned that increasing the relative density in tyre treated specimens is effective to improve liquefaction resistance of the sand.

The literature review on past studies on improvement of the liquefaction resistance of soil shows that most of the investigations have been conducted on traditional agents such as cement. Also, the literature review shows that previous studies mainly applied reinforcement agents to improve the liquefaction resistance of the soil, and no study has considered effect of other innovative materials on liquefaction resistance of the soil.

2.4. Conclusions

A liquefaction event can be controlled or less destructive if the ground improvement techniques applies before its occurrence. A series of applicable ground improvement techniques to mitigate liquefaction were reviewed and discussed. These methods are physical methods, reinforcement and application of chemical additives. The physical techniques refer to changing the physical nature of soil particles by increasing the soil density and interlocking forces using heavy machinery such as which usually are expensive techniques. The soil reinforcement technique has a concept similar to mechanical technique since the soil strength increases due to an increase in interlocking forces amongst soil particles and reinforcement agent. The soil reinforcement method was categorised in two sub-categories of the geo-synthetics group and tyre products. It was determined that the third method in ground improvement is performed by application of chemicals additives into the soil to improve its strength and durability properties. The applied additives usually have a hydration and pozzolanic characteristics, which provide bonds amongst soil particles and increase the soil strength characteristics. Portland cement (PC) and lime are two popular chemical agents with a broad range of application in geotechnical engineering projects. The chemical agents are divided into two main groups of environmentally friendly and non-environmentally friendly products. The literature review showed that most of the investigations on liquefaction mitigation have considered the effect of reinforcement techniques and rarely studies investigated the effect of additives on liquefaction strength of the soil. Although, Portland cement (PC) and lime are effective agents, they are expensive, and their application is hazardous for the environmental. Hence, application of the environmental friendly additives has been encouraged. The ground granulated blast-furnace slag (GGBFS) and fly ash (FA) are by-products from

the steel and fired coal industry respectively with hydration and pozzolanic characteristics similar to lime. They are eco-friendly additives and can reduce the carbon foot print. Therefore, their applications have been encouraged by researchers in ground improvement.

Table 2.1. shows a summary of the conducted studies on improvement of the cyclic resistance of soil using different agents. As shown, past studies on improvement of the liquefaction resistance of soil conducted to investigate the effect of traditional agents such as cement and geotextile, and no study has considered effect of other innovative materials on cyclic resistance of the soil. Therefore, current study on improvement of the cyclic behaviour of soil using by-product agents is a gap in the literature, and is a broad and novel area of research

Table. 2.1. main studies conducted on improvement of the liquefaction resistance of soil using different agents

No.	Reference	Used by-product agent
1	Chegenizadeh et al. (2018a)	Bulk continuous filament (BCF)
2	Mashiri et al. (2016)	Tyre chips
3	Hong et al. (2015)	Tyre chips
4	Noorzad and Fardad Amini (2014)	Randomly distributed fibre
5	Naeini and Gholampoor (2014).	Geotextile
6	Hamidi and Hooresfand (2013)	Reinforced cemented sand
7	Maheshwari et al. (2012)	Geogrid
8	Kaneko et al. (2012)	Rubber
9	Neaz Sheikh et al. (2012).	Tyre chips

10	Maheshwari et al. (2012)	Geogrid
11	Ibraim et al. (2010)	Discrete flexible fibre (DFF)
12	Towhata (2008).	Tyre chips
13	Uchimura et al. (2007)	Tyre chips
14	Liao et al. (2003)	Colloid silica grouting
15	Boominathan and Hari (2002)	Fibre
16	Haeri et al. (2000)	Geotextile reinforcement.
17	Vercueil et al. (1997)	Woven and non-woven geosynthetics
18	Maher et al. (1994)	Grouting
19	Maher and Ho (1993)	Fibre-reinforced cemented
20	Clough et al. (1989)	Cementation
21	Saxena et al. (1988),	Cement content

Chapter 3

Applied Experimental Devices

3. Applied Experimental Devices

3.1. Introduction

A variety of experimental devices are applicable to evaluate the soil behaviour and the particle interaction at different testing conditions. From an overall point of view and according to the purpose of the analysis, these experimental devices can be divided into two main groups of micro-structural analysis devices and geotechnical experimental devices. The microstructural analysis devices are mainly focused on the particle interactions in the micro level and can be used for evaluation of the soil particles and constituent minerals before and after geotechnical experimental. On the other hand, the geotechnical experimental devices are focused on overall behaviour of a soil system which is known as the specimen and have been prepared based on the special requirements. In compare with in-situ testing, the experimental investigation of the soil behaviour is an inexpensive and reliable way to simulate the soil condition similar in real condition. There are a wide variety of experimental devices which are applicable to evaluate the soil strength under different stress conditions. This chapter briefly introduces the apparatuses used to evaluate the micro-structural and mechanical behaviour of soil used in this study.

3.2. Geotechnical Experimental Devices

The experimental apparatus has a key role to simulate the different soil and materials loading conditions in geotechnical engineering. They are reliable and cost-effective methods to investigate the soil mechanical characteristics in comparison with the in-situ testing. However, there are a wide range of geotechnical experimental apparatuses, each device is manufactured to simulate a specific testing condition.

3.2.1. Direct Shear Device

A direct shear device is used to evaluate the shear strength of the soil. The tests can be performed on disturbed or undisturbed specimens. The sample holder consisted of two parts of the upper halves and the downer halves which hold the sample within a shear box. The upper halve is pulled of horizontally until the sample failure is occurred. During the testing, a desired loading is vertically applied to the specimen to simulate the overhead weight in a real condition. If the direct shear testing is conducted in a fully saturated condition, selection of the shearing rate is very critical since it might lead to generation of the pore water pressure at higher shearing rates. The data recording should be stepwise and be performed in similar intervals to have a uniform and reliable results. Fig. 3.1 shows sample container of a direct shear device and Fig. 3.2 shows a direct shear testing device used to conduct the tests.



Fig. 3.1. The sample container in direct shear test

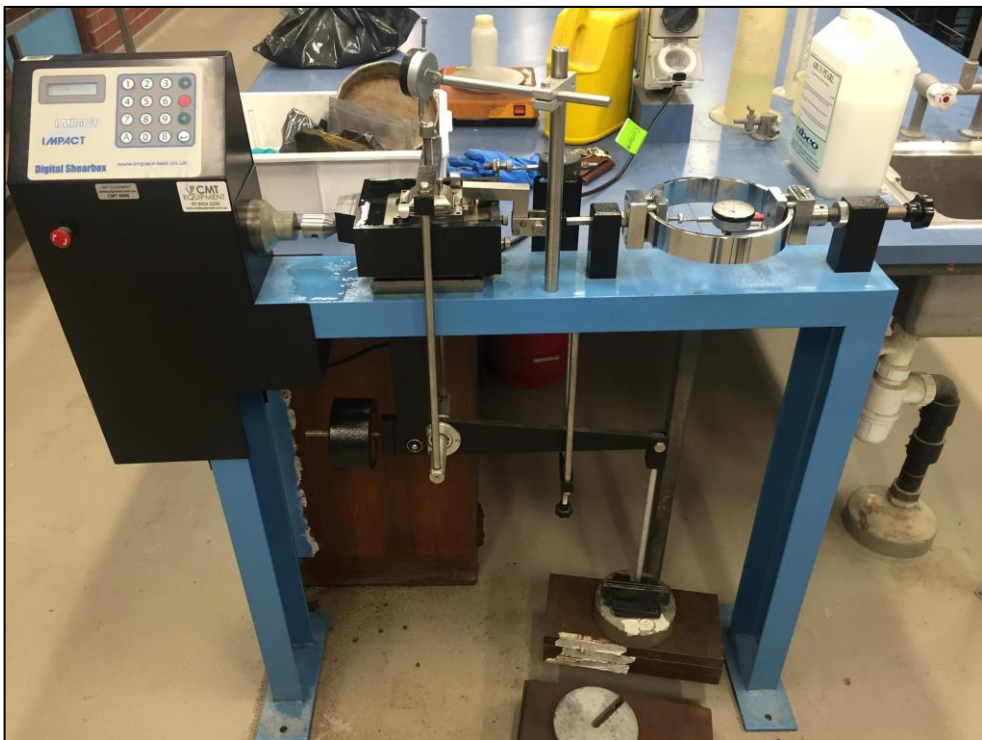


Fig. 3.2. A direct shear testing apparatus used to conduct the tests in this study

3.2.2. Ring Shear Device

A ring shear device is used to evaluate the residual shear strength of soil. The ring shear device has an annular sample container which an upper ring is placed on top of the soil to simulate the overhead weight and rotates. The ring shear device can be sheared unlimitedly and uni-directionally. The sample preparation in ring shear device is very important since it may cause the upper ring slightly tilt over and the loading applies non-uniformly on samples. Another problem which ring shear devices are facing is the wall friction, and sample extrusion during the tests which can be reduce by selecting an appropriate level of hearing rate. Fig. 3.3 shows a Bromhead ring shear device used in this study to conduct the tests. In addition, Fig. 3.4 shows a prepared sample in a ring shear container.

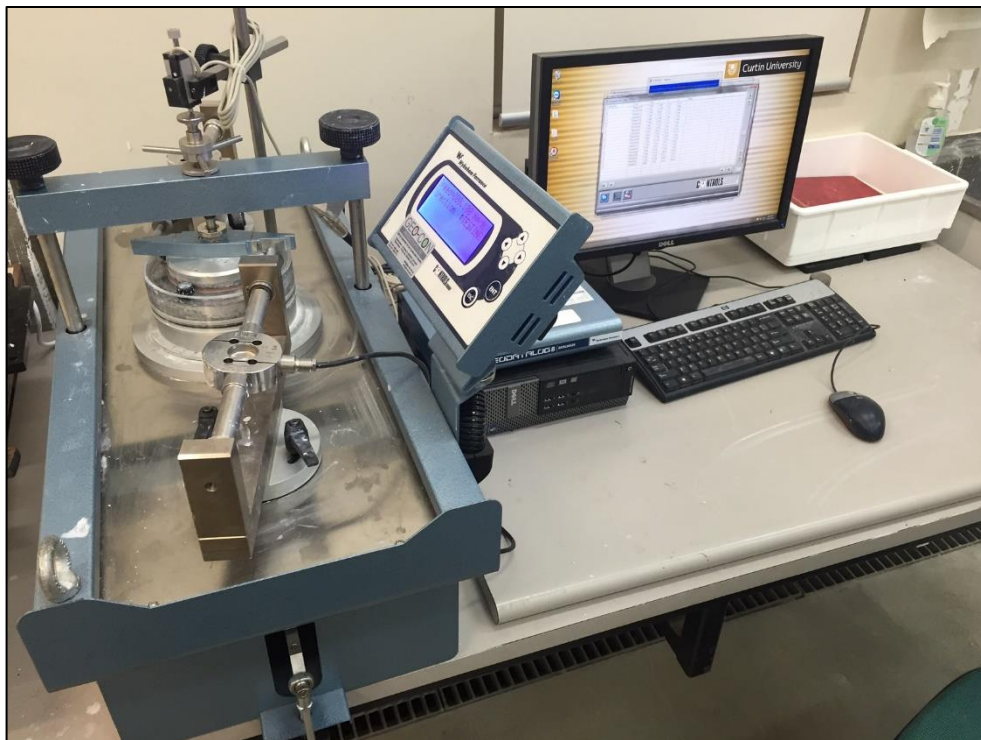


Fig. 3.3. A Bromhead ring shear device used to conduct the tests

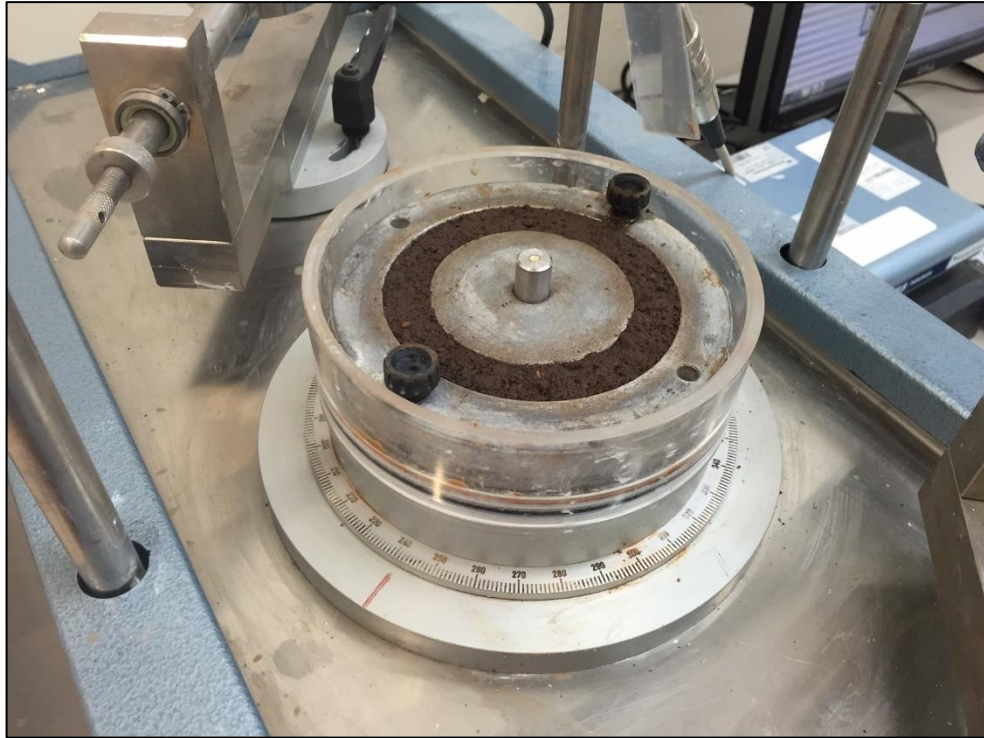


Fig. 3.4. A prepared sample in the container in the ring shear device

3.2.3. Oedometer Apparatus

An oedometer device is used to evaluate the settlement and drainage behaviours of the soil under a series of sequential one-dimensional loading condition in a real condition. Both the disturbed or undisturbed specimens can be used for consolidation testing. Two porous stones with a filter paper are placed on top and underneath of the sample holder (i.e., a relatively small steel ring) to simulate the drainage condition from the sample. The consolidation is a time-dependent process and an appropriate time is required to be considered for completion of each loading sequence. Fig. 3.5 shows a prepared sample inside of the consolidation ring and container. Furthermore, Fig. 3.6 shows an oedometer device.

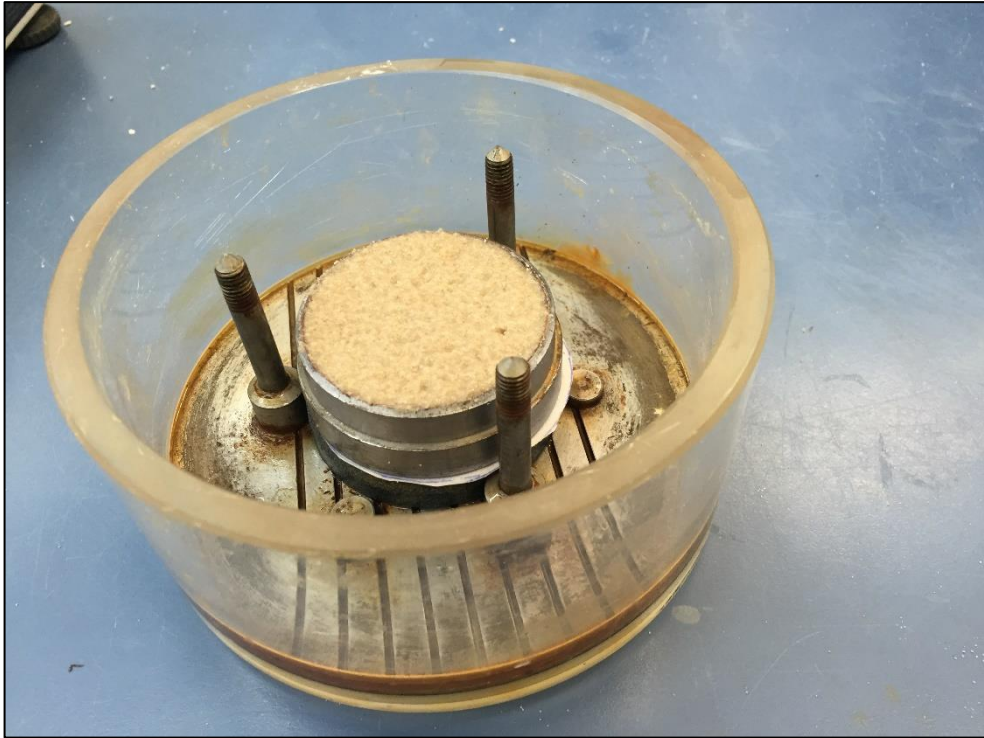


Fig. 3.5. A prepared sample in the container in the ring shear device



Fig. 3.6. An oedometer device to measure the consolidation of the sample

3.2.4. Unconfined Compressive Strength (UCS) Test

The unconfined compressive strength test is a quick way to evaluate the compressive strength of the soil. This test is not applicable for cohesion-less and coarse grained soils. The results of this test are used in stability analysis for the slopes and embankments. The cylindrical specimens with an aspect ratio of 2 are prepared to conduct the UCS testing. Fig. 3.7 shows a sample in a UCS testing device.

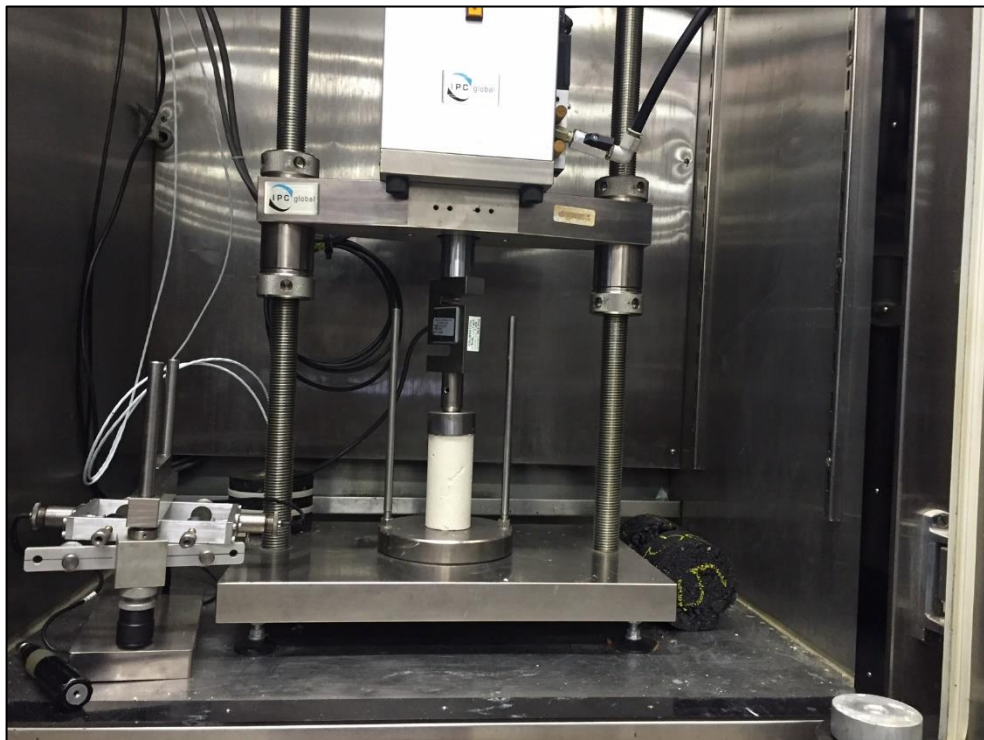


Fig. 3.7. A cylindrical sample in a UCS testing device

3.2.5. Triaxial Testing Device

A triaxial testing apparatus is a comprehensive and advanced device to evaluate the shear strength and stiffness of the different types of soils. The ability of this device to control the pore water pressure and drainage of the specimens privilege this device in compare with similar devices such as direct shear or ring shear to measure the shear

strength of the specimens. Fig. 3.8 shows a typical cyclic triaxial testing machine and its components. The triaxial testing is consisted of three main stages of saturation, consolidation, and shearing stages. There are three types of the triaxial testing which consisted of unconsolidated undrained test (UU), consolidated undrained test (CU), and consolidated drained test (CD) (GDS 2013). The UU testing condition is a quick way to evaluate the undrained shear strength of the soil. The CU testing condition is the most applicable type of triaxial testing. To saturate the sample two actions are taken to ensure the pores amongst soil particles are filled with water. Firstly, a vacuum pressure is applied into the specimens to remove the air and draw water toward the drainage line, and secondly, by a constant increase of cell pressure and pore pressure. The consolidation stage is initiated by increasing the cell pressure while the pore pressure is maintained constant. This process is continued until the volumetric strain of the specimens are not significant. The CD testing condition is a time taking test that is used to simulate long-term loading condition and provide the data.

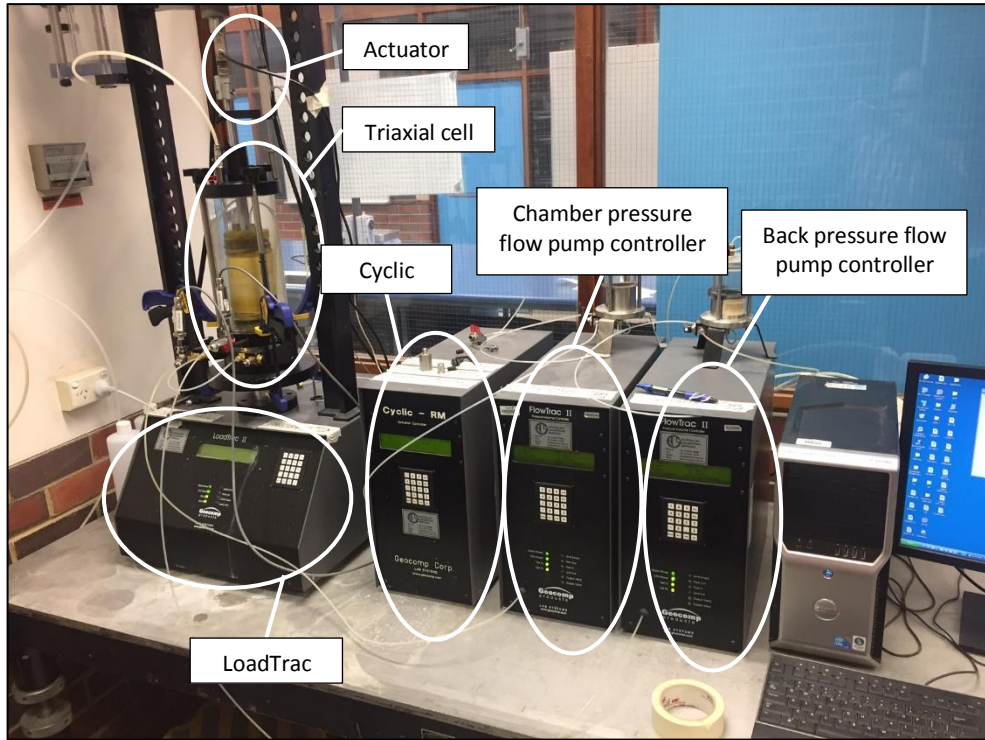


Fig. 3.8. Gecomp cyclic triaxial device used to perform the tests in this study

3.2.5.1. Stress State in Triaxial Testing

During triaxial testing, the confining pressure (σ_c) is simulated by pressurising the specimen using a fluid in the triaxial cell. The confining pressure is equal to radial stress (σ_r) or minor principle stress (σ_3). In addition, the deviatoric stress (q) is generated by applying the actuator in the vertical direction and the axial strain (ϵ_a) is recorded using an automated dial gauge. The combination of deviatoric stress (q) and confining pressure (σ_c) is equal to axial stress (σ_a) or major principal stress (σ_1). If testing condition is in isotropic state when $\sigma_1 = \sigma_3$ and is in anisotropic state when $\sigma_1 \neq \sigma_3$. Fig. 3.9 shows an overview for stress-strain ($q-p'$) and pore water pressure ratio ($r_u-\epsilon_a$) phases in triaxial tests.

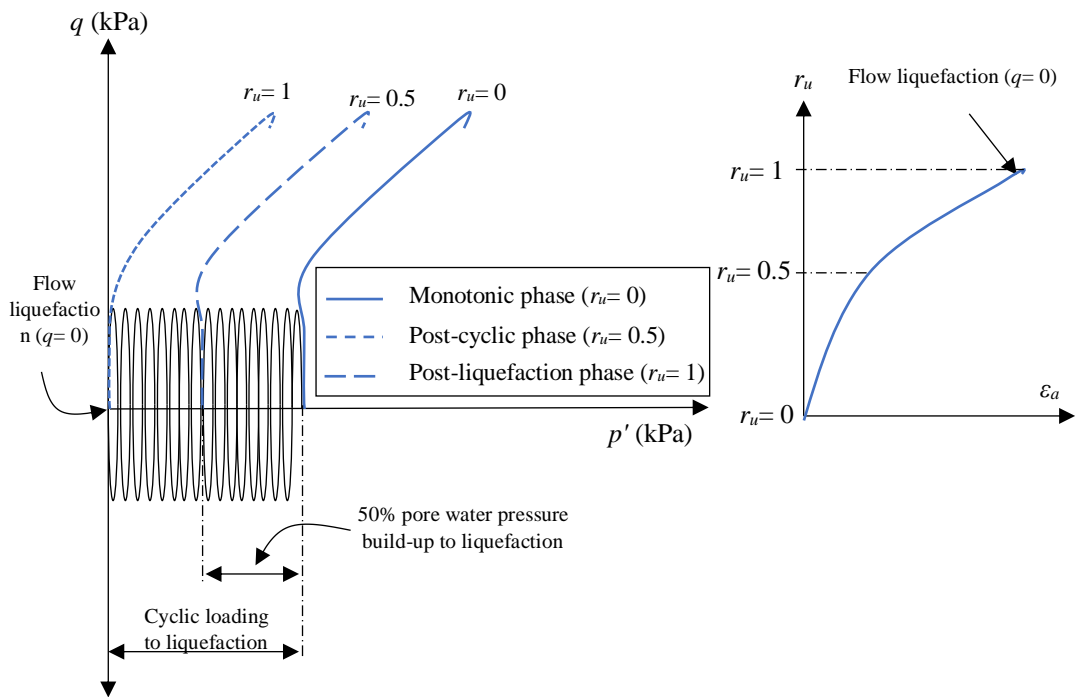


Fig. 3.9. Schematic overview for stress-strain (q - p') and pore water pressure ratio (r_u - ϵ_a) phases in triaxial tests

3.2.5.2. Sample Preparation

There are different techniques in triaxial sample preparations. The moist tamping method is usually used for granular soils like sand. Other sample preparation methods such as slurry depositions are used mainly for fine-grained soils such as silt and clay. In a triaxial testing device, samples are prepared within a cylindrical steel split mould while a membrane is pulled of inside of the mould. The specimens usually have an aspect ratio of 2. Fig. 3.10(a) shows a sand sample in the split mould prepared according to the moist tamping method. In addition, Fig. 3.10(b) shows a prepared specimen before installing the chamber and mounting on the triaxial device.



Fig. 3.10. Sample preparation in a triaxial device using moist tamping method (a) Sample preparation in a steel split mould; and (b) prepared sample on pedestal and ready for the tests.

3.2.5.3. Triaxial Testing Phases

Triaxial testing is consisted of three phases of three phases as mentioned below

- Saturation;
- Consolidation;
- and shearing.

In saturation stage, the empty voids fill with fluid, and the pore pressure transducer and drainage lines are de-aired (GDS 2013). To achieve a full saturation state, the back pressure and the cell pressure is linearly increased. The level of saturation is controlled using a coefficient known as Skempton coefficient (B -value). The B -value is a ratio, which is computed by dividing the pore pressure with cell pressure ($\Delta u/\Delta\sigma_3$). The soil is supposed as fully saturated when a B -value ≥ 0.95 is achieved.

After saturation stage, the specimen is consolidated to simulate the desired effective stress condition before shearing. This stage is completed by increasing the cell pressure and maintaining a constant value for pore pressure. This process is continued until the recorded volume change for the specimen is negligible. The specimen is sheared upon completion of consolidation stage by applying a constant rate of shearing.

3.2.5.4. Triaxial Testing Types

There are three types of the triaxial testing conditions, which is defined by various loading and drainage conditions as indicated below;

- Unconsolidated - Undrained (UU);
- Consolidated – Drained (CD);
- Consolidated - Undrained (CU).

The unconsolidated – undrained (UU) is one of the most common types of the triaxial testing on cohesive soils as provide a quick test setup and the outcome on undrained shear strength value. This test is more suitable for short-term stability analysis of a slope (GDS 2013).

In contrast, the consolidated – drained (CD) is a time taking test type as it simulates a long-term loading condition on soil. The required time to conduct this test is even longer if a cohesive soil to be tested. The parameters such as shear strength, cohesiveness, and friction angle can be obtained by performing this test. Selection of a shearing rate is critical in this test type as selecting an inappropriate shearing rate can cause a generation of the pore water pressure ratio and accordingly inaccurate test results (GDS 2013).

Similar to consolidated – drained (CD) test condition, the strength parameters can be obtained in a consolidated – undrained (CU), however in a faster way, and by recording the pore water pressure ratio variations. These characteristics has made it as a favourable test type for most of soils (GDS 2013).

3.3. Micro-structural Analysis Devices

In general, the micro-structural analysis apparatus of the soil materials is divided into two main groups of the scanning electron microscopy (SEM) imaging and x-ray powder diffraction (XRD) analysis. The SEM imaging mainly is focused on the shape particles analysis and its morphology while the XRD's focus is mainly on the constituent mineral of the soil from a chemical point of view. The following sections introduce the microstructural devices in more detail.

3.3.1. Scanning Electron Microscopy (SEM) Imaging

In a SEM imaging device is consisted of a series of electron detectors (i.e., secondary and backscattered), sample chamber, lenses and electron source. This device provides the imaging information about the surface and topography of the soil by scanning a focused electron beam over a surface. The electron in the beam generates various signals by interacting with the sample, which is resulted in generation of the imaging. Fig. 3.12 shows a typical SEM device for imaging purposes of the soil and used to conduct the studies. The prepared samples for SEM testing are coated using carbon or platinum with different thicknesses. Fig. 3.13 shows a series of samples after carbon coating placed on sample holder prepare for SEM testing.

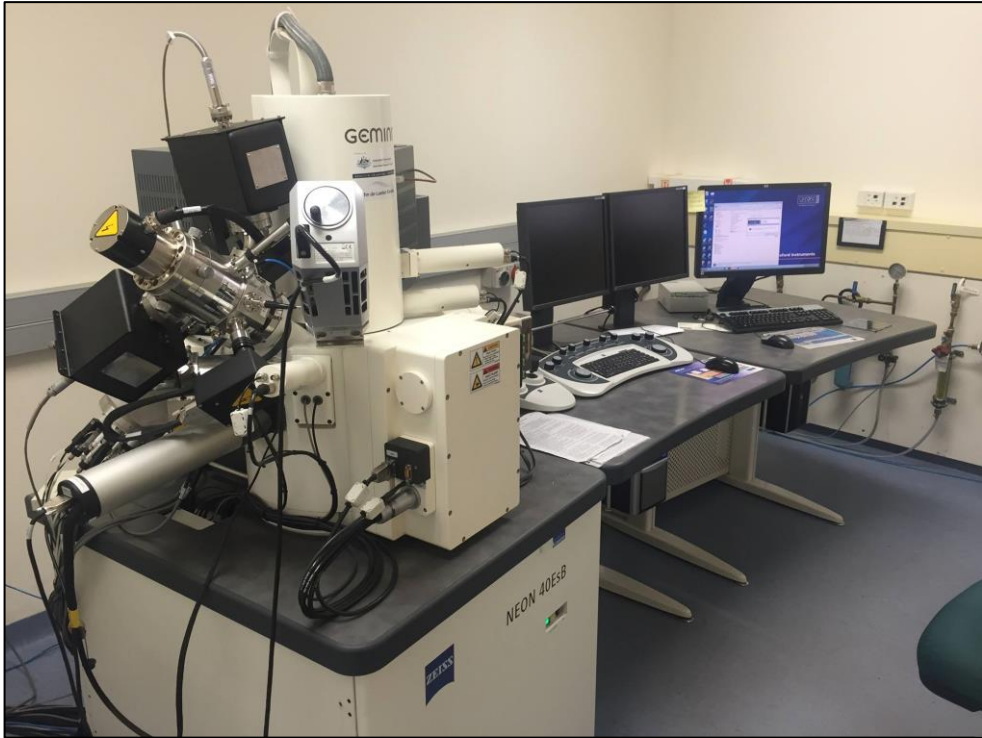


Fig. 3.11. A typical scanning electron microscopy (SEM) image used to conduct the microstructural analysis of the study

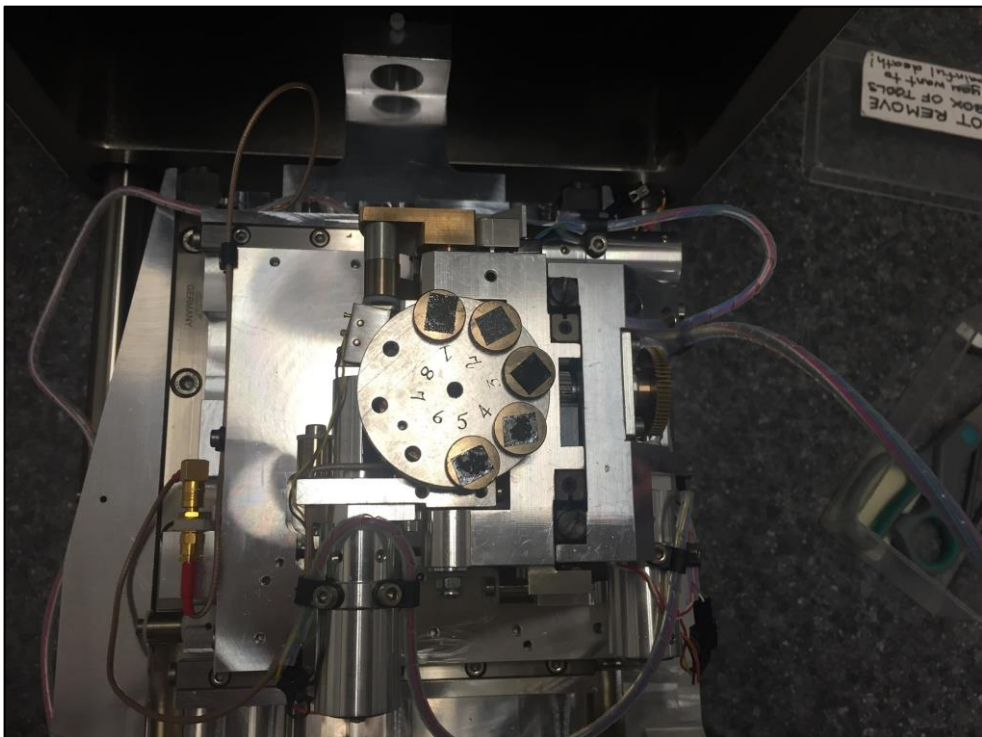


Fig. 3.12. Prepared specimens for SEM testing in sample holder of the SEM device

3.3.2. X-ray Powder Diffraction (XRD) Analysis

The x-ray powder diffraction (XRD) analysis is a method for phase identification, microcrystalline quantification, and structural characterisations. The test is conducted on the homogenised and powdered specimens which are grinded using a heavy ball mill. The results of the XRD analysis is an x-ray diffraction pattern which is a unique pattern for each material and is interpreted using phase identification applications which have a vast database of different phases.

Chapter 4

Preliminary Tests & Materials Selection

CHAPTER INTRODUCTION

In this chapter, a series of the preliminary experimental analysis have been conducted on the representative ground improvement materials in order to evaluate their effectiveness to improve the mechanical behaviour of the soil, and to select the most effective of them in order to continue the liquefaction study in the next stages.

The sawdust and recycled tyre are two abundant environmental friendly materials that have been selected as the representative for the reinforcement group, and the investigations on their effect on mechanical behaviour of soil have been presented in part one and two respectively. These two parts consist of a series of 1-D consolidation tests and rigid-wall hydraulic conductivity tests conducted to investigate the effect of sawdust and recycled tyre as two reinforcement agents on compressibility and hydraulic conductivity of soil.

The lime was selected as the representative for the traditional chemical agents and a series of experimental analysis conducted on the effect of lime addition on mechanical behaviour of the soil. The results of this analysis presented in the third part of this chapter in a series of comprehensive experimental study consisted of a series of the volumetric shrinkage tests, unconfined compressive strength (UCS) tests, and ring shear tests to investigate the effect of lime on mechanical behaviour of soil and the effect of partially replacement of the lime with GGBFS.

The GGBFS was selected as the representative for the environmental-friendly chemical binders to investigate its effect on mechanical behaviour of the soil by performing a series of direct shear tests on over-consolidated clay.

Finally, the results have been analysed and discussed, and the most effective method and additives have been selected in conclusion section. In order to have a complete

understanding of the response of the intended materials, the experimental analysis have been conducted on sand mixed with 5% bentonite. Since a higher amount of hydration and pozzolanic reactions occurs in fine-grained soils, third and fourth parts of this chapter focused to investigate two types of clayey soils.

The analysis of the effect of sawdust on consolidation and hydraulic conductivity of soil published by Keramatikerman et al. (2017a). Furthermore, the results of the effect of recycled tyre on consolidation and hydraulic conductivity of soil published in form of a paper by Chegenizadeh et al. (2018). The results of experimental study on the effect of lime published by Keramatikerman et al. (2016) and the results of the investigations on the effect of GGBFS on mechanical behaviour of clay published by Keramatikerman et al. (2018a).

Part 1

Effect of Sawdust on Permeability and
Compressibility of Soil

4.1. Effect of Sawdust on Permeability and Compressibility of Soil

4.1.1. Abstract

Landfills containing municipal solid waste (MSW) are increasing with growing population and consumption rate in Australia. However, construction of conventional containment systems such as slurry walls are a cost-effective and timesaving approach to control the leachate diffusion, they are weak barriers when exposed to volatile organic compounds (VOCs) or heavy metals, which are abundant in municipal solid wastes. This study investigates effect of sawdust addition on hydraulic conductivity and compressibility of the Soil-Bentonite (SB) slurry cut-off wall. A series of hydraulic conductivity and consolidation tests performed on SB backfill amended with 2%, 5% and 10% sawdust contents. The results showed that application of sawdust reduced the final hydraulic conductivity (k_f) in the range of $2.13 \times 10^{-10} \leq k_f \leq 3.5 \times 10^{-10}$ m/s. The computed hydraulic conductivity values using consolidation theory (k_{theory}) also showed an identical decreasing trend in the range of $5.10 \times 10^{-11} \leq k_{theory} \leq 3.50 \times 10^{-10}$ m/s under $24 \leq \sigma'_n \leq 1,280$ kPa effective overburden pressure (σ'_n). The coefficient of consolidation (c_v) was computed using Casagrande and Taylor methods showed a good agreement range value. Additionally, the computed compression index (C_i) and swelling index (C_s) were calculated using void ratio and effective overburden pressure graphs ($e - \log \sigma'_n$) showed that application of sawdust had no significant impact on settlement of the SB backfill.

4.1.2. Introduction

A significant growth in production of the waste has been reported in recent years in Australia due to increase in population and consumption rate. There is 12% increase

in volume of waste deposited to landfill from 2001 to 2007 (Plant et al. 2014). The statistics showed that 19 million tonnes of waste were disposed to landfill in 2001. The amount has increased to more than 21.3 million tonnes in 2007. Moreover, it has been indicated that during 2006–2007, nearly half (i.e., 48%) of all waste was released in landfill (Plant et al. 2014). Similar conditions have been reported in different areas around the globe (Nabavi-Pelesaraei et al. 2017; Rong et al. 2017). It has been proved that landfills contain a wide range of volatile organic compounds (VOCs), and the leachates from municipal solid waste (MSW) can contaminate the surrounding land and groundwater (Malusis et al. 2009). The VOCs contain some toxic elements that migrate to the environment and enter into the human body through food (Haque 2016). The conventional soil-bentonite (SB) slurry cut-off walls are non-structural and in-situ barriers that isolate the contaminated lands from uncontaminated areas. Construction of slurry-cut of walls is a well-established approach to control the contamination (Ressi and Cavalli 1985; Philip 2001; Du et al. 2015; Wang et al. 2016). Although, these vertical barriers have a low hydraulic conductivity due to application of bentonite, they are weak barriers when exposed to VOCs or heavy metals, which are abundant in municipal solid wastes (MSWs) (Malusis et al. 2009). It has been indicated that application of materials containing a high amount of carbon such as activated carbon and tyre chips can be useful to increase the adsorption capability of the SB slurry cut-off walls while enhancing the compressibility characteristics of these barriers (Malusis et al. 2009; Hong et al. 2012).

Sawdust (SD) is known as a strong adsorbent for heavy metal contaminants (Shukla et al. 2002) and its application in the ground improvement projects is a well-established practice (Keller 2016). Application of the sawdust is not only an environmental friendly approach, but also reduces the carbon emission in the nature (Fogarasi and

Cormos 2017). Application of sawdust is also cost effective (Fogarasi and Cormos 2015). However, its effect on the hydraulic conductivity and compressibility characteristics of a SB backfill is unknown. This study aims to investigate hydraulic conductivity and compressibility behaviour of a SB slurry cut-off wall when amended with different sawdust contents.

4.1.3. Materials and Methods

4.1.3.1. Constituent Materials

Sand used in this study was supplied from Baldivis in Western Australia. This sand was clean and classified as the poorly graded sand according to the unified soil classification systems (USCS) [(ASTM D2487, (ASTM 2011a)]. The used sodium bentonite had a liquid limit (LL) of 455 and a plastic limit (PL) of 387 according to ASTM D4318 (ASTM 2010) and classified as a high plasticity (CH) clay. The used sawdust (SD) was dried in an oven before the application. It had a specific gravity (G_s) of 1.35, [ASTM D854, (ASTM 2014a)], coefficient of curvature (C_c) of 1.10, and a uniformity coefficient (C_u) of 2.33. The particle size distribution analysis was performed according to the ASTM C136 (ASTM 2014b) and ASTM D4221 (ASTM 2011b) and the results were presented in Fig. 4.1.

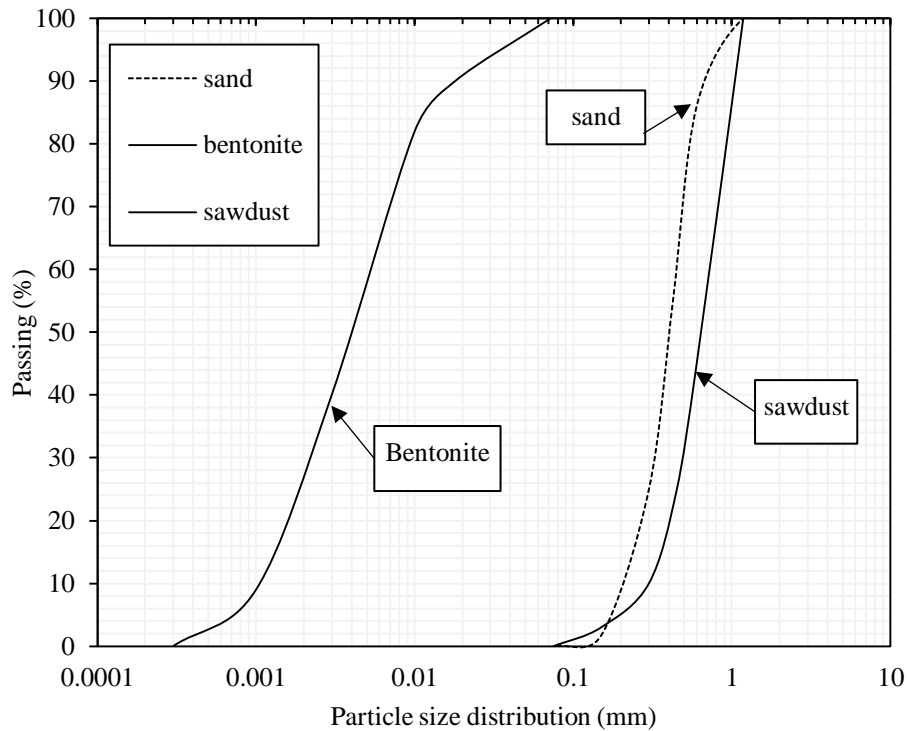


Fig. 4.1. Particle size distribution (PSD) of the used materials.

4.1.3.2. Sample Preparation

In the first stage, the bentonite-slurry (BS) was prepared by mixing 5% bentonite (by dry weight) with tap water and mixed in an automated mixer machine for 30 minutes. After 24 hours of hydration, the electric conductivity (EC) and pH of the prepared bentonite slurry were 115.5 mS/m and 8.80 respectively. In addition, the measured density and marsh funnel viscosity were 1.035 g/cm³ and 40 s respectively. To prepare the base mixture (unamended), the dried sand was mixed with 8% water similar to its original gravimetric moisture content, and then 4% bentonite (by dry weight) was added to it and mixed in the automated mixer machine for 30 minutes (Malusis et al. 2009; Hong et al. 2012). The unamended backfill was prepared by mixing the bentonite-slurry (BS) to the base mixture until a targeted slump of 125 ± 12.5 mm was achieved according to ASTM C143 (ASTM 2015a). The measured total amount of the

included bentonite to the control mixture was 5.8%. To prepare the sawdust amended mixtures, it was necessary to add more bentonite-slurry (BS) to the mixture in order to have a desired slump value. In addition, more bentonite was added to the base mixture to omit the bentonite content as a variable and keep it constant for all mixtures. Table 4.1 shows the characteristics of each backfill mixture.

Table 4.1. Characteristics of each backfill mixture

No.	ID	Sand, (%)	Bentonite, (%)	Sawdust, (%)	Liquid limit (LL)	Water content, w (%)	Slump, (mm)
1	SB backfill	94.2	5.8	-	28	44.1	125
2	2%SD	92.2	5.8	2	34	48.4	127
3	5%SD	89.2	5.8	5	37	52.6	125
4	10%SD	84.2	5.8	10	39	57.8	126

4.1.3.3. Methodology

To figure out the hydraulic conductivity of the sawdust amended backfill mixtures rigid-wall hydraulic conductivity tests using falling head method were conducted according to ASTM D5856 (ASTM 2015b). The tests were conducted in moisture and temperature controlled room. A compaction permeability mould with 140 mm diameter and 150 mm height was used to perform the tests. To prevent the side-wall leakage, a rubber membrane was stretched inside of the used mould before pouring the specimens inside of the mould (Aldaef and Rayhani 2014). The backfill mixtures were poured in the mould in three layers and were rodded to remove the voids (Daniel et al. 1985). The tap water was used as the permeating liquid with a pH and electrical

conductivity (EC) of 6.7 and 5.5 mS/m respectively. The specimens after preparation were left for saturation. The data were recorded when a steady flow was observed from the effluent outflow. The hydraulic conductivity was measured three times in a similar permeating and testing conditions (i.e., outflow rate and hydraulic gradient) for each backfill mixture. The final hydraulic conductivity (k_f) was the mean of the three readings. Furthermore, 1-D consolidation tests were performed using a conventional fixed-ring Wykeham Farrance oedometer device in accordance with ASTM D2435 (ASTM 2011c). The specimens were prepared in a cylindrical mould with 50 mm diameter and 19 mm height. The specimens were rodded to remove any void. They were under a sequential series of effective overburden pressures of 24, 48, 96, 192, 383, 766, and 1,280 kPa, and then unloaded in the reversed order. Each sequence completed in 24 hours, and the hydraulic conductivity was computed based on the Terzaghi consolidation theory (k_{theory}) at the end of each loading stage.

4.1.4. Results and Discussion

4.1.4.1. Hydraulic Conductivity Tests (k_f)

The measured final hydraulic conductivity (k_f) values were shown in Table 4.2. The control backfill mixture has a final hydraulic conductivity of 5.23×10^{-10} m/s. This value decreased to 3.5×10^{-10} , 2.9×10^{-10} m/s, and 2.13×10^{-10} m/s when 2%, 5% and 10% sawdust were added to the SB backfill mixture. The results in this section indicated that addition of sawdust was effective to reduce hydraulic conductivity of the SB backfill. It has been indicated that the sawdust has an adsorption capacity due to ion exchange or hydrogen binding mechanism (Shukla et al. 2002), which might be

the main reason in reduction of the hydraulic conductivity of the sawdust amended specimens.

Table 4.2. A summary of hydraulic conductivity test results.

Specimen	Porosity, n	Density γ_d , (t/m ³)	Measured Hydraulic Conductivity	
			k , (m/s)	
			k , (m/s)	k_f average (m/s)
SB backfill	0.48	1.36	5.3 x 10 ⁻¹⁰	5.23 x 10 ⁻¹⁰
			4.8 x 10 ⁻¹⁰	
			5.6 x 10 ⁻¹⁰	
2%SD	0.47	1.41	3.8 x 10 ⁻¹⁰	3.5 x 10 ⁻¹⁰
			3.5 x 10 ⁻¹⁰	
			3.2 x 10 ⁻¹⁰	
5%SD	0.51	1.42	2.9 x 10 ⁻¹⁰	2.9 x 10 ⁻¹⁰
			2.7 x 10 ⁻¹⁰	
			3.1 x 10 ⁻¹⁰	
10%SD	0.49	1.43	2.4 x 10 ⁻¹⁰	2.13 x 10 ⁻¹⁰
			2.2 x 10 ⁻¹⁰	
			1.8 x 10 ⁻¹⁰	

4.1.4.2. Consolidation Tests

4.1.4.2.1. Compression Index (C_c) and Swelling

Index (C_s)

Fig. 4.2 shows the variation of the void ratio versus logarithm effective overburden pressure ($e - \log \sigma'_n$) for Control SB backfill and sawdust amended specimens. As can be seen, void ratio for the control backfill is in the range of $0.82 \leq e \leq 1.18$ under $24 \leq \sigma'_n \leq 1280$ kPa effective overburden pressure. Addition of the sawdust caused a reduction in void ratio values. For instance, the void ratio values were in the range of $0.78 \leq e \leq 1.15$, $0.74 \leq e \leq 1.13$, and $0.70 \leq e \leq 1.10$ when 2%, 5% and 10% sawdust was added to the SB backfill respectively. The compression index (C_i) and swelling index (C_s) computed using $e - \log \sigma'_n$ graphs were showed in Fig. 4.2(b). As can be seen, addition of the sawdust had no impact on compression index (C_i) and this parameter remained constant after increasing the sawdust content of the SB backfill (i.e., 0.2). This behaviour shows that addition of the sawdust has no impact in rigidity of the SB backfill (Malusis et al. 2009). However, addition of the sawdust caused a decrease in swelling index (C_s) values of the mixtures, these values were in the range of $0.009 \leq C_s \leq 0.04$ when 2% to 10% sawdust was added.

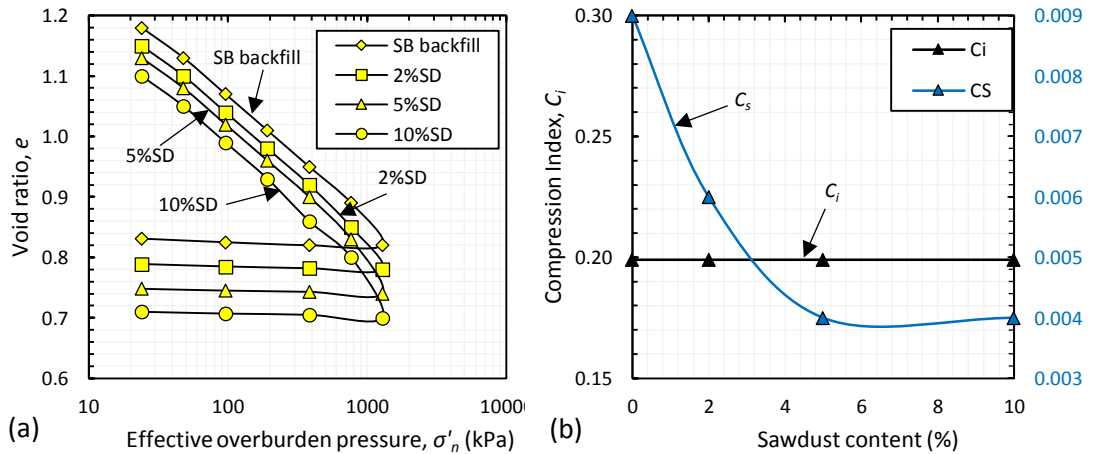


Fig. 4.2. (a) Variation of void ratio (e) versus logarithm of effective overburden pressure ($e - \log \sigma'_n$) for control SB backfill mixture and sawdust amended specimens; (b) Variation of compression index (C_i) and swelling index (C_s) versus sawdust contents

4.1.4.2.2. Coefficient of Consolidation (c_v)

The coefficient of consolidation (c_v) was computed using Casagrande and Taylor methods and the results were shown in Fig. 4.3. As can be seen in Fig. 4.3(a), addition of the sawdust slightly decreased the c_v values computed based on the Casagrande method. For instance, while the coefficient of consolidation for control mixture was in the range of $1.7 \times 10^{-8} \leq c_v \leq 6.53 \times 10^{-7}$ m²/s under $24 \leq e \leq 1280$ kPa effective overburden pressure (σ'_n), this value decreased to $1.65 \times 10^{-8} \leq c_v \leq 6.01 \times 10^{-7}$, $1.51 \times 10^{-8} \leq c_v \leq 5.54 \times 10^{-7}$, and $1.35 \times 10^{-8} \leq c_v \leq 5.13 \times 10^{-7}$ m²/s after addition of 2%, 5% and 10% sawdust. Identical trend was recorded when the c_v values were calculated using Taylor method as shown in Fig. 4.3(b). For instance, the c_v values computed based on the Taylor method was in the range of $3.4 \times 10^{-8} \leq c_v \leq 6.73 \times 10^{-7}$ m²/s while addition of 2% sawdust caused a reduction in the range $3.2 \times 10^{-8} \leq c_v \leq 6.24 \times 10^{-7}$ m²/s. This decreasing trend was followed to the ranges of $2.87 \times 10^{-8} \leq c_v \leq 5.86 \times 10^{-7}$ m²/s and $2.54 \times 10^{-8} \leq c_v \leq 5.62 \times 10^{-7}$ m²/s by addition of 5% and 10% sawdust. The decreasing trend of the c_v values computed based on Casagrande and Taylor methods can be seen in Fig. 4.4. In addition, Fig. 4.5 shows the computed c_v values based on the Taylor method relative to c_v values computed based on the Casagrande method (i.e., $c_{v, Taylor} / c_{v, Casagrande}$) versus logarithm effective overburden pressure ($\log \sigma'_n$). It can be seen that the acquired c_v values in Taylor method are greater than the Casagrande method as the compressibility changing with effective stress and the rate of strain (Yeo et al. 2005) and as the secondary compression happens during the primary consolidation (Olson, 1986; Yeo et al. 2005).

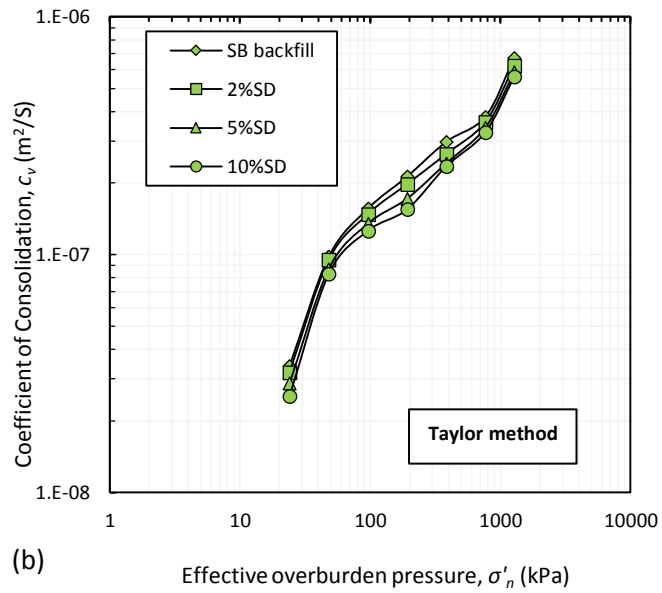
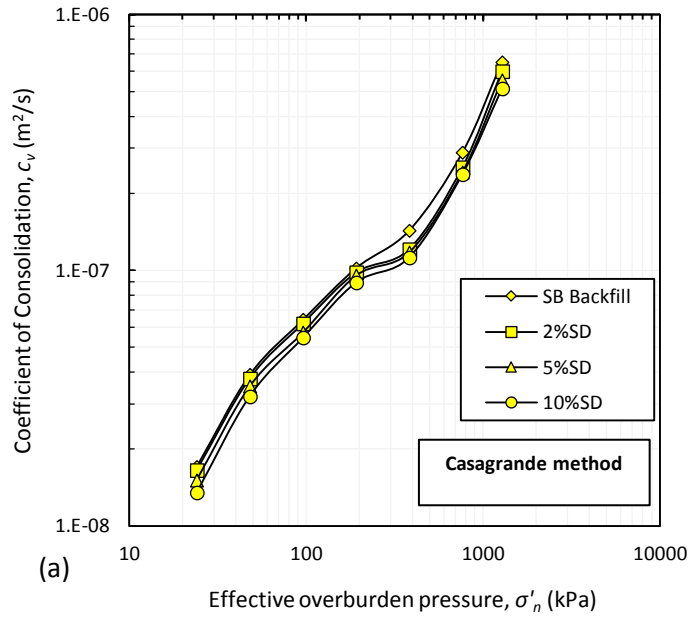


Fig. 4.3. Computed c_v values versus effective overburden pressure (σ'_n) for SB backfill mixture and sawdust amended mixtures based on (a) Casagrande method; (b) Taylor method

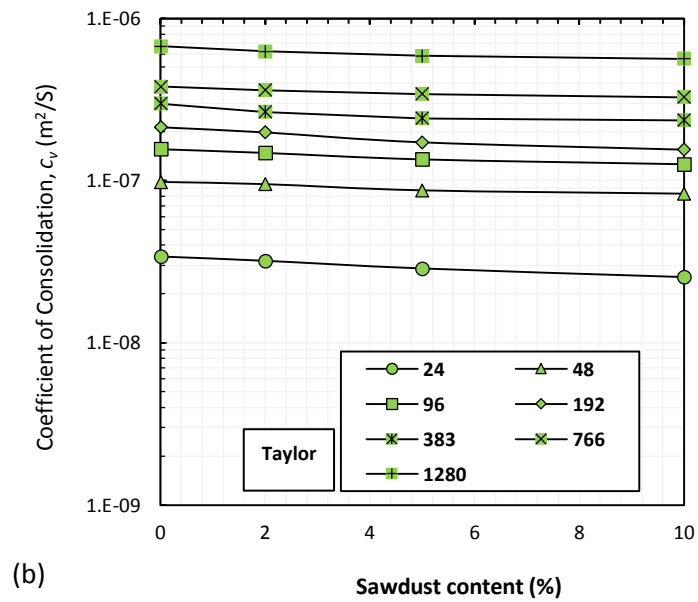
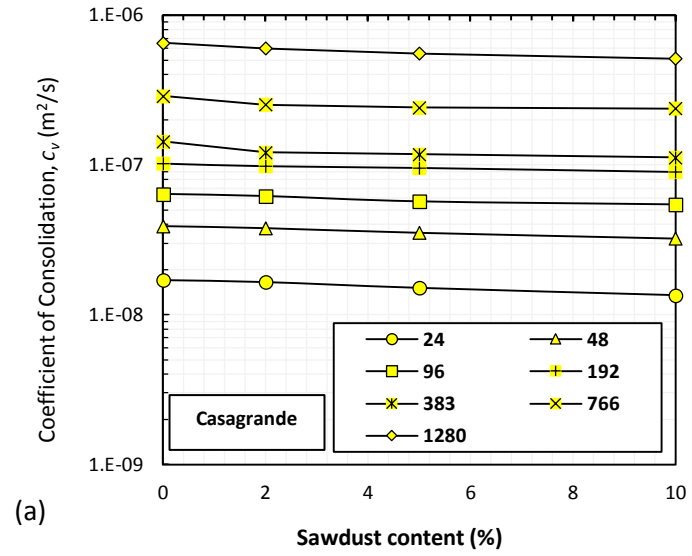


Fig. 4.4. Computed c_v values versus sawdust content for SB backfill mixture and sawdust amended mixtures based on (a) Casagrande method; (b) Taylor method

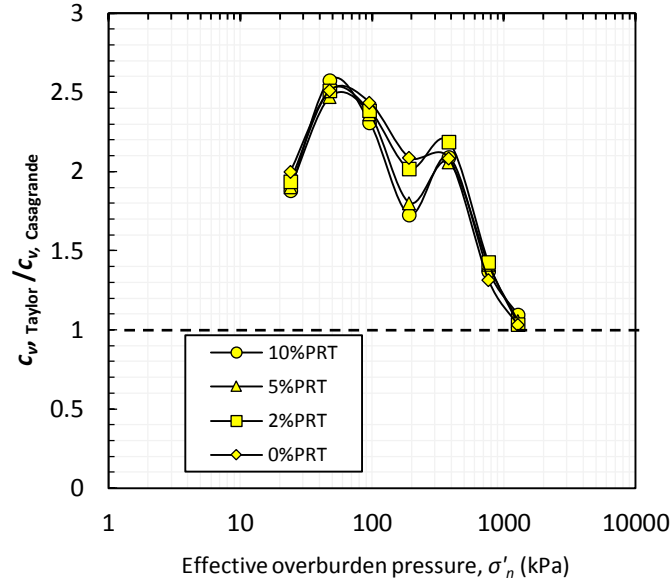


Fig. 4.5. Computed c_v values based on the Taylor method relative to c_v values computed based on the Casagrande method versus σ'_n for sawdust amended specimens

4.1.4.2.3. Coefficient of Volume Compressibility (m_v) and Coefficient of Compressibility (a_v)

Fig. 4.6(a) shows the variation of coefficient of volume compressibility versus logarithm effective overburden pressure ($m_v - \log \sigma'_n$). As can be seen, increasing the sawdust content of the SB backfill caused a reduction in m_v values of the SB backfill. For instance, the m_v values for the control mixture are in the range of $2.36 \times 10^{-5} \leq m_v \leq 2.82 \times 10^{-3} \text{ kPa}^{-1}$ under 1280 to 24 kPa effective overburden pressure. This range decreased to $1.44 \times 10^{-5} \leq m_v \leq 2.16 \times 10^{-3}$, $1.31 \times 10^{-5} \leq m_v \leq 2.09 \times 10^{-3}$, and $1.01 \times 10^{-5} \leq m_v \leq 1.89 \times 10^{-3} \text{ kPa}^{-1}$ after addition of 2%, 5% and 10% sawdust. Similar decreasing trend was recorded for coefficient of compressibility (a_v) as shown in Fig. 4.6(b). For instance, the control SB backfill has a_v values in the range of $7.07 \times 10^{-5} \leq a_v \leq 8.45 \times 10^{-3} \text{ kPa}^{-1}$ under 1280 to 24 kPa effective overburden pressure. Addition of 2% sawdust caused a decrease in the range of $4.33 \times 10^{-5} \leq a_v \leq 6.49 \times 10^{-3} \text{ kPa}^{-1}$ under the same

effective overburden pressure range. This decreasing trend was continued to $3.92 \times 10^{-5} \leq a_v \leq 6.28 \times 10^{-3} \text{ kPa}^{-1}$ and $3.04 \times 10^{-5} \leq a_v \leq 5.66 \times 10^{-3} \text{ kPa}^{-1}$ when 5% and 10% sawdust were added to the mixtures. Reduction of m_v and a_v indicates that addition of sawdust reduces the rate of compression in the sawdust treated specimens.

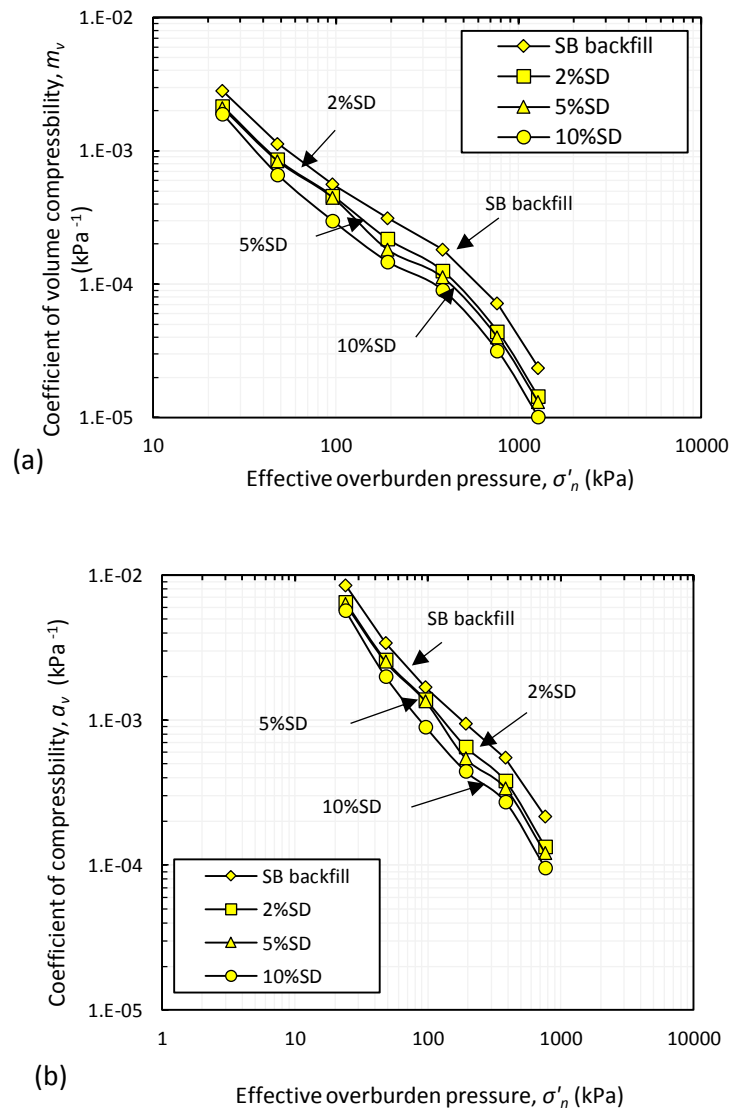


Fig. 4.6. (a) Coefficients of volume compressibility (m_v) versus effective overburden pressure (σ'_n) for SB backfill and sawdust amended mixtures; (b) coefficient of compressibility (a_v) versus effective overburden pressure (σ'_n) for SB backfill and sawdust amended mixtures

4.1.4.2.4. Computed Hydraulic Conductivity (k_{theory})

The hydraulic conductivity was computed using Terzaghi consolidation theory similar to Kang and Shackelford (2010) at the end of each loading sequence, and the results were presented in Fig. 4.7. As shown in the figure, the computed hydraulic conductivity values for the control SB backfill mixture was in the range of $1.51 \times 10^{-10} \leq k_{theory} \leq 4.70 \times 10^{-10}$ m/s under $24 \leq \sigma'_n \leq 1280$ kPa effective overburden pressure. Addition of 2% sawdust caused a reduction in the range of $8.50 \times 10^{-11} \leq k_{theory} \leq 3.50 \times 10^{-10}$ m/s. This trend reached to the range of $7.10 \times 10^{-11} \leq k_{theory} \leq 3.10 \times 10^{-10}$ m/s and $5.10 \times 10^{-11} \leq k_{theory} \leq 2.50 \times 10^{-10}$ m/s when 5% and 10% sawdust were added to the specimens. Variation of the computed hydraulic conductivity (k_{theory}) with void ratio was shown in Fig. 4.8. As can be seen, the hydraulic conductivity decreased by decreasing the void ratio. In addition, the variations of the hydraulic conductivity with sawdust for measured (k_f) and computed (k_{theory}) conductivity were shown in Fig. 4.9. As can be seen, the measured k_f values have a good agreement with computed k_{theory} values at low effective overburden pressure.

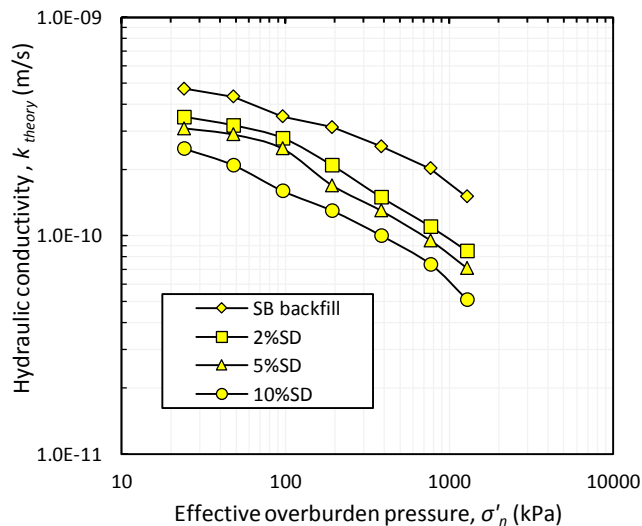


Fig. 4.7. Hydraulic conductivity (k_{theory}) as a function of effective overburden pressure ($\log \sigma'_n$) for control SB backfill mixture and sawdust amended specimens

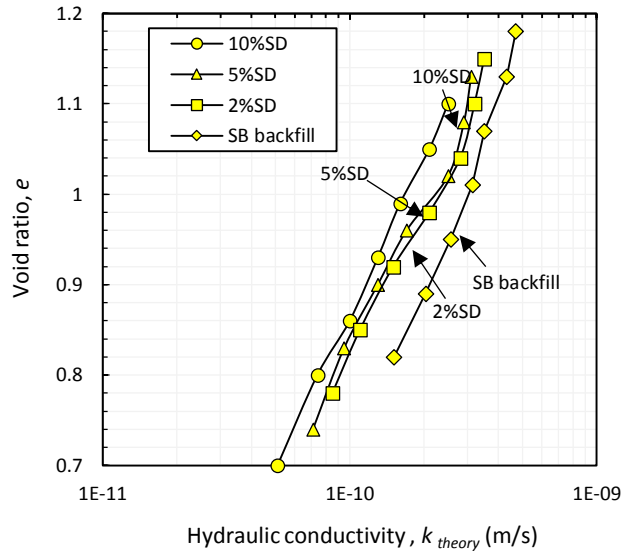


Fig. 4.8. Hydraulic conductivity (k_{theory}) as a function of void ratio (e) for control backfill mixture and sawdust amended specimens

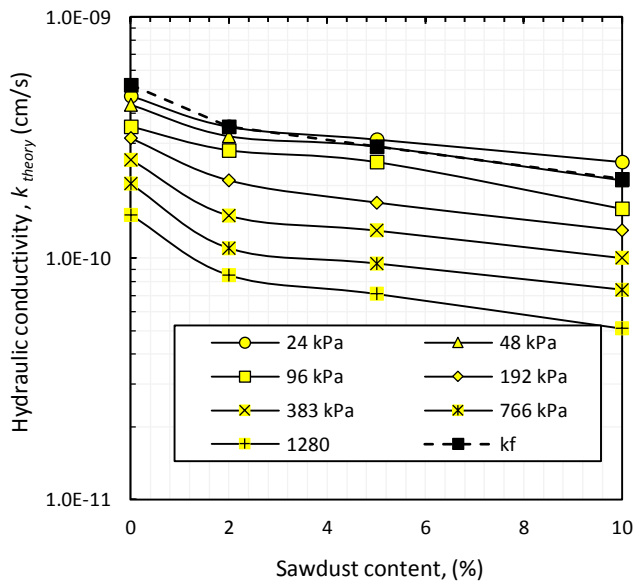


Fig. 4.9. Comparison between the computed and measured hydraulic conductivity (i.e., k_f and k_{theory}) as a function of sawdust content for SB control mixture and sawdust amended specimens

4.1.5. Conclusions

This study investigated effect of sawdust addition on hydraulic conductivity and compressibility of the sand bentonite (SB) backfill mixture by performing a series of falling head hydraulic conductivity and 1-D consolidation tests. The following conclusions can be drawn from the results;

- The results showed that the SB backfill mixture has a hydraulic conductivity of 5.23×10^{-10} m/s, and addition of 2%, 5%, and 10% sawdust caused a reduction in the range of 3.5×10^{-10} , 2.9×10^{-10} , and 2.13×10^{-10} for hydraulic conductivity values respectively.
- Investigations showed that the control backfill mixture has a hydraulic conductivity in the range of $1.51 \times 10^{-10} \leq k_{theory} \leq 4.70 \times 10^{-10}$ under $24 \leq \sigma'_n \leq 1280$ kPa effective overburden pressure when computed based on Terzaghi consolidation theory, and addition of sawdust caused a reduction in the range of $8.50 \times 10^{-11} \leq k_{theory} \leq 2.50 \times 10^{-10}$ m/s for the mixtures. The measured k_f and computed k_{theory} values showed a good agreement at low effective overburden pressure.
- The results showed that addition of sawdust caused a reduction for the coefficient of consolidation (c_v) in both Casagrande and Taylor methods.
- The investigations showed that addition of sawdust has no impact on compression index (C_i) and consequently on rigidity of the sawdust amended mixtures. In addition, it was revealed that the swelling index (C_s) decreased by addition of the sawdust in a very low range.

Part 2

Effect of Recycled Tyre on Mechanical Behaviour
of Soil

4.2. Effect of Recycled Tyre on Mechanical Behaviour of Soil

4.2.1. Abstract

Disposing scrap tyre has increased in recent years, and finding innovative reusing methods is of interest to researchers. This study aims to investigate the hydraulic conductivity and one-dimensional consolidation behaviour of soil-bentonite (SB) backfill amended with powdered recycled tyre (PRT) and crumbed recycled tyre (CRT) by performing a series of oedometer consolidation and rigid-wall hydraulic conductivity tests. Three values of PRT and CRT (i.e., 2%, 5% and 10% by dry weight) were used to prepare the specimens. The investigation on vertical strain-time graphs showed that the addition of PRT and CRT caused an increase in settlement characteristics of the SB backfill. The results also showed that the addition of PRT and CRT caused an increase in the compression index (C_i) and the swelling index (C_s) of the SB specimens. The coefficient of consolidation (c_v) based on the Casagrande and Taylor methods showed a consistent increasing trend by increasing the PRT and CRT. The hydraulic conductivity was computed based on the Terzaghi consolidation theory (k_{theory}), and the results showed that increasing the PRT and CRT caused an increase in hydraulic conductivity of the SB backfill. The hydraulic conductivity (k_f) measured using a rigid-wall permeability compaction mould showed a similar increasing trend by increasing the PRT and CRT contents of the backfills.

4.2.2. Introduction

Australia is facing a significant growth in waste production due to increases in population and consumption rates in recent years ([Keramatikerman et al. 2017a](#); [Plant et al. 2016](#)). The tyre industry is one of the sectors growing the most, with around 52.2

M tyres disposed each year in Australia, only 13% of which are recycled, and the rest is stockpiled in landfills (Chegenizadeh et al. 2017; SUEZ 2016). Along with this increasing trend of scarp tyre generation emerges serious environmental and health issues for the future, and highlights the importance of innovative reusing methods. The scarp tyre has some natural characteristics that make it useful when applied to drainage, insulation, and lightweight aggregate backfill purposes (Edil et al. 2004). Previous studies investigated the potential reuse of tyres in structural engineering and in particular in improving the strength characteristics of concrete (Kashani et al. 2017; Hesami et al. 2016; Bravo and de Brito 2012; Pelisser et al. 2011), however many more studies need to be conducted to fully investigate the potential application of scarp tyres in various sectors. This material also has a wide range of usage in environmental studies (Ghazavi 2004; Rao and Dutta 2006; Bhalla et al. 2010; Turner and Rice 2010; Lian et al. 2011; Lian et al 2013). Since carbon is the main constituent of the scarp tyre, this material has a high potential for the absorption of waste containing volatile organic compounds (VOCs) and can be applied in the waste management industry as well. As an example, Cokca and Yilmaz (2004) investigated effect of rubber and fly ash mixed bentonite as a liner material. They indicated that the mixture of bentonite and fly ash, with up to 10% rubber, provided a satisfactory barrier system with an appropriate hydraulic conductivity required for liner systems. In another example, Park et al. (2003) investigated the suitability of the shredded tyre as a collection medium for landfill leachate in a large scale tank, and concluded that tyre chips are good for the absorption of contamination. Park et al. (1993) also reported on the effectiveness of ground tyre to absorb the VOCs in a series of laboratory scale column tests.

The construction of soil-bentonite (SB) slurry cut-off walls is a well-established approach to control the migration of contaminants into an uncontaminated area. This method is a cost-effective and time-saving approach in comparison to the construction of a treatment plant (Hong et al. 2012). The SB barriers have an intrinsic low sorption capacity when exposed to volatile organic compounds (VOCs) and require modification with some amendments that have a high capability for carbon absorption (Malusis et al. 2009; Park et al. 1993). It has been indicated that materials such as activated carbon, fly ash, zeolite, and scarp tyre etc. contain a high level of carbon that are effective in increasing the absorption capacity of SB slurry walls (Hong et al. 2012; Malusis et al. 2009; Mott and Weber 1992), however some of their most crucial engineering characteristics (i.e., hydraulic conductivity and compressibility) are not clear after amendments. For instance, Hong et al. (2012) investigated the effect of zeolite amendment on compressibility and hydraulic conductivity of the SB slurry walls by performing a series of laboratory scale hydraulic conductivity and consolidation tests. It was indicated that the addition of zeolite had little impact on the settlement and permeability characteristics of the SB backfill. In another example, Malusis et al. (2009) investigated the effect of two types of activated carbon (i.e., powdered and granular) amendment on permeability and consolidation characteristics of the SB slurry walls. They indicated that the application of powdered activated carbon marginally reduced the hydraulic conductivity and increased the compressibility of the SB backfill.

In aforementioned literature, it was determined that the generation of the scarp tyre is increasing day to day and finding innovative solutions to reuse this material is of interest to the researchers. In addition, it was mentioned that the scarp tyre, like some other materials (i.e., fly ash carbon, and zeolite etc.), has a high level of VOCs

absorption that has the potential for application in SB slurry walls, however their effect on engineering characteristics such as hydraulic conductivity and compressibility of the SB slurry walls is unknown. Thus, this study aims to investigate the effect of two types of scrap tyre after recycling, powdered recycled tyre (PRT) and crumbed recycled tyre (CRT), on hydraulic conductivity and compressibility of the SB slurry cut-off wall.

4.2.3. Materials and Methods

The materials used to prepare the backfill consist of sand, sodium bentonite, powdered recycled tyre (PRT) and crumbed recycled tyre (CRT) at 0, 2, 5 and 10% by dry weight. The sand used is classified as poorly graded sand (SP) according to the Unified Soil Classification System (USCS) [(ASTM D2487, (ASTM 2011a)], and was obtained from Baldivis, Western Australia. The bentonite used has a liquid limit (LL) and a plastic limit (PL) of 455 and 387, respectively [ASTM D4318 (ASTM 2010)], and is classified as a high plasticity (CH) clay according to the USCS. Both the PRT and the CRT have a specific gravity of solids (G_s) of 1.2. They were made from recycled truck tyres using a tyre buffing machine and purified of any other waste materials such as wood, glass, fibre or metal by the supplier. The uniformity coefficient (C_u) was 2.5 and 1.20, and the coefficient of curvature (C_c) was 1.02 and 1.20 for PRT and CRT, respectively. The particle size distribution (PSD) tests were performed for the materials in accordance with ASTM C136 (ASTM 2014b) and ASTM D422 (ASTM 2011b), and the results are presented in Fig. 4.10.

A Bentonite-water (BW) slurry was prepared by the addition of 5% bentonite (by dry weight) to tap water. The slurry was then mixed for 30 minutes in an automated Hobart mixer machine and left to hydrate for 24 hours (Hong et al. 2012). The prepared slurry had a density and marsh funnel viscosity of 1035 kg/m³ and 40 s, respectively. In addition, the electrical conductivity (EC) and pH of the slurry at 25°C were equal to 115.5 mS/m and 8.80. The unamended SB backfill was prepared by mixing sand with 4% bentonite (by dry weight) in the automated mixer for 30 minutes (Malusis et al. 2009; Hong et al. 2012). During preparation, water content equal to 8% of the sand (similar to the original gravimetric water content) was added to the backfill to keep its uniformity (Hong et al. 2012). To prepare the unamended SB backfill, the BW slurry was mixed with the base mixture and blended in the mixer machine until a targeted slump of 125 ± 12.5 mm was obtained [ASTM 2015a (ASTM C143)]. The total bentonite content of the final SB mixture was 5.8% (by dry weight of the soil). Fig. 4.11 shows a typical slump test performed for the SB backfill mixture. To prepare the PRT and CRT amended backfills, a greater amount of slurry was required to be added to each mixture due to the difference in nature of the tyre with sand. Furthermore, the amount of added dry bentonite was adjusted to maintain a similar total bentonite content for each PRT and CRT amended mixture. This modification was necessary to maintain a constant bentonite content in each backfill in order to compare the hydraulic conductivity and consolidation characteristics under the same condition. Table 4.3 shows the characteristics of each backfill mixture.

Table 4.3. Characteristics of each backfill mixture

No.	ID	Sand (%)	PRT (%)	CRT (%)	Liquid limit (LL)	Water content w (%)	Slump (mm)
1	SB	94.2	-	-	28	44.1	125
2	2PRT	92.2	2	-	32	45.3	126
3	5PRT	89.2	5	-	35	47.8	128
4	10PRT	84.2	10	-	37	51.3	127
5	2CRT	92.2	-	2	30	44.7	126
6	5CRT	89.2	-	5	31	45.4	127
7	10CRT	84.2	-	10	34	46.9	124

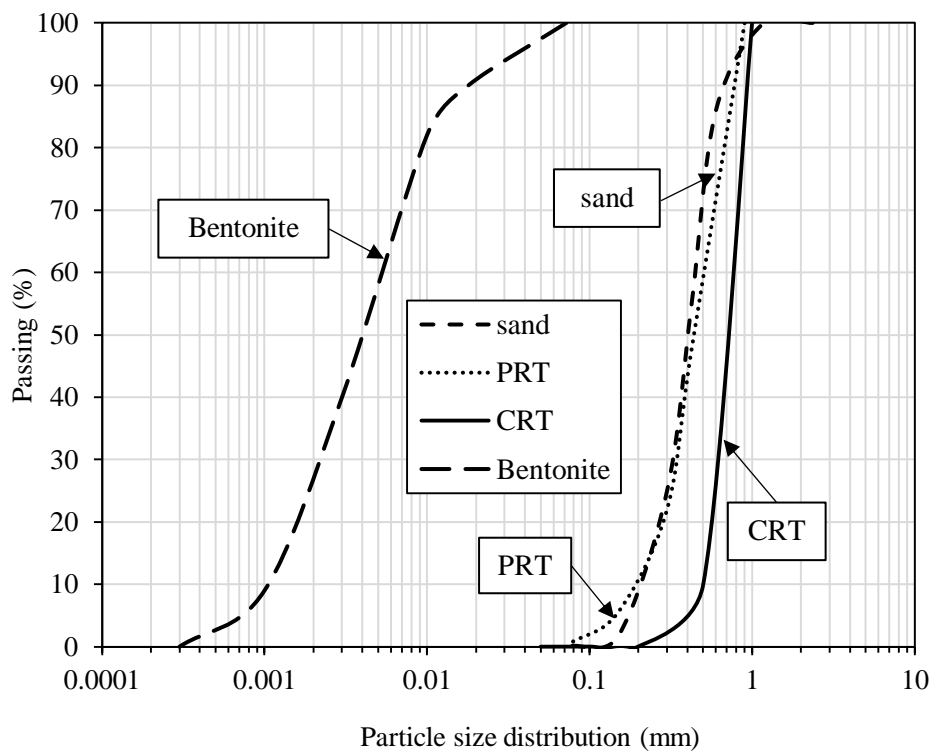


Fig. 4.10. Particle grading of the used materials.

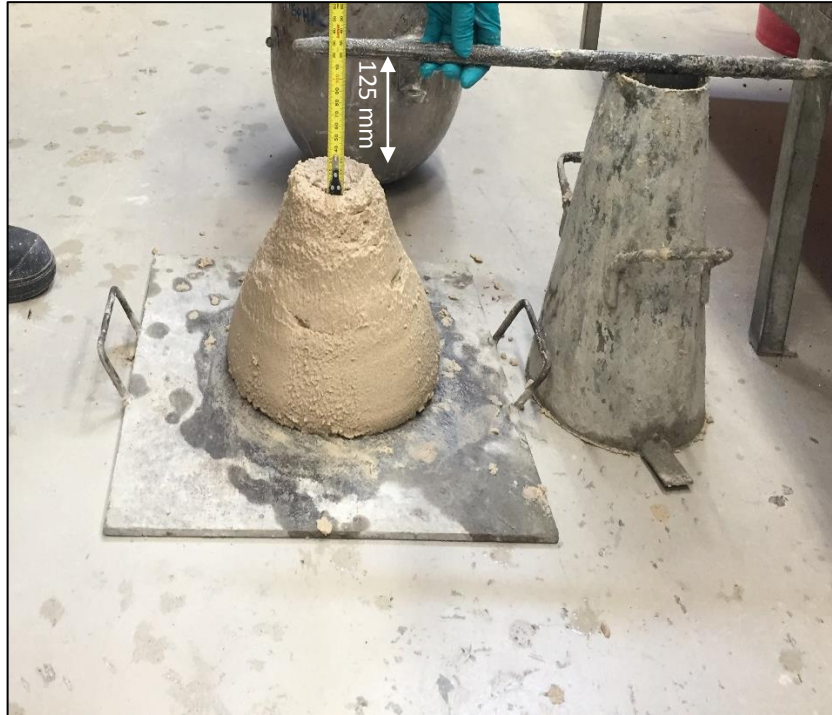


Fig. 4.11. A typical slump test performed on SB backfill.

4.2.4. Laboratory Test Setup

A series of rigid-wall hydraulic conductivity tests based on the falling head technique, in accordance with ASTM D5856 (ASTM 2015), were conducted in a moisture controlled room at $25 \pm 1^\circ\text{C}$ temperature. The tests were conducted in a compaction permeability mould with an inner diameter of 140 mm, and 150 mm height. Tap water with a pH and electrical conductivity (EC) of 6.7 and 5.5 mS/m was used as the permeant liquid. The rubber membrane was stretched inside the mould before depositing each backfill mixture to avoid sidewall leakage during the test (Aldaef and Rayhani 2014). Each mixture was deposited into the mould in three layers and rodded to avoid the formation of unwanted significant voids (Daniel et al. 1985). The recording started when the specimen reached the fully saturated state, and a steady outflow was observed. The hydraulic conductivity tests were measured three times for each mixture in a similar permeating and testing condition (i.e., outflow rate and

hydraulic gradient) and final hydraulic conductivity (k_f) was calculated by taking their mean value.

The one-dimensional consolidation tests were performed using a conventional fixed-ring Wykeham Farrance oedometer device in accordance with ASTM D2435 (ASTM 2011c). A cylindrical steel ring with a 50 mm diameter and 19 mm height was used to perform the tests on each mixture. The mixtures were rodded when placed in the ring to remove the significant pores. The applied vertical overburden stress started from 24 kPa and increased to 48, 96, 192, 383, 766 and 1,280 kPa and unloaded in a reverse order. Each sequence was completed after 24 hours. The hydraulic conductivity was also computed using Terzaghi consolidation theory (k_{theory}).

4.2.5. Results and Discussion

4.2.5.1. Consolidation Tests

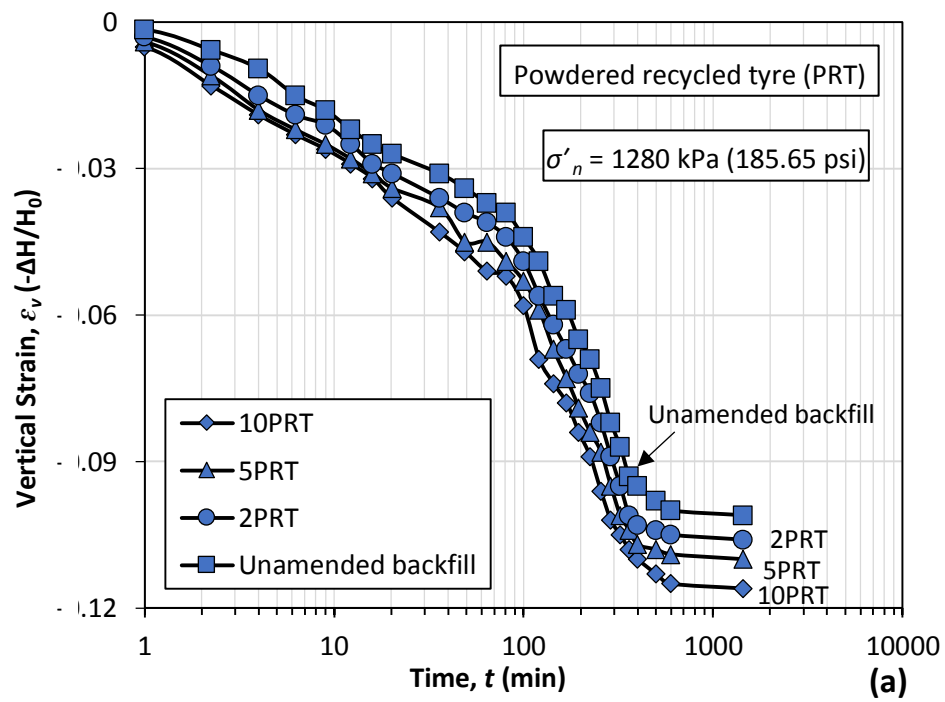
4.2.5.1.1. Deformation vs Time Relations

Fig. 4.12 shows typical variations of vertical strain versus time ($\varepsilon_v - t$) for unamended and PRT amended SB backfills when the tests were conducted under 1280 kPa effective confining stress. The variations of the deformation illustrated based on logarithm of the time ($\log t$) and square root of the time ($t^{1/2}$) in Fig. 4.12 (a) and Fig. 4.12 (b), respectively. It is seen from the figure that increasing the PRT contents of the specimens caused an increase in settlement characteristics of the specimens over time. For instance, while the unamended backfill has a vertical strain in the range of $0.2\% \leq \varepsilon_v \leq 10.1\%$ when the test duration was in the range of $1 \leq t \leq 1440$ min, addition of 2, 5, and 10% PRT to the backfill caused a deformation in the range of $0.3\% \leq \varepsilon_v \leq 10.6\%$, $0.4\% \leq \varepsilon_v \leq 11.0\%$, and $0.5\% \leq \varepsilon_v \leq 11.6\%$ in a test duration of $1 \leq t \leq 1440$ min

respectively. This trend clearly indicates that the addition of PRT to the backfill increased the settlement characteristics of the specimens. In addition, typical variations of the vertical strain with time for unamended and CRT amended backfills under 1280 kPa effective overburden stress were shown in Fig. 4.13. Similarly, these variations were shown based on logarithm of the time ($\log t$) and square root of the time ($t^{1/2}$) in Fig. 4.13(a) and Fig. 4.13(b), respectively. As shown in the figure, increasing the CRT content of the specimens caused an increase in vertical strain of the backfills. The settlement in CRT amended backfills is more pronounced than PRT amended ones. For instance, while the control backfill has a vertical strain in the range of $0.2\% \leq \varepsilon_v \leq 10.1\%$ during the consolidation time in the range of $1 \leq t \leq 1440$ min, amendment of the specimens with 2, 5, and 10% CRT caused a vertical strain in the range of $0.3\% \leq \varepsilon_v \leq 11.1\%$, $0.4\% \leq \varepsilon_v \leq 12.0\%$, and $0.5\% \leq \varepsilon_v \leq 12.7\%$ during $1 \leq t \leq 1440$ min respectively. This trend also shows that the amendment of the SB backfills with CRT caused a higher amount of settlement.

The acquired curves in vertical strain-logarithm time ($\varepsilon_v - \log t$) graphs for control backfill and both PRT and CRT amended specimens show an identical trend with three distinct inclinations during 27 interval times from 0.25 to 1440 min under 1280 kPa effective overburden stress. These inclinations clearly highlight that the rate of settlement was greater at earlier steps and reduced by over time until the last intervals (i.e., 500, 600, and 1440 min), where a very low amount of settlement was recorded, and the primary consolidation fully completed. This trend can be clearly seen from vertical strain-square root of time ($\varepsilon_v - t^{1/2}$) graphs. This trend was identical when the tests were conducted under the other effective overburden pressures.

The PRT is a flexible fine material with a lower elastic modulus than sand (Cokca and Yilmaz 2004), this characteristic caused a greater deformation to be recorded when the backfill was mixed with a greater PRT content. The flexibility is more pronounced in CRT since it has a larger structure than PRT, therefore, it has a lower elastic modulus than PRT and a greater amount of deformation was recorded in CRT amended specimens.



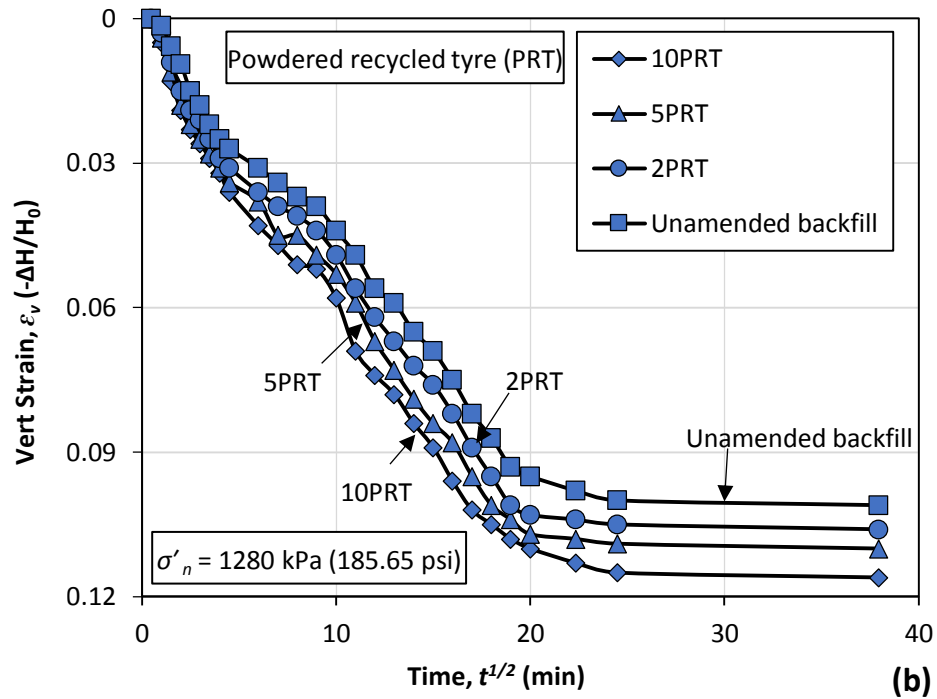
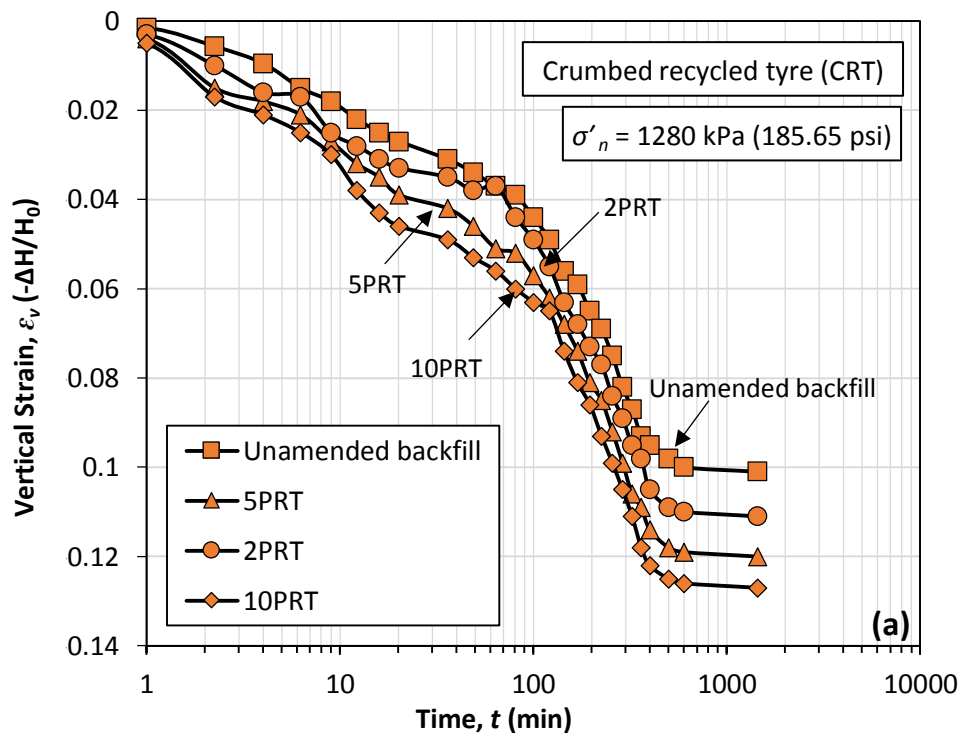


Fig. 4.12. Typical settlement behaviour for control SB and PRT amended backfills as a function of the vertical strain (ϵ_v): (a) $\log t$; (b) $t^{1/2}$ under 1280 kPa (185.65 psi) effective overburden stress (σ'_n).



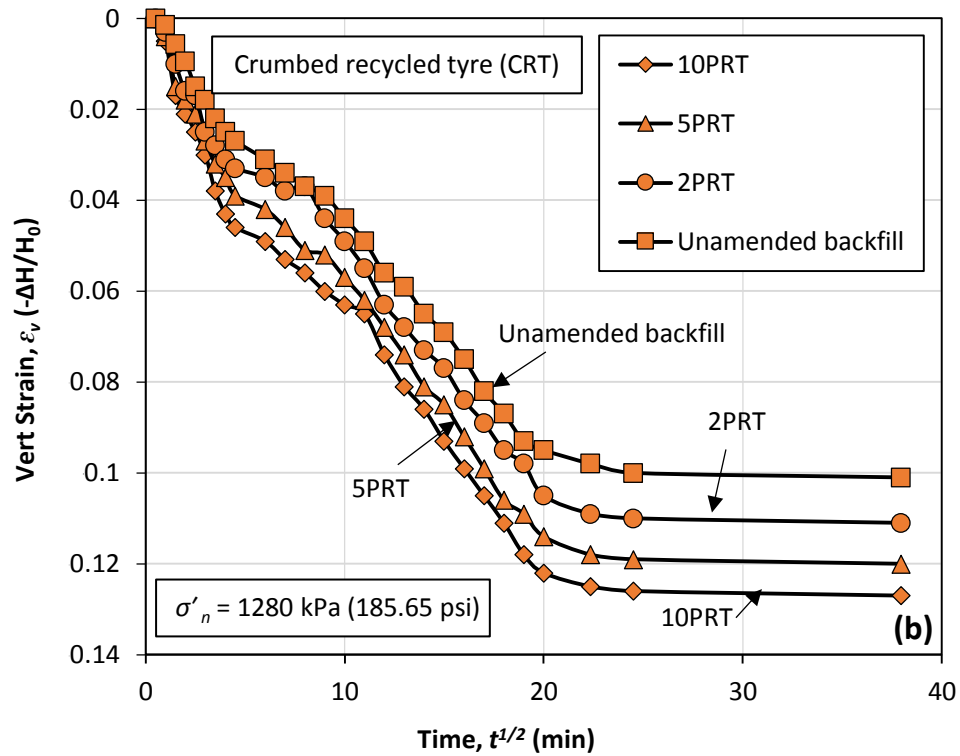


Fig. 4.13. Typical settlement behaviour for control SB and CRT amended backfills as a function of the vertical strain (ϵ_v): (a) $\log t$; (b) $t^{1/2}$ under 1280 kPa (185.65 psi) effective overburden stress (σ'_n).

4.2.5.2. Compression Index and Swelling Index

Variations of the void ratio (e) with logarithm of the effective overburden stress (i.e., $e - \log \sigma'_n$) for control, PRT and CRT amended specimens are shown in Fig. 4.14. As can be seen in Fig. 4.14(a), the control SB backfill mixture has a void ratio in the range of $0.82 \leq e \leq 1.18$ at an effective overburden stress in the range of $24 \leq \sigma'_n \leq 1280 \text{ kPa}$, whereas for the same range of effective overburden stress (σ'_n), the void ratio values (e) for PRT amended specimens are in the range of $0.85 \leq e \leq 1.22$, $0.87 \leq e \leq 1.26$, and $0.90 \leq e \leq 1.30$ when 2, 5, and 10% PRT added to the specimens respectively. Similarly, amendment of the SB backfills with CRT slightly increased the void ratio values. As shown in Fig. 4.14(b), addition of 2% CRT caused an increase in void ratio in the range of 0.84 to 1.20. This value increased to the range of 0.85-1.22 and 0.87 to

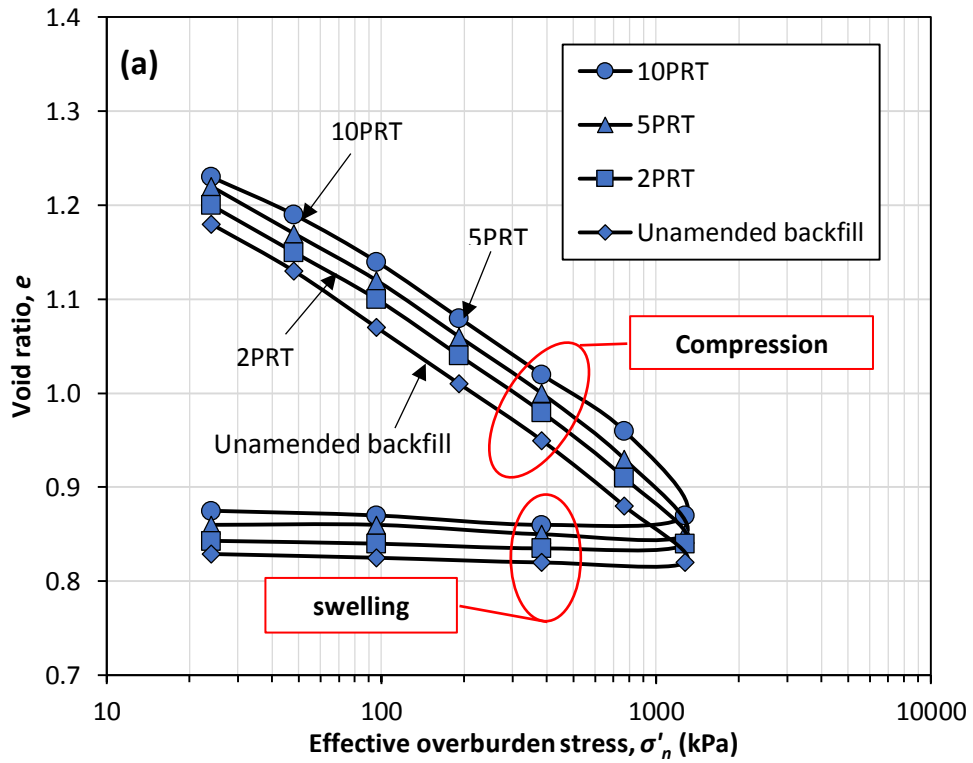
1.23 when 5% and 10% of CRT was added to the specimens under an effective confining stress range of $24 \leq \sigma'_n \leq 1280$ kPa, respectively.

The PRT used in this study has a relatively similar particle size distribution (PSD) to the sand (i.e., the main component of the backfill). Although, the PRT can be classified as the poorly graded (SP) category based on the USCS, some portions of its grading has larger particles than the sand used, which might be the main reason for the increase in void ratio. Increasing the PRT content caused this portion in the specimens to increase and a greater void ratio value to be recorded. Since the CRT contents has a larger grading, a similar condition is governed for the case of CRT amended backfills, and a greater value of void ratio was recorded after the addition of CRT and increasing its contribution in the backfill.

The compression index (C_i) and swelling index (C_s) values computed using $e - \log \sigma'_n$ graphs, and were shown versus PRT and CRT contents in Fig. 4.15. The computed compression index values for the PRT added specimens showed a greater range value (i.e., $0.314 \leq C_i \leq 0.404$) than the SB backfill control mixture (i.e. $C_i = 0.269$). Similarly, the compression index values for all CRT included SB backfill mixtures, were lower than the control mixture (i.e., $0.292 \leq C_i \leq 0.359$). The reported variations in compression index values show that the addition of the PRT and CRT to the SB backfill mixture have a slight impact on the settlement characteristics of the SB backfills and increasing their contribution caused an increase in these characteristics. The recorded behaviours in this section were consistent with results acquired from vertical strain-time graphs in the previous section.

An identical increasing trend was recorded for swelling index values when the PRT and CRT contribution of the SB backfill increased. For instance, while the compression index of the unamended specimen was 0.009, the addition of 2 to 10%

PRT and CRT caused a compression index value range of $0.009 \leq C_s \leq 0.017$ and $0.007 \leq C_s \leq 0.013$, respectively. This trend can be attributed to the flexible characteristics of the PRT and CRT, and reflects the low range of the fine materials used in the mixtures (Yeo et al. 2005; Malusis et al. 2009).



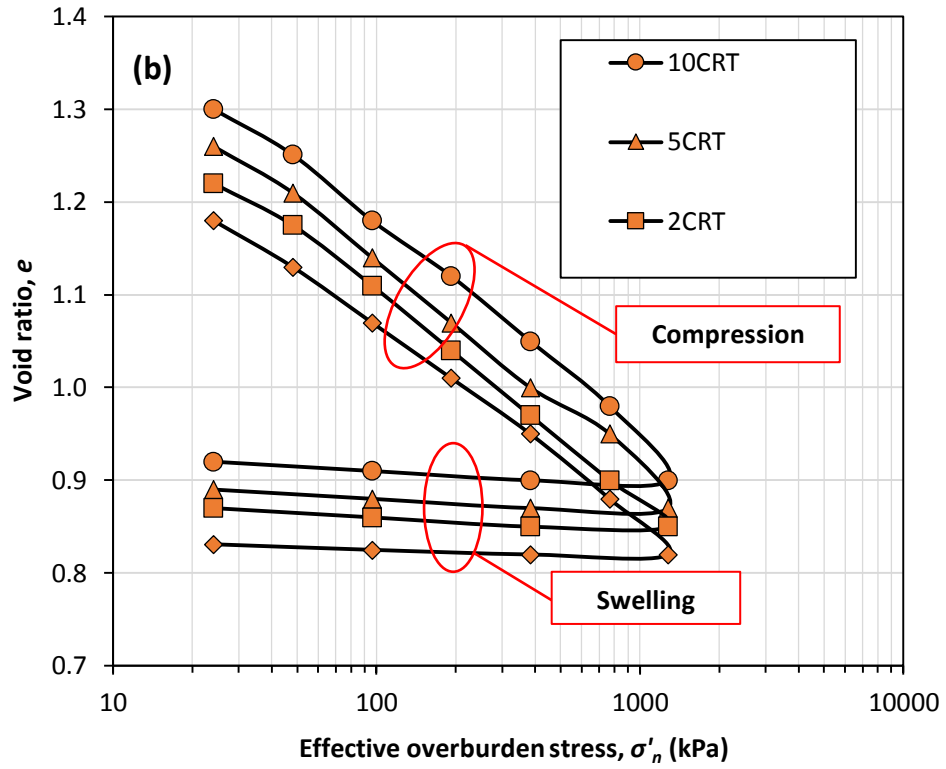


Fig. 4.14. Void ratio (e) versus logarithm of effective overburden stress ($\log \sigma'_n$) for control SB backfill mixture and (a) PRT amended specimens and; (b) CRT amended specimens

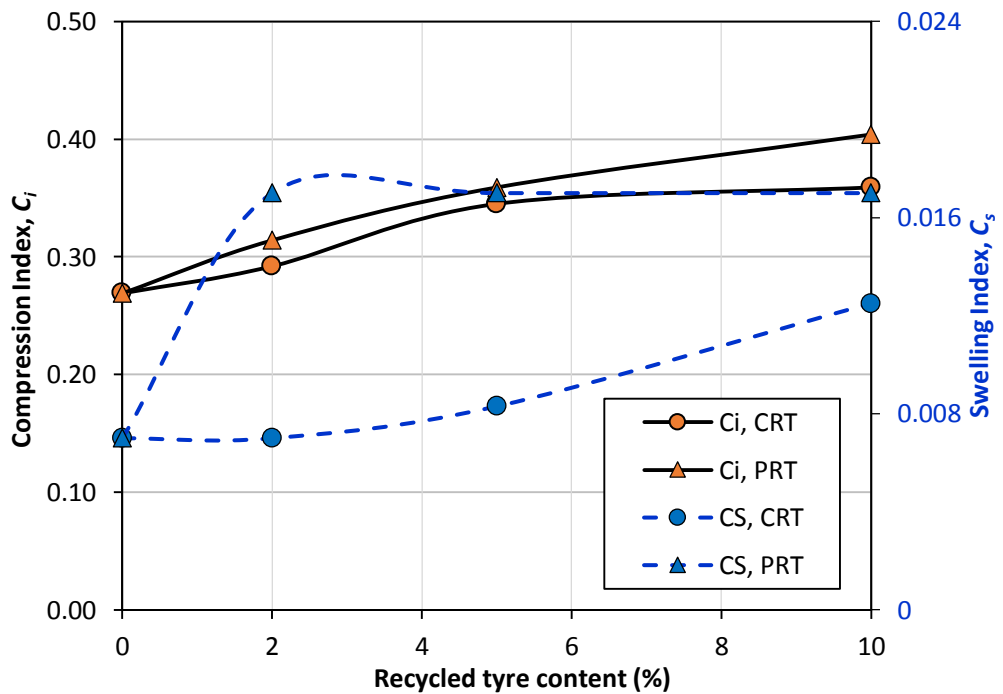


Fig. 4.15. Variation of the compression index (C_i) and swelling index (C_s) versus recycled tyre content

4.2.5.3. Coefficient of Consolidation

The coefficient of consolidation (c_v) was computed using Casagrande and Taylor methods, and the results are presented in Fig. 4.16 and 4.17, respectively. As shown in both figures, the reported coefficient of consolidation values have a similar trend and range in both calculated methods for both the PRT and CRT amended backfills. For instance, in Casagrande method, the control SB backfill mixture has a coefficient of consolidation value in the range of $1.13 \times 10^{-8} \leq c_v \leq 3.97 \times 10^{-7} \text{ m}^2/\text{s}$ under $24 \leq \sigma'_n \leq 1280 \text{ kPa}$ effective overburden stress, while this range increased to $1.22 \times 10^{-8} \leq c_v \leq 4.32 \times 10^{-7} \text{ m}^2/\text{s}$, $1.37 \times 10^{-8} \leq c_v \leq 5.23 \times 10^{-7} \text{ m}^2/\text{s}$, and $1.70 \times 10^{-8} \leq c_v \leq 6.53 \times 10^{-7} \text{ m}^2/\text{s}$ after the addition of 2, 5, and 10% PRT respectively [see Fig. 4.16(a)]. A similar trend was recorded for the c_v values in the results computed based on the Taylor method. For instance, addition of the PRT caused a decrease in the range of $1.7 \times 10^{-8} \leq c_v \leq 5.27 \times 10^{-7}$, $2.8 \times 10^{-8} \leq c_v \leq 6.24 \times 10^{-7}$, and $3.4 \times 10^{-8} \leq c_v \leq 6.73 \times 10^{-7} \text{ m}^2/\text{s}$ when 2, 5, and 10% PRT included in the specimens, respectively. The control SB backfill range was $1.0 \times 10^{-8} \leq c_v \leq 4.5 \times 10^{-7} \text{ m}^2/\text{s}$ [see Fig. 4.17(a)].

An identical trend was observed for CRT included specimens in both Casagrande and Taylor methods. For instance, while the coefficient of consolidation for unamended backfill was $1.13 \times 10^{-8} \leq c_v \leq 3.97 \times 10^{-7} \text{ m}^2/\text{s}$ under $24 \leq \sigma'_n \leq 1280 \text{ kPa}$ effective overburden stress, amendment of the backfill with 2, 5, and 10% CRT caused a coefficient of consolidation in the range of $1.27 \times 10^{-8} \leq c_v \leq 5.56 \times 10^{-7} \text{ m}^2/\text{s}$, $1.42 \times 10^{-8} \leq c_v \leq 5.76 \times 10^{-7} \text{ m}^2/\text{s}$, and $1.55 \times 10^{-8} \leq c_v \leq 6.02 \times 10^{-7} \text{ m}^2/\text{s}$ under $24 \leq \sigma'_n \leq 1280 \text{ kPa}$ effective overburden stress when computed using Casagrande method. Similarly, the unamended backfill in the Taylor method had a coefficient of consolidation of $1 \times 10^{-8} \leq c_v \leq 4.5 \times 10^{-7} \text{ m}^2/\text{s}$ under $24 \leq \sigma'_n \leq 1280 \text{ kPa}$ effective overburden stress, and the addition of 2, 5, and 10% CRT caused a coefficient of

consolidation in the range of $1.8 \times 10^{-8} \leq c_v \leq 6.01 \times 10^{-7} \text{ m}^2/\text{s}$, $2.41 \times 10^{-8} \leq c_v \leq 6.37 \times 10^{-7} \text{ m}^2/\text{s}$, and $3.20 \times 10^{-8} \leq c_v \leq 6.51 \times 10^{-7} \text{ m}^2/\text{s}$ under $24 \leq \sigma'_n \leq 1280 \text{ kPa}$ effective overburden stress. The results reported in this section indicated that increasing the contribution of the PRT and CRT in the specimens caused an increase in coefficient of consolidation. This characteristic can be attributed to the flexible characteristics of the PRT and CRT. In fact, the substitution of sand with a higher rigidity than tyre caused a higher value of coefficient of consolidation to be recorded in PRT and CRT amended specimens.

Generally, the coefficient of consolidation computed based on the Taylor method has a greater value than those values computed using the Casagrande method. This fact can be seen clearly in Fig. 4.18, which shows variations of the computed c_v values based on the Taylor method divided by c_v values computed based on the Casagrande method (i.e., $c_{v, Taylor} / c_{v, Casagrande}$) versus logarithm of effective overburden pressure ($\log \sigma'_n$) in PRT and CRT amended SB backfill. It is seen from the figure that almost all values are greater than one. This trend can be attributed to the changes of the compressibility with effective stress and the rate of strain (Yeo et al., 2005), and is due to the secondary compression which happens during the primary consolidation (Olson, 1986; Yeo et al. 2005).

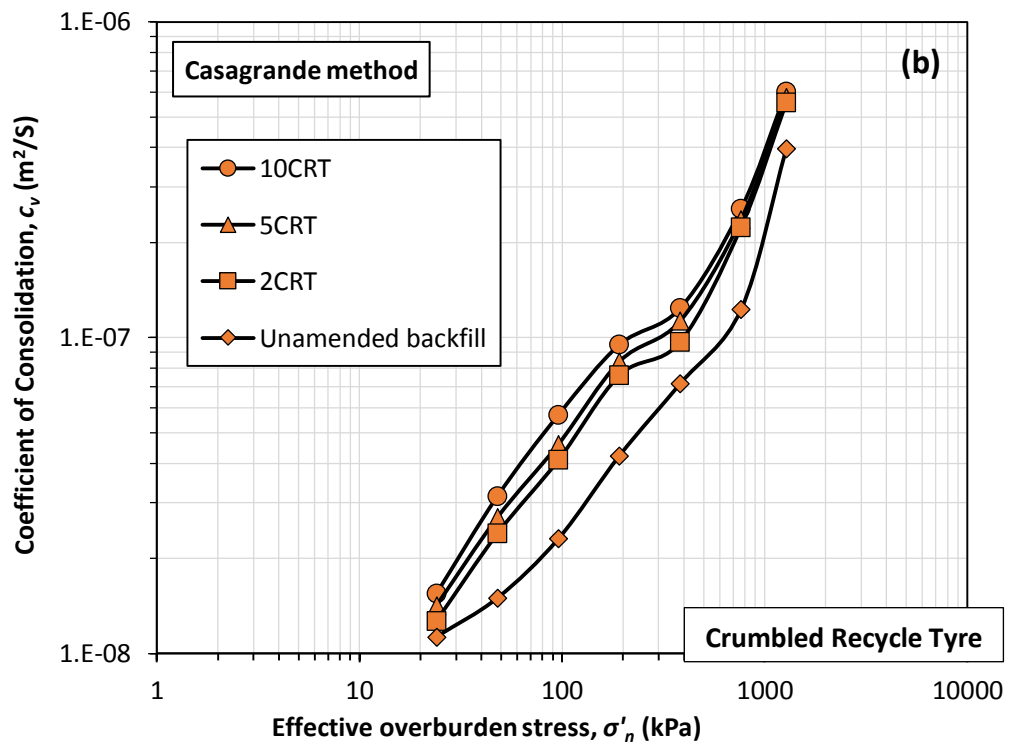
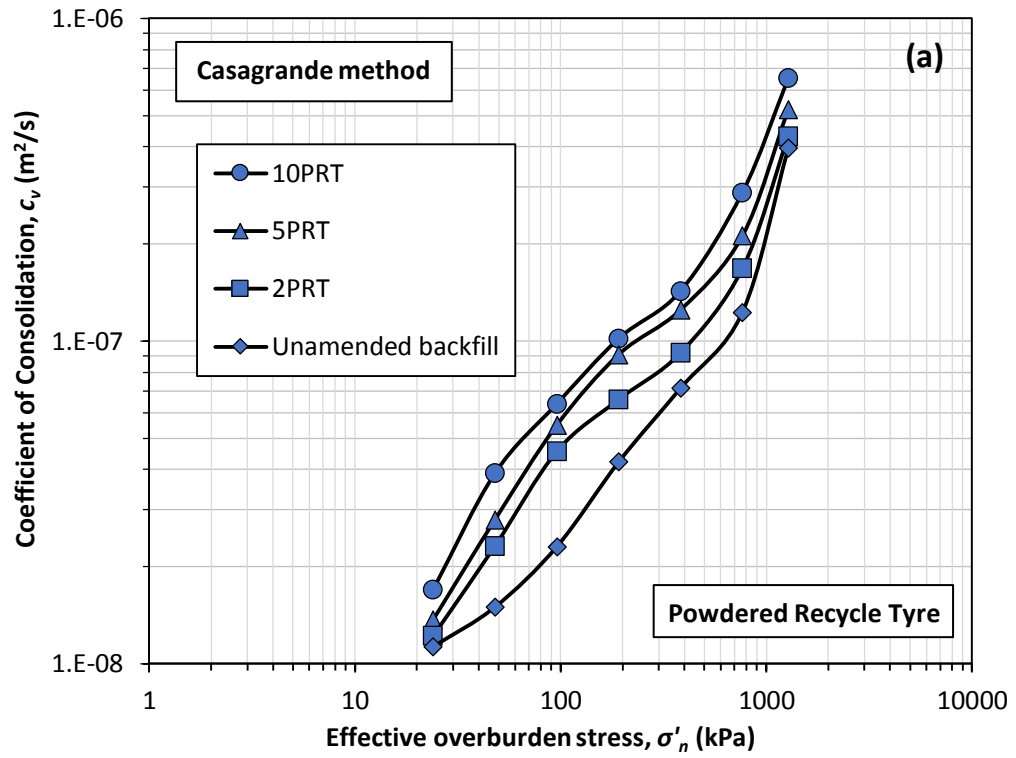


Fig. 4.16. Computed c_v values based on Casagrande method versus logarithm effective overburden stress (σ'_n) for SB backfill mixture and (a) PRT amended specimens; (b) CRT amended specimens

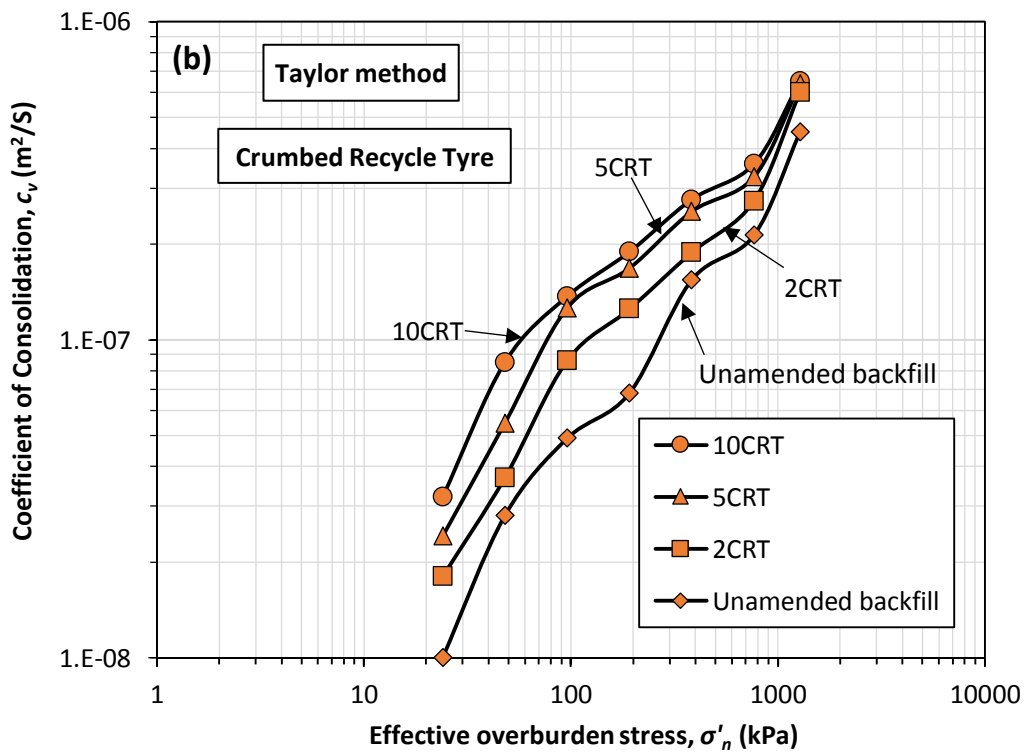
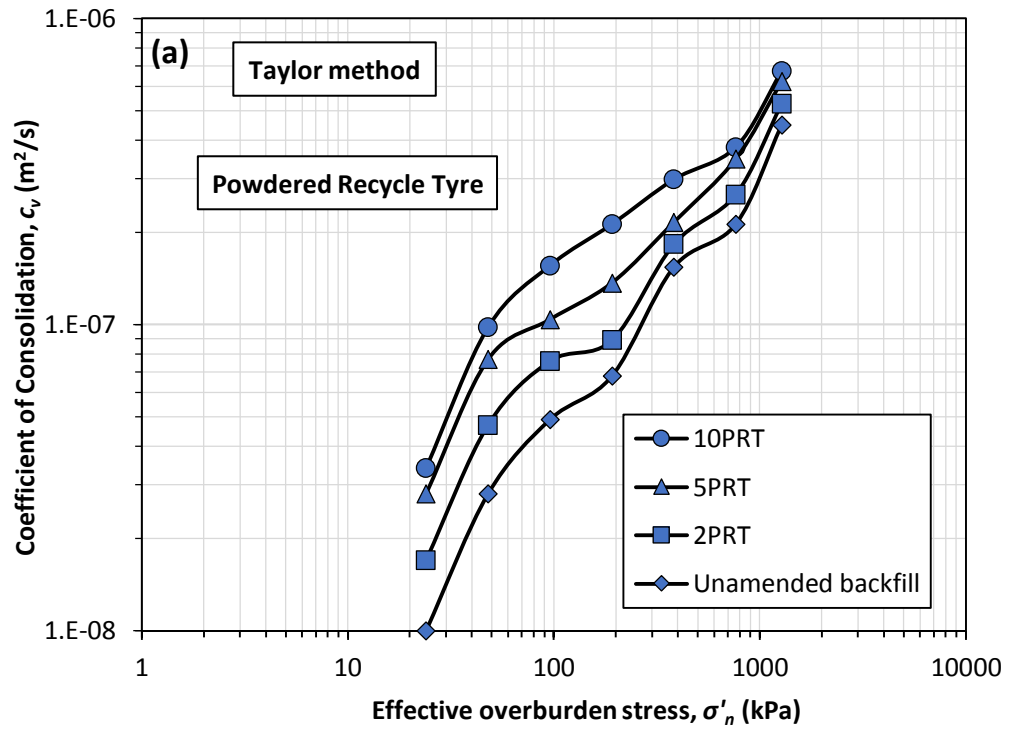


Fig. 4.17. Computed c_v values based on Taylor method versus logarithm effective overburden stress (σ'_n) for SB backfill mixture and (a) PRT amended specimens and; (b) CRT amended specimens

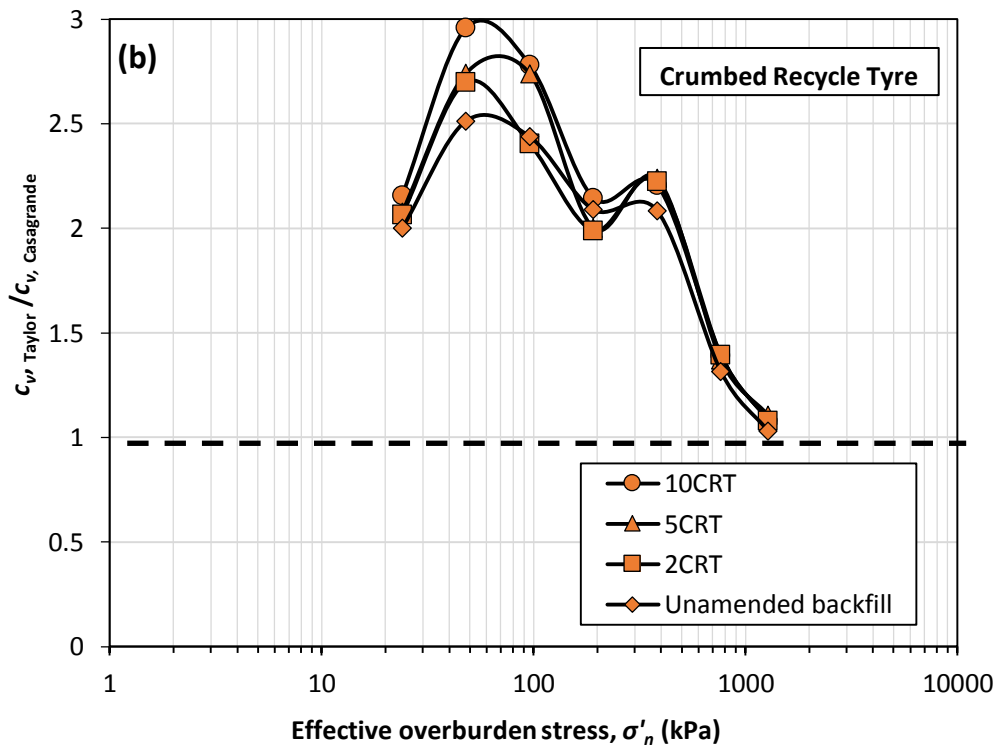
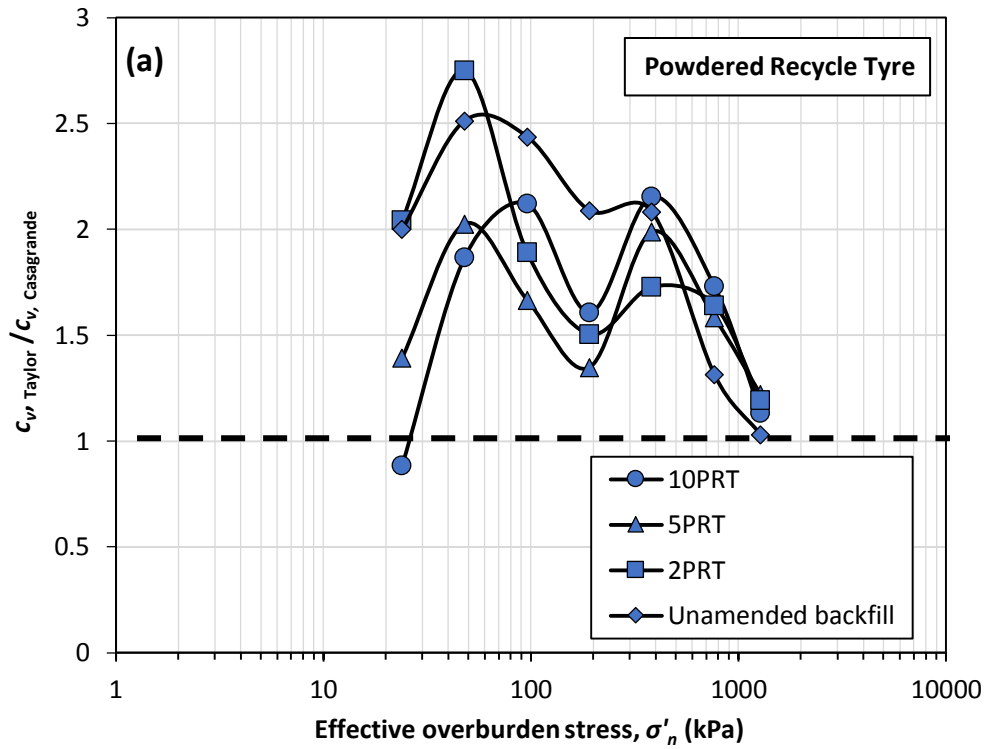
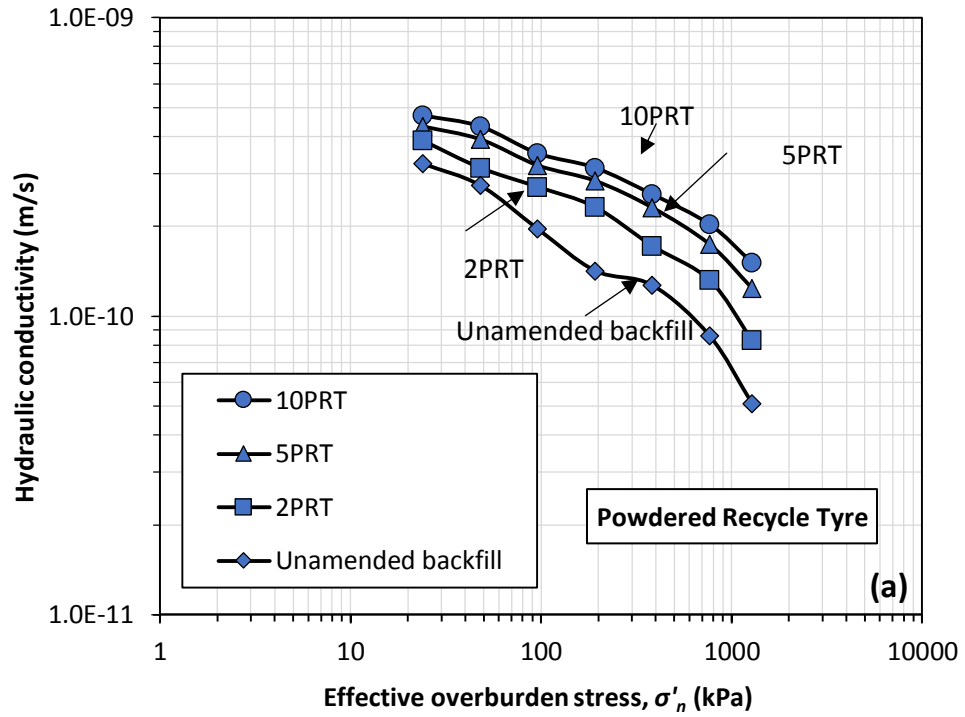


Fig. 4.18. Computed c_v values based on the Taylor method relative to c_v values computed based on the Casagrande method versus σ'_n for (a) PRT amended specimens and; (b) CRT amended specimens

4.2.5.4. Terzaghi Hydraulic Conductivity (k_{theory})

Hydraulic conductivity values were computed based on the Terzaghi consolidation theory (k_{theory}) similar to Kang and Shackelford (2010), and the results were plotted versus logarithm effective overburden stress ($\log \sigma'_n$) as shown in Fig. 4.19. The computed k_{theory} for PRT amended specimens showed an increasing trend in the range of $8.30 \times 10^{-11} \leq k_{theory} \leq 3.87 \times 10^{-10}$, $1.24 \times 10^{-10} \leq k_{theory} \leq 4.32 \times 10^{-10}$, and $1.51 \times 10^{-10} \leq k_{theory} \leq 4.70 \times 10^{-10}$ m/s when a PRT content of 2, 5, and 10% was added, under 24 and 1280 kPa effective overburden stress, respectively. The control backfills had a hydraulic conductivity in the range of $5.10 \times 10^{-11} \leq k_{theory} \leq 3.24 \times 10^{-10}$ m/s when the test was conducted under an effective overburden stress of $24 \leq \sigma'_n \leq 1280$ kPa. A similar increasing trend was recorded for the hydraulic conductivity values of the CRT amended specimens. This increasing trend was more pronounced than those recorded in PRT added backfills. For instance, while the hydraulic conductivity of the unamended backfill was in the range of $5.10 \times 10^{-11} \leq k_{theory} \leq 3.24 \times 10^{-10}$ m/s under an effective overburden stress of $24 \leq \sigma'_n \leq 1280$ kPa, increasing the CRT contents of the specimens caused a hydraulic conductivity in the range of $7.4 \times 10^{-11} \leq k_{theory} \leq 3.89 \times 10^{-10}$, $1.01 \times 10^{-10} \leq k_{theory} \leq 4.52 \times 10^{-10}$, and $1.57 \times 10^{-10} \leq k_{theory} \leq 5.23 \times 10^{-10}$ m/s when 2, 5, and 10% CRT were added in the specimens, respectively. Increases in hydraulic conductivity by increasing the contribution of the PRT and CRT can be attributed to increases in void ratio of the specimens as shown in Fig. 4.20. As indicated earlier, the PRT and CRT grading characteristics caused an increase in void ratio of the specimens, which caused an increase in the hydraulic conductivity of the amended backfills. Fig. 4.21 shows the variations of the hydraulic conductivity with different PRT and CRT contents when the tests were conducted under different effective overburden stress. It is noteworthy to mention that an increase in effective

overburden stress caused a decrease in recorded hydraulic conductivity values. For instance, the recorded hydraulic conductivity values had the lowest values when the tests were conducted under an effective confining stress of 1280 kPa in comparison with lower effective overburden stresses.



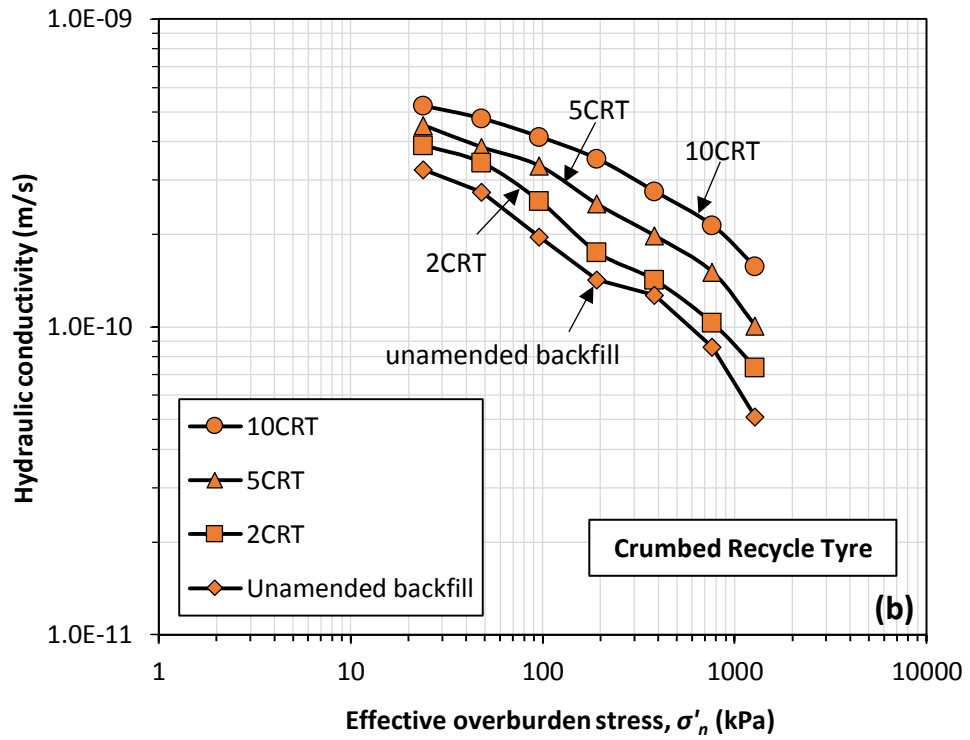
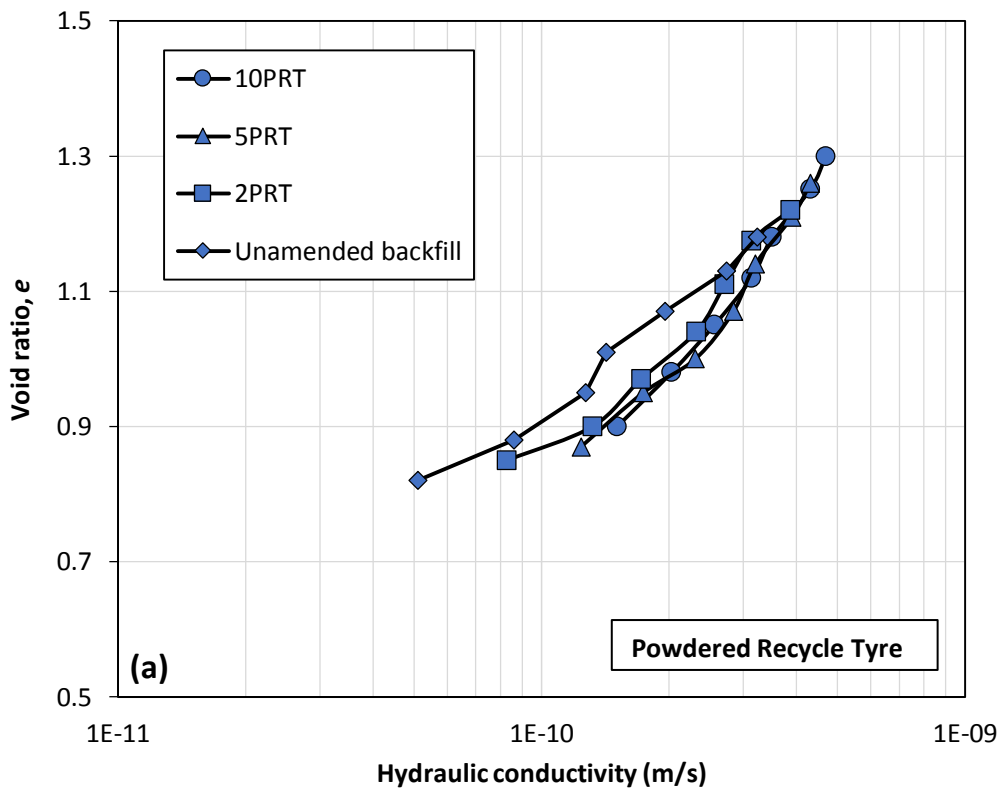


Fig. 4.19. Hydraulic conductivity (k_{theory}) as a function of effective overburden stress (σ'_n) for control SB backfill mixture and (a) PRT amended specimens; (b) CRT amended specimens



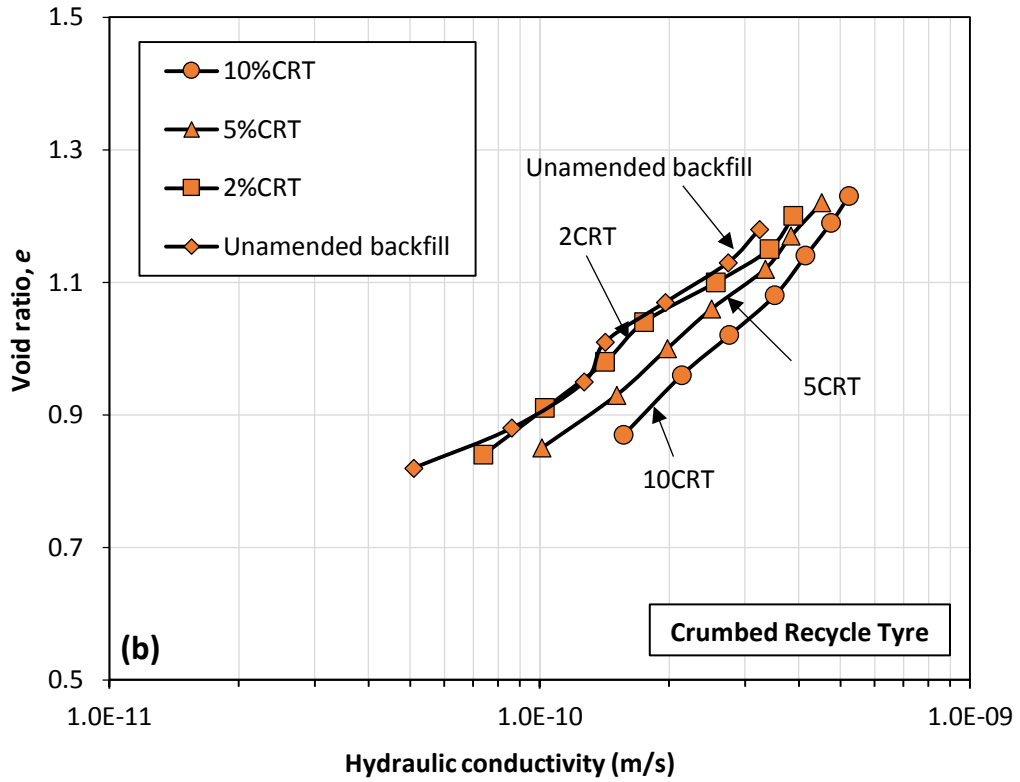
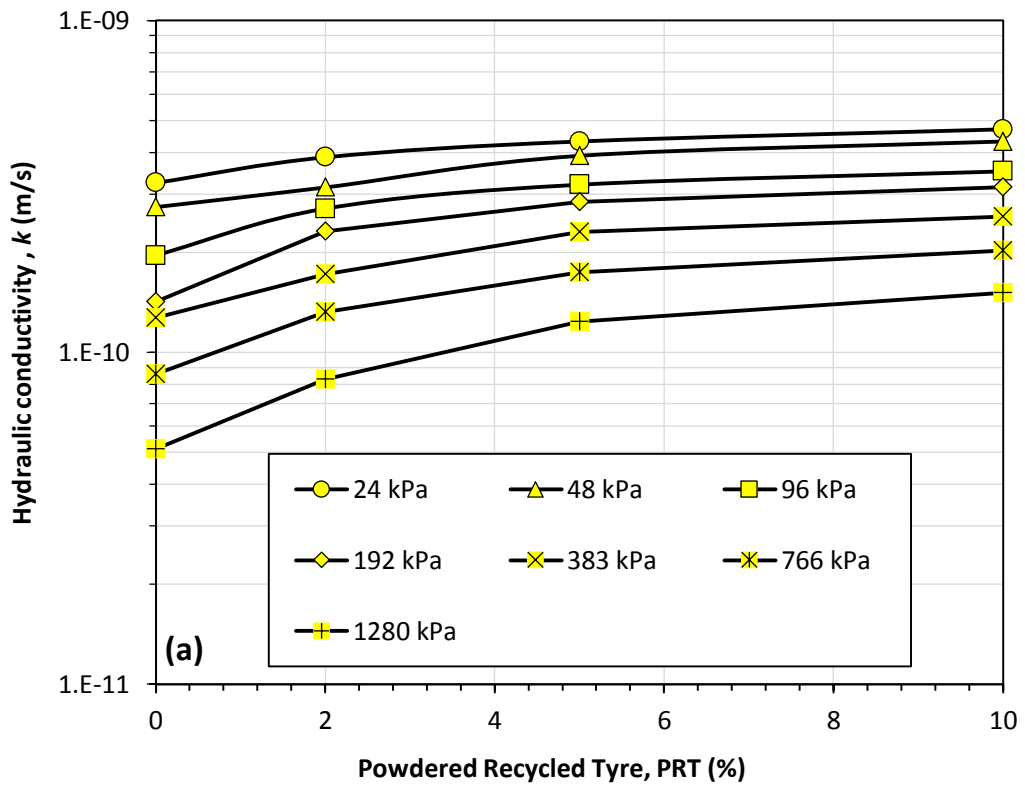


Fig. 4.20. Hydraulic conductivity (k_{theory}) as a function of void ratio (e) for control backfill mixture and (a) PRT amended specimens; (b) CRT amended specimens



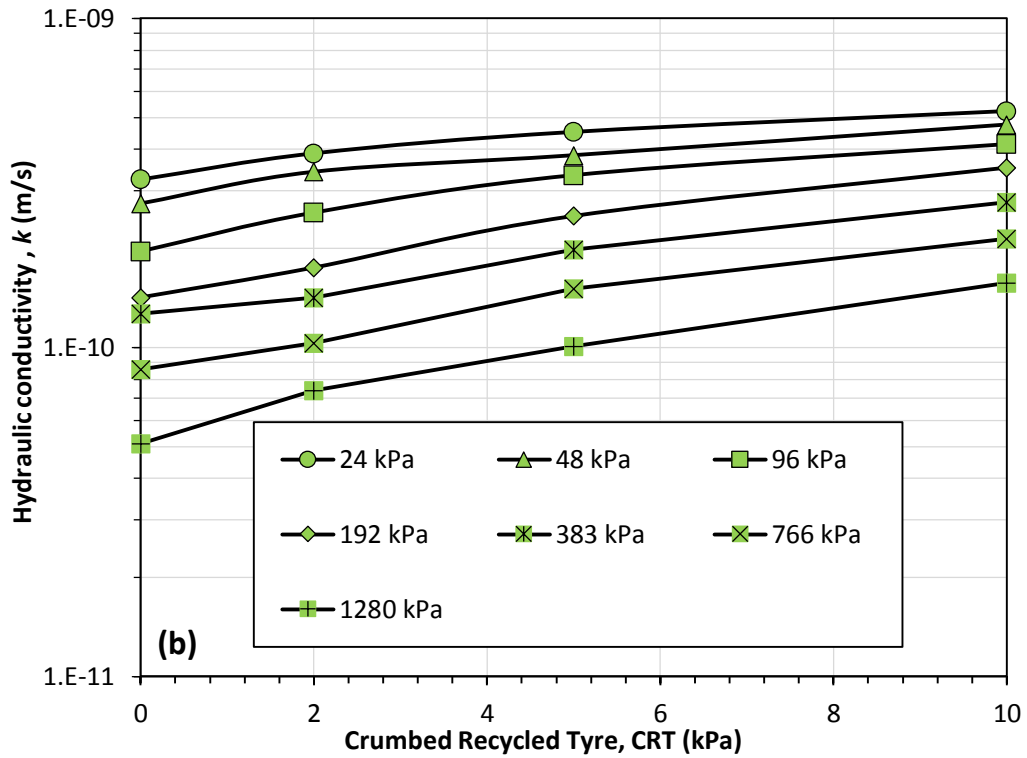


Fig. 4.21. The computed hydraulic conductivity based on Terzaghi consolidation theory (i.e., k_{theory}) as a function of tyre content for SB control mixture and (a) PRT amended specimens; (b) CRT amended specimens

4.2.5.5. Rigid-Wall Hydraulic Conductivity Tests (k_f)

Table 4.4 shows the results of rigid-wall hydraulic conductivity tests conducted on unamended SB backfill and SB amended with PRT and CRT. The results showed that, while the control SB backfill mixture has a final hydraulic conductivity (k_f) value equal to 5.2×10^{-10} . This value increased to the range of $5.3 \times 10^{-10} \leq k_f \leq 5.8 \times 10^{-10}$ m/s when the specimens were mixed with 2% to 10% PRT. The k_f values increased even more (i.e., $6.1 \times 10^{-10} \leq k_f \leq 6.6 \times 10^{-10}$ m/s) when the SB backfill mixtures were mixed with a CRT content in the range of 2% to 10%. The results in this section suggest that the addition of the PRT and CRT increased the hydraulic conductivity of the SB backfill mixtures. As indicated before, increases in hydraulic conductivity by increasing the PRT and CRT contents of the backfills can be attributed to increases in

void ratio of the specimens. The reported trend in this section is consistent with the acquired hydraulic conductivity values by Terzaghi consolidation theory in the previous section.

Table 4.4. A summary of hydraulic conductivity test results.

Specimen	Porosity, n	Density γ_d (t/m ³)	Measured Hydraulic Conductivity k (m/s)	
			k , (m/s)	$k_{f\text{average}}$
SB backfill	0.48	1.36	5.3×10^{-10}	5.2×10^{-10}
			4.8×10^{-10}	
			5.6×10^{-10}	
2PRT	0.49	1.39	5.2×10^{-10}	5.3×10^{-10}
			5.5×10^{-10}	
			5.3×10^{-10}	
5PRT	0.49	1.36	5.9×10^{-10}	5.6×10^{-10}
			5.3×10^{-10}	
			5.5×10^{-10}	
10PRT	0.48	1.39	5.5×10^{-10}	5.8×10^{-10}
			5.9×10^{-10}	
			5.9×10^{-10}	
2CRT	0.48	1.38	5.8×10^{-10}	6.1×10^{-10}
			6.1×10^{-10}	
			6.3×10^{-10}	
5CRT	0.48	1.39	6.2×10^{-10}	6.3×10^{-10}
			6.3×10^{-10}	
			6.5×10^{-10}	
10CRT	0.48	1.38	6.5×10^{-10}	6.6×10^{-10}
			6.5×10^{-10}	
			6.8×10^{-10}	

4.2.6. Conclusions

The generation of the scrap tyre has been an increasing trend in recent years, and finding innovative reusing methods is of great importance to reduce the negative impacts of these materials on the environment. Tyre has a high intrinsic sorption capacity of volatile organic compounds (VOCs) and has the potential for application in containment barriers, however, its effect on hydraulic conductivity and compressibility, two crucial engineering characteristics of the soil, is unknown. This study investigated the effect of powdered recycled tyre (PRT) and crumbed recycled tyre (CRT) addition on hydraulic conductivity and consolidation characteristics of the soil-bentonite (SB) backfill mixture. Investigation on deformation characteristics showed that the addition of PRT and CRT to the SB backfills mixtures increased the settlement characteristics of the specimens. In addition, investigations showed that the addition of PRT and CRT to the SB backfill mixtures increased the compression index (C_i) and swelling index (C_s) of the specimens. The coefficient of consolidation (c_v) values calculated using the Casagrande and Taylor methods showed a good agreement between recorded ranges and trends. Furthermore, it was revealed that the addition of the PRT and CRT increased the c_v values of the specimens. The hydraulic conductivity values computed using the Terzaghi consolidation theory (k_{theory}) incremented by increasing the PRT and CRT contents of the specimens. In addition, the rigid-wall hydraulic conductivity tests showed an increase after the addition of PRT and CRT contents.

Part 3

Effect of lime and GGBFS on engineering properties of Soil

4.3. Effect of Lime and GGBFS on Engineering Properties of Soil

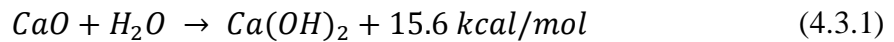
4.3.1. Abstract

Although lime is one of the most suitable binders in soil improvement projects, the associated environmental impact and some accompanying mechanical deficiencies should not be ignored. Partial substitution of lime with other binders is one of the ways of reducing the associated harm and improving the engineering properties of lime. This study investigated the effect of the partial substitution of lime with ground granulated blast furnace slag (GGBFS) on the strength and mechanical properties of lime stabilised clay by performing a total of 246 volumetric shrinkage strain (VSS), unconfined compressive strength (UCS) and ring shear (RS) tests. The VSS results demonstrated that the addition of GGBFS to lime is very effective in reducing the volumetric shrinkage of lime stabilised clay, and that the reduction in volumetric shrinkage behaviour is linearly related to curing period. The UCS results revealed that the partial replacement of lime with GGBFS led to significantly higher compressive strength for all ageing periods. The ring shear results also demonstrated that the partial replacement of lime with GGBFS led to a greater shear strength. Moreover, microstructural studies were performed to better understand the reactions of the mixtures. Scanning electron microscopy (SEM) and energy dispersive X-ray spectroscopy (EDS) carried out on selected specimens revealed that the addition of GGBFS in a lime stabilised clay results in production of the cementitious products in a faster rate. X-ray powder diffraction (XRD) test results revealed that the main hydration products are cementitious products such as calcium silicate hydrates (CSH), calcium aluminates (CAH).

4.3.2. Introduction

Clay in lightly loaded foundation systems such as road and railway networks, compresses and changes its volume due to applied stresses and loss of moisture content (reactive clays) respectively. These defects lead to some irreversible failures to the structures that cost billions of dollars to remedy (Petry and Little 2002). The main goal in improvement of the mechanical behaviour of a fine-grained soil is to reduce the volume changes and to increase the strength (Petry and Little 2002). Many studied, tried to stabilise clay using different agents (Phetchuay et al. 2016; Brooks 2009; Kamruzzaman et al. 2009; Lee et al. 2005). However, lime (CaO) is known as the most applicable agent in pavement projects (Bell 1996; Prusinski and Bhattacharja 1999; Eades and Grim 1960) especially in improvement of a clayey subgrade (Petry and Little 2002).

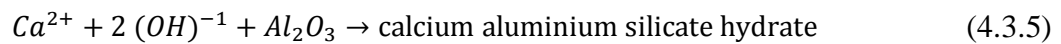
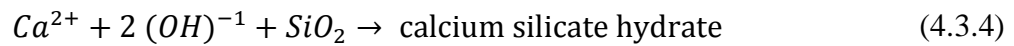
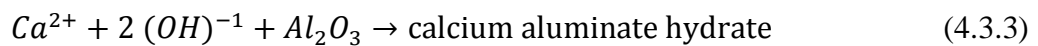
Addition of lime to a clay soil system containing water results in hydration, cation exchange and pozzolanic reactions. The lime absorbs the moisture of the soil and becomes hydrated lime ($Ca(OH)_2$) through a rapid reaction that produces a large amount of heat through the hydration process. This reaction is illustrated in Eq. (4.3.1) (Kitazume and Terashi 2013).



The hydrated lime dissolves into the existing pore water and increases the concentration of calcium (Ca^{2+}) and hydroxyl ($(OH)^{-1}$) ions (See Eq. (4.3.2)). Then cation exchange occurs between the ions of the clay grains and the calcium ions of the lime on the surface of the clay minerals (Bell 1996).



The Ca^{2+} and $(OH)^{-1}$ ions react with Al and Si minerals in the clay particles while they are in the pore water and undergo pozzolanic reactions and generate hydration products such as calcium aluminate hydrate (CAH), calcium silicate hydrate (CSH), and calcium aluminium silicate hydrate (CASH). These hydration products play the main role in soil stabilisation by lime. Eq. (4.3.3), (4.3.4) and (4.3.5) show the generation of hydration products (Bell, 1996; Al-Mukhtar et al. 2012).



Lime is very similar to Portland cement (PC) in terms of the internal reactions that occur in soil stabilisation and the associated production process and environmental hazards (Higgins 2007, Yi et al. 2013). Nowadays, the environmental impacts associated with lime application in terms of carbon emissions, energy consumption and cost have become a significant issue. For instance, European commission (2013) reported that the major environmental concerns associated with lime manufacturing are consumption of a highly amount of energy and major air pollutions. Another report raised same issues and indicated that lime production process is along with generation of toxic elements such as arsenic, lead, mercury, nickel, etc. which put the public health at risk (EPA 2004).

In addition, although the application of lime enhances the engineering properties of soil to a certain extent, there are also some deficiencies. For instance, lime stabilisation has been shown to decrease the plasticity of the soil (Clare and Cruchley 1957) and lead to fragile collapse characteristics in specimens that rapidly lost strength at the time

of failure (Sabry et al. 1996). Therefore, the application of other additives such as fibre along with the lime to reduce its contribution or partial or full replacement of the lime with more environmentally friendly products has been encouraged by many researchers (Cai et al. 2006; Wild et al. 1998; 1999; James et al. 2008; Oti et al. 2014; Yi et al. 2015).

Developments in knowledge have led to the production of new materials and consequently some new by-products. One of the by-products recently considered for use in geotechnical engineering is ground granulated blast furnace slag (GGBFS), which remains after the steel manufacturing process. Application of GGBFS in civil engineering projects is not only cost effective and energy saving but also reduces the carbon emissions and is environmentally friendly (Higgins 2007). Stabilisation clay using GGBFS has been subject of some recent studies (Vakili et al. 2016; Yi et al. 2013). For instance, James et al. (2008), investigated effect of the GGBFS on a lime treated clay and concluded that addition of GGBFS for a fixed proportion of the lime caused an increase in production of the pozzolanic products and greater values of the unconfined compressive strength. In another study, Nidzam and Kinuthia (2010), indicated that application of the GGBFS, improves the engineering properties of the soil including strength, durability and its resistance to swelling. They also highlighted that application of the GGBFS has a lower environmental impact and is more cost effective in compare with other additives when applies as a soil stabiliser. Wild et al. (1999) indicated that the partially substitution of the lime with GGBFS to a certain amount, significantly reduced the sulphate expansion associated with sulphate bearing clay soil.

Some researchers have employed GGBFS along with lime in their studies. For instance, Yi et al. (2015) partially substituted quick lime and hydrated lime with

GGBFS and compared the effect on mechanical and microstructural properties in the stabilisation of marine clay, reporting that the unconfined compressive strength (UCS) of the hydrated lime activated GGBFS was slightly better than for quick lime activated GGBFS.

In another study, Wild et al. (1998) investigated the effect of partial replacement of lime with GGBFS in a clay soil stabilisation including sulphate. They reported that with regard to long-term effects, the stabilisation of clay using more GGBFS and less lime is very effective. When the percentage of GGBFS is lower and lime is higher, the addition of the gypsum is very effective for soil stabilisation. For short-term soil stabilisation, the addition of more GGBFS and less lime with gypsum was more effective due to acceleration of the hydration process.

The aforementioned literature showed that although lime is an effective binder for soil stabilisation especially in pavement area, but the application of lime significantly consumes energy and is accompanied by some environmental impacts and negative mechanical characteristics. Therefore, this study designed to investigate effect of the reduction of lime contribution in clay stabilisation. There is a huge body of literature that investigates the soil's characteristics such as volume changes, UCS and shear strength that highlights the importance of these properties of the soil (Wild et al. 1998; 1999; James et al. 2008; Yi et al. 2013; Vakili et al. 2016). In one example, Cai et al. (2006) highlighted the importance of these characteristics by performing a series of shrinkage, UCS and shear strength tests on a clay treated with lime and fibre. In fact, the variations in the soil's volume cause destructive risks for the structures such as deflection, settlement and damages to foundation (Petry and Little, 2002). Besides, ignorance of the strength characteristics makes a vulnerable structure for the soils against different stresses. Therefore, to figure out effect of the GGBFS addition on the

volume changes, compressive strength and shear strength of a lime treated clay, a series of experimental studies consist of VSS, UCS and RS tests were designed to investigate the effect of partially replacement of the lime with GGBFS. Moreover, some specimens were chosen for SEM and XRD analysis after being tested to understand the governing mechanisms in the specimens' microstructures.

4.3.3. Material Used

The clay kaolinite employed to conduct the tests is commercially known as prestige NY and is supplied by Sibelco a local provider in Western Australia. It contains around 93% kaolinite and roughly 7% quartz (Sibelco 2011) and has a liquid limit (LL) of 58%, a plastic limit (PL) of 31% and a plasticity index of 27 (Purwana 2013), classifying it as a highly plastic soil group. The applied kaolinite has a specific gravity in a range of 2.66 to 2.7 and a pH value from 5.7 to 8.1 (Sibelco 2011). Fig. 4.22 illustrates the particle size distribution (PSD) of the kaolinite and Fig. 4.23 is an SEM micrograph of its structure. The ordinary Portland cement (PC) used had a specific gravity ranging from 3 to 3.4 Mgram/m³ (BGC Cement 2013).

The lime and GGBFS used in this study were purchased from Cockburn Cement and BGC Cement two local suppliers based in Perth, Western Australia. The used alkali GGBFS is a white powder that has a specific gravity in a range of 2.8 to 3.1 and a melting point of 1350°C (BGC Cement 2013). In addition, the employed lime has a specific gravity in a range between 2.1 and 2.3 and a bulk density of 200 to 500 kg/m³ (Cockburn Cement 2012). Fig. 4.24 shows the SEM micrographs of the used GGBFS. Table 4.5 lists the chemical properties of the lime and Table 4.6 revealed the properties of the employed GGBFS.

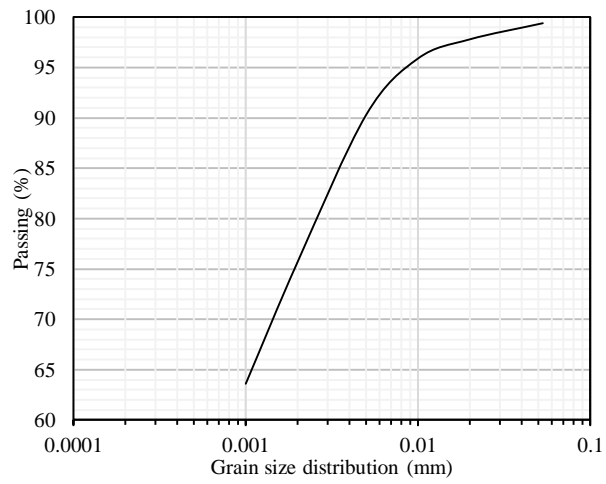


Fig. 4.22. Particle size distribution of kaolinite.

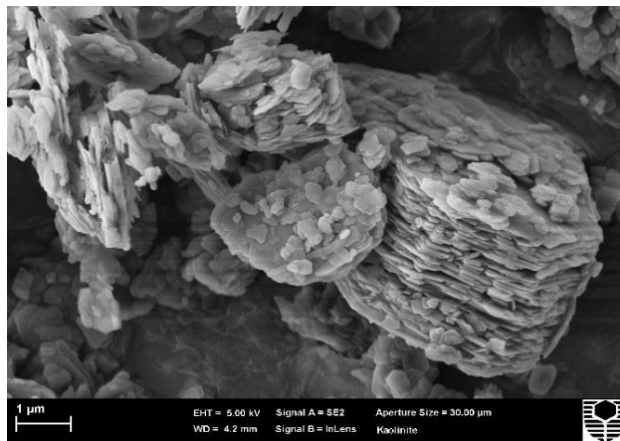


Fig. 4.23. SEM micrograph of the used kaolinite.

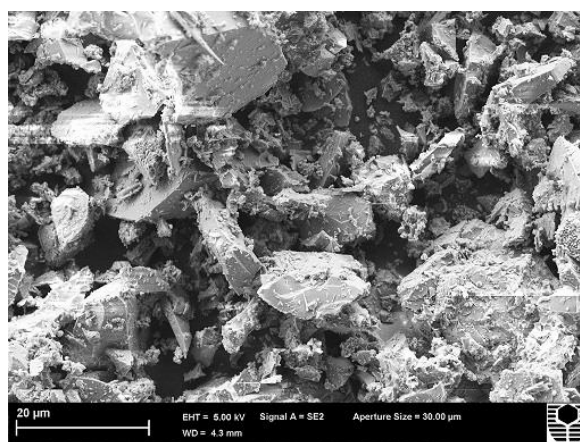


Fig. 4.24. SEM micrograph of the used GGBFS

Table 4.5. The chemical properties of the lime (Cockburn Cement 2012)

Lime composition	Formula	Percentage
Calcium hydroxide	Ca(OH) ₂	80–95%
Magnesium hydroxide	Mg(OH) ₂	0–6%
Crystalline silica	SiO ₂	<1%
Silicon dioxide, quartz	SiO ₂	0–8%

Table 4.6. The chemical properties of the GGBFS used in this study (BGC Cement 2013).

GGBFS composition	Formula	Percentage
Calcium oxide	CaO	30–50%
Silica, amorphous	SiO ₂	35–40%
Aluminium oxide	Al ₂ O ₃	5–15%
Sulphur	S	<5%

4.3.4. Methodology

To determine the effect of partial replacement of lime with GGBFS, two types of experimental study and microstructural study were performed. In the experimental section, three geotechnical laboratory tests including the volumetric shrinkage strain (VSS), unconfined compressive strength (UCS) and ring shear (RS) test were carried out and the microstructure was studied using X-ray powder diffraction (XRD), energy dispersive X-ray spectroscopy (EDS) and scanning electron microscopy (SEM).

4.3.4.1. Volumetric shrinkage Strain Tests

Puppala et al. (2004) proposed a three-dimensional volumetric shrinkage strain test to combat the deficiencies in the conventional linear shrinkage bar test. This method has also been applied by other researchers (Fatahi et al. 2012; Fatahi et al., 2013; Puppala et al. 2013). In this method, the use of a cylindrical specimen means that there is no contact between the mould and specimens after extrusion, making the results more realistic. Moreover, different compaction conditions based on different moisture contents and dry densities can be simulated, which is not possible with the linear shrinkage bar test method (Puppala et al. 2013).

To perform the tests, the materials were mixed in dry mode and thoroughly blended. When a dry uniform mixture was obtained, 75% water by volume was added to the mixture according to the recommendations made by Lorenzo and Bergado (2004), Fatahi et al. (2012a; 2012b), and Fatahi et al. (2013). The prepared mixture was poured into a 100 mm × 50 mm cylindrical mould in different layers and shaken using a vibration machine in order to minimise the trapped air and achieve a uniform sample with the minimum voids possible. The moulds had been lubricated for ease of extrusion before the pouring of the mixture. To help the hydration process and minimise the loss of moisture from the samples, the samples were sealed with caps placed on top of the moulds and left for 24 hours in a temperature-controlled room for bonding (Fatahi et al. 2013).

After a 24 hour bonding period, the specimens were extruded from the moulds and samples were then placed in a water curing bath for 3, 7, 14, 21 and 28 days. In this study, a total of 150 three-dimensional volumetric shrinkage strain tests were performed.

Next, the variations in the diameter and height of each sample were recorded and the total volumetric shrinkage of specimens was calculated. Eq. (4.3.6) was used to calculate the volumetric variations (Fatahi et al. 2013).

$$V = \frac{V_w - V_d}{V_w} \times 100\% \quad (4.3.6)$$

Where V is the total volumetric shrinkage, V_w is the wet volume and V_d is the dry volume of the sample.

In this study, a lime content and GGBFS content of 2, 4 and 6% was added to the clay as specified by Khemissa and Mahamedi (2014) and Wild et al. (1998). In addition, cement at percentages of 5, 10 and 15% with a 1:1 ratio of water was added to each specimen to promote the hydration process and to obtain a satisfactorily workable mixture (Mardani et al. 2015; Fatahi et al. 2013). The prepared samples were cured over five different ageing periods namely 3, 7, 14, 21 and 28 days. Table 4.7 represents a summary of the mix designs for full and partial replacement of the lime with GGBFS for volumetric shrinkage strain tests.

Table 4.7. A summary of the mix design for the volumetric shrinkage strain tests

No.	ID	PC (%)	Lime (%)	GGBFS (%)	Curing time (%)
1	5PC	5	-	-	3, 7, 14, 21, 28
2	5PC-2L	5	2	-	3, 7, 14, 21, 28
3	5PC-4L	5	4	-	3, 7, 14, 21, 28
4	5PC-6L	5	6	-	3, 7, 14, 21, 28
5	5PC-2G	5	-	2	3, 7, 14, 21, 28
6	5PC-4G	5	-	4	3, 7, 14, 21, 28
7	5PC-6G	5	-	6	3, 7, 14, 21, 28
8	10PC	10	-	-	3, 7, 14, 21, 28
9	10PC-2L	10	2	-	3, 7, 14, 21, 28
10	10PC-4L	10	4	-	3, 7, 14, 21, 28
11	10PC-6L	10	6	-	3, 7, 14, 21, 28
12	10PC-2G	10	-	2	3, 7, 14, 21, 28
13	10PC-4G	10	-	4	3, 7, 14, 21, 28
14	10PC-6G	10	-	6	3, 7, 14, 21, 28
15	15PC	15	-	-	3, 7, 14, 21, 28
16	15PC-2L	15	2	-	3, 7, 14, 21, 28
17	15PC -4L	15	4	-	3, 7, 14, 21, 28
18	15PC-6L	15	6	-	3, 7, 14, 21, 28
19	15PC-2G	15	-	2	3, 7, 14, 21, 28
20	15PC-4G	15	-	4	3, 7, 14, 21, 28
21	15PC-6G	15	-	6	3, 7, 14, 21, 28
Partial lime replacement tests					
No.	ID	PC (%)	Lime (%)	GGBFS (%)	Curing time (%)
1	10PC-2L-2G	10	2	2	3, 7, 14, 21, 28
2	10PC -2L-4G	10	2	4	3, 7, 14, 21, 28
3	10PC -2L-6G	10	2	6	3, 7, 14, 21, 28
4	10PC -4L-2G	10	4	2	3, 7, 14, 21, 28
5	10PC -4L-4G	10	4	4	3, 7, 14, 21, 28
6	10PC -4L-6G	10	4	6	3, 7, 14, 21, 28
7	10PC -6L-2G	10	6	2	3, 7, 14, 21, 28
8	10PC -6L-4G	10	6	4	3, 7, 14, 21, 28
9	10PC -6L-6G	10	6	6	3, 7, 14, 21, 28

4.3.4.2. Unconfined Compressive Strength Tests

Lime and GGBFS were mixed at the same percentages used for the shrinkage tests and the 50 mm × 100 mm cylindrical moulds were applied to perform the UCS tests. The methodology and sample preparation procedures were those recommended in ASTM D1633 (ASTM 2007) and by Yi et al. (2015). The specimens were wrapped in plastic bags and cured at three ageing periods of 3, 7 and 14 days in a moisture and temperature controlled room. Table 4.8 shows a summary of the designed and performed UCS tests.

Table 4.8. A summary of the mix design for the unconfined compressive strength (UCS)

No.	ID	PC (%)	Lime (%)	GGBFS (%)	Curing time (%)
1	10PC	10	-	-	3, 7, 14
2	10PC-2L	10	2	-	3, 7, 14
3	10PC-4L	10	4	-	3, 7, 14
4	10PC-6L	10	6	-	3, 7, 14
5	10PC-2G	10	-	2	3, 7, 14
6	10PC-4G	10	-	4	3, 7, 14
7	10PC-6G	10	-	6	3, 7, 14
8	10PC-2L-2G	10	2	2	3, 7, 14
9	10PC-2L-4G	10	2	4	3, 7, 14
10	10PC-2L-6G	10	2	6	3, 7, 14
11	10PC-4L-2G	10	4	2	3, 7, 14
12	10PC-4L-4G	10	4	4	3, 7, 14
13	10PC-4L-6G	10	4	6	3, 7, 14
14	10PC-6L-2G	10	6	2	3, 7, 14
15	10PC-6L-4G	10	6	4	3, 7, 14
16	10PC-6L-6G	10	6	6	3, 7, 14

4.3.4.3. Ring Shear Tests

The effect of partial substitution of lime with GGBFS on the shearing strength of clay was determined by performing a series of ring shear tests. To perform the tests, a Bromhead ring shear apparatus was used with a modified (knurled surface) top bronze porous platen (Meehan et al. 2007). The specimen container had an inner diameter of 70 mm and an outer diameter of 100 mm. The tick top platen had a hole in the top to release air pressure to reduce the impact of wall friction due to soil intrusion, according to the standard method for the torsional ring shear test to determine the drained residual shear strength of cohesive soils [(ASTM D6467 (ASTM 1999))].

In order to prepare the samples, the reconstituted specimens with a moisture content equal to the plastic limit of the mixture (Harris and Watson 1997; Anayi et al. 1989) were kneaded into a 5 mm thick specimen container using a spatula and levelled off below the surface of the one-piece specimen container using a blade. The tests were run at an extremely low shearing rate to avoid generation of excess pore water pressure and the specimens were tested under three normal stresses of 50, 100 and 150 kPa. Table 4.3.5 shows the mix design of samples for this section.

Table 4.9. A summary of the mix design for the ring shear tests

No.	ID	PC (%)	Lime (%)	GGBFS (%)	Normal stress
1	10PC	10	-	-	50, 100, 150
2	10PC-2L	10	2	-	50, 100, 150
3	10PC -4L	10	4	-	50, 100, 150
4	10PC-6L	10	6	-	50, 100, 150
5	10PC-2G	10	-	2	50, 100, 150
6	10PC-4G	10	-	4	50, 100, 150
7	10PC-6G	10	-	6	50, 100, 150
8	10PC-2L-2G	10	2	2	50, 100, 150
9	10PC -2L-4G	10	2	4	50, 100, 150
10	10PC -2l-6G	10	2	6	50, 100, 150
11	10PC -4L-2G	10	4	2	50, 100, 150
12	10PC -4L-4G	10	4	4	50, 100, 150
13	10PC -4L-6G	10	4	6	50, 100, 150
14	10PC -6L-2G	10	6	2	50, 100, 150
15	10PC -6L-4G	10	6	4	50, 100, 150
16	10PC -6L-6G	10	6	6	50, 100, 150

4.3.5. Results and Discussion

4.3.5.1. Volumetric Shrinkage Strain Tests

4.3.5.1.1. Effect of Lime Addition

Fig. 4.25(a) depicts the typical relationship between volumetric shrinkage strain and curing time for different lime contents. The effect of adding lime to the mixture is obvious in comparison with the untreated specimen. The figure shows that there is a gradual decrease in volumetric strain with an increase in curing time. In addition, Fig. 4.25(b) shows the variation in volumetric shrinkage versus lime content after different curing periods. It can be clearly seen that the addition of lime at various percentages reduced the shrinkage capacity of the soil.

There is a systematic mechanism in the shrinkage process that the flaky clay particles with a negative charge on their surface and positive charges at their edges react with the cations in the water, creating a balance in electrical charge. In fact, when the balance between the internal electrochemical force of the soil and water with external stresses and matric suction is broken, shrinkage occurs (Nelson and Miller 1997). Temperature as an external force can break the inter-particle balance and cause the shrinkage.

A decrease in the width of the clay's double layers or substitution of the existing ions by bivalent cations of calcium reduces the volume shrinkage capacity in the lime stabilised clay, however this reduction is negligible (Sivapullaiah et al. 2000). Lambe (1958) noted that the main reason for the reduction in the shrinkage capacity of lime stabilised clay could be the average grain inclination of the flaky clay particles. In fact, parallel-oriented clay grains have a greater volume shrinkage capacity than a clay with a fluctuated/agglomerated particle texture. The rate of fluctuation increases even more with an increase in curing time. Bell (1996) and Cai et al. (2006) have reported the same trend in the shrinkage behaviour of clay after the addition of lime.

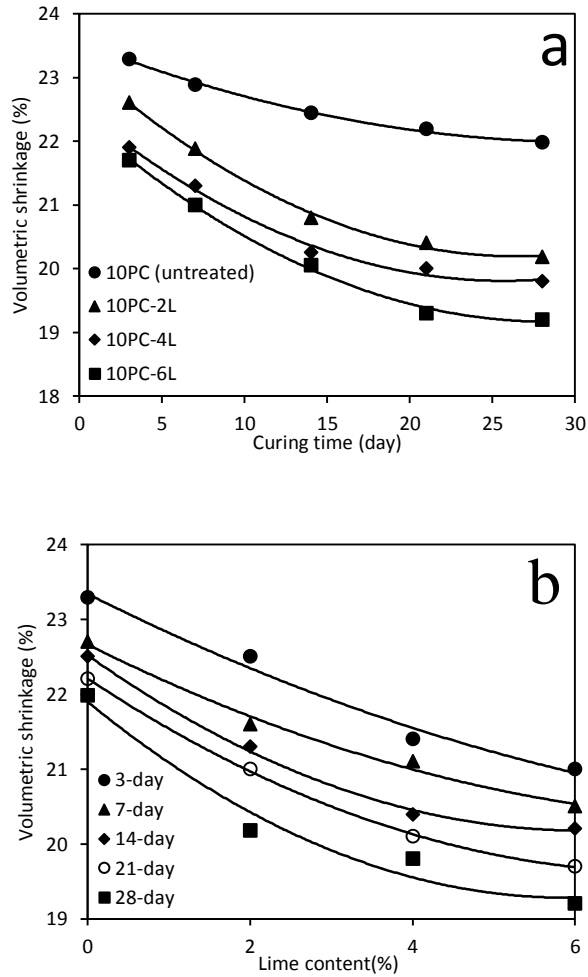


Fig. 4.25. (a) Typical relationship between volumetric shrinkage and curing time for different percentages of lime. (b) Typical relationship between volumetric shrinkage and different percentages of lime after different curing times.

4.3.5.1.2. Effect of GGBFS on Shrinkage

The variations in volumetric shrinkage versus curing time in terms of different percentages of GGBFS content were plotted in Fig. 4.26(a). It can be clearly seen that the addition of GGBFS reduced the volumetric shrinkage capacity. Fig. 4.26(b) also shows the relationship between volumetric shrinkage and GGBFS percentages for different curing periods. It can be seen that the volumetric shrinkage decreased by increasing the curing time.

Puppala et al. (2004) noted that the reduction of shrinkage capacity can be due to an improvement in the tensile strength of the soil. They indicated that internal soil reactions lead to the enhancement of cohesion, increasing the soil's tensile resistance. Addition of GGBFS increases the tensile strength of soil (Gennadii and Ilya 2013), therefore reducing its shrinkage capacity. Fig. 4.27(a) depicts the cracking observed after shrinkage due to a lack of tensile strength. Fig. 4.28(b) shows that the addition of GGBFS to the clay improved the tensile strength of the soil and reduced the cracking.

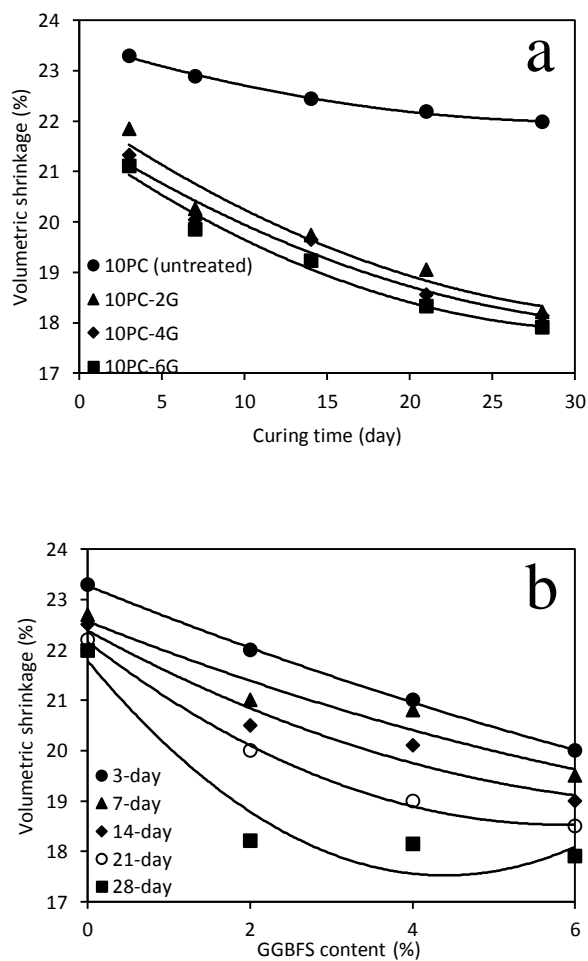


Fig. 4.26. (a) Typical relationship between volumetric shrinkage and curing time for different percentages of GGBFS (b) Typical relationship between volumetric shrinkage and different percentages of GGBFS after different curing periods

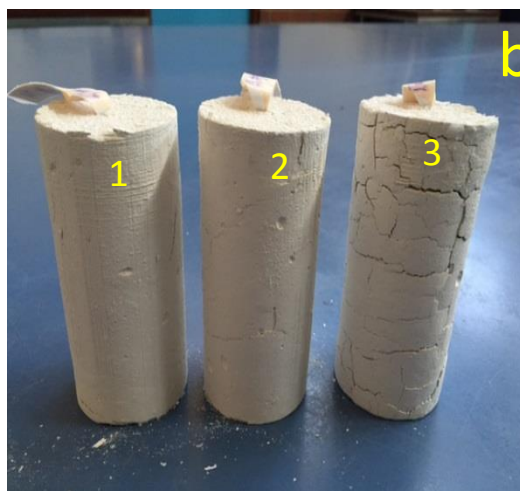
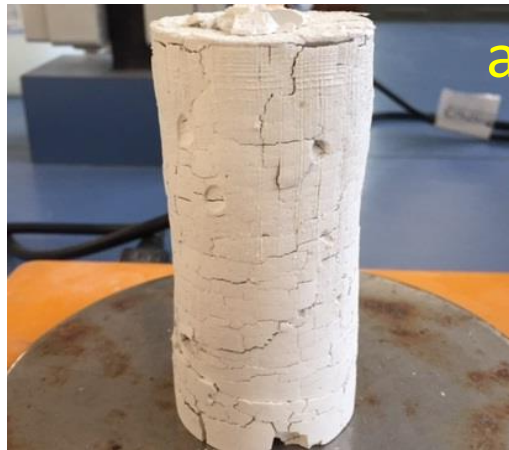


Fig. 4.27. (a) The cracks that developed due to shrinkage in an untreated specimen after 28 days curing (b) Samples (1) 10PC-6G, (2) 10PC-4G and (3) 10PC-2G after 28 days curing, showing the effect of the GGBFS in reducing cracking due to shrinkage

4.3.5.1.3. Effect of Partial Replacement of Lime with GGBFS

Fig. 4.28(a) illustrates the variation in volumetric shrinkage with different percentages of GGBFS mixed with 2% lime, while Fig. 4.28(b) depicts the variation in volumetric shrinkage with different percentages of lime mixed with 2% GGBFS at different curing times.

It can clearly be seen that the addition of GGBFS with a certain amount of lime (2%) decreased the volumetric shrinkage strain in the clay. The rate of shrinkage reduction by the addition of lime with a fixed percentage of GGBFS showed a declining trend, however it was less steep, meaning that the addition of GGBFS is more effective than the addition of lime in reducing the shrinkage behaviour of the soil. In fact, the addition of GGBFS to the specimens, compared with lime, accelerated the production of cementitious crystalline products such as CSH, CAH and CASH and promoted the fluctuation and agglomeration of the soil, consequently reducing the volumetric shrinkage (Obuzor et al. 2012).

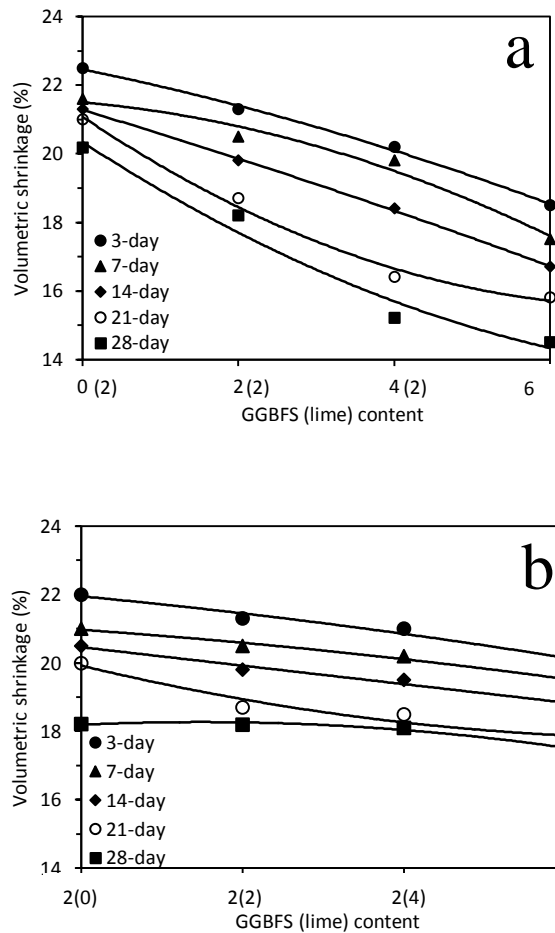


Fig. 4.28. (a) The relationship between volumetric shrinkage and different percentages of GGBFS content and 2% lime for different curing times. (b) The relationship between volumetric shrinkage and different percentages of lime content and 2% GGBFS for different curing times

4.3.5.2. Effect of GGBFS-Lime Ratios on Compressive Strength

Fig. 4.29(a) shows the variations in unconfined compressive strength (UCS) with lime content for different curing periods. As expected, there was a gradual increasing trend with the addition of lime and increase in curing time.

Fig. 4.29(b) shows the relationship between unconfined compressive strength with GGBFS-lime ratios at different curing periods. The results showed that the addition of different percentages of GGBFS to a certain percentage of lime (2%) significantly improved the compressive strength of the specimens. This trend could be attributed to the role of GGBFS in the acceleration of the production of the cementitious crystalline products in the lime stabilised clay specimens.

The effect on the pozzolanic reactions of an increase in curing time is more pronounced. In fact, the calcium ions (Ca^{++}) generated from GGBFS and lime become distributed among the clay flaky particles, promoting the formation of pozzolanic products such as CSH, CAH and CASH (James et al. 2008). This causes an increase in UCS with an increase in curing time. This trend can be accelerated by the addition of higher percentages of GGBFS to the mixture in order to produce more crystalline products and consequently increase the compressive strength (Obuzor et al. 2012).

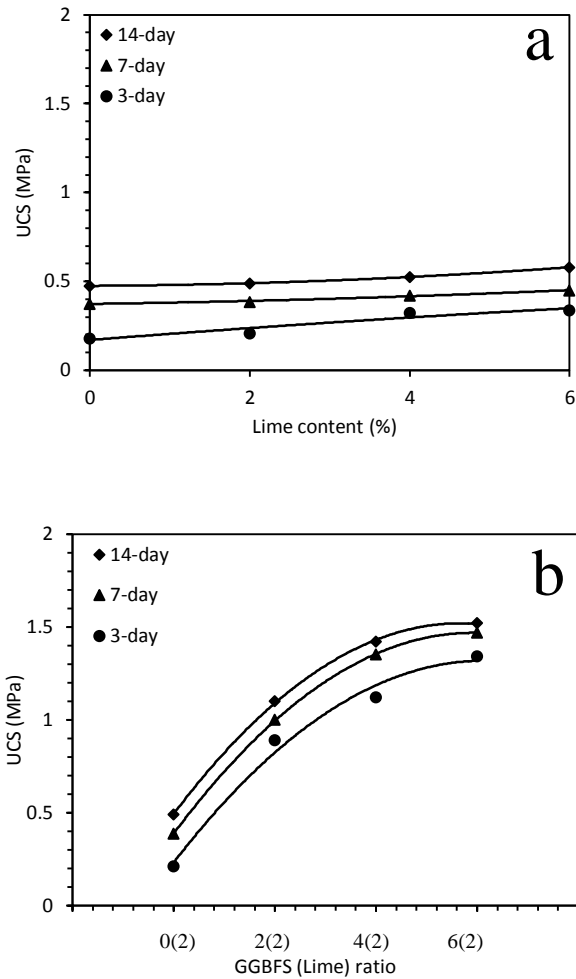


Fig. 4.29. (a) Results for unconfined compressive strength (UCS) in mixtures of clay with different ratios of lime. (b) Results for unconfined compressive strength (UCS) in mixtures of clay with different ratios of GGBFS-lime.

4.3.5.3. Effect of GGBFS-Lime Ratios on Shear Strength

Fig. 4.30(a) depicts the typical results of ring shear tests on lime treated clay and Fig. 4.30(b) illustrates the shear strength for different percentages of GGBFS and 2% lime under different vertical stresses.

As can be seen, the shear strength of the lime treated specimens increased with an increase in lime content and curing time, however the addition of GGBFS to lime resulted in a higher percentage of shear strength. This increasing trend could be

attributed to the pozzolanic reactions occurring during the curing period, generating of the cementitious products that promote bonding and interlocking forces amongst clay grains and consequently leading to greater shear strength. An increase in lime content promoted the production of these cementitious products and increased the strength of the soil, but the addition of GGBFS accelerated the generation of the pozzolanic products and led to an increase in the shear strength (Obuzor et al. 2012).

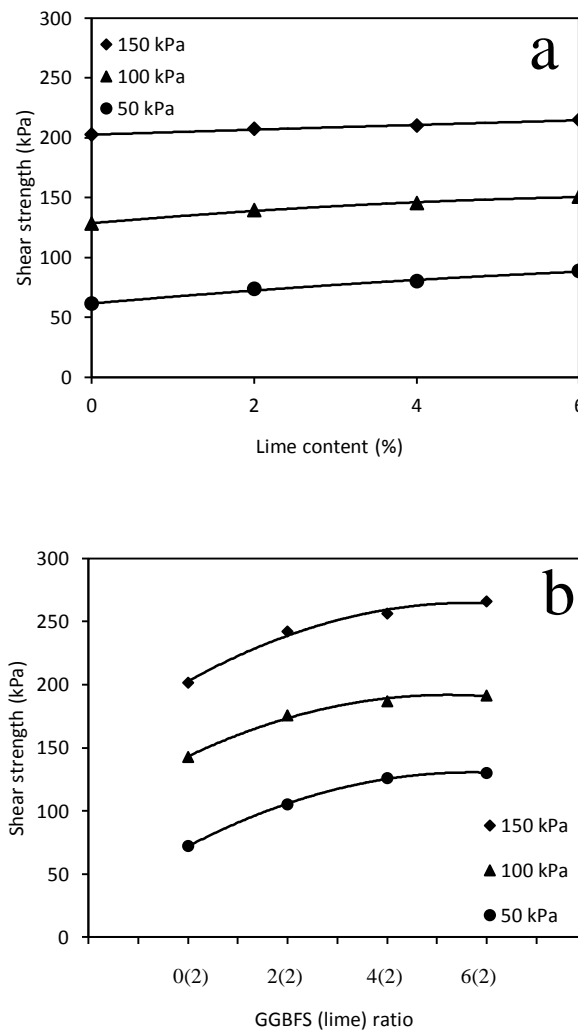


Fig. 4.30. (a) Results of shear strength tests on mixtures of clay and cement with different S/L ratios under 50 kPa normal stress. (b) Results of shear strength tests on mixtures of clay and cement with different S/L ratios under 100 kPa normal stress

4.3.5.4. Microstructural Study

To fully understand the inter-particle reactions of GGBFS and lime mixed with clay, it was necessary to perform a series of micro-analytical studies. In the following sections, SEM/EDS and XRD studies were presented.

4.3.5.4.1. SEM/EDS Characterisation

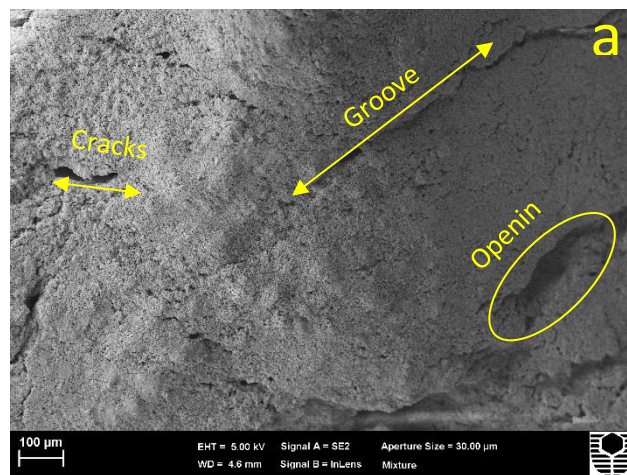
Fig. 4.31(a-d) illustrates a series of typical scanning electron micrograph (SEM) characterisations of a 28-day specimen of clay mixed with 6% GGBFS and 2% lime for a morphological analysis of the reactions occurring amongst the minerals.

A uniform surface with a series of grooves, openings and cracks can be seen in Fig. 4.31(a). This can be attributed to water reduction due to evaporation that increased the porosity and consequently a permeable texture for the soil structure. Fig. 4.31(b-d) shows the porous nature of the mixture from a more detailed micrograph. Yi et al. (2015) indicated that lime and GGBFS mixed clay specimens have a reticulated structure however with less porosity than PC treated clay due to different nature and amount of generated hydration products. The larger-size pores were filled due to hydration reactions and converted to the small-size pores in the specimens of GGBFS-lime mixed with clay.

Similarly, the cracks and grooves were observed in the mixtures of GGBFS-lime mixed with clay by James et al. (2008). They also noted that increasing of the lime proportion to a certain amount of the GGBFS increased the fragility properties of the mixture comparison with lime mixed with clay and increasing the proportion of GGBFS to a constant amount of lime led to generation of more cementitious products and consequently more strength for the mixture. Effect of the mentioned cementitious

products such as CSH, CAH and CASH can be seen in the Fig. 4.31(b-d). Although, the nature and the morphology of the observed cementitious products in Fig. 4.31(d) was similar to that was observed in Fig. 4.31(b-c) that is a fluctuated and gel-like microstructure but an amorphous and fibrous spot of the hydration products was observed in the Fig. 4.31(d) as it can be attributed to the different ratios of the calcium and silicate was produced by cementitious products (Yi et al. 2015).

Fig. 4.31(c) depicted that only a small amount of the needle-like ettringite was generated due to presence of the sulphate (Obuzor et al. 2012). In fact, addition of the GGBFS was led to suppression of the ettringite formation due to increasing the formation of the cementitious products and more density and consequently more strength for the mixture (Wild et al. 1999; Puppala et al. 2003). In other words, progressive substitution of the lime with GGBFS was led to progressive adjustment of the ettringite formation of the mixture (Tasong et al. 1999). The above mentioned conclusions are in coincidence with acquired results in the mechanical properties sections and with XRD analysis in the next section.



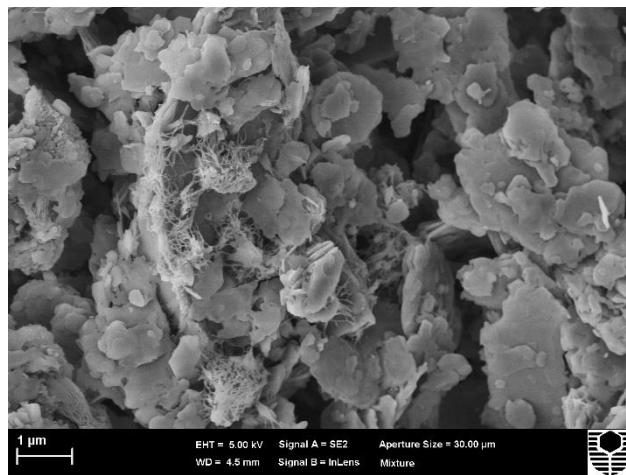
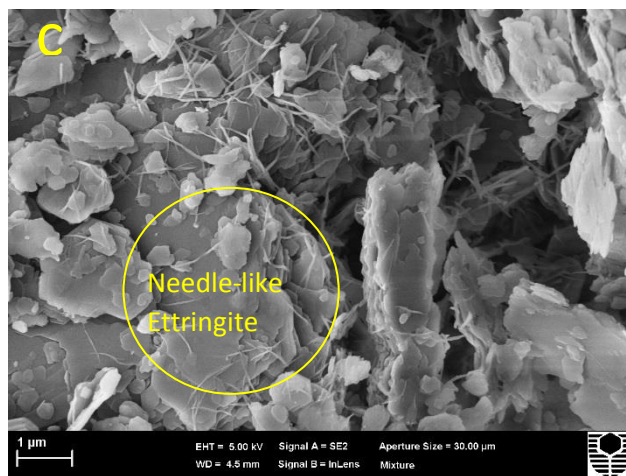
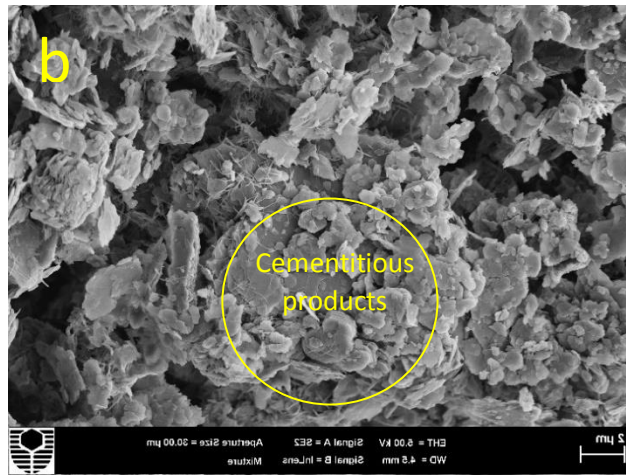


Fig. 4.31. (a) Scanning electron micrograph of a 28 day cured GGBFS mixed with lime at a ratio of (6:2) at a micrograph of 100 µm and (b) scanning electron micrograph of a 28 day cured GGBFS mixed with lime at a ratio of (6:2) showing the formation of cementitious crystalline products after pozzolanic reactions, (c) showing the presence of a small amount of needle-like ettringite, and (d) showing other forms of cementitious material (amorphous and fibrous).

4.3.5.4.2. XRD Analysis

A series of 28-day cured samples were selected to perform the XRD analysis. Fig. 4.32 shows the XRD patterns for untreated soil, clay mixed with 6% GGBFS, clay mixed with 6% lime and clay mixed with GGBFS-lime with a 6:2 ratio. In all patterns, the kaolinite ($Al_2Si_2O_5(OH)_4$) and quartz (Si_2O_4) were common detected minerals presenting the nature of the applied kaolinite. Presence of the halloysite (H) in the acquired xrd pattern of the untreated soil clearly indicates that the employed clay belongs to the kaolinite group.

GGBFS when mixed with clay without any other activator is able to produce only a low amount of the hydration products after a long time curing period (Nidzam and Kinuthia 2010). In fact, when the GGBFS is in a moist condition, it forms a $Al - Si - O$ layer on the surface of its particle. However, the pH of the mixture and OH^- increase due to absorbed H^+ ions by this layer, but it is not sufficient to break the $Al - O$ and $Si - O$ bonds to generate the hydration products and only a small amount of the CSH will be generated after a long time curing time. Therefore, application of the GGBFS is based on the power of its activator for breaking these bonds (Caijun and Day 1993). The analysed pattern for the mixture of the GGBFS with clay presenting formation of the CSH that is due to addition of the PC as an activator.

Ettringite was not observed in the GGBFS mixed with clay pattern as it is an early hydration product generated in GGBFS activation (Nidzam and Kinuthia 2010).

In the XRD pattern of lime mixed with clay the cementitious products were observed. In fact, the CSH gel forms due to reactions of the alumina and silica in the clay structure and water and lime become stronger and binds the soil structure together and

produce a relatively fragile structure (Arabi and Wild 1989). This strength increased by addition of the curing period as the Al_2O_3 and SiO_2 progressively dissolve in reactions to generate the CSH (Croft, 1964). In addition, trace of the ettringite was observed indicating the presence of the sulphate in the clay (Nidzam and Kinuthia 2010).

No trace of the portlandite was detected in the mixture of the GGBFS-lime mixed with clay as the pozzolanic reactions and activation of the GGBFS consumed it (Nidzam and Kinuthia 2010). GGBFS is able to produce only a low amount of the cementitious products by its own. Addition of the lime led to provision of the required alkali for activation of the GGBFS and generating the hydration products and increasing the production of the cementitious products and consequently increasing the strength of the mixture (Higgins 1998). The stronger reflections from cementitious products was seen in the GGBFS-lime treated clay than in specimens treated only with GGBFS or lime (see Fig. 4.32), confirming the results of the shrinkage and strength tests.

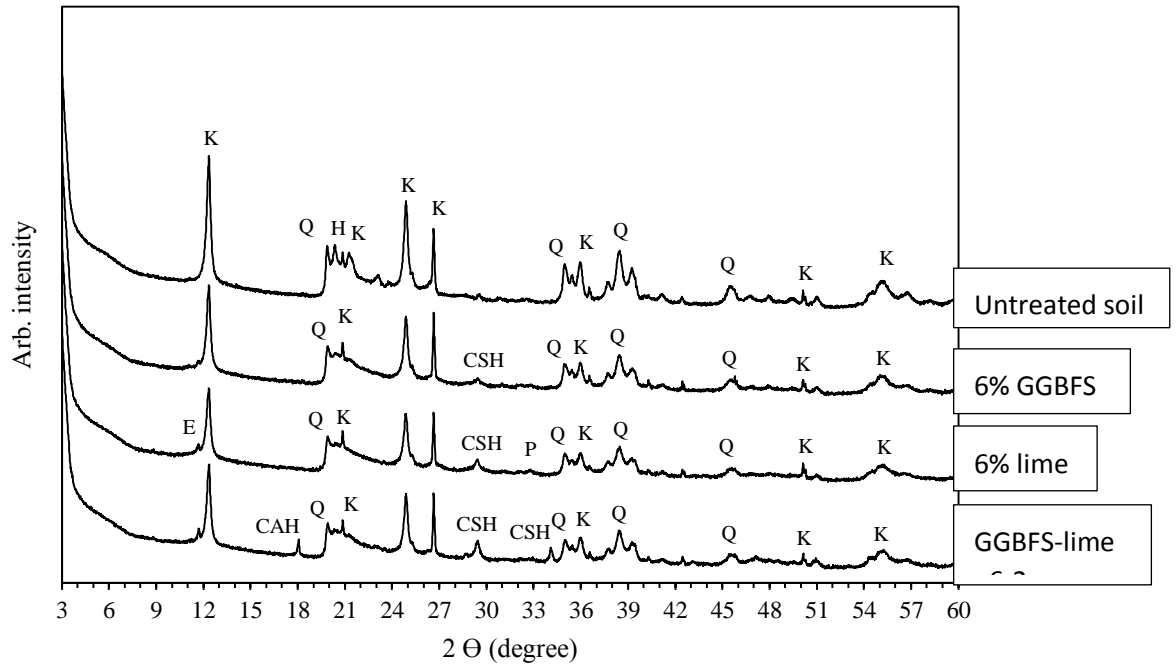


Fig. 4.32. XRD crystalline phase analysis of untreated clay, 28 day cured clay treated with 6% GGBFS, 6% lime and GGBFS-lime at a ratio of (6:2). The abbreviations are: Q-quartz, K-kaolinite, CSH-calcium silicate hydrate, CAH-calcium aluminate hydrate, P-portlandite, E-ettringite. H-halloysite

4.3.6. Conclusions

In this study, a total of 246 shrinkage, unconfined compressive strength and ring shear tests were performed to investigate the effect of lime mixed with GGBFS on the engineering properties of clay at different curing periods. The following conclusions can be drawn from the results of the tests performed:

1. Application of GGBFS as a by-product material led to a reduction in the cracks generated due to shrinkage by increasing the tensile strength of the soil.
2. Addition of GGBFS to a certain amount of lime mixed with clay significantly reduced the shrinkage capacity of the clay compared to the lime mixed with clay, due to accelerated generation of cementitious products leading to greater

fluctuation and agglomeration and consequently less shrinkage behaviour. In addition, the pozzolanic reactions that occurred showed a positive effect in reducing volumetric shrinkage.

3. Addition of GGBFS to a certain amount of lime significantly improved the unconfined compressive strength and shear strength properties of the soil compared with lime mixed with clay mixtures, due to the acceleration of the production of cementitious products such as CSH and CAH and the pozzolanic reactions occurring during the curing time.
4. The microstructural analysis results showed that the mixture of GGBFS and lime produced cementitious crystalline products and a small quantity of ettringite, as seen in the SEM micrographs. Furthermore, the intense effect of hydration products such as CSH, and CAH was observed in the XRD patterns of the GGBFS-lime mixture.

Part 4

Shear Strength Characteristics of Over-consolidated Clay Treated with GGBFS

4.4. Shear Strength Characteristics of Over-consolidated Clay Treated with GGBFS

4.4.1. Abstract

Ground granulated blast furnace slag (GGBFS) is an industrial by-product material that its application in ground improvement projects is a well-established practice. This study is focused on investigating the effect of GGBFS on drained shear strength characteristics of an over-consolidated clay by performing a series of direct shear tests. The tests are conducted on untreated clay and clay treated with 3%, 5%, and 7% GGBFS (by dry weight of the soil). The results depicted that increasing the GGBFS contents increased the mobilised peak and residual shear strength of the tested clays. In addition, the specimens containing GGBFS showed a greater and more contradictive peak due to sudden breakage of the cementitious bonds. The cohesion (c) values in fully softened and residual conditions showed an increasing trend upon increasing the GGBFS contents and curing time. However, in the residual condition, it dropped to a very low range ($2.8 \leq c_r \leq 8$ kPa). Further investigation showed that friction angle (ϕ) and slope (m) values slightly decreased by increasing the GGBFS content and curing time in both peak and residual condition.

4.4.2. Introduction

Each year 1.4 billion tonnes production of Portland cement (PC) is responsible for 5% of carbon dioxide emission in the atmosphere ([Higgins 2007](#)). Application of an environmental-friendly alternative for PC helps to reduce the energy use, emission of carbon dioxide and promotes sustainable development. Numerous studies have investigated substitution effect of ground granulated blast furnace slag (GGBFS) with

PC (Keramatikerman et al. 2016; Vakili et al. 2016; James et al. 2008; Wild et al. 1998). The GGBFS is a by-product material that is manufactured from iron blast furnaces in steel companies. This product consists of silicates and alumino-silicates of lime and has potential cementitious reactivity similar to PC (Nidzam and Kinuthia 2010; Lee 1974).

In general, fully softened and residual shear strength are considered as the drained shear strength of the clay (Stark et al. 2005). The residual shear strength applies to clayey slopes and shearing zones. The fully softened corresponds to the situation after an over-consolidated clay has absorbed the maximum amount of water and reached the equilibrium condition (Stark et al. 2005). It has been indicated by Skempton (1970) that fully softened shear strength is equal to the drained peak shear strength of a consolidated specimen in a normal condition.

To study stability analysis of the slopes and landslides, evaluation of the shear strength of the clay is one of the most crucial factors as it presents the largest uncertainty (Stark et al. 2005). The fully softened shear strength, residual shear strength, cohesion and friction angle are effective parameters to study drained shear strength characteristics of a slope.

Although, many studies have been conducted to investigate the effect of GGBFS on mechanical characteristics of the soil, behaviour of clay treated with GGBFS in an over-consolidated condition is a gap in the literature. Therefore, this study aims to investigate drained shear strength characteristics of a type of Western Australian local clay after treatment with GGBFS by performing a series of direct shear tests.

4.4.3. Materials Used

The used clay was collected from Rockingham area a suburb located in southern part of Perth, Western Australia. To collect the soil, 1 meter of the top soils were removed, and the clay was collected. The clay after the collection was left in an oven at a temperature of 105 ± 5 °C for 24 hours to be dried. Next, it was manually crushed and subjected to the particle size analysis [ASTM D4221 ([ASTM 2011b](#))], index properties [ASTM D4318 ([ASTM 2010](#))], X-ray powder diffraction (XRD) and the scanning electron microscopic (SEM) tests. The results of the particle size distribution (PSD) and index properties tests are summarised in Table 4.10. According to the unified soil classification system (USCS) [ASTM D2487 ([ASTM 2011a](#))], the used soil is classified as a high plasticity clay (CH). The XRD analysis showed that the used clay belongs to the kaolinite clay group and mainly contains kaolinite, some nontronite and montmorillonite minerals. The scanning electron microscopy (SEM) studies showed that the used clay has a polygonal flaky topography with formed small pores and grooves on its surface [See Fig. 4.33]. The GGBFS used in this study was purchased from BGC cement, a local supplier in Perth. GGBFS has a specific gravity in the range of 2.8-3.1 and a melting point of 1350° C ([BGC Cement 2013](#)). Fig. 4.34 shows the SEM micrograph of the used GGBFS.

Table 4.10. Particle size distribution (PSD) and index properties of the Rockingham clay used to perform the tests

Rockingham clay properties			
Soils properties		Sieve analysis	
Description	value	PSD (mm)	Passing (%)
G_s	2.81	0.0001	1
LL	88	0.0004	10
PL	37	0.008	25
PI	51	0.01	35
C_c	1.69	0.04	55
C_u	6.25	0.075	75
-	-	0.15	100

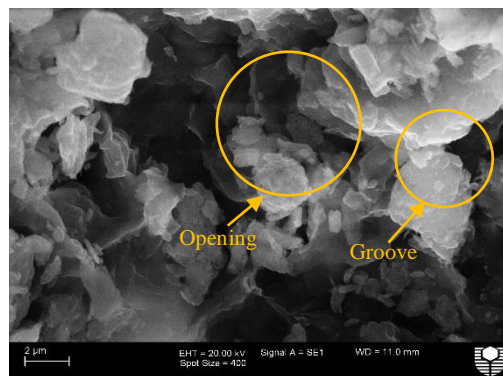


Fig. 4.33. Scanning electron microscopic (SEM) image of the used Rockingham clay.

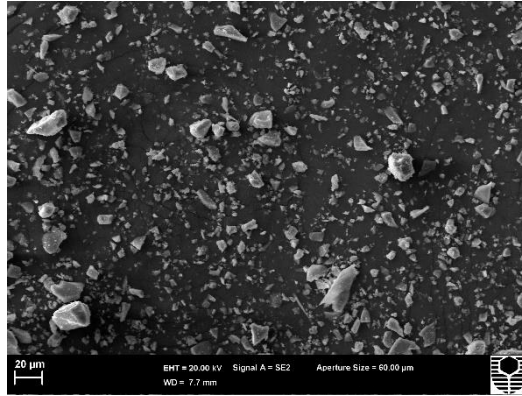


Fig. 4.34. Scanning electron microscopic (SEM) image of the used GGBFS.

4.4.4. Methodology

To investigate the effect of GGBFS on drained shear strength characteristics of the over-consolidated clay, a series of direct shear tests were designed and conducted. A digital Impact direct shear device was employed to perform the test. To prepare the mixtures, GGBFS was mixed with clay in the percentages of 3%, 5%, and 7% (by dry weight of the soil) in dry condition and thoroughly mixed. When a uniform dry mixture was attained a moisture content equal to optimum moisture content (OMC) was added to each mixture acquired from the standard compaction proctor test [ASTM D698 (ASTM 2012a)]. The mixture was completely blended until a uniform texture was obtained. A square 60 x 60 mm steel mould was used to prepare the specimens. The mixtures were placed in the mould in three layers and compacted with a specific energy according to ASTM D698 (ASTM 2012a) until the targeted maximum dry density (MDD) was acquired. To over-consolidate the specimens, the mould containing specimen after preparation were mounted on the direct shear device and subjected to an incremental loading of 1, 5, 10, 20, 40, 80, 160, 320, 640 and 1280 kPa according to the ASTM D3080 (ASTM 2011d). The specimens were then unloaded in the reverse order of loading. The loading and unloading of specimens was conducted in a fully

inundate condition. Each loading and unloading stage took 24 hours for completion. When the last stage of unloading completed and swelling of the specimen stopped, the water contained inside the direct shear carriage was discharged, and the specimen was extruded from the mould. The specimens were wrapped in a sealed plastic bag and left in a moist and temperature controlled room to be cured for 7, 14, and 28 days. It has been indicated that the residual shear strength condition in an over-consolidated clay with a flattened-like appearance of clay minerals occurred after a major consecutive plane of discontinuity (Askarani and Pakbaz 2016; Terzaghi et al. 1996). Therefore, the specimens were sheared in a series of discontinued shearing displacements. Initially, the test was performed on the intact specimen until 5 mm displacement was observed (Askarani and Pakbaz 2016). The mould containing the specimen brought out carefully from the carriage and cut off from the sheared line which was placed in the middle of upper and lower halves. The test continued by connecting the disconnected upper and lower halves and sheared until another 5 mm displacement. The recent step was repeated until the final residual state of the specimen recorded. In fact, this step is the maximum mobilised shear strength in two consecutive sequences, and are almost equal. The specimens were sheared under an effective normal stress (σ'_n) of 50, 100, 200, and 400 kPa. Table 4.11 shows the experimental program designed to perform the tests. The specimens were sheared at a very slow shearing rate of 0.018 mm/min to avoid generation of the excess pore water pressure.

Table 4.11. Experimental program to perform the tests in this study

No.	ID	GGBFS (%)	Normal load	Curing time
1	C	0	50, 100, 200, 400	7
2	C-3%G	3	50, 100, 200, 400	7
3	C-5%G	5	50, 100, 200, 400	7
4	C-7%G	7	50, 100, 200, 400	7
5	C-7%G	7	50, 100, 200, 400	14, 28

4.4.5. Results and Discussion

4.4.5.1. Effect of GGBFS Contents

Fig. 4.35 shows typical discontinued graphs for variation of shear strength versus displacement (τ - ε) for untreated clay and clay treated with 3%, 5%, and 7% GGBFS under 100 kPa effective normal stress (σ'_n) after 7 days curing time. As can be seen from Fig. 4.35(a) for untreated clay specimen, it took a longer time and distance (6 sequences) to reach the residual condition in comparison with GGBFS treated specimens (5 sequences). The untreated clay has a fully softened shear strength (τ_{fs}) of 79 kPa at the first step and a final residual shear strength (τ_r) of 46 kPa at the final step. The recorded fully softened and residual shear strength of 3% GGBFS treated specimens increased to 105 and 57 kPa as can be seen from Fig. 4.35(b). A similar trend was recorded for fully softened and residual shear strength when the GGBFS contents of the soil increased to 5% and 7% [see Fig. 4.35(c, d)]. This increase was in the range of $128 \leq \tau_{fs} \leq 142$ kPa and $65 \leq \tau_r \leq 74$ kPa for fully softened and residual shear strength values respectively. Fig. 4.36 shows a typical continued graph for variation of the shear strength versus displacement for different GGBFS contents under 100 kPa effective normal stress which acquired from discontinued graphs. As

can be seen, the untreated specimen has a less contractive peak in comparison with GGBFS treated specimens whereas, the GGBFS treated specimens showed more dilative peaks. This behaviour might be attributed to the addition of GGBFS that caused the formation of the cementitious products amongst soil particles. In GGBFS treated specimens, due to sudden breakage of the cementitious bonds that created amongst particles, the recorded peaks are more distinct in comparison with the untreated clay ([Askarani and Pakbaz 2016](#)). The clay particles in GGBFS treated specimens have a lower capability to absorb water due to cementitious reactions amongst clay and GGBFS grains. Therefore, the capability of swelling for GGBFS treated specimens is less than that of untreated specimens, and they have lower dilations.

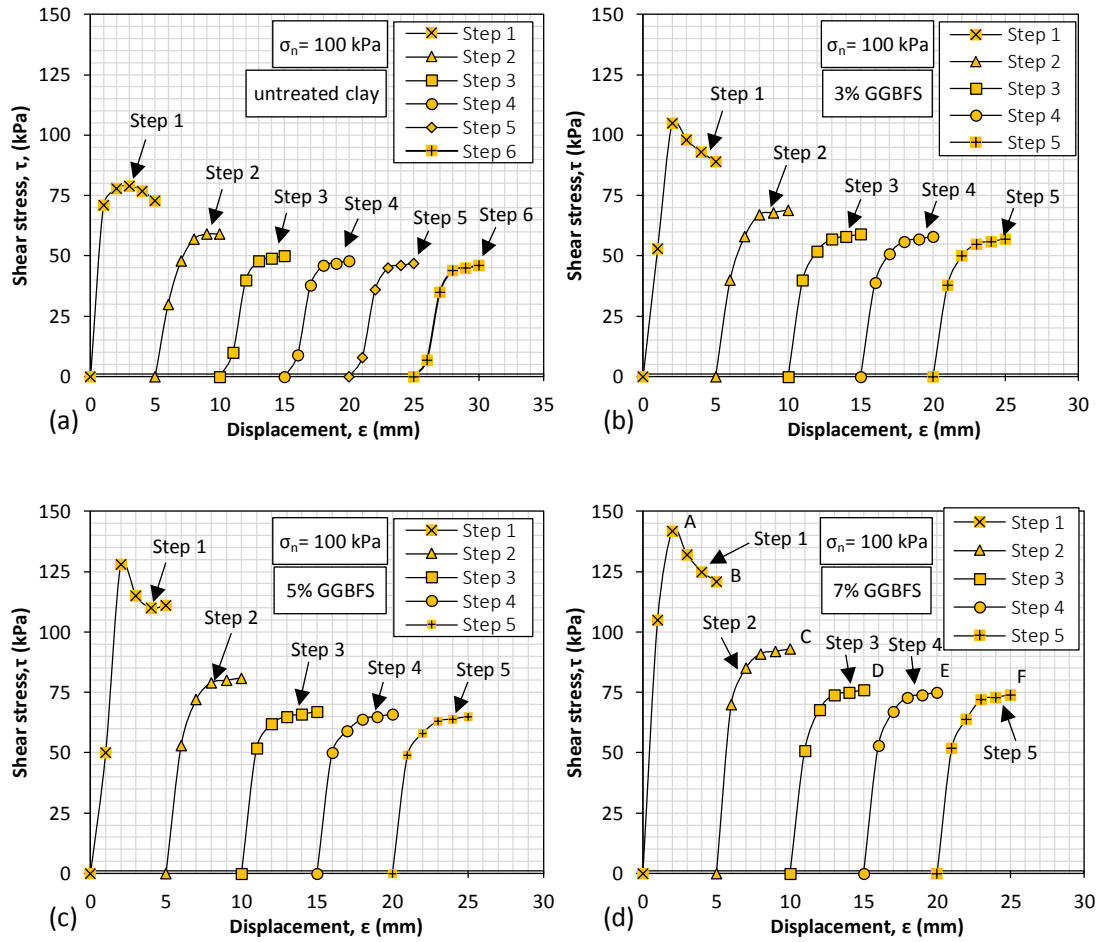


Fig. 4.35. Typical discontinued graphs for variation of shear stress versus displacement (τ - ϵ) under 100 kPa effective normal stress for (a) untreated clay; (b) clay treated with 3% GGBFS; (c) clay treated with 5% GGBFS; (d) clay treated with 7% GGBFS.

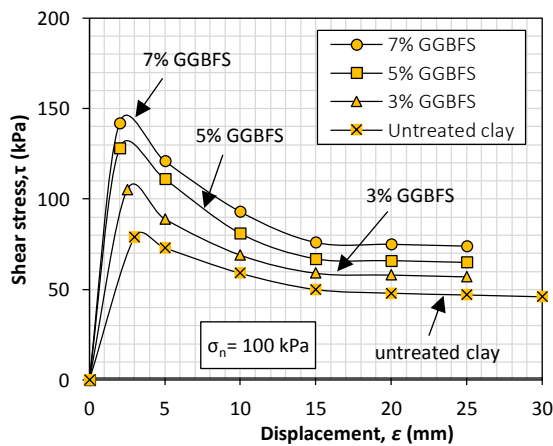


Fig. 4.36. A typical graph for variation of shear stress versus displacement (τ - ϵ) under 100 kPa effective normal stress acquired from discontinued graphs

4.4.5.2. Effect of Effective Normal Stress (σ'_n)

Fig. 4.37 shows the failure envelopes for untreated and GGBFS treated specimens under 50, 100, 200, and 400 kPa effective normal stresses (σ'_n) in fully softened and residual conditions. As can be seen in both figures, the computed failure envelopes have a non-linear relation due to the generation of the cementation bonds. The failure envelope for fully softened shear strength showed more distinct peaks as can be seen in Fig. 4.37(a). The fully softened shear stress values for 7% GGBFS treated specimens were the highest and in the range of $158 \leq \tau_{fs} \leq 331$ kPa under 50 and 400 kPa effective normal stress respectively whereas, the fully softened shear strength of the untreated specimens was at the lowest and in the range of 103 to 267 kPa under 50 and 400 kPa effective normal stress. However, the failure envelopes of the untreated and GGBFS treated specimens were non-linear but they showed more dilative trend as shown in Fig. 4.37(b). Similar to fully softened condition, the 7% GGBFS treated specimen had the highest values in the range of $52 \leq \tau_r \leq 152$ kPa under 50 and 400 kPa effective normal stress (σ'_n) and untreated specimens had the lowest values of the residual shear strength (i.e., $28 \leq \tau_r \leq 121$ kPa under 50 and 400 kPa effective normal stress respectively).

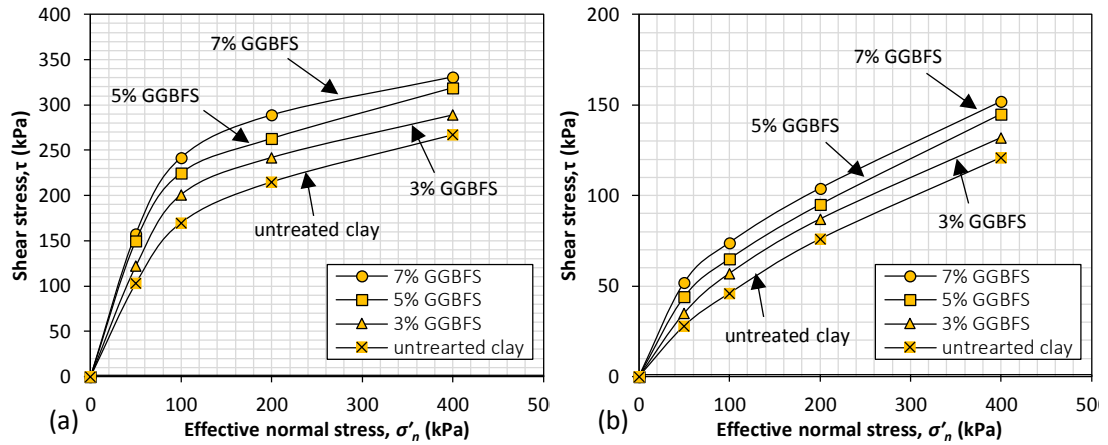


Fig. 4.37. Failure envelope for untreated and GGBFS treated clay specimens (a) fully softened; (b) residual.

Terzaghi et al. (1996) proposed Eq. (4.4.1) to calculate drained shear strength of an over-consolidated clay.

$$\tau_p = \sigma'_n \tan \varphi. [OCR]^{1-m} \quad (4.4.1)$$

Where τ_p = intact mobilised shear strength; σ'_n = effective normal stress; OCR = over-consolidation ratio; φ = internal friction angle; m = slope. The Eq. (4.4.1) indicates that the drained shear strength of an over-consolidated clay is greater than the normally consolidated clay by multiplying the $[OCR]^{1-m}$ parameter. The m value in each specimen is a factor of normal stress and curvature of the failure envelope. Fig. 4.38 shows variation of logarithm fully softened shear strength versus logarithm effective normal stress ($\log \varepsilon_p - \log \sigma'_n$) for untreated and GGBFS treated specimens. The m values were computed for each specimen based on those graphs. Generally, the m value of a normally consolidated clay is 1 and this value is 0 for the intact or the cemented clay (Terzaghi et al. 1996; Mesri and Abdel-Ghafar 1993). As can be seen from the figures, the m value for 7% GGBFS treated specimen is 0.494, while this value increased to 0.50, 0.509 and 0.514 for 5%, 3% GGBFS treated and untreated

specimens respectively. The cohesion (c_{fs}) values also, were computed according to the presented failure envelopes. It can be seen that addition of GGBFS increased the c_p values of the specimens. For instance, while this value for untreated clay was 10 kPa, this value increased to 23, 35, and 40 kPa for 3%, 5%, and 7% GGBFS treated specimens. The increase in c_p values of the GGBFS treated specimens attributed to promotion of the cementitious bonds amongst soil particles.

Table 4.12 shows a summary of the computed m_r and c_r values in residual condition. As can be seen from the table, increasing the GGBFS content caused a slight decrease for m_r parameter. For instance, the untreated soil has a m_r value of 0.27 whereas this value decreased to 0.268, 0.262, and 0.257 by addition of 3%, 5%, and 7% GGBFS to the specimens. The cohesion (c_r) values showed an increasing trend; however, in a much lower range in comparison with fully softened condition. For instance, the c_r value for untreated specimen was 2.8 kPa, whereas this value increased to the range of $4 \leq c_r \leq 8$ kPa when 3% to 7% GGBFS was added to the specimens.

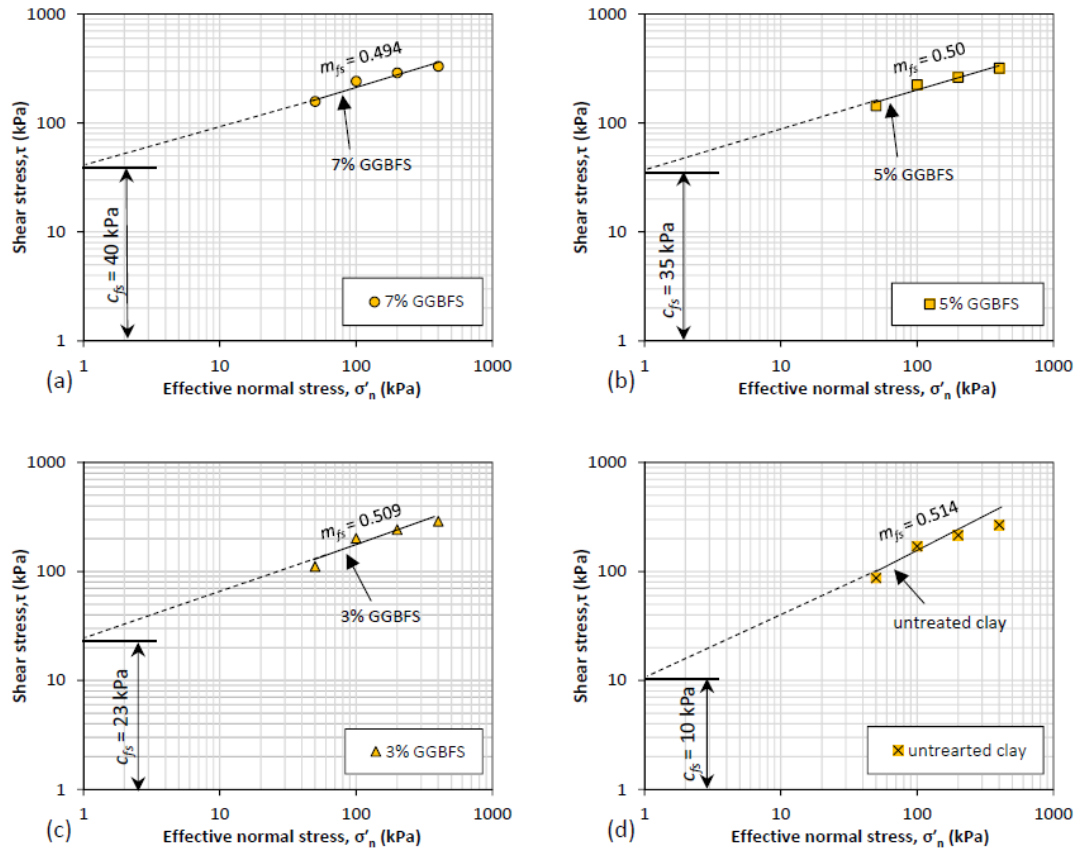


Fig. 4.38. Failure envelope shows drained shear strength characteristics in fully softened condition for (a) 7% GGBFS treated specimens; (b) 5% GGBFS treated specimens; (c) 3% GGBFS treated specimens; (d) untreated specimens.

Table 4.12. A summary of drained fully softened and residual shear strength characteristics of untreated clay and clay treated with different GGBFS contents.

Parameter	Untreated clay	3% GGBFS	5% GGBFS	7% GGBFS
Cohesion, c_{fs} (kPa)	10	23	35	40
Friction angle, ϕ_{fs} (degree)	27.2	27	26.6	26.3
Slope, m_{fs}	0.514	0.509	0.500	0.494
Cohesion, c_r (kPa)	2.8	4	6	8
Friction angle, ϕ_r (degree)	15.1	15.0	14.68	14.41
Slope, m_r	0.27	0.268	0.262	0.257

4.4.5.3. Effect of Curing Time

To investigate the effect of curing time on GGBFS treated over-consolidated clay, the specimens containing 7% GGBFS were selected and cured for 7, 14, and 28 days. The observed fully softened, and residual shear strength curves were similar to those reported in the previous section in terms of contraction and dilation. Increase in both fully softened and residual shear strength values of the GGBFS treated specimens can be attributed to the generation of the pozzolanic reactions amongst GGBFS and clay particles that caused the production of more hydration products and accordingly led to a higher value of shear strength (Vakili et al. 2016).

Table 4.4.4 shows a summary of drained shear strength characteristics of untreated clay and clay treated with 7% GGBFS after 7, 14, and 28 days curing time. As can be seen from the table, cohesion (c_p) values of the specimens increased by increasing the curing time. For instance, this value was in the range of $40 \leq c_{fs} \leq 49$ kPa and $8 \leq c_r \leq$

13.6 kPa for fully softened and residual shear strength of the GGBFS treated specimens after 7 to 28 days curing time. Conversely, friction angles showed a decreasing trend in both fully softened and residual conditions. For instance, friction angle was in the range of $25.7^\circ \leq \phi_{fs} \leq 26.3^\circ$ and $13.9^\circ \leq \phi_r \leq 14.4^\circ$ for 7% GGBFS treated specimens after 28 to 7 days curing time.

Table 4.13. A summary of drained fully softened and residual shear strength characteristics of untreated clay and clay treated with 7% GGBFS at 7, 14, and 28 days curing time

Parameter	Untreated clay	7 days curing (days)	14 days curing (days)	28 days curing (days)
Cohesion, c_{fs} (kPa)	10	40	44	49
Friction angle, ϕ_{fs} (degree)	27.2	26.3	26	25.7
Slope, m_{fs}	0.514	0.494	0.487	0.481
Cohesion, c_r (kPa)	2.8	8	10.2	13.6
Friction angle, ϕ_r (degree)	15.1	14.41	14.09	13.87
Slope, m_r	0.27	0.257	0.251	0.247

4.4.6. Conclusions

A series of direct shear tests were performed on reconstituted specimens of the Rockingham clay to investigate the effect of GGBFS addition on drained shear strength characteristics of the clay in the over-consolidated condition. The following conclusions can be drawn from the results;

- Increasing the GGBFS contents of the specimens caused the formation of contradictive peaks for GGBFS treated specimens and a dilative peak for the untreated specimen. This behaviour was attributed to sudden breakage of cementitious bonds of the GGBFS treated specimens.
- The drawn failure envelope curves for untreated and GGBFS treated specimens showed a non-linear trend. This trend was more distinct especially for GGBFS treated specimens where production of the hydration products was promoted.
- The fully softened cohesion (c_{fs}) and residual cohesion (c_r) values increased by increasing the GGBFS contents and curing time, however, the friction angle (ϕ_{fs} , ϕ_r) and slope (m_{fs} , m_r) slightly decreased by increasing the GGBFS contents and curing time in both fully softened and residual conditions. The cohesion values in residual conditions had a very low range (i.e., $2.8 \leq c_r \leq 8$ and $2.8 \leq c_r \leq 13.6$ kPa).
- Increasing the curing time of the GGBFS treated specimens caused generation of the pozzolanic hydration products and increased the fully softened and residual shear strength values.

4.5. CHAPTER CONCLUSIONS

A series of comprehensive preliminary experimental studies conducted on the representative additives in order to evaluate their effectiveness on improvement of the mechanical behaviour of soil, and to select the most effective additives to conduct the liquefaction analysis in the next chapters. For investigating the effect of reinforcement techniques, the sawdust and recycled tyre were selected, and a series of 1-D consolidation and rigid-wall hydraulic conductivity tests were conducted to investigate their effect on mechanical behaviour of the soil. The lime was selected as the representative of the non-environmental friendly chemical additives to investigate its effect on mechanical behaviour of the soil by performing a series of volumetric shrinkage, unconfined compressive strength (UCS), and ring shear tests. Finally, the GGBFS was selected as the representative for the environmental-friendly chemical binders to investigate its effect on mechanical behaviour of the soil by performing a series of direct shear tests on over-consolidated clay. In addition, in order to have a complete understanding of the response of the intended materials, the experimental analysis has been conducted on sand mixed with 5% bentonite and the experimental analysis on the effect of lime and GGBFS has been conducted on two types of clayey soils since the maximum hydration and pozzolanic reactions occurred in a clayey type of soil.

The first part of this chapter investigated the effect of sawdust addition on hydraulic conductivity and compressibility of the sand-bentonite (SB) mixture by performing a series of falling head hydraulic conductivity and 1-D consolidation tests. The results showed that the SB mixture has a hydraulic conductivity of 5.23×10^{-10} m/s, and addition of 2%, 5%, and 10% sawdust caused a reduction in the range of 3.5×10^{-10} , 2.9×10^{-10} , and 2.13×10^{-10} for hydraulic conductivity values respectively. In the next

stage of analysis, investigations showed that the control backfill mixture has a hydraulic conductivity in the range of $1.51 \times 10^{-10} \leq k_{theory} \leq 4.70 \times 10^{-10}$ under $24 \leq \sigma'_n \leq 1280$ kPa effective overburden pressure when computed based on Terzaghi consolidation theory, and addition of sawdust caused a reduction in the range of $8.50 \times 10^{-11} \leq k_{theory} \leq 2.50 \times 10^{-10}$ m/s for the mixtures. The measured k_f and computed k_{theory} values showed a good agreement at low effective overburden pressure. In continue the analysis showed that addition of sawdust caused a reduction for the coefficient of consolidation (c_v) in both Casagrande and Taylor methods. Finally, the investigations showed that addition of sawdust has no impact on compression index (C_i) and consequently on rigidity of the sawdust amended mixtures. Furthermore, it was revealed that the swelling index (C_s) decreased by addition of the sawdust in a very low range.

The second part of this study investigated the effect of powdered recycled tyre (PRT) and crumbed recycled tyre (CRT) addition on hydraulic conductivity and consolidation characteristics of the sand-bentonite (SB) mixtures. Analysis on deformation characteristics showed that the addition of PRT and CRT to the SB backfills mixtures increased the settlement characteristics of the specimens. In addition, investigations showed that the addition of PRT and CRT to the SB backfill mixtures increased the compression index (C_i) and swelling index (C_s) of the specimens. The coefficient of consolidation (c_v) values calculated using the Casagrande and Taylor methods showed a good agreement between recorded ranges and trends. Furthermore, it was revealed that the addition of the PRT and CRT increased the c_v values of the specimens. The hydraulic conductivity values computed using the Terzaghi consolidation theory (k_{theory}) incremented by increasing the PRT

and CRT contents of the specimens. In addition, the rigid-wall hydraulic conductivity tests showed an increase after the addition of PRT and CRT contents.

In third part of this chapter, a series of shrinkage, unconfined compressive strength and ring shear tests were performed to investigate the effect of fully or partially replacement of GGBFS with lime on the engineering properties of clay at different curing periods. The analysis showed that increasing the replacement of the GGBFS with lime led to a reduction in the cracks generated due to shrinkage by increasing the tensile strength of the soil. Furthermore, the results showed that the replacement of the GGBFS to a certain amount with lime significantly reduced the shrinkage capacity of the clay compared to the lime mixed with clay, due to accelerated generation of cementitious products leading to greater fluctuation and agglomeration and consequently less shrinkage behaviour. In addition, the pozzolanic reactions that occurred showed a positive effect in reducing volumetric shrinkage. The results showed that the addition of GGBFS to a certain amount of lime significantly improved the unconfined compressive strength and shear strength properties of the soil compared with lime mixed with clay mixtures, due to the acceleration of the production of cementitious products such as CSH and CAH and the pozzolanic reactions occurring during the curing time, and the microstructural analysis results showed that the mixture of GGBFS and lime produced cementitious crystalline products and a small quantity of ettringite, as seen in the SEM micrographs. Furthermore, the intense effect of hydration products such as CSH, and CAH was observed in the XRD patterns of the GGBFS-lime mixture.

In the final part, a series of direct shear tests were performed on reconstituted specimens of the clay to investigate the effect of GGBFS addition on drained shear strength characteristics of the clay in the over-consolidated condition. The results

showed that increasing the GGBFS contents of the specimens caused the formation of contradictive peaks for GGBFS treated specimens and a dilative peak for the untreated specimen. This behaviour was attributed to sudden breakage of cementitious bonds of the GGBFS treated specimens. The drawn failure envelope curves for untreated and GGBFS treated specimens showed a non-linear trend. This trend was more distinct especially for GGBFS treated specimens where production of the hydration products was promoted. The fully softened cohesion (c_{fs}) and residual cohesion (c_r) values increased by increasing the GGBFS contents and curing time, however, the friction angle (ϕ_{fs} , ϕ_r) and slope (m_{fs} , m_r) slightly decreased by increasing the GGBFS contents and curing time in both fully softened and residual conditions. The cohesion values in residual conditions had a very low range (i.e., $2.8 \leq c_r \leq 8$ and $2.8 \leq c_r \leq 13.6$ kPa). Increasing the curing time of the GGBFS treated specimens caused generation of the pozzolanic hydration products and increased the fully softened and residual shear strength values.

The analysis on the compressibility and hydraulic conductivity of the recycled tyre added specimens in the second part of the chapter showed that the addition of recycled tyre is not effective to reduce the compressibility and hydraulic conductivity of the soil. In addition, the conducted analysis on compressibility and hydraulic conductivity of sawdust added specimens showed that the addition of sawdust is relatively effective to reduce the deformation and the hydraulic conductivity of the soil. Hence, their application is not recommended to improve the mechanical characteristics of the soil. However, the analysis of the effect of lime on mechanical characteristics of the clay showed that the application of lime is effective to improve the mechanical behaviour of the soil, its application is accompanying with some technical deficiencies such as generation of cracks and it was recommended the lime to be fully or partially replaced

with the GGBFS. In the final part of the study, the analysis showed that the shear strength of the specimens increased by increasing the GGBFS contents of the specimens. Based on the acquired results in this chapter for the GGBFS, and the abundancy and the cost effectiveness of the GGBFS it is recommended that the GGBFS to be used to conduct the experimental analysis on improvement of the liquefaction strength in the next stage. In addition, FA has been selected as another environmental chemical additive to conduct the analysis and confirmation of the results.

Chapter 5

Monotonic Behaviour of Sand-FA Mixture

CHAPTER INTRODUCTION

This chapter investigates the effect of FA on the monotonic liquefaction of sand by performing a series of undrained monotonic triaxial compression tests. The investigations have been conducted on the effect of FA contents, initial relative density, initial mean effective stress, and curing periods and the results have been presented and analysed. This chapter does not investigate the effect of GGBFS on monotonic liquefaction behavior of sand since this study already has been conducted by Sabbar et al. ([2017](#)).

5. Monotonic Behaviour of Sand-FA Mixture

5.1. Abstract

Liquefaction is one of the most disastrous phenomena in the world and mitigation of its destructive impacts is a big challenge. Fly ash (FA) is a by-product additive and has hydration and pozzolanic characteristics similar to Portland cement (PC) and has a potential of application in ground improvement projects. This study investigates the effect of FA addition on liquefaction resistance of sand by conducting a series of undrained monotonic triaxial compression tests. The effect of four FA contents (i.e., 0, 2, 4, and 6%), three initial mean effective stresses (i.e., 50, 70, and 90%), and three initial relative densities (i.e., 20, 40, and 60%) were investigated. In addition, the effect of two curing periods of 14 and 28 days were evaluated on selected specimens and the results were presented. The analysis of the effect of FA contents showed that the specimens with a greater FA contents have a higher ultimate deviatoric stress (q_u). This behavior was attributed to the filled existing micro pores amongst soil particles by FA which reduced the pore water pressure build-up. The investigation of the effect of initial mean effective stress showed that the FA added specimens tested under a greater initial mean effective stress have a lower ultimate deviatoric strength value. This was attributed to the suppression of dilatancy and consistent with critical state of soil. The investigation on effect of initial mean effective stress showed that increasing the initial mean effective stress is effective to increase the ultimate deviatoric strength of the soil. The results showed that the densification is more effective in FA added specimens as these specimens showed a greater q_u value in all relative densities than the untreated soil. The investigation of the effect of curing time on FA added specimens showed that the specimens with a greater curing period have a greater ultimate deviatoric strength.

5.2. Introduction

Application of chemical admixtures to increase the strength characteristics of the soil is a common approach in ground improvement. Previous studies reported on effectiveness of the additives such as Portland cement (PC) and lime to increase the strength characteristics of the soil, however these materials are expensive and not environmental-friendly. There are some by-product materials remain from different industries such as steel manufacturing which have a hydration and pozzolanic characteristic similar to PC and lime. Not only these materials are cheap and cost-effective but also their application is environmental friendly as it helps in reduction of the carbon foot print. Fly ash (FA) is a by-product material with hydration characteristics remains from process of fired coal in power plants. This study aims to investigate the effect of FA addition on liquefaction mitigation of the soil.

The application of fly ash (FA) in the ground improvement area has been reported on by previous researchers in the literature ([Keramatikerman et al 2017b](#); [Horpibulsuk et al. 2011](#); [Prabakar et al. 2004](#) amongst other). Fly ash is a pozzolanic material and is a product which remains after processing in electrical power plants. This by-product additive is effective at improving the mechanical behaviour of the soil such as swelling, controlling the volume change, and increasing the compressibility ([Horpibulsuk et al. 2009](#)). Fly ash increases the reactive surfaces of the soil grains and causes an increase in production of hydration and pozzolanic reactions amongst soil particles. These characteristics show that fly ash could be a good potential replacement for Portland cement (PC) ([Horpibulsuk et al. 2009](#)).

The liquefaction behaviour is triggered when a saturated soil substantially loses its strength due to the abrupt generation of pore water pressure when soil is subjected to

undrained monotonic or cyclic loadings (Schofield and Wroth 1968; Kramer 1996). Many investigations have been conducted to mitigate the disastrous impacts of liquefaction. For instance, Keramatikerman et al. (2017b) investigated the effect of fly ash on cyclic liquefaction behaviour of the soil and indicated that fly ash is effective in improving liquefaction behaviour of the soil. In another example, Sabbar et al. (2017) investigated the effect of slag addition on the liquefaction behaviour of sand mixture and indicated that slag is effective in improving the liquefaction behaviour of the sand.

5.3. Materials Used

The sand was sourced from south of Perth metropolitan area, Western Australia. The sieve analysis was conducted on the used sand based on ASTM C136 (ASTM 2014b). The results as can be seen from Fig. 5.1 showed that it has a uniformity coefficient of (C_u) and a coefficient of curvature (C_c) of 2.5 and 1.19 respectively. This sand is a poorly graded soil (SP) based on the Unified Soil Classification System (USCS) [(ASTM D2487, (ASTM 2011a)], and has a specific gravity (G_s) of 2.67. The X-ray powder diffraction (XRD) investigations revealed that quartz (Q) is the main constituent of the used sand. Fig. 5.2 shows the results of XRD analysis on the used sand. In addition, a scanning electron microscopy (SEM) image of the used sand was shown in Fig. 5.3. The used fly ash (FA) was sourced from a local supplier in Perth, Western Australia (Flyash Australia 2016). The XRD analysis showed that quartz (Q), Mullite (Mu), and hematite (H) are the main constituent minerals of the used FA as can be seen from Fig. 5.3. Furthermore, the specific gravity of the used FA was 3.1. The conducted SEM analysis on the used FA showed that the FA has well-rounded particles. Fig. 5.4 shows the results of SEM imaging on used FA.

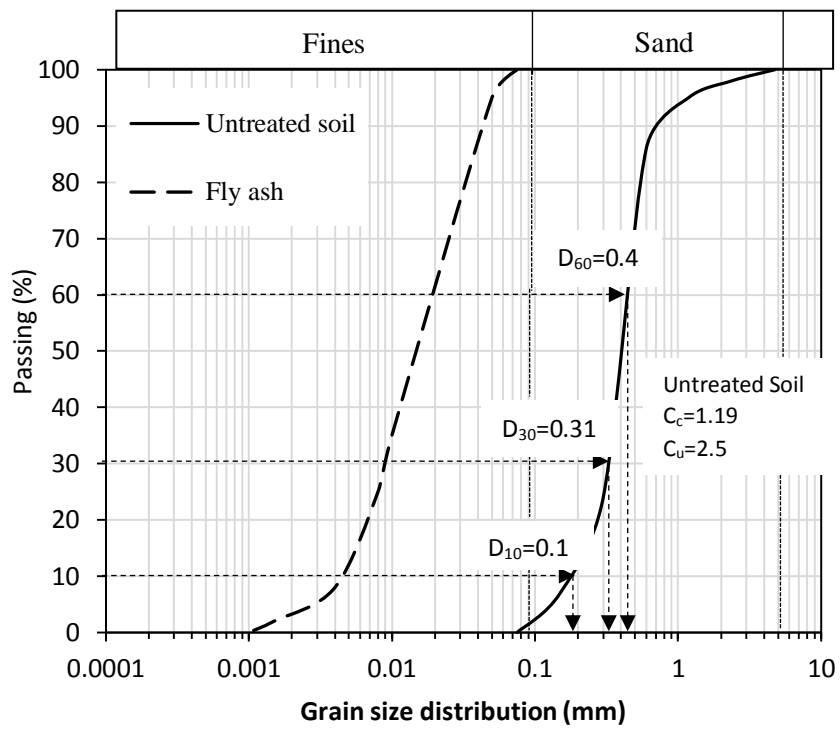


Fig. 5.1. Particle size distribution of used materials

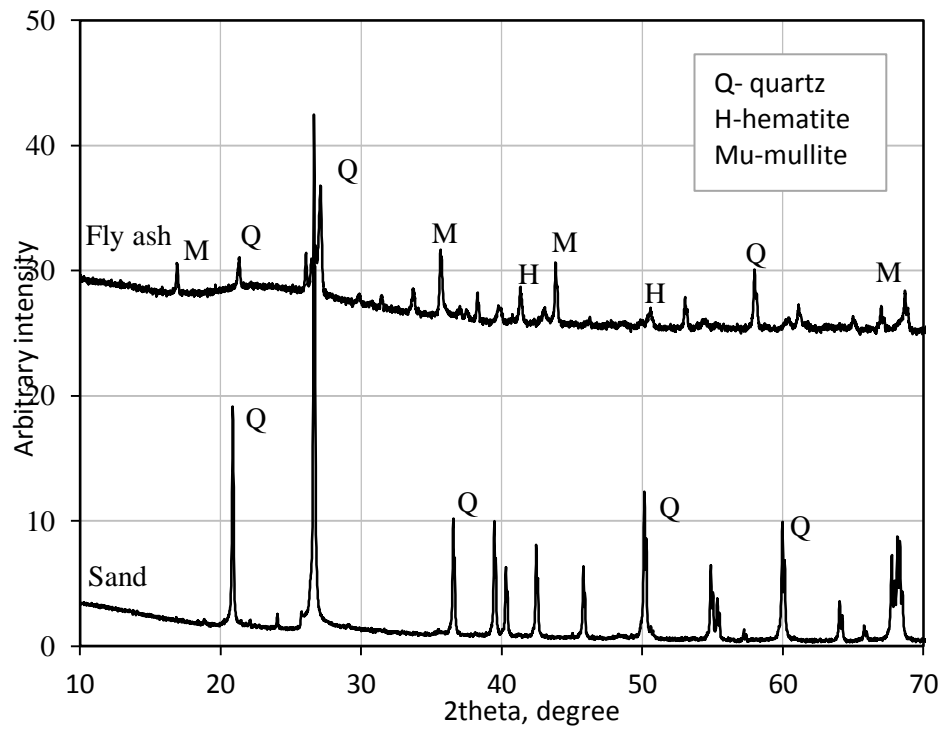


Fig. 5.2. X-ray powder diffraction (XRD) analysis of used sand and FA

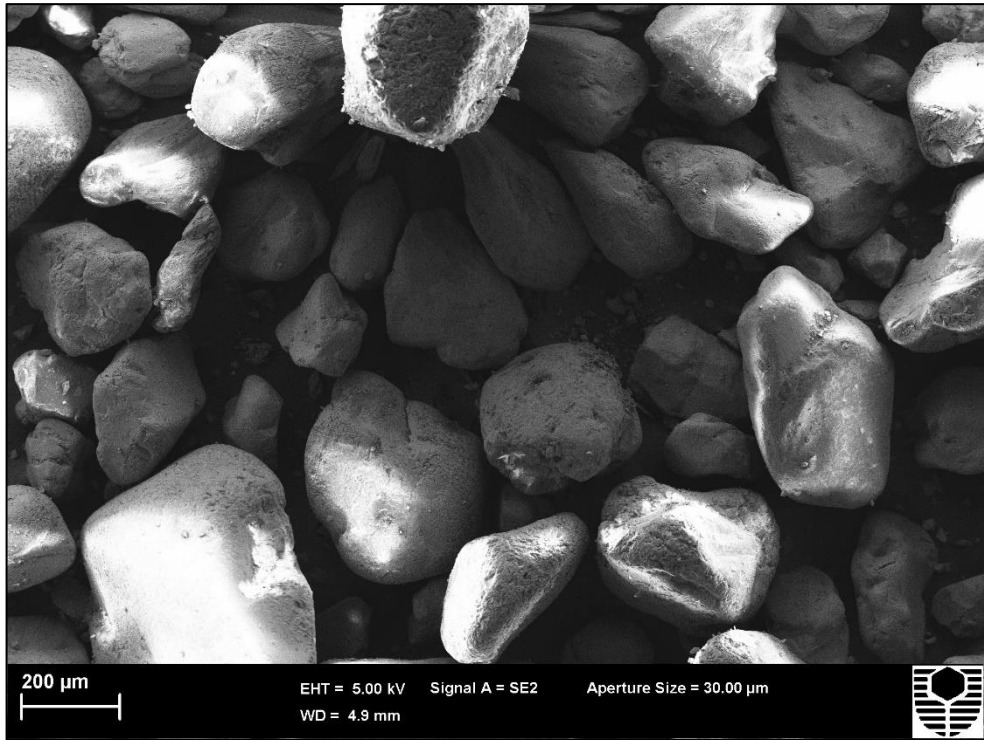


Fig. 5.3. Scanning electron microscopic (SEM) of used sand

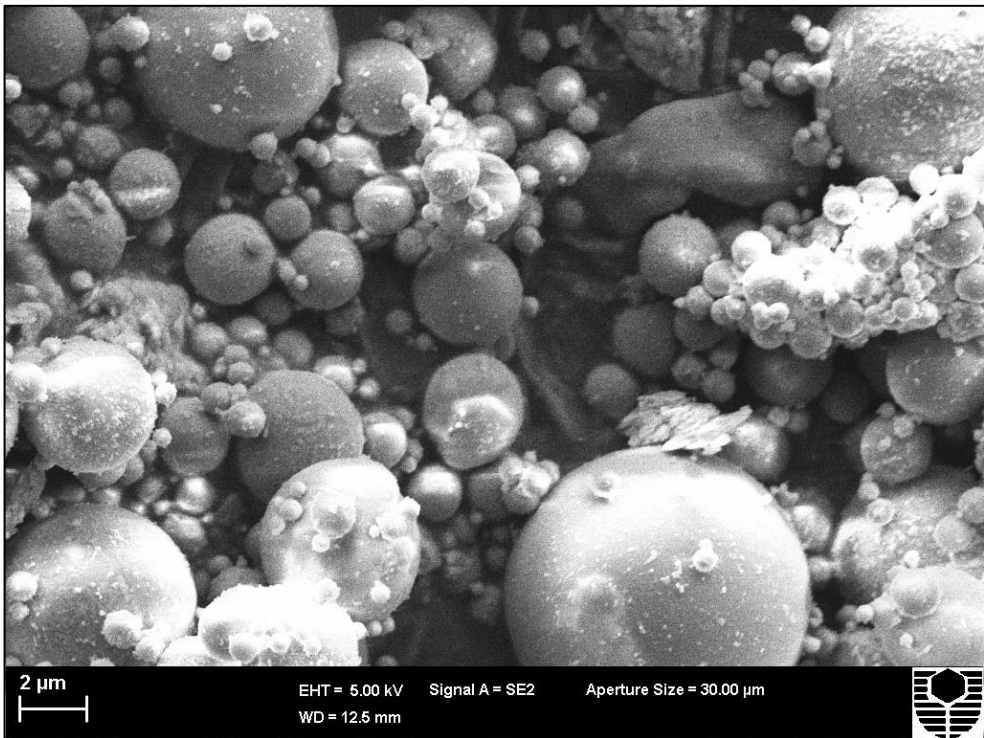


Fig. 5.4. Scanning electron microscopic (SEM) of used FA

5.4. Specimen Preparation and Triaxial Testing

In this study, a series of undrained monotonic triaxial compression tests were conducted according to ASTM D7181 (ASTM 2011e) by means of an automated triaxial device (Bishop and Wesley 1975). The specimens with 62.5 mm diameter and 125 mm height were prepared by moist tamping method, which is proposed as the under compaction method by Ladd (1978). Four FA contents of 0, 2, 4, and 6% were used to investigate the effect of FA contents on sand. To prepare the mixtures, initially, the desired amount of FA was added into the soil and thoroughly mixed, then water was added according to the optimum moisture content (OMC) of each mixture acquired from standard proctor tests. Each mixture was compacted in five layers into a cylindrical split mould until the desired height was obtained based on the maximum dry density (MDD). To investigate the effect of curing time, the specimens after preparation were cured for 14 and 28 days periods in a moisture and temperature controlled room. After completion of the sample preparation, the triaxial testing procedure initiated and water was injected through the sample until a Skempton value of ≥ 0.95 was recorded, and the saturation stage completed. Then, the samples isotropically were consolidated until the initial mean effective stress of 50, 70, or 90 kPa. The post-consolidation void ratio (e_p) of each specimen was recorded according to the pre-consolidation void ratio (e_0) and the occurred volumetric strain during consolidation stage. Table 5.1 shows the test program used to conduct the tests.

Table 5.1. Experimental program and mixtures characteristics

No.	Test ID	FA content (%)	D_r	D_{rp}	p' (kPa)	Curing time (day)	B -Value
1	S1	-	20	21.6	50	-	0.95
2	S2	-	20	22.1	70	-	0.96
3	S3	-	20	22.5	90	-	0.95
4	S4	-	40	41.5	50	-	0.95
5	S5	-	60	61.4	50	-	0.95
6	SF1	2	20	21.6	50	-	0.95
7	SF2	2	20	22.1	70	-	0.96
8	SF3	2	20	22.5	90	-	0.95
9	SF4	2	20	21.6	50	14	0.95
10	SF5	2	20	21.6	50	28	0.95
11	SF6	2	40	41.5	50	-	
12	SF7	2	60	61.4	50	-	
13	SF8	4	20	21.6	50	-	0.95
14	SF9	4	20	22.1	70	-	0.95
15	SF10	4	20	22.5	90	-	0.95
16	SF11	4	20	21.6	50	14	
17	SF12	4	20	21.6	50	28	
18	SF13	6	20	21.6	50	-	0.95
19	SF14	6	20	22.1	70	-	0.96
20	SF15	6	20	22.5	90	-	0.96
21	SF16	6	20	21.6	50	14	
22	SF17	6	20	21.6	50	28	

5.5. Triaxial Test Results

5.5.1. Effect of FA Contents

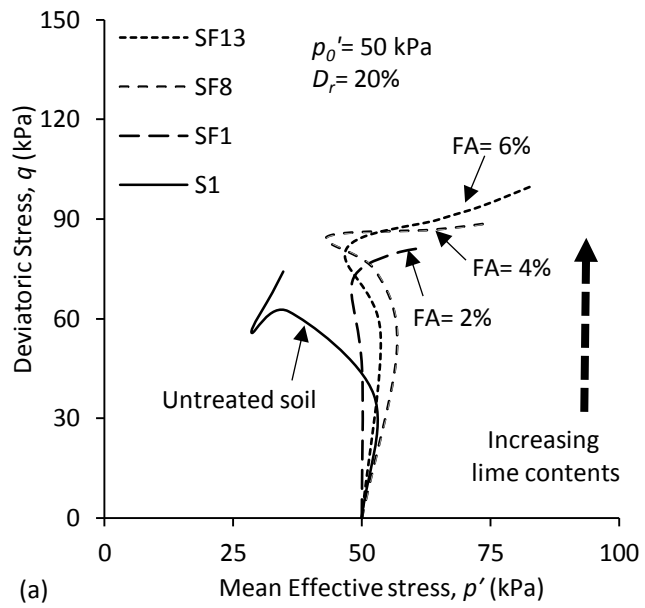
Deviator stress (q) and mean effective normal stress (p') in triaxial tests were computed using Eq. (5.1) and (5.2) respectively.

$$q = \sigma'_1 - \sigma'_3 \quad (5.1)$$

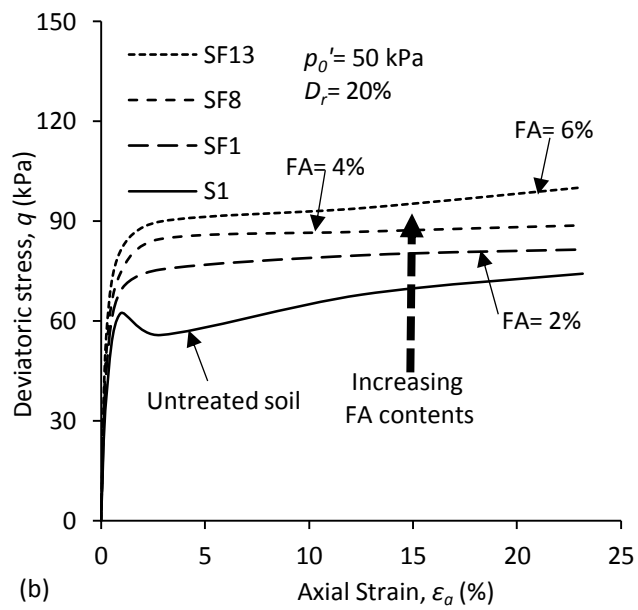
$$p' = \frac{(\sigma'_1 + 2\sigma'_3)}{3} \quad (5.2)$$

Where σ'_1 = effective major principal stress; and σ'_3 = effective minor principal stress. Fig. 5.5 shows the typical stress-strain behaviour for untreated soil and FA treated specimens with an initial relative density of 20% under an initial mean effective stress (p') of 50 kPa. It is seen from the figure that the untreated soil (i.e., S1) has a contractive behaviour until a deviatoric stress of 56 kPa at around 1% axial strain, then dilated and reached the ultimate deviatoric stress (q_u) of 74 kPa after around 20% axial strain. The increasing trend of the excess pore water pressure for this specimen is aligned with recorded behaviour for the variation of the deviatoric stress and mean effective stress. The untreated soil also shows a limited liquefaction.

Addition of FA into the specimens changed the behaviour of the soil from semi-contractive to fully dilative and a greater deviatoric stress value. For instance, addition of 2% FA, caused an ultimate deviatoric stress of 81 kPa to be recorded for 2% FA treated specimen (i.e., SF1). Addition of 4% FA into the sand increased the ultimate deviatoric stress of the specimen even more. For instance, a peak deviatoric stress of 89 kPa was recorded when the specimen was mixed with 4% axial strain. Similar trend was recorded when the specimen was mixed with 6% FA. For instance, an axial deviatoric stress of 100 kPa was recorded when 6% FA was added into the specimens. In fact, addition of FA filled the micropores which exist between the soil particles and reduced the generation of the pore water pressure. This may be the main reason for increasing the ultimate deviatoric stress and reducing the pore water pressure for FA added specimens.



(a)



(b)

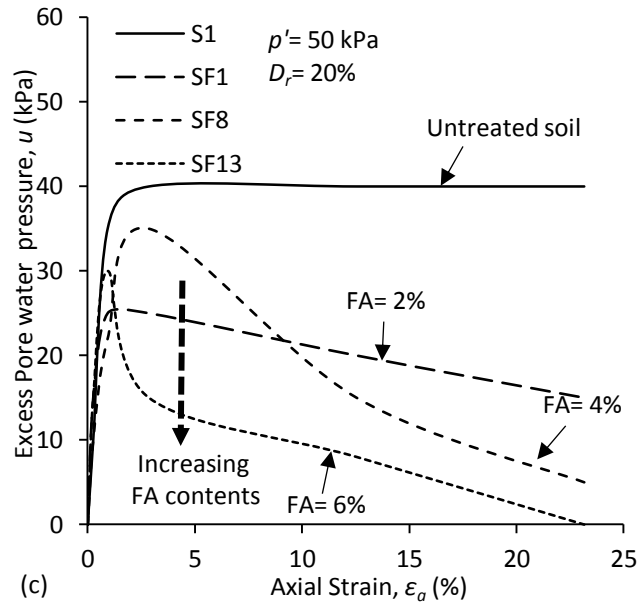
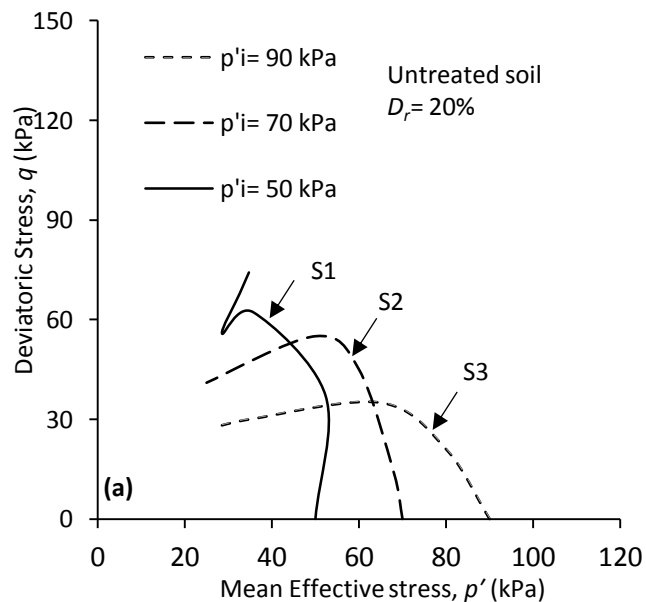


Fig. 5.5. Undrained shear response for untreated soil and FA treated specimens with an initial relative density of 20% under 50 kPa initial mean effective stress acquired from monotonic triaxial tests (a) stress path ($q-p'$); (b) stress-strain relation; and (c) excess pore water pressure versus axial strain.

5.5.2. Effect of Initial Mean Effective Stress

Fig. 5.6 shows the effect of initial mean effective stress on shearing behaviour of the untreated and FA treated specimens with an initial relative density of 20% when tested under an initial mean effective stress (p') of 50, 70, and 90 kPa. It is seen from the figure that increasing while increasing the FA content improved the ultimate deviatoric strength of the soil, increasing the initial mean effective stress reduced the ultimate deviatoric strength in each set of conducted tests. For instance, in untreated soil, ultimate deviatoric stresses of 74, 41, and 28 kPa was recorded when specimens were tested under initial mean effective stress of 50, 70, and 90 kPa respectively. Similar trend was recorded when 2% FA was added into the specimens. For instance, an ultimate deviatoric stress of 81, 75, and 64 kPa was recorded when the tests conducted under 50, 70, and 90 kPa initial mean effective stress respectively. However, the

addition of 4% FA into the sand increased the ultimate deviatoric stress, increasing the initial mean effective stress reduced the ultimate deviatoric stress for this tested set of specimens as well as other tested set. For instance, an ultimate deviatoric stress of 89, 72, and 72 kPa was recorded when the specimen tested under 50, 70, and 90 kPa initial mean effective stress respectively. Similarly, testing the specimens set mixed with 6% FA caused an ultimate deviatoric stress of 100, 94, and 86 kPa under initial mean effective stress of 50, 70, and 90 kPa respectively. Fig. 5.7 shows a summary of the recorded ultimate deviatoric strength values for untreated and FA treated specimens under different initial mean effective stress. As shown, increasing the initial mean effective stress reduced the ultimate deviatoric stress in all tested specimens. The reported results can be attributed to the soil suppression of dilatancy behaviour and consistent with critical state of soil. Seed and Harder (1990) also reported the same behaviour for the tested specimens under different effective confining pressures.



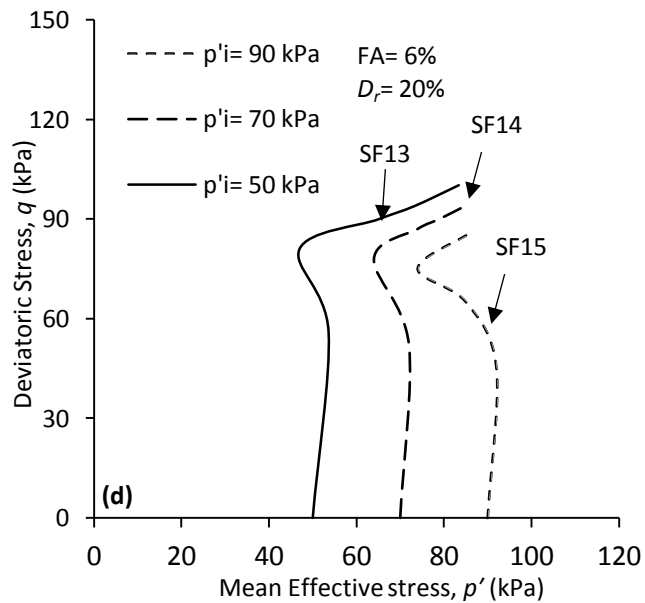
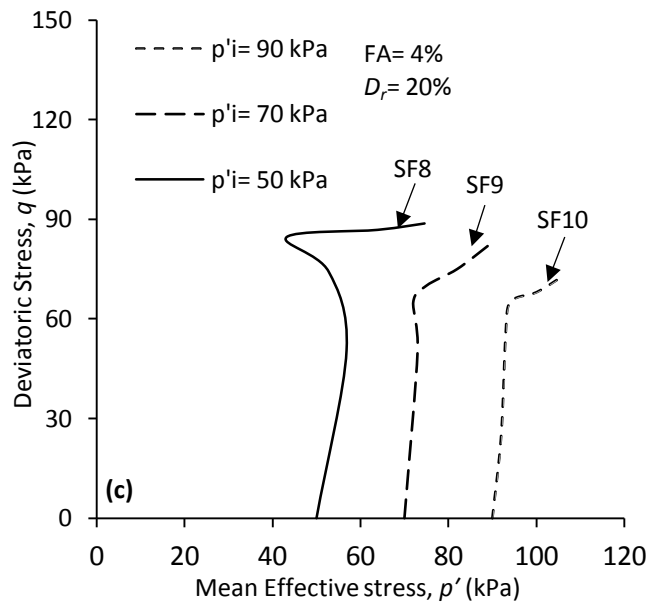
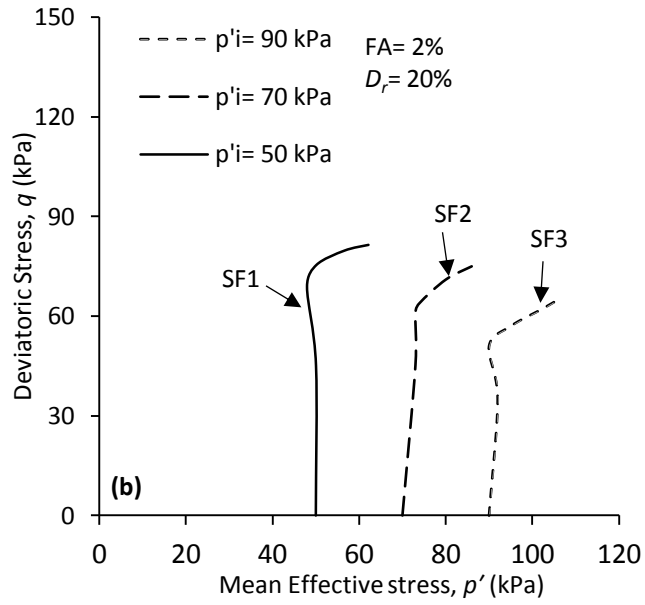


Fig. 5.6. Effect of FA contents on stress path ($q-p'$) in post-cyclic tests (a) untreated soil; (b) FA=2%; (c) FA=4%; and (d) FA=6%.

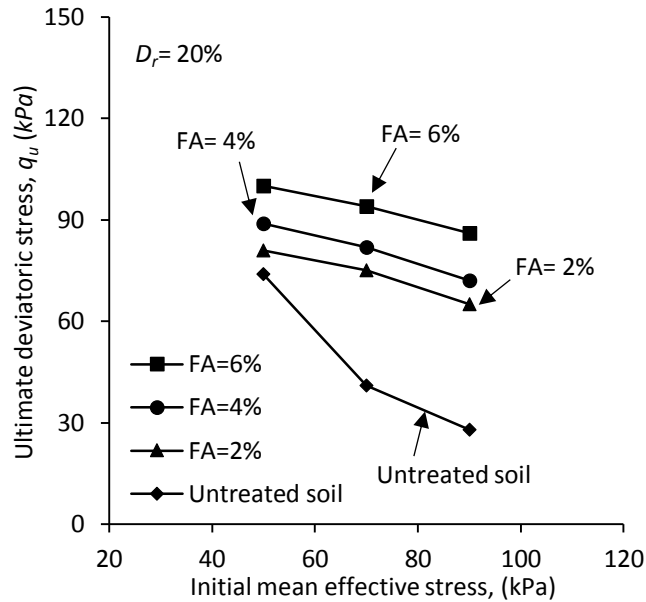
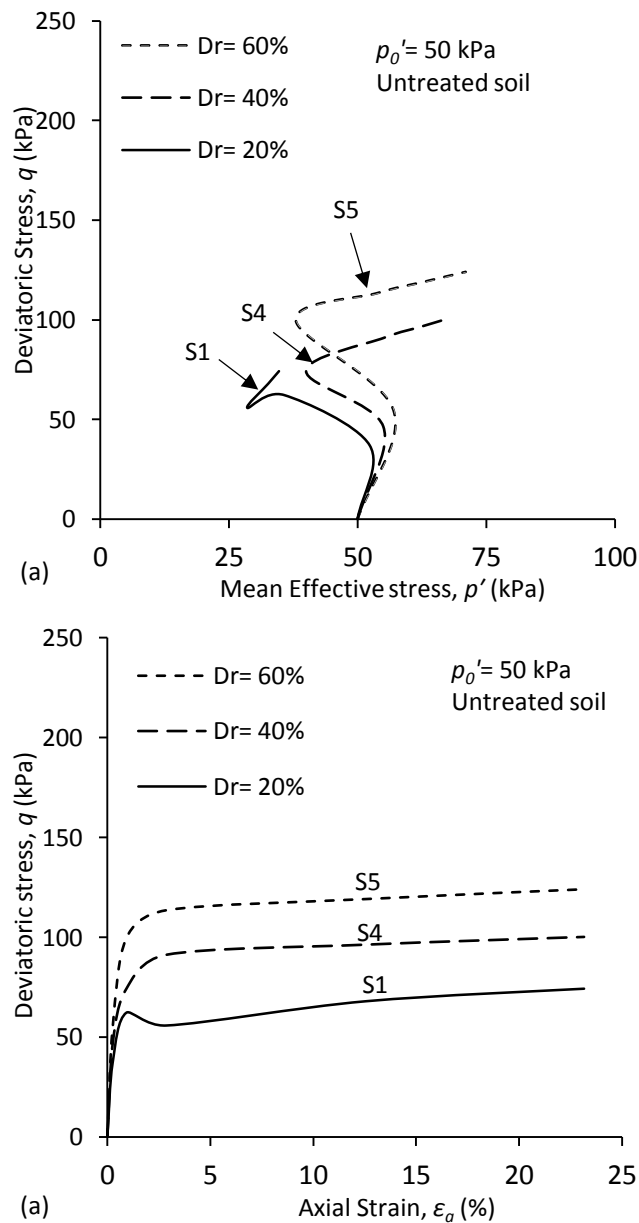


Fig. 5.7. Variations of the ultimate deviatoric stress acquired from post-cyclic tests for untreated and FA treated specimens

5.5.3. Effect of Relative Density

Fig. 5.8 shows the effect of relative density on shearing responses of the untreated soil, and 2% FA treated specimens under an initial mean effective stress of 50 kPa when the specimens were prepared with an initial relative density of 20%, 40%, or 60%. It is seen from the figure that increasing the initial relative density increased the ultimate deviatoric strength of the soil. For instance, the untreated specimens have an ultimate deviatoric strength of 74, 100, and 124 kPa when the tests conducted for the specimens with an initial relative density of 20, 40, and 60% respectively. Similar trend was recorded for 2% FA added specimens, however in a greater range. For instance, an ultimate deviatoric strength of 81, 115, and 161 kPa when the specimens tested with an initial relative density of 20, 40, and 60% respectively.

Fig. 5.9 shows a summary of the acquired results for the effect of initial relative density. As shown, the specimens prepared with a greater relative density have a higher ultimate deviatoric strength. This increase in FA added specimens was more apparent which shows the densification of the FA added specimens is more effective than untreated soil.



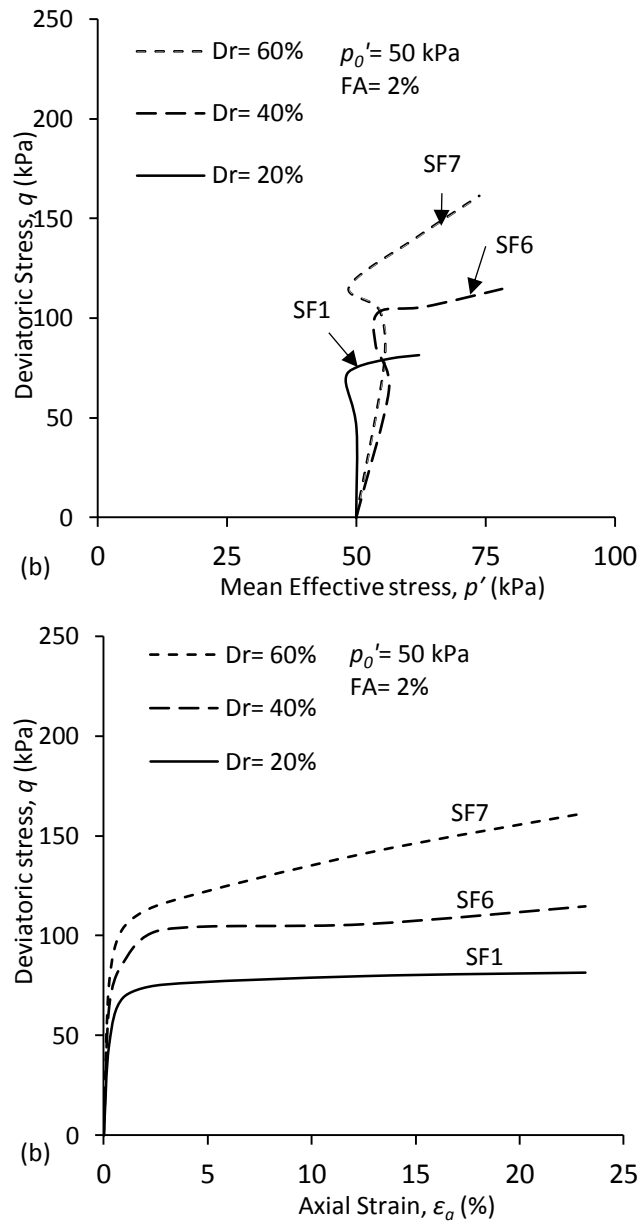


Fig. 5.8. Typical stress path ($q-p'$) and stress-strain ($q-\epsilon_a$) acquired from post-cyclic tests for (a) untreated soil; and (b) FA=2%

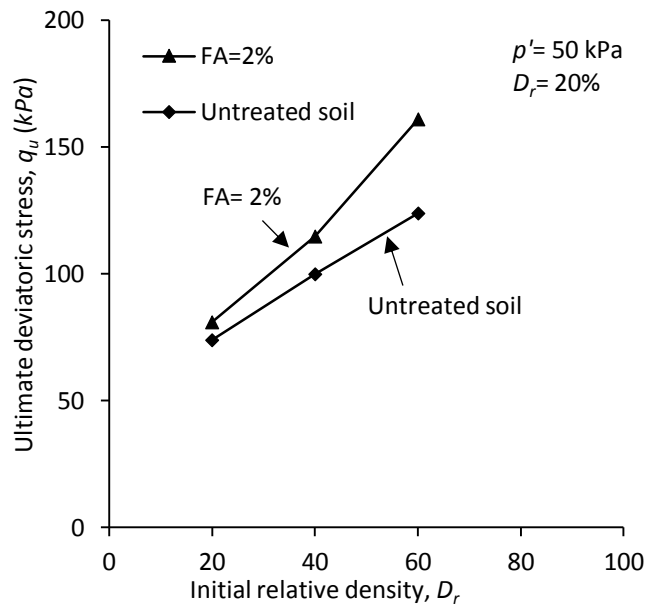


Fig. 5.9. Variations of the ultimate deviatoric stress acquired from monotonic tests for untreated and 2% FA treated specimens

5.5.4. Effect of Curing Time

To investigate the effect of curing time on ultimate deviatoric stress of the specimens, a series of undrained monotonic triaxial compression tests conducted on the specimens treated with 2%, 4%, and 6% FA and cured for 14 and 28 days. Fig. 5.10 shows a summary of the results for the effect of curing time on ultimate deviatoric stress of the specimens when the specimens prepared with a relative density of 20% and tested under 50 kPa initial mean effective stress. It is seen from the figure that increasing the curing time increased the ultimate deviatoric of the specimens. For instance, while 2% FA treated specimen showed an ultimate deviatoric strength of 81 kPa when tested without curing time, 14 and 28 days curing time caused an ultimate deviatoric strength of 96 and 108 kPa for the specimens respectively. Similar trend was recorded for 4% FA treated specimens when tested after 14 and 28 days curing time. For instance, while this specimen without curing time have an ultimate deviatoric strength of 89 kPa, testing the specimens after 14 and 28 days curing time caused an ultimate deviatoric

strength of 105 and 117 kPa respectively. Similarly, an increasing trend of 100, 114, and 125 kPa was recorded for the specimens treated with 6% FA when the specimens tested without and with 14 and 28 days curing time respectively.

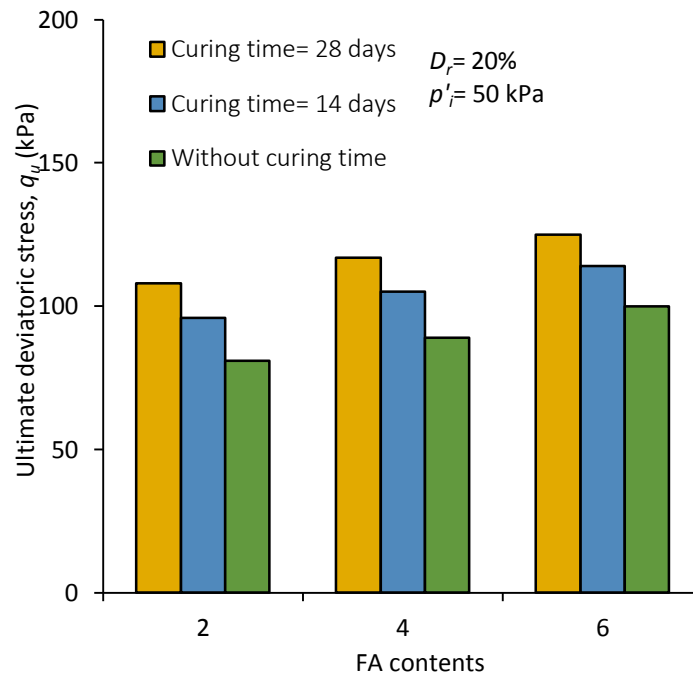


Fig. 5.10. Effect of curing time in variations of ultimate deviatoric stress acquired from monotonic tests for FA treated specimens.

5.6. Conclusions

Liquefaction is one of the main disastrous phenomena in the world which its mitigation is of great importance. Application of chemical admixtures to increase the strength characteristics of the soil is a common approach in ground improvement. Previous studies reported on effectiveness of the additives such as Portland cement (PC) and lime to increase the strength characteristics of the soil, however these materials are expensive and not environmental-friendly. There are some by-product materials remain from different industries such as steel manufacturing which have a hydration and pozzolanic characteristic similar to PC and lime. Not only these materials are

cheap and cost-effective but also their application is environmental friendly as it helps in reduction of the carbon foot print. Fly ash (FA) is a by-product material with hydration characteristics which is remained from process of fired coal in plants. This study aims to investigate the effect of FA addition on liquefaction mitigation of the soil. A series of undrained monotonic triaxial compression tests conducted to investigate the effect of fly ash (FA) on compression behavior of the soil. This study investigated the effect of four FA contents (i.e., 0, 2, 4, and 6%), three initial mean effective stresses (i.e., 50, 70, and 90%), and three initial relative densities (i.e., 20, 40, and 60%). In addition, the effect of two curing periods of 14 and 28 days were evaluated on selected specimens. The investigations of the effect of FA contents showed that the specimens with a greater FA contents have a higher ultimate deviatoric stress (q_u). This behavior was attributed to the filled existing micro pores amongst soil particles by FA which reduced the pore water pressure build-up. The investigation of the effect of initial mean effective stress showed that the FA added specimens tested under a greater initial mean effective stress have a lower ultimate deviatoric strength value. This was attributed to the suppression of dilatancy and consistent with critical state of soil. The investigation on effect of initial mean effective stress showed that increasing the initial mean effective stress is effective to increase the ultimate deviatoric strength of the soil. The results showed that the densification is more effective in FA added specimens as these specimens showed a greater q_u value in all relative densities than the untreated soil. The investigation of the effect of curing time on FA added specimens showed that the specimens with a greater curing period have a greater ultimate deviatoric strength.

Chapter 6

Effect of Binders on Cyclic Behaviour of Sand

CHAPTER INTRODUCTION

The chapter six is divided into two parts. The first part investigates the effect of fly ash (FA) on cyclic liquefaction strength of sand by performing a series of stress-controlled undrained cyclic triaxial tests. In this part the effect of FA contents, initial relative density, effective confining pressure, and curing time on cyclic liquefaction resistance of the soil has been investigated and the results have been analysed. The second part, investigates the effect of ground granular blast furnace slag (GGBFS) on cyclic liquefaction resistance of the sand by performing a series of stress-controlled undrained cyclic triaxial tests. In this part, similar to the part one, the effect of different parameters such as GGBFS contents, initial relative density, effective confining pressure, and curing time on cyclic liquefaction strength of the soil have been investigated and the results were presented and analysed.

The results of the first part of this chapter were published as Keramatikerman et al (2017b) and the results of the second part of this chapter currently are under preparation to submit to a high quality journal.

Part 1

Effect of FA on Cyclic Behaviour of Sand

6.1. Effect of FA on Cyclic Behaviour of Sand

6.1.1. Abstract

A series of cyclic triaxial tests were performed to determine the liquefaction resistance of sand stabilised with fly ash (FA). In order to understand the cyclic behaviour of the FA stabilised sand, the effect of relative density (D_r), FA content, effective confining pressure (CP) and curing time liquefaction resistance were considered. In the first stage of the laboratory tests, specimens of sand mixed with 2% FA under 50 kPa CP and 0.2 CSR with relative density of 20%, 40%, 60%, and 80%, were tested and compared with untreated soil. The results indicated that mixtures of sand-FA in all relative densities have more resistance to liquefaction failure in comparison with untreated soil, and mixture of sand-FA for relative density of 80% has the greatest resistance value. In the second stage, two types of sand-FA mixture (i.e., 4% and 6% FA) with a relative density of 20% under three ranges of confining pressure, namely 50, 70 and 90 kPa, were tested. The results in this stage suggested that the addition of 6% FA to the sand led to an increase in the cyclic response of the soil to the liquefaction in comparison with the specimens of sand mixed with 4% FA in all tested effective confining pressures. In the last part of the study, variation of the CSR with the number of cycles to liquefaction for a mixture of sand and 2% FA with 20% relative density under 50, 70 and 90 kPa effective confining pressure were presented and results indicated that the specimens under greater CP liquefied at earlier cycle numbers and vice versa. In continuing to investigate the effect of curing time, the specimens containing 2% FA were cured for 14 and 28 days and tested under 50 kPa CP and 20% relative density. The result showed that an increase in curing time led to an increase in the liquefaction strength of the sand containing FA.

6.1.2. Introduction

Studying the behaviour of soil under cyclic loading and seismic waves is a complicated matter in geotechnical earthquake engineering. This issue is even more complicated when these seismic waves happen in saturated soils. This phenomenon has been known as liquefaction in geotechnical engineering. Liquefaction is a natural disaster that happens due to loss of strength and stiffness during seismic events and usually occurs in sandy soils. Many studies have been conducted to improve sandy soil performance in liquefaction events. For instance, Porcino et al. (2015) investigated the effect of cement treated sand on liquefaction resistance and reported that liquefaction strength increased. Ye et al. (2015) figured out the pre-shearing effect on liquefaction strength of a sandy soil. They observed that medium to large pre-shearing loadings led to a decrease in the resistance of the liquefaction. Noorzad and Fardad Amini (2014) tried to increase the liquefaction resistance of sand using fibre. They reported that increasing fibre length and number led to an increase in liquefaction strength of the sand. In a similar study on the effect of fibre reinforced sand (Liu et al. 2011), increasing inconsistency in shear strength has been reported by increasing the fibre content of the specimens. In another study, Karim and Alam (2014) studied the effect of non-plastic silt on liquefaction resistance of the sand-silt specimens for a constant relative density. They observed a primary increase in excess pore water pressure by the addition of silt content until a limiting amount was attained. This trend reversed when the silt content passed the limit. An adverse behaviour for cyclic strength has also been reported (Karim and Alam 2014). The effect of colloidal silica grout on the liquefaction strength of sand was investigated by Gallagher and Michell (2002). They found that the addition of colloidal silica as an agent led to an increase in the deformation strength of the sand. The liquefaction resistance of three types of sand were compared in another

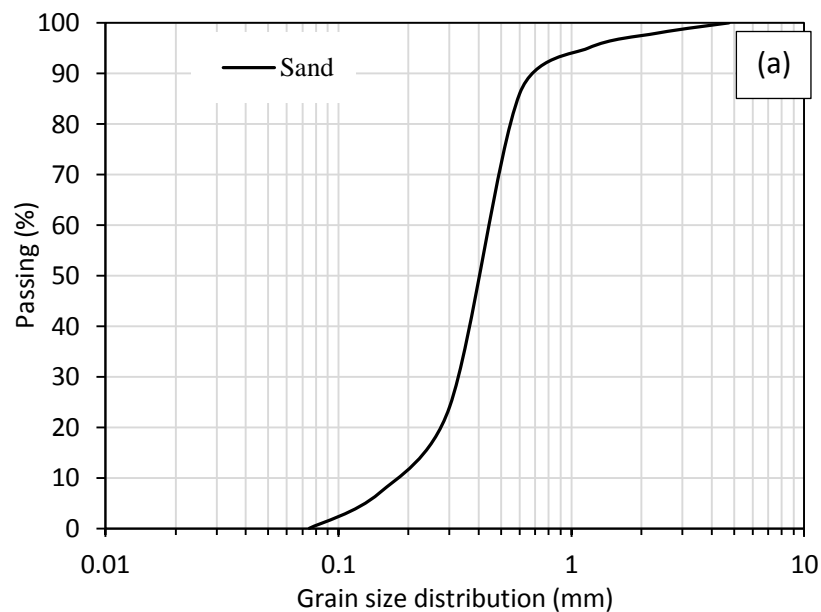
study ([Monkul et al. 2015](#)). In this study, dry and saturated samples of clean and silty sand were subjected to a drained constant volume cyclic shear test and it was reported that the liquefaction possibility of the saturated samples could also be estimated by dry specimens. It was also reported that the results of the cyclic behaviour of the saturated and dry sand is different for clayey sand and this soil type needs to be saturated in order to assess its liquefaction strength characteristics.

Application of a chemical agent is one of the main techniques in the soil stabilisation area to improve soil strength. Fly ash is one of the chemical additives that recently has drawn attention of scholars ([Kaniraj and Havanagi 1999](#); [Prabakar et al. 2004](#); [Singh et al. 2015](#); [Al-Malack et al. 2016](#)). The studies that have been performed on effect of fly ash or other additives as an agent, have focused on investigating the mechanical properties of the soil from the static viewpoint of geotechnical engineering ([Boominathan and Hari 2002](#); [Zand et al. 2009](#); [Ibraim 2010](#); [Jakka et al. 2010](#)). However, there are some studies on the cyclic behaviour of the impounded or reinforced FA ([Boominathan and Hari 2002](#); [Zand et al. 2009](#); [Ibraim 2010](#); [Jakka et al. 2010](#)). Investigation of the behaviour of the FA stabilised sand under cyclic loading is a novel issue and a gap in the literature. Similarly, the effect of curing time is a less considered issue in the investigation of cyclic behaviour of soils mixed with additives. Therefore, this study aims to determine the cyclic behaviour of the sand mixed with FA by considering effective parameters such as FA content, curing time, CP and D_r .

6.1.3. Testing Materials

6.1.3.1. Sand

The selected sand for this study was obtained from the Baldivis area located 50 km south of Perth in Western Australia. This sand is known as concrete yellow sand and is widely used in construction projects. It is a uniform semi-rounded sand that includes more than 80% crystalline silica (quartz) and less than 20% other minerals and organic materials. Hydraulic conductivity of the sand is equal to 7.67×10^{-3} cm/sec and has a moisture content of 13.94% and a dry density of 1.62 gr/cm³ according to the results of standard proctor compaction test. Fig. 6.1(a) shows a scanning electron microscope (SEM) of the applied yellow sand used in this study. Fig. 6.1(b) also shows the particle size distribution (PSD) of the employed sand.



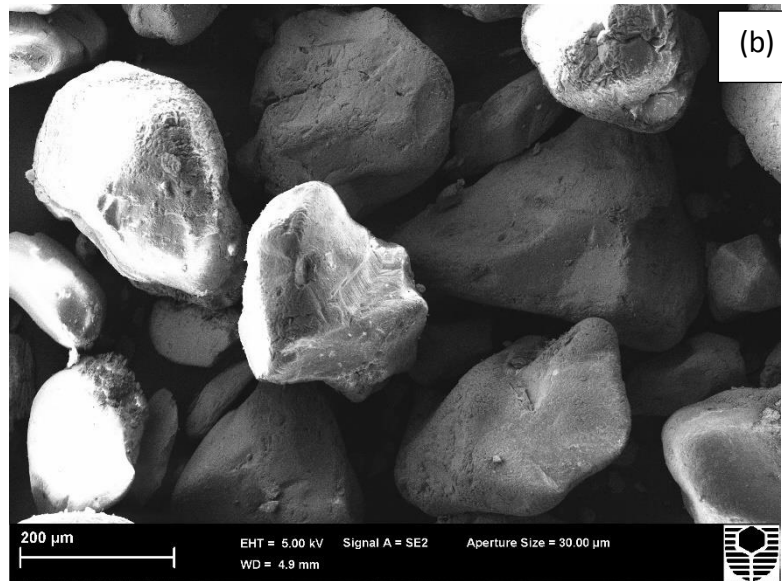


Fig. 6.1. (a) Particle size distribution (PSD) of the employed Baldivis yellow sand and
; (b) Scanning electron microscopy (SEM) of the used sand in this study

6.1.3.2. Fly Ash (FA)

The applied FA in this study is a class F category FA which was obtained from Fly ash Australia Pty Ltd. This product is known as Collie fly ash. It is normally used as an additive in soil stabilisation and a filler in asphalt. Fig. 6.2 shows scanning electron microscopy (SEM) of the employed FA. Table 6.1 also shows the chemical composition of the Collie fly ash (Flyash Australia 2016).

Table 6.1. Chemical compositions of the employed Collie Fly ash (Flyash Australia 2016)

No.	Element	Formula	Percentage
1	Silicon dioxide	SiO ₂	51.80%
2	Aluminium oxide	Al ₂ O ₃	26.40%
3	Ferric oxide	Fe ₂ O ₃	13.20%
4	Calcium oxide	CaO	1.61%
5	Titanium dioxide	TiO ₂	1.44%
6	Phosphorus pentoxide	P ₂ O ₅	1.39%
7	Magnesium oxide	MgO	1.17%
8	Potassium oxide	K ₂ O	0.68%
9	Sodium oxide	Na ₂ O	0.31%
10	Manganese oxide	MnO	0.10%

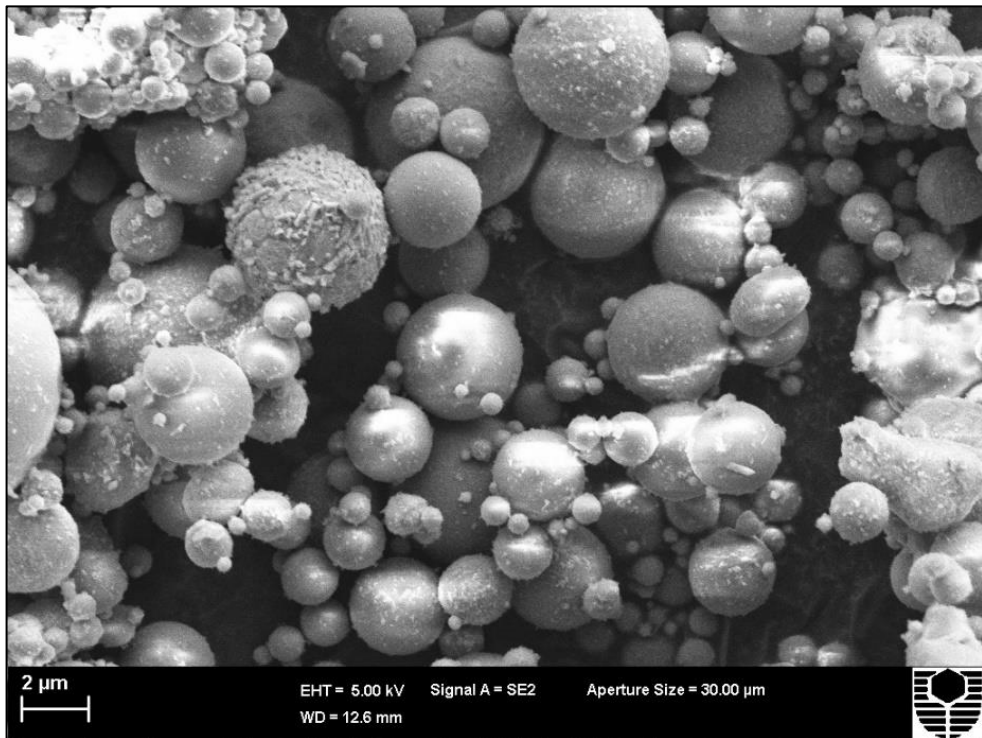


Fig. 6.2. Scanning electron microscopic (SEM) image of the employed FA

6.1.4. Methodology

To investigate the cyclic behaviour of the mixture of sand-FA, a series of cyclic triaxial tests were performed. All the tests were in compliance with the procedure described in ASTM D5311 (2013). In this study, the effect of four parameters, namely D_r , FA contents, CP, and curing time, have been considered. Table 6.2 shows the designated experimental program to investigate effect of the mentioned parameters. To perform the tests, specimens were initially consolidated according to the designated effective confining pressure. Stress controlled method in an undrained condition was applied after consolidation stage. Then, axial stress, vertical strains and pore water pressure were recorded at short periodic intervals for the applied cyclic stresses with the frequency of 1 Hz.

Table 6.2. Experimental program designed to investigate effect of the relative density (D_r), FA content, effective confining pressure (CP) and curing time (CT) on cyclic behaviour of the fly ash (FA) treated soil.

No.	Test ID	CP (σ)	D_r (%)	CSR	FA (%)	Curing time (day)
Relative Density						
1	20-S	50	20	0.2	-	-
2	40-S	50	40	0.2	-	-
3	60-S	50	60	0.2	-	-
4	80-S	50	80	0.2	-	-
5	20-2FA	50	20	0.2	2	-
6	40-2FA	50	40	0.2	2	-
7	60-2FA	50	60	0.2	2	-
8	80-2FA	50	80	0.2	2	-
FA content						
9	50-4FA	50	20	0.2	4	-
10	70-4FA	70	20	0.2	4	-
11	90-4FA	90	20	0.2	4	-
12	50-6FA	50	20	0.2	6	-
13	70-6FA	70	20	0.2	6	-
14	90-6FA	90	20	0.2	6	-
Effective confining pressure and curing time						
15	50-2FA	50	20	0.2, 0.35, 0.5	2	-
16	70-2FA	70	20	0.2, 0.35, 0.5	2	-
17	90-2FA	90	20	0.2, 0.35, 0.5	2	-
18	2FA	50	20	0.2, 0.35, 0.5	2	0
19	14-2FA	50	20	0.2, 0.35, 0.5	2	14
20	28-2FA	50	20	0.2, 0.35, 0.5	2	28

6.1.5. Results and Discussion

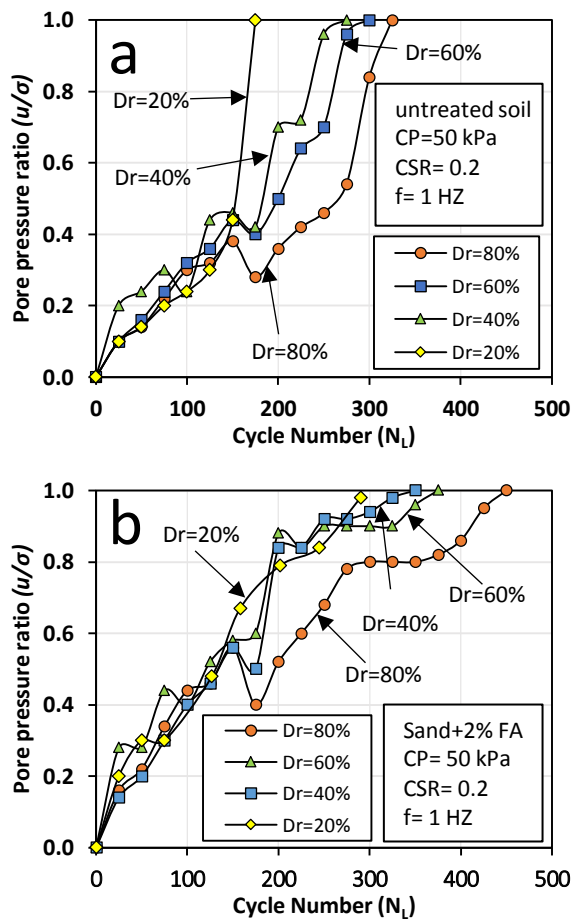
6.1.5.1. Effect of Relative Density on Liquefaction Resistance

To investigate effect of relative density on liquefaction resistance of the mixture of sand-FA, eight cyclic triaxial tests for untreated soil and sand mixed with 2% FA under 50 kPa effective confining pressure were performed. In this section, four values of relative density, namely 20%, 40%, 60% and 80% with 0.2 CSR, were tested and compared. Fig. 6.3(a-c) compares the results achieved for untreated soil and mixture of sand-FA at different relative densities.

For the relative density of 20%, it is seen from Fig. 6.3(b) that the sand mixed with 2% FA had higher values for the pore pressure ratio (u/σ) from the start point to the 150th cycle number in comparison with the untreated soil with 20% relative density plotted in Fig. 6.3(a). It is also seen that the untreated soil liquefies earlier than sand mixed with FA. Using a relative density of 40%, many fluctuations at the same cycle number could be seen in both tested specimens. However, sand mixed with 2% FA had lower values of pore pressure ratio (u/σ) and tended to be liquefied later in comparison with untreated soil. A major drop that was followed with a peak point for the mixture of sand and 2% FA with relative density of 60% is very noticeable. Except for this, a gradual increasing trend can be seen for the rest of the graph. A similar trend, but with lower values of pore pressure ratio (u/σ), can be seen for the untreated soil with 60% relative density in Fig. 6.3(a). The untreated soil has lower values of pore pressure ratio (u/σ) in comparison with mixture of sand mixed with 2% FA and liquefies earlier.

For 80% relative density, a peak point that has been followed with an immediate drop point for both graphs is very noticeable. It can be seen that the specimen with the mixture of sand and 2% FA has lower values of pore pressure ratio (u/σ) and liquefies

later than untreated soil with relative density of 80% same as previous tests. In this section, it can be concluded that the relative density of 80% has the highest impact on cyclic response of the mixture of sand and 2% FA to increase its resistance, and the relative density of 20% provides the lowest resistance of liquefaction. A summary of the results for the effect of relative density are shown and compared in the Fig. 6.3(c) and Table 6.3.



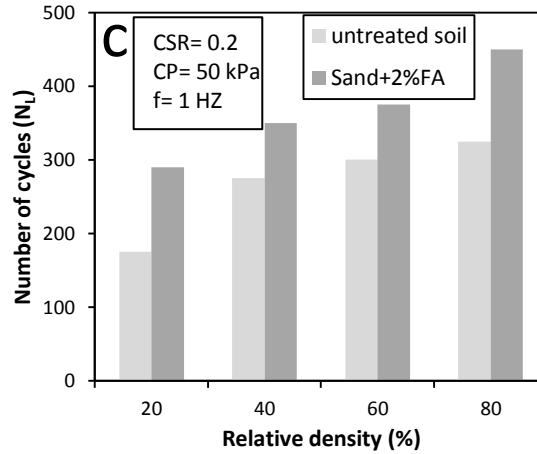


Fig. 6.3. (a) Effect of relative density on liquefaction behaviour of the untreated soil under 50 kPa CP and 0.2 CSR. (b) Effect of relative density on liquefaction strength of the sand mixed with 2% FA under 50 kPa CP and 0.2 CSR. (c) Comparison of the cyclic behaviour of the untreated soil and sand mixed with 2% FA with 20%, 40%, 60% and 80% relative density and 0.2 CSR under 50 kPa CP.

Table 6.3. Effect of relative density on liquefaction strength of the untreated soil and sand mixed with 2% FA under 50 kPa CP and 0.2 CSR and 1 HZ frequency.

No.	Specimen	Effective confining pressure, CP (kPa)	Relative density, D_r , (%)	Number of cycles to liquefaction, N_L
1	Untreated soil	50	20	175
2			40	275
3			60	300
4			80	325
5	Sand+2%FA	50	20	300
6			40	350
7			60	375
8			80	450

6.1.5.2. Effect of FA Content on Liquefaction of the Soil

The effect of the FA contents on the cyclic behaviour of the FA stabilised sand was investigated by comparing six cyclic triaxial tests on sand mixed with 4% and 6% FA with 20% relative density and 0.2 CSR. Fig. 6.4(a-b) compares the cyclic behaviour of the mentioned specimens under 50, 70 and 90 kPa CP. The effect of sand mixed with 4% FA under 50, 70 and 90 kPa CP was investigated by performing three cyclic triaxial tests. There is a rapid increasing trend for the specimen under 90 kPa effective confining pressure. This specimen liquefied in earlier cycles than the specimens under 70 and 50 kPa effective confining pressures as shown in Fig. 6.4(a). In final stage of this section, the effect of effective confining pressure on the liquefaction strength of sand mixed with 6% FA was determined by undertaking three cyclic triaxial tests under 50, 70 and 90 kPa CP. It is seen from Fig. 6.4(b) that there is a rapid increasing trend for the pore pressure ratio (u/σ) for the sample under 90 kPa effective confining pressure in initial cycle numbers. This trend follows a transitional increase. In contrast with 90 kPa effective confining pressure, the specimen under 70 and 50 kPa effective confining pressure had lesser fluctuations and liquefied later respectively.

A summary of the results was presented in Table 6.4. According to the presented results in this section, it could be concluded that generally, specimens under greater effective confining pressure have more tendency toward liquefaction in comparison with the specimens that are under lower CP. The presented results in this section are in strong agreement with critical state of the soil behaviour explained by Seed and Harder (1990). In addition, it can be concluded that addition of the FA increased the cyclic strength of the tested soils in all cases.

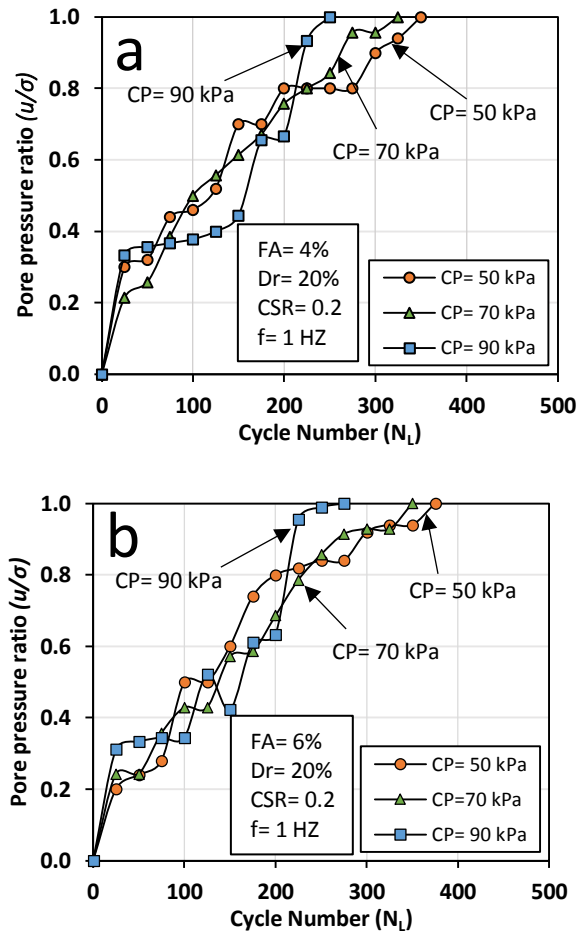


Fig. 6.4. (a) Effect of 4% FA addition on liquefaction strength of the sand with a 20% relative density and 0.2 CSR under 90, 70 and 50 kPa effective confining pressure (b) Effect of 6% FA addition on liquefaction strength of the sand with a 20% relative density and 0.2 CSR under 90, 70 and 50 kPa effective confining pressure.

Table 6.4. A summary of the results to investigate effect of the 4% and 6% FA addition on liquefaction strength of the sand with 20% relative density and under 50, 70 and 90 kPa effective confining pressure.

No.	Specimen	Relative density, D_r , (%)	Effective confining pressure, CP (kPa)	Number of cycles to liquefaction, N_L
1			50	350
2	Sand+4%FA	20	70	325
3			90	250
4			50	375
5	Sand+6%FA	20	70	350
6			90	275

6.1.5.3. Effect of Effective Confining Pressure and Curing Time on Liquefaction Strength

Fig. 6.5(a) illustrates the variation of the cyclic stress ratio with changes in number of cycles to liquefaction for specimens of sand mixed with 2% FA with 20% relative density under 50, 70, 90 kPa CP. The results indicated that the specimens under greater effective confining pressures liquefied at earlier cycle numbers. A summary of the results was shown in Table 6.5 in this section. In addition, Fig. 6.5(b) illustrates the alteration of the cyclic stress ratio (CSR) with changes in the number to liquefaction for specimens cured for 14 and 28 days. According to the figure, liquefaction resistance of the sand mixed with 2% FA with 20% relative density and under 50 kPa effective confining pressure increased with an increase in the curing time. Table 6.6 summarised the presented results in this section.

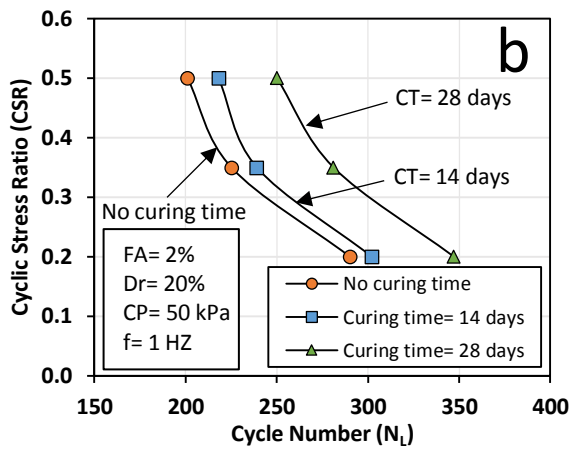
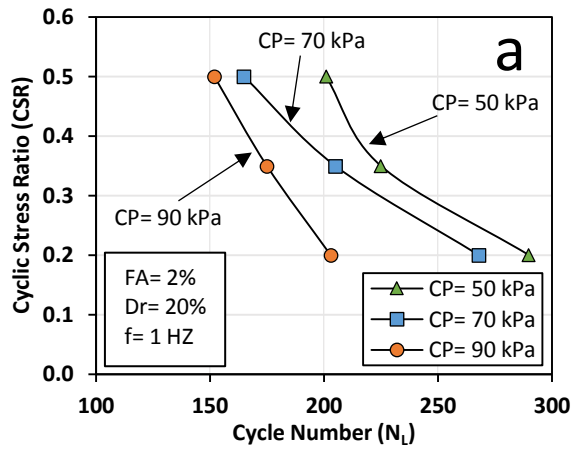


Fig. 6.5. (a) Variation of CSR with cycle number to liquefaction at different effective confining pressure for sand mixed with 2% FA and 20% relative density. (b) Variation of CSR with cycle number to liquefaction for different curing times for sand mixed with 2% FA and 20% relative density under 50 kPa effective confining pressure.

Table 6.5. A summary of the results to investigate effect of the 50, 70 and 90 kPa effective confining pressure on liquefaction strength of the sand mixed with 2% FA and 20% relative density.

No.	Specimen	Relative density, D_r , (%)	Effective confining pressure, CP (kPa)	CSR	Number of cycles to liquefaction, N_L
1				0.5	201
2			50	0.35	225
3				0.2	290
4				0.5	165
5	Sand+2%FA	20	70	0.35	205
6				0.2	268
7				0.5	152
8			90	0.35	175
9				0.2	203

Table 6.6. A summary of the results to investigate effect of the 14 and 28 days curing time on liquefaction strength of the sand mixed with 2% FA and 20% relative density under 50 kPa effective confining pressure.

No.	Specimen	Relative density, D_r , (%)	Effective confining pressure, CP (kPa)	CSR	Curing time (days)	Number of cycles to liquefaction, N_L
1				0.5		201
2				0.35	0	225
3				0.2		290
4				0.5		218
5	Sand+2%FA	20	50	0.35	14	239
6				0.2		302
7				0.5		250
8				0.35	28	281
9				0.2		347

6.1.6. Conclusion

In this study, a series of cyclic triaxial tests have been performed to investigate the effect of fly ash (FA) on the liquefaction strength of sand. The effect of relative density, FA content, effective confining pressure and curing time have been compared and presented. To investigate the effect of relative density, two types of specimens, including untreated soil and sand mixed with 2% FA with 0.2 CSR under 50 kPa effective confining pressure with relative density of 20%, 40%, 60% and 80%, have been tested. The results suggested that specimens of sand mixed with 2% FA with 80% relative density have the most resistance for liquefaction in comparison with other relative densities. In continuing to determine the effect of FA content, a series of cyclic triaxial tests for the specimens mixed with 4% and 6% FA conducted under 50, 70 and 90 kPa effective confining pressure with 20% relative density and 0.2 CSR. The results suggested that specimens with a higher FA content have a lower tendency to be liquefied. In the last stage of the study, effect of the effective confining pressure and curing time was studied. The results showed that the specimens of sand mixed with 2% FA liquefied earlier under higher effective confining pressures. Furthermore, to investigate the effect of curing time, two specimens with 2% FA content were cured for 14 and 28 days and tested under 50 kPa effective confining pressure and 20% relative density. The results were then compared with an instantly tested specimen in a cyclic stress ratio (CSR) versus number to liquefaction (N_L) graph. Results showed that an increase in curing time led to an increase in liquefaction resistance.

Part 2

Effect of GGBFS on Cyclic Behaviour of Sand

6.2. Effect of GGBFS on Cyclic Behaviour of Sand

6.2.1. Abstract

Traditional agents such as Portland cement (PC) and lime are potential sources of carbon emission into the environment, and their applications have been discouraged by the environmental agencies. Ground granulated blast furnace slag (GGBFS) is a by-product material that recently has drawn attention of the geotechnical engineers as an alternative for those mentioned hazardous agents. Previous studies mainly investigated mechanical behaviour of the GGBFS treated soil in static condition and dynamic behaviour of the GGBFS amended soil has not considered yet. This study investigates effect of GGBFS addition on liquefaction resistance of sand. Effect of three GGBFS contents (i.e., 3%, 5%, and 7% by dry weight), three effective confining stress (i.e., 100, 200, and 400 kPa), three relative densities (i.e., 40%, 60%, and 80%), and three curing periods of 7, 14 and 28 days were investigated, and the results were presented. The investigations showed that increasing the GGBFS contents was effective to increase the liquefaction resistance of the soil. In addition, the results showed that the effective confining stress has an opposite relation with liquefaction resistance, and increasing the effective confining stress reduced the liquefaction resistance of the specimens. Moreover, the investigations on effect of relative density showed that increasing the relative density increased the cyclic strength of the GGBFS stabilised soil. Finally, investigations on effect of curing time showed that increasing the curing time is effective to enhance the liquefaction resistance of the GGBFS treated soils.

6.2.2. Introduction

When the excess pore water pressure ratio (i.e., $r_u = u_e/\sigma'_3$) reaches one, the soil loses its strength and stiffness and liquefies (Elgamal et al. 2003; Karim and Allam 2014). Previous studies showed that the mitigation of liquefaction risks using chemical grouting is an effective method (Gouvenot 1998; Ishii et al. 2011; Porcino et al. 2015). More studies conducted on effect of fibres and geotextiles also showed that their application is an effective method to reduce liquefaction of the soil (Vercueil et al. 1997; Maheshwari et al. 2012; Noorzad and Amini 2014). Keramatikerman et al. (2017b) conducted a series of experimental study on liquefaction strength of fly ash added specimens and indicated that application of fly ash is effective to reduce cyclic behaviour of the soil.

Application of chemical additives is a well-established approach in ground improvement projects. It has been proofed that traditional additives such as Portland cement (PC) and lime has adverse impacts on the environment and increase the carbon emission into the environment. In a study conducted by Higgins (2007), it was mentioned that production of one tons PC led to generation of 0.95 tone CO₂ in the environment, 5000 MJ energy use, 1.5 tone mineral extraction, and 0.02 waste disposal. These negative impacts promote the practitioners to used environmental friendly alternatives (Higgins 2007; Keramatikerman et al. 2016; Vakili et al. 2016). Ground granulated blast-furnace slag (GGBFS) is a by-product from the steel industry, which application of this material is a well-accepted practice in ground improvement project as it improves the durability, sulphate and chloride resistance of the soil. It also provides protection against alkali silica reaction. This product has a hydration phases very similar to the PC and lime. For instance, generation of the ettringite, calcium silicate hydrate, calcium aluminium hydrate, and calcium aluminium silicate hydrate

are similar to PC. GGBFS has a low hydration product by itself and it is required to be mixed with a chemical activator such as PC (Keramatikerman et al. 2016). It has been indicated that production one tone of GGBFS lead to generation of 0.07 tone CO₂ in the environment (carbon emission), usage of 1300 MJ energy, no mineral extractions and saving 1 tone waste disposal (Higgins 2007).

Chand et al. (2017) conducted a series of short-term leaching tests such as strong acid digestion test (SADT), toxicity characteristics leaching procedure (TCLP), batch leach test (BLT), and American Society for Testing and Materials (ASTM) shake tests on slag. They indicated that the most of heavy metals such as lead (Pb), chromium (Cr), copper (Cu), iron (Fe), vanadium (V) nickel (Ni), Cadmium (Cd), selenium (S), and zinc (Zn), Cobalt (Co), manganese (Mn), and arsenic (As) are below the detection limit in slag, which categorise it as a non-hazardous since it has the minimum risk for the environment (Chand et al. 2017).

In aforementioned literature importance of the liquefaction mitigation has been highlighted. In addition, it was revealed that application of traditional agents such PC and lime has been discouraged by the environmental agencies and there are some environmental friendly alternatives such as GGBFS. This study investigates effect of GGBFS on liquefaction behaviour of sand.

6.2.3. Materials Used

The sand used in this study was collected from Baldivis, a suburb in Perth, Western Australia. To investigate the physical characteristics of the collected soil, sieve analysis conducted in accordance with ASTM C136 (ASTM 2014b), and the results were presented in Fig. 6.6. The PSD analysis showed that the used sand has a D₁₀ and D₃₀ value of 0.18 and 0.3 mm respectively. In addition, it was determined that the used

soil has a D_{50} and D_{60} value of 0.4 and 0.45 mm respectively. This soil has a coefficient of uniformity (C_u) of 2.5 and a coefficient of curvature (C_c) of 1.19. The sieve analysis showed that the used soil is categorised as the well-graded soil in Unified Soil Classification System (USCS) [ASTM D2487, (ASTM 2011a)]. To investigate the constituent minerals of the used sand, X-ray powder diffraction (XRD) analysis performed, and the results showed that the used sand contains more than 80% quartz. This soil also has a specific gravity of (G_s) 2.67 based on pycnometer specific gravity test [ASTM D854, (ASTM 2014a)]. A series of standard compaction tests based on ASTM D1557 (ASTM 2012b) conducted on the used sand, and the results showed that this soil has an optimum moisture content (OMC) and a maximum dry density (MDD) of 13.94% and 1.62 t/m³ respectively. Fig. 6.7 shows a scanning electron micrograph (SEM) of the used sand. The GGBFS sourced from BGC Cement, a local provider in Perth, Western Australia. The used GGBFS has a specific gravity in the range of 2.8-3.1, with a melting point of 1350 °C (BGC Cement, 2013). The PSD analysis conducted on used GGBFS based on ASTM C136 (ASTM 2014b) and ASTM D4221 (ASTM 2011b), and the results showed that the D_{10} and D_{30} are equal to 0.01 and 0.035 mm respectively. Furthermore, it was determined that the D_{50} and D_{60} are equal to 0.06 and 0.065 mm respectively. The PSD analysis on GGBFS showed that this by-product material has a coefficient of uniformity (C_u) of 6.5 and a coefficient of curvature (C_c) 1.88. The GGBFS has a compacted unit weight in a range of 1.12 t/m³ to 1.36 t/m³. Table 6.7 and Table 6.8 shows its mineral constituents and physical characteristics of used GGBFS respectively.

Table 6.7. Chemical composition of used GGBFS (BGC Cement 2013).

GGBFS composition	Formula	Percentage
Calcium oxide	CaO	30–50%
Silica, amorphous	SiO ₂	35–40%
Aluminium oxide	Al ₂ O ₃	5–15%
Sulphur	S	5%

Table 6.8. Physical characteristics of used GGBFS (BGC Cement 2013).

Characteristics	Value
pH in dry state	>7.0
pH in wet plastic state	>10.0
Odour:	ammonia
Melting point:	>1200° C
Solubility:	Not soluble
Specific gravity	2.5
Flash Point:	Not applicable
Hazardous Decomposition:	None
Hazardous Reactions	None
Ignition Temp:	Not applicable

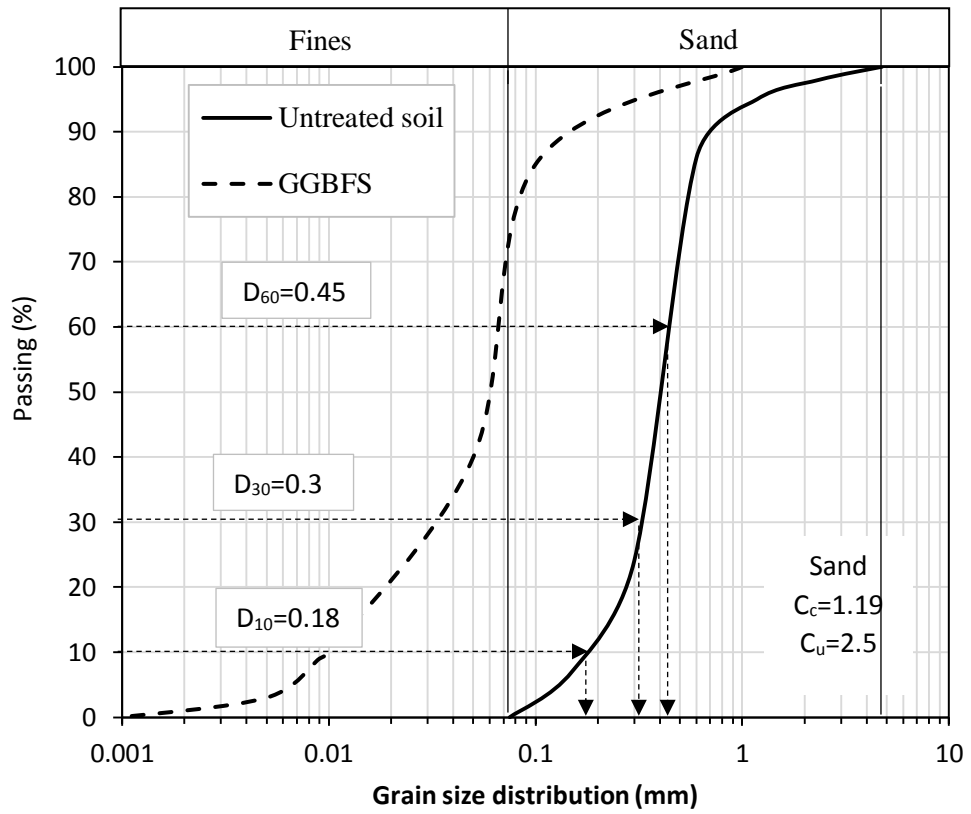


Fig. 6.6. Particle size distribution of used sand and GGBFS.

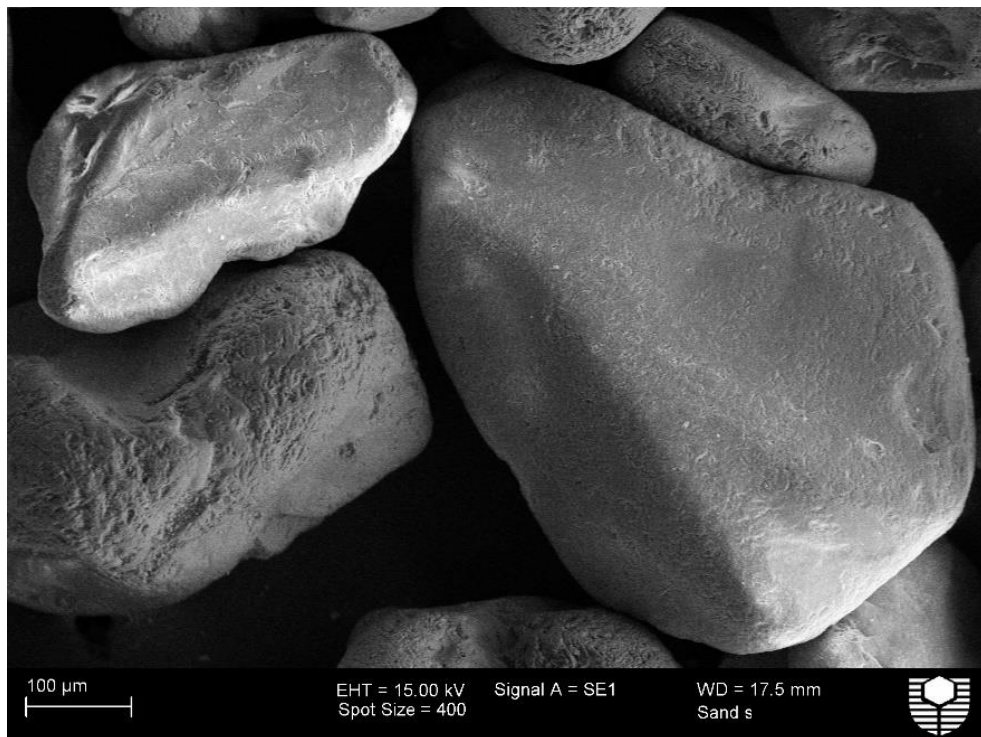


Fig. 6.7. A typical SEM image shows geometry of the used sand in this study

6.2.4. Sample Preparation and Laboratory Test Setup

To investigate effect of GGBFS on cyclic behaviour of the soil, a series of cyclic triaxial compression tests were performed in accordance with ASTM D5311 (ASTM 2013) using an automated Bishop and Wesley triaxial apparatus. The tests were performed in a stress-controlled and consolidated undrained (CU) condition. In addition, to control the effect of temperature on the specimens, the tests were conducted in a moisture-controlled room with a temperature of $22\pm 1^\circ\text{C}$. The specimens were prepared with 62.5 mm diameter and 125 mm height (i.e., aspect ratio of 2) according to the under-compaction method by moist-tamping the mixtures (Ladd 1978; El Takch et al. 2015). To prepare the specimens, initially, the desired amount of soil was mixed with GGBFS and thoroughly mixed. When a uniform mixture was achieved, water was added based on the optimum moisture content (OMC) of each mixture obtained from standard proctor compaction tests, and completely mixed. Then, the soil was compacted in a steel, cylindrical, split mould in five layers until the desired height was achieved based on its maximum dry density (MDD) [ASTM D1557, (ASTM 2012b)]. Three different relative density values used to prepare the specimens of (i.e., 40, 60, and 80%). The relative density of each specimen computed using Eq. (6.2.1).

$$D_r (\%) = \frac{e_{max} - e}{e_{max} - e_{min}} \times 100 \quad (6.2.1)$$

Where, e_{max} = maximum void ratio; e_{min} = minimum void ratio; and e = global void ratio. Based on the required relative density for each specimen, the mass of each mixture was computed and put into the mould in five layers and by the use of a small tamper according to moist tamping method (Ladd 1978). In this method, densification of the

lower layers is controlled by compaction of the upper layer. In fact, compaction of a new layer causes the lower layers have a density more than previously targeted. This linear variation in each layer from the first until the last layer helps to control the final relative density of the specimens during the preparation stage (Ladd 1978). Fig. 6.8 shows a typical untreated sample during preparation. After the completion of sample preparation, the moulds were wrapped with a plastic bag and were stored for 7, 14, and 28 days for curing (Schnaid et al 2001; Asghari 2003). When the curing period completed, the specimens were saturated by injecting de-aired water from bottom of the specimens. The saturation stage was completed when a B -value (Skempton constant) of at least 0.96 was achieved. The specimens were consolidated at three effective confining stress (σ'_3) of 100, 200, and 400 kPa. The amount of the post-consolidation relative density (D_r) values were computed before conducting the test. Table 6.9 shows a summary of the conducted tests and key results in this study. Fig. 6.9 shows an overview of structure of the study.



Fig. 6.8. A typical specimen during preparation in split mould.

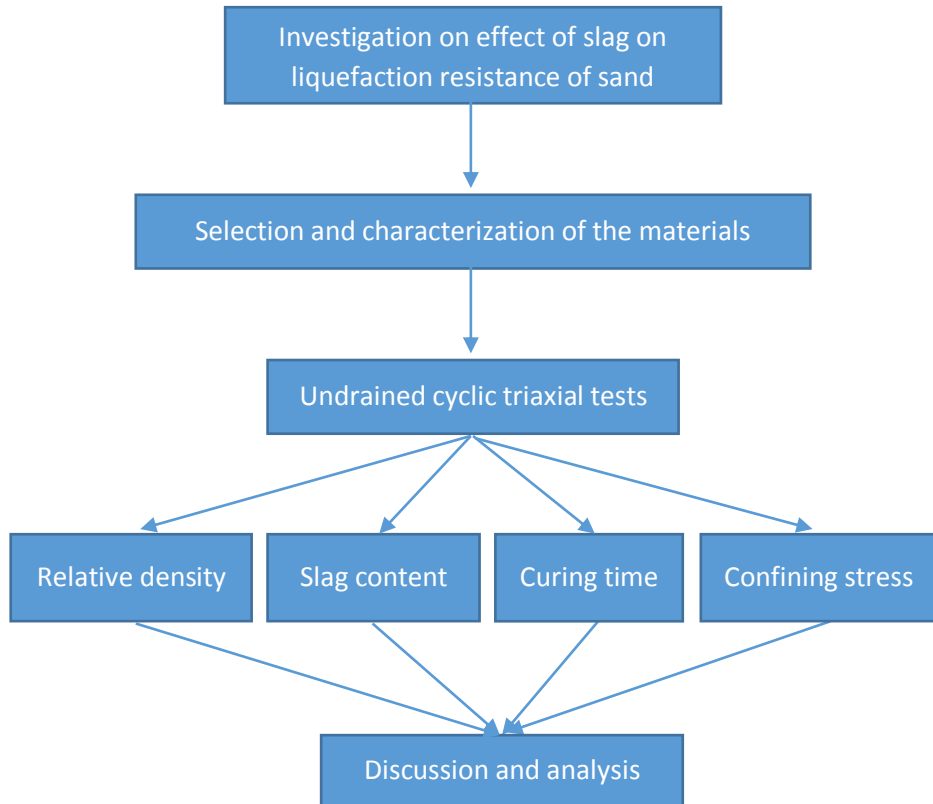


Fig. 6.9. An overview of structure of the study

Table 6.9. Experimental program to investigate cyclic behaviour of the GGBFS treated soil.

No.	ID	σ'_3 (kPa)	GGBFS (%)	Curing time (days)	CSR	Pre-consolidation D_r (%)	Post-consolidation D_r
1	S1	200	-	-	0.20	60	62.5
2	S2	200	-	-	0.35	60	62.5
3	S3	200	-	-	0.50	60	62.5
4	S-3G	200	3	7	0.20	60	62.5
5	S-3G	200	3	7	0.35	60	62.5
6	S-3G	200	3	7	0.50	60	62.5
7	S-5G	200	5	7	0.20	60	62.5
8	S-5G	200	5	7	0.35	60	62.5
9	S-5G	200	5	7	0.50	60	62.5
10	S-7G	200	7	7	0.20	60	62.5
11	S-7G	200	7	7	0.35	60	62.5
12	S-7G	200	7	7	0.50	60	62.5
13	S-5G	100	5	7	0.20	60	62.5
14	S-5G	100	5	7	0.35	60	62.5
15	S-5G	100	5	7	0.50	60	62.5
16	S-5G	400	5	7	0.20	60	62.5
17	S-5G	400	5	7	0.35	60	62.5
18	S-5G	400	5	7	0.50	60	62.5
19	S1	200	-	-	0.2	40	43.6
20	S2	200	-	-	0.2	80	81.4
21	S-5G	200	5	7	0.20	40	43.6
22	S-5G	200	5	7	0.35	40	43.6
23	S-5G	200	5	7	0.50	40	43.6
24	S-5G	200	5	7	0.20	80	81.4
25	S-5G	200	5	7	0.35	80	81.4
26	S-5G	200	5	7	0.50	80	81.4
27	S-5G	200	5	14	0.20	60	62.5
28	S-5G	200	5	14	0.35	60	62.5
29	S-5G	200	5	14	0.50	60	62.5
30	S-5G	200	5	28	0.20	60	62.5
31	S-5G	200	5	28	0.35	60	62.5
32	S-5G	200	5	28	0.50	60	62.5

6.2.5. Results and Discussions

6.2.5.1. Effect of GGBFS Contents

Fig. 6.10 shows typical results of cyclic triaxial tests for specimen treated with 5% GGBFS, at a CSR value of 0.20, a pre-consolidation relative density of 60% (Post-consolidation relative density of 62.5%), under an effective confining pressure of 200 kPa. In general, the effective mean principal stress (p') reduces at low shearing strain due to tendency of the specimen to contraction and generation of the excess pore water pressure. A dilation behaviour happens for effective mean principal stress when the phase transformation line has been passed, and an increase in effective stress, and a reduction in pore water pressure happens due to dilative behaviour of the path which inclined the path toward right. This contractive and dilative cycle continues until the phase transformation line to be crossed (Elgamal et al. 2003). The main difference between effective stress path of untreated and GGBFS treated specimens is in the rate of decrement. In GGBFS treated specimens, generation of cementitious bonds amongst soil particles blocks generation of the pore water pressure and a lower rate of reduction happens, whereas, in the untreated specimens the pore water pressure easily generates amongst the voids and liquefies.

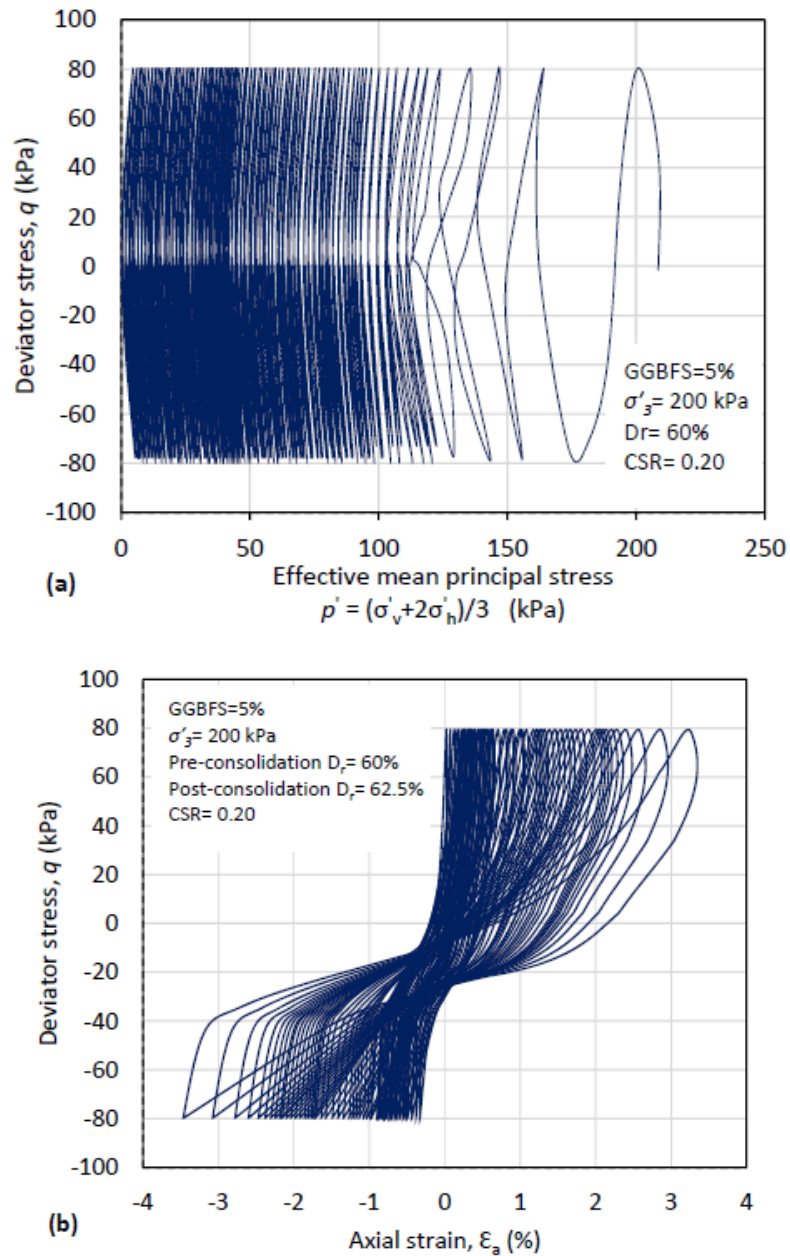


Fig. 6.10. Typical results of cyclic triaxial tests for GGBFS treated specimen (a) Effective stress path; (b) stress-strain relationship (hysteresis loop).

Variations of the number of cycles to liquefaction (N_L) with cyclic stress ratio (CSR) for untreated soil and GGBFS treated soil specimens under 400 kPa effective confining pressure at a pre-consolidation relative density of 60% (i.e., Post-consolidation relative density of 62.5%) were shown in Fig. 6.11(a) and (b) respectively. As can be seen, increasing the GGBFS contents of the specimens caused an increase for number of cycles to liquefaction. For instance, at a CSR of 0.20, the N_L value for untreated soil

was 175, whereas, this value increased to 192, 207, and 215 when 3%, 5%, and 7% GGBFS were added to the specimens respectively. Similar trends were followed when the CSR value changed from 0.20 to 0.35, and 0.50. For example, at CSR of 0.35, untreated soil liquefied after 145 cycle numbers while, the specimens liquefied after 161, 175, and 188 cycle numbers after addition of 3%, 5%, and 7% GGBFS contents. Similarly, at CSR value of 0.50, the untreated specimen liquefied after 115 cycle numbers while, addition of 3%, 5%, and 7% caused the specimens were liquefied at cycle's numbers of 134, 141, and 159 respectively.

Variations of the pore water pressure ratio (r_u) with number of cycles to liquefaction (N_L) for untreated and GGBFS treated specimens at CSR value of 0.2 were shown in Fig. 6.12. As can be seen, untreated soil liquefied earlier than the GGBFS treated specimens.

Noorzad and Amini (2014) used Eq. (6.2.2) to quantify improvement of the specimens after application of an agent.

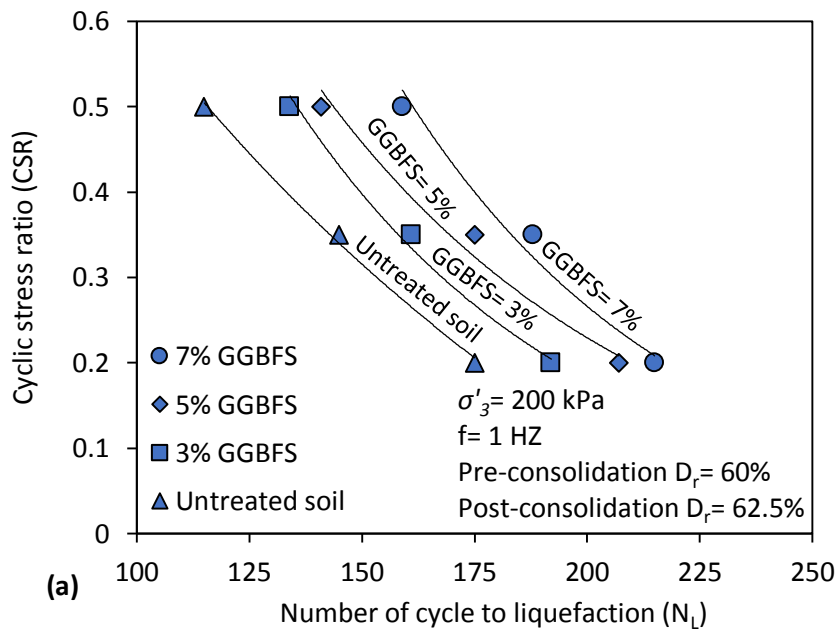
$$IMP (\%) = \frac{N_G - N_S}{N_S} \times 100\% \quad (6.2.2)$$

Where, N_G = number of cycles to liquefaction for GGBFS treated specimens; N_S = number of cycles to liquefaction for untreated specimen. The improvement of the specimens using GGBFS were quantified using Eq. (6.2.2) in this study and were summarised in Table 6.10. As shown, the percentage of improvement increased by addition of GGBFS. For instance, an improvement in the range of $9.7\% \leq IMP \leq 16.5\%$ was recorded when the tests conducted at a CSR value of 0.20. Similarly, at the CSR values of 0.35 and 0.50, an improvement in the range of $18.3\% \leq IMP \leq 22.6\%$ and $22.9\% \leq IMP \leq 38.3\%$ observed when a GGBFS content of 5% and 7% was applied in the specimens. Application of GGBFS in soil caused production of the cementitious

bonds such as calcium silicate hydrate and calcium aluminate hydrate amongst soil particles. Production of the cementitious bonds reduced the existing voids between soil particles and dissipated the pore water pressure.

Table 6.10. Effect of GGBFS contents on improvement of the liquefaction resistance of the specimens under 200 kPa effective confining pressure and a pre-consolidation relative density of 60%.

CS R	Untreated soil	GGBFS= 3%		GGBFS= 5%		GGBFS= 7%	
	N _L	N _L	Improvement (%)	N _L	Improvement (%)	N _L	Improvement (%)
0.20	175	192	9.7	207	18.3	215	22.9
0.35	145	161	11.0	175	20.7	188	29.7
0.50	115	134	16.5	141	22.6	159	38.3



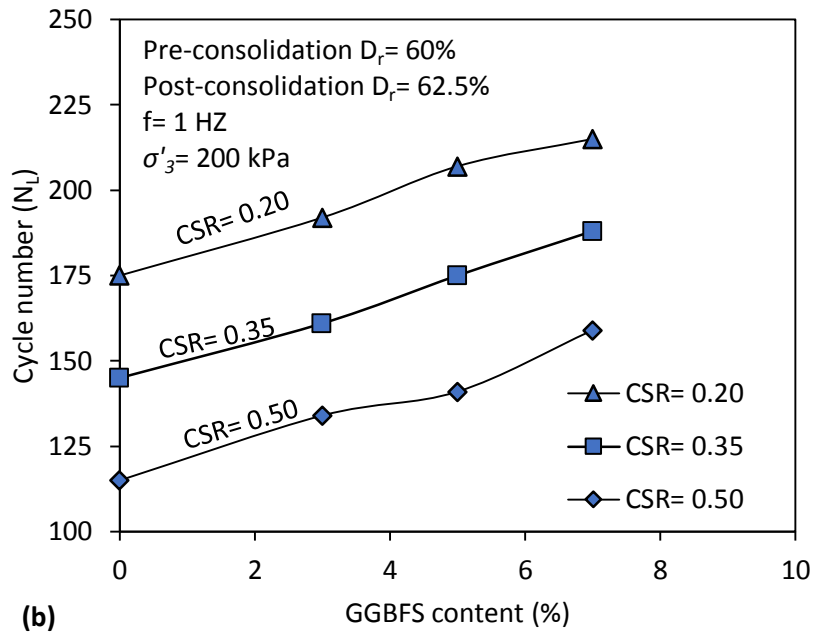


Fig. 6.11. Effect of GGBFS contents on liquefaction resistance of the soil for specimens under effective confining pressure of 200 kPa and an initial relative density of 60% (a) variations of the cyclic stress ratio (CSR) versus number of cycles to liquefaction (N_L); (b) variation of the cycle numbers (N_L) versus GGBFS contents.

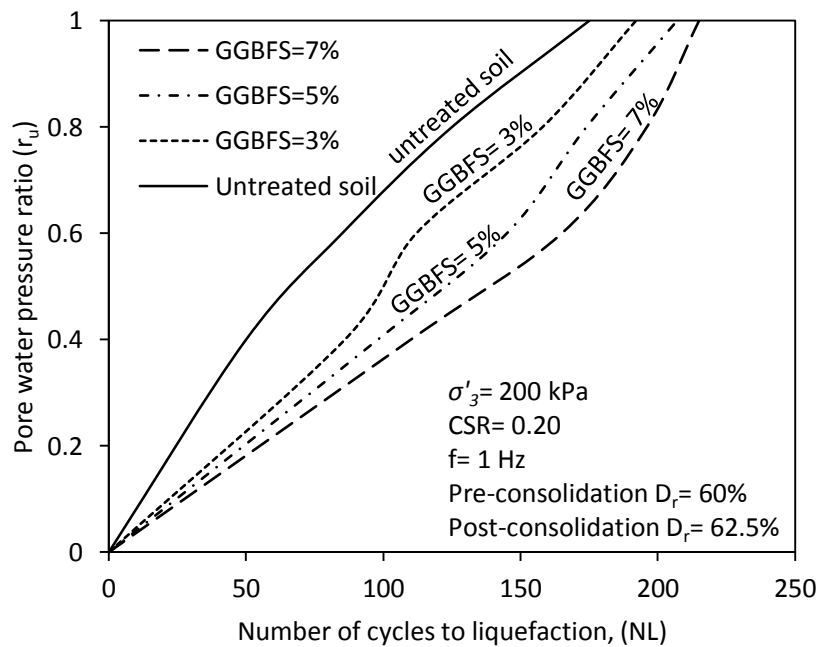


Fig. 6.12. Effect of GGBFS contents on pore water pressure ratio of the specimens under 200 kPa effective confining pressure, CSR value of 0.20, and an initial relative density of 60%

6.2.5.2. Effect of Effective Confining Pressure (σ'_3)

Figs. 6.13 (a) and (b) shows effect of effective confining stress (σ'_3) on liquefaction behaviour of GGBFS treated soil at a pre-consolidation relative density of 60% (i.e., Post-consolidation relative density of 62.5%). As can be seen, increasing the effective confining pressure, reduced the liquefaction strength of the GGBFS treated specimen. For instance, the specimen liquefied at a cycle number of 219, 184, and 161 when the tests conducted under 100 kPa effective confining pressure at a CSR value of 0.20, 0.35, and 0.50 respectively. Similarly, a cycle number in the range of $141 \leq N_L \leq 207$ and $131 \leq N_L \leq 187$ was recorded when the tests conducted under 200 and 400 kPa effective confining pressure. In addition, it is seen from figures that the liquefaction resistance of the GGBFS treated specimens reduced by increasing the CSR value.

Fig. 6.14 shows the typical curves for variations of the pore water pressure ratio (r_u) with number of cycles to liquefaction (N_L) for specimens treated with 5% GGBFS at a relative density of 60% under 100, 200, and 400 kPa effective confining pressure. As can be seen, increasing the effective confining pressure reduced the liquefaction resistance of the specimens. The recorded behaviour in this section is in agreement with reported results by Seed and Harder (1990).

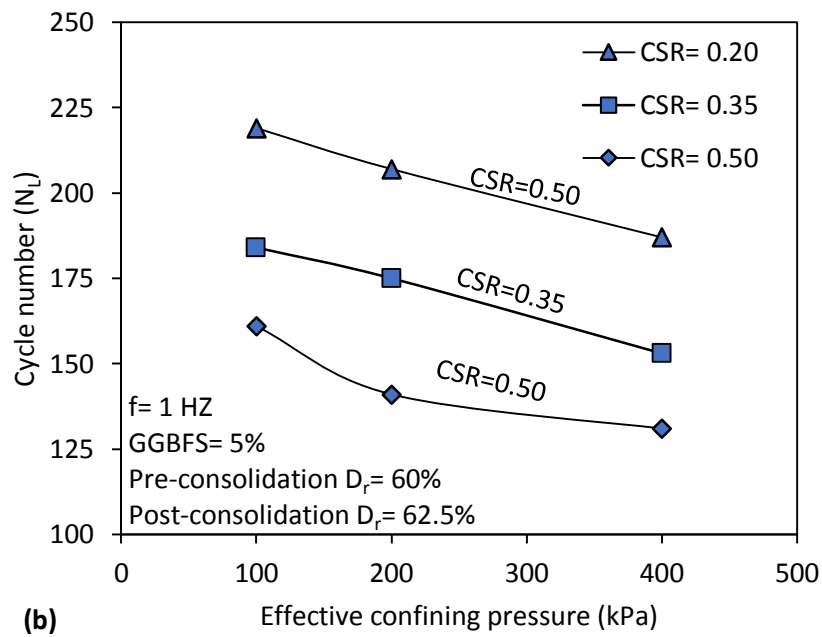
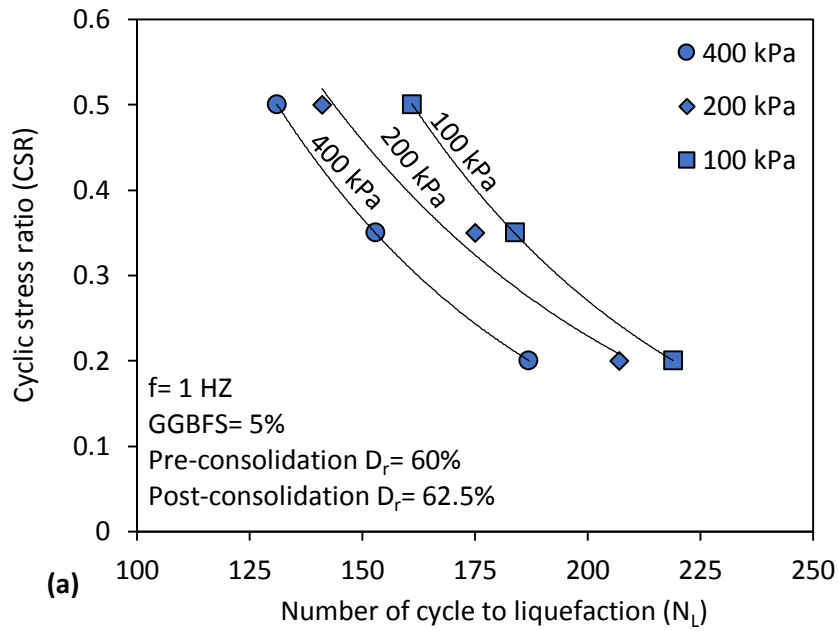


Fig. 6.13. Effect of effective confining pressure on liquefaction resistance of the 5% GGBFS treated specimens at a pre-consolidation relative density of 60% (a) variations of the cyclic stress ratio (CSR) versus number of cycles to liquefaction (N_L); (b) variation of the cycle numbers (N_L) versus effective confining pressures.

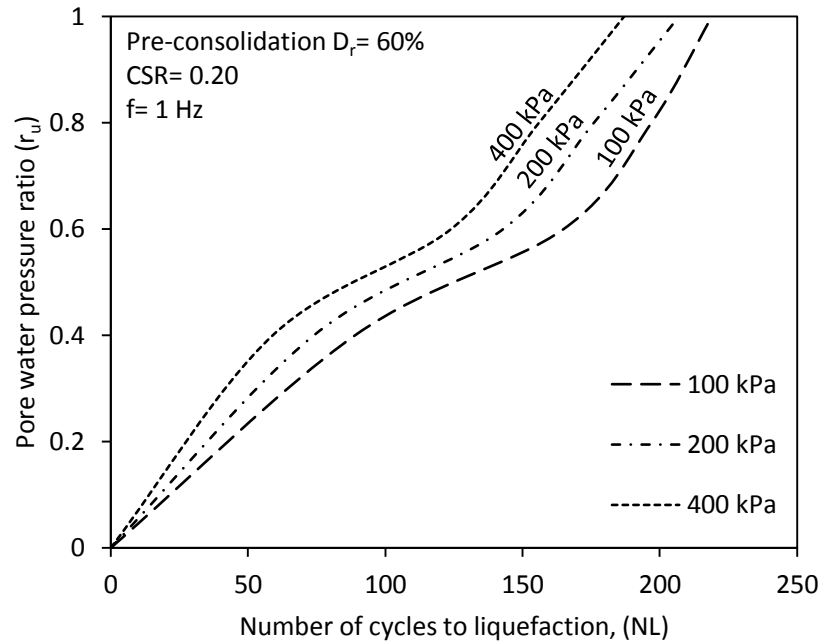


Fig. 6.14. Effect of effective confining pressure on pore water pressure ratio of the GGBFS treated specimens for a CSR value of 0.20, a pre-consolidation relative density of 60%, GGBFS= 5%.

6.2.5.3. Effect of Relative Density (D_r)

Effect of relative density on liquefaction resistance of the GGBFS treated specimens was shown in Figs. 6.15(a) and (b). Effect of three pre-consolidation relative densities of 40%, 60%, and 80% (i.e., Post-consolidation relative density of 43.6%, 62.5%, and 81.4%) for the soil when mixed with 5% GGBFS and tested under 200 kPa effective confining pressure were shown in these figures. As can be seen in the figure, increasing the relative density value caused an increase for liquefaction resistance of the soil. For instance, when the tests conducted at a relative density of 40%, the specimens were liquefied at a liquefaction numbers of 189, 152, and 134 at the CSR numbers of 0.20, 0.35, and 0.50 respectively. The N_L values followed an increasing trend by increasing the relative density value. For example, a liquefaction resistance number in the range of $141 \leq N_L \leq 207$ and $158 \leq N_L \leq 221$ were recorded when the specimens prepared at

the relative densities of 60% and 80%. Furthermore, the figures showed that increasing the number of liquefaction at different relative density has an opposite relation with number of cyclic stress ratio (CSR), and the N_L value decreased by increasing the CSR. Fig. 6.16 shows the effect of relative density for untreated and 5% GGBFS treated specimens, as can be seen, GGBFS treated specimens have more resistance to liquefaction than untreated specimens at the same relative density. For instance, the GGBFS treated specimens liquefied at the cycle numbers of 221, 207, and 189 at the relative density of 40%, 60%, and 80%, whereas the untreated specimens have N_L values of 204, 187, and 175 at the same relative densities. Increasing relative density of the specimens caused reduction of void numbers amongst soil particles, which decline generation of the pore water pressure. Application of the GGBFS in the soil and filling the remained voids by hydration product such as calcium silicate hydrate and calcium aluminate hydrate provide more difficulties for generation of the pore water pressure. This behaviour promotes liquefaction strength of GGBFS treated sand in a greater D_r (Noorzad and Amini 2014; Keramatikerman et al. 2017b).

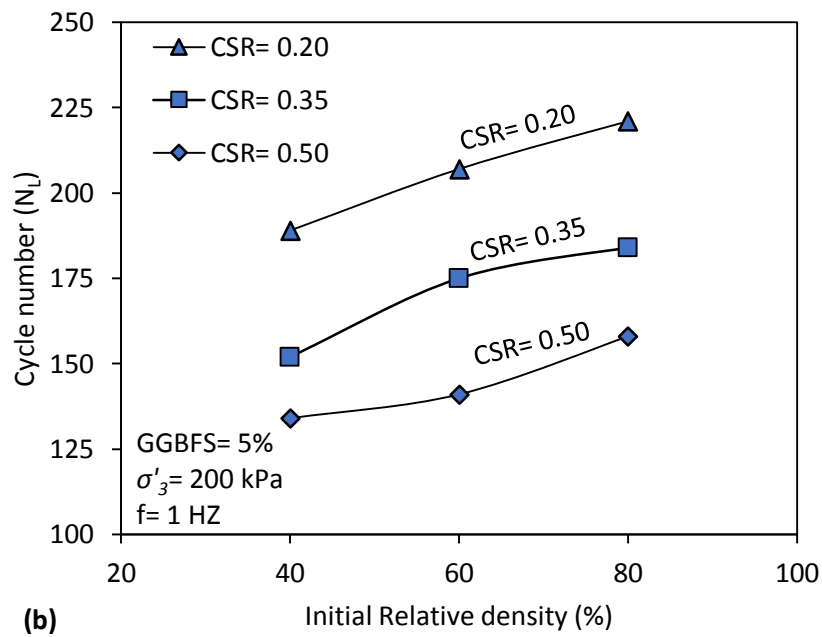
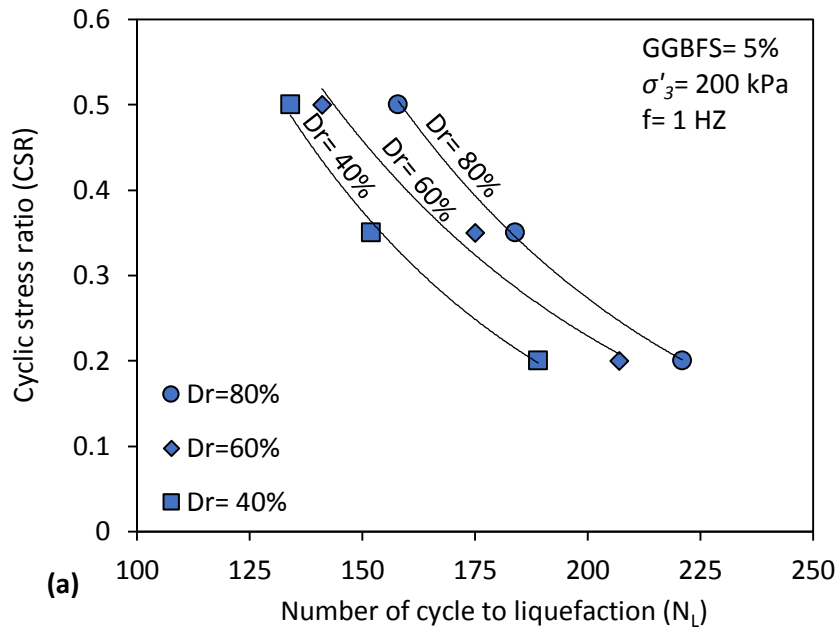


Fig. 6.15. Effect of initial relative density on liquefaction resistance of the GGBFS treated soil for specimens under effective confining pressure of 200 kPa (a) variations of the cyclic stress ratio (CSR) versus number of cycles to liquefaction (N_L); (b) variation of the cycle numbers (N_L) versus initial relative densities.

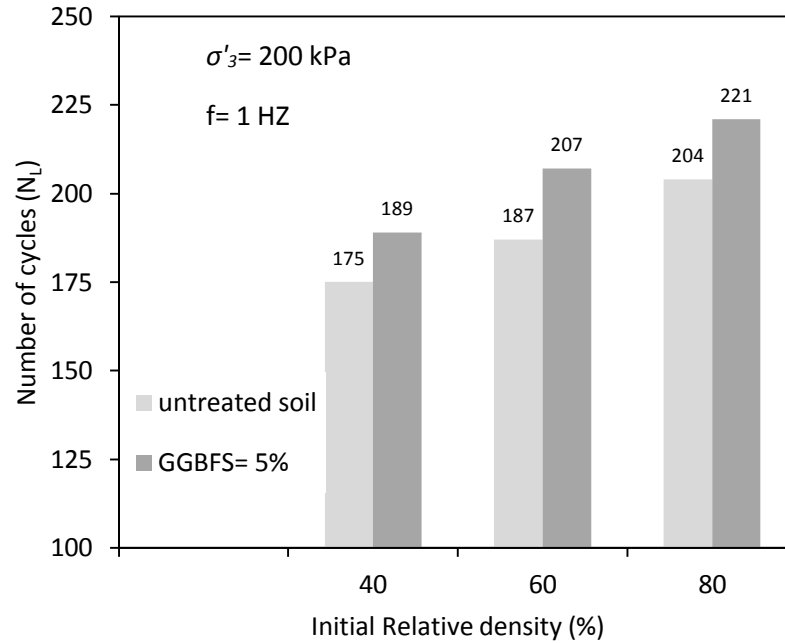


Fig. 6.16. Effect of relative density on liquefaction resistance of the untreated and GGBFS treated specimens for a pre-consolidation relative density of 60%, a GGBFS content of 5%, and a CSR value of 0.20.

6.2.5.4. Effect of Curing Time

To investigate effect of curing time on liquefaction resistance of the GGBFS treated specimens a series of the cyclic triaxial tests conducted on the specimens cured at 7, 14 and 28 days. Figs. 6.17(a) and (b) shows effect of curing periods on cyclic resistance of GGBFS treated specimens tested under 60 kPa effective confining pressure and prepared at a pre-consolidation relative density of 60%. It seen from the figure that number of cycles to liquefaction has a linear relation with curing time and increased by increasing the curing time. For instance, while the specimens after 7 days curing time showed a N_L in the range of 207, 175, and 141 at a CSR value of 0.20, 0.35, and 0.50, this value increased to the range of $163 \leq N_L \leq 223$ and $175 \leq N_L \leq 236$ when the samples cured for 14 and 28 days for the same CSR values respectively. The analysis

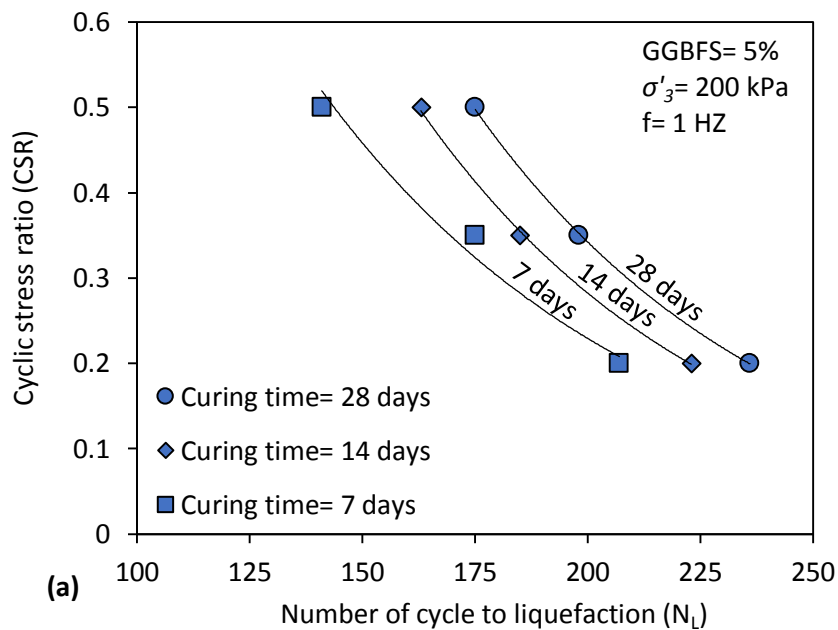
also shows that greater values of liquefaction resistance recorded at lower values of CSR.

Fig. 6.18 shows typical curves for variations of the pore water pressure ratio for GGBFS treated specimens after 7, 14, and 28 days curing time. As can be seen, increasing the curing time caused a delay to reach maximum value of pore water pressure ratio (i.e., $r_u=1$).

Effect of curing time on cyclic strength of the GGBFS treated specimens were compared with untreated specimens and its improvement quantified in Table 6.11. As can be seen, curing of the specimen for 7 days, caused an improvement in the range of $18.3\% \leq IMP \leq 22.6\%$ for a CSR value in the range of $0.20 \leq CSR \leq 0.50$. The improvement of the GGBFS treated specimens followed its increasing trend in the range of $27.4\% \leq IMP \leq 41.7\%$ and $34.9\% \leq IMP \leq 52.2\%$ when 5% GGBFS treated specimens were cured for 14 and 28 days at the mentioned CSR range values respectively. Application of GGBFS causes production of the hydration products such as calcium silicate hydrate, calcium aluminate hydrate, and calcium silicate aluminate hydrate. As the time goes by, the pozzolanic reactions caused generation of the hydration products to be accelerated and greater amount of bonds to be formed amongst soil particles that hardly is broken during cyclic loads. It might be the main reason for increasing the liquefaction resistance of the soil by increasing the curing time.

Table 6.11. Effect of curing time on improvement of the liquefaction resistance of the specimens at a pre-consolidation void ratio of 60% and a GGBFS content of 5%.

CS R	Untreated soil	Curing time= 7 days		Curing time= 14 days		Curing time= 28 days	
	N_L	N_L	Improvement (%)	N_L	Improvement (%)	N_L	Improvement (%)
0.20	175	207	18.3	223	27.4	236	34.9
0.35	145	175	20.7	185	27.6	198	36.6
0.50	115	141	22.6	163	41.7	175	52.2



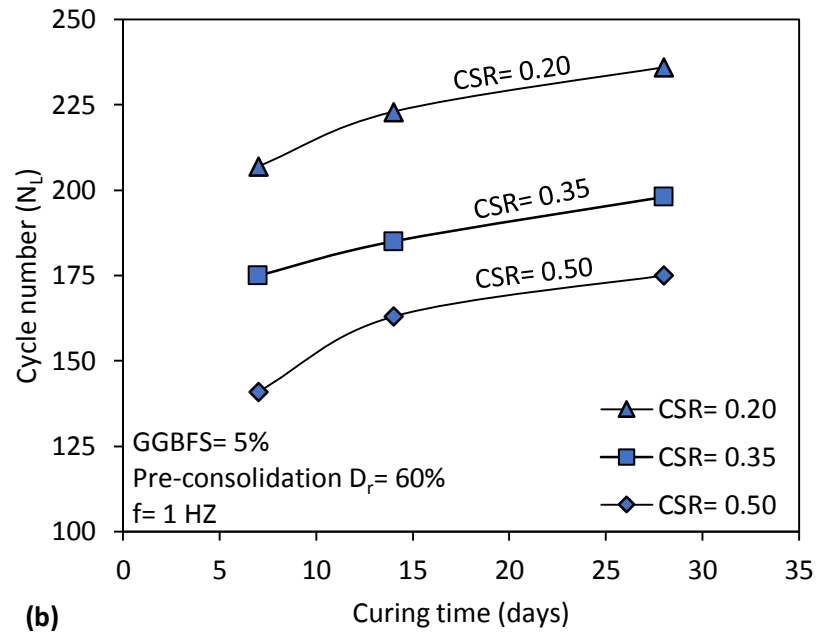


Fig. 6.17. Effect of curing time on liquefaction resistance of the GGBFS treated soil for specimens under effective confining pressure of 200 kPa and a pre-consolidation relative density of 60% (a) variations of the cyclic stress ratio (CSR) versus number of cycles to liquefaction (N_L); (b) variation of the cycle numbers (N_L) versus curing time.

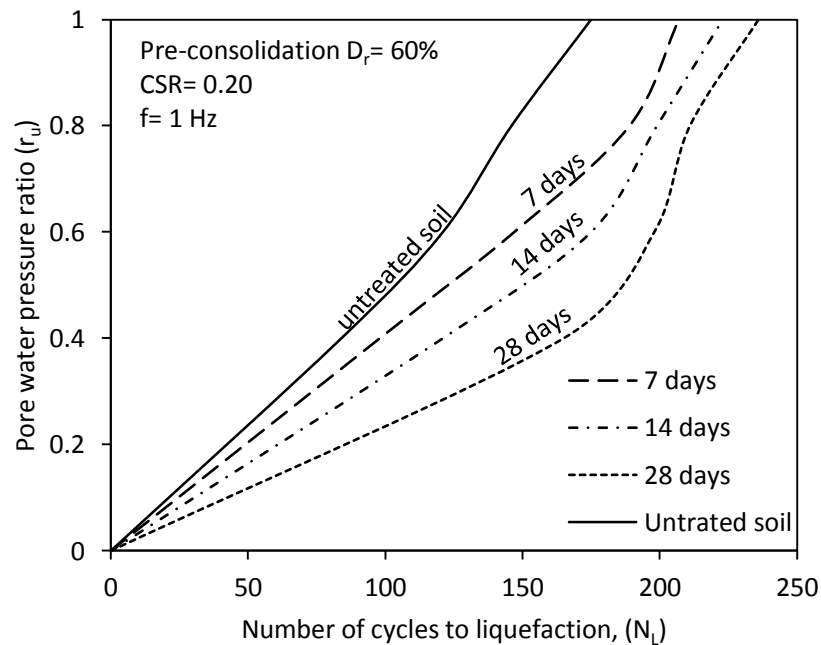


Fig. 6.18. Effect of curing time on pore water pressure ratio of the specimens at 200 kPa effective confining pressure, CSR value of 0.20, and a pre-consolidation relative density of 60%

6.2.6. Conclusion

Application of traditional agents to improve mechanical behaviour of the soils have been discouraged due to their carbon footprint, and their impact on the environment. Besides, more environmental friendly alternatives such as GGBFS have been proposed and used by previous researchers. Previous studies investigated mechanical behaviour of the GGBFS in a static state and no study conducted to investigate its dynamic behaviour. This study investigated liquefaction strength of GGBFS amended sand by performing undrained cyclic triaxial tests. Following conclusions can be drawn from the results:

- Addition of 3%, 5%, and 7% GGBFS in the specimens caused an increase for the liquefaction resistance and improved in the range of $9.7\% \leq IMP \leq 16.5\%$, $18.3\% \leq IMP \leq 22.6\%$, and $22.9\% \leq IMP \leq 38.3\%$ respectively.
- The investigations showed that the effective confining pressure has an opposite behaviour with liquefaction resistance of the GGBFS treated soil, and the specimens under greater effective confining pressures showed a lower value of the cyclic strength.
- Increasing the relative density of the GGBFS treated specimens, increased the liquefaction resistance of the specimens. A comparison between N_L values of untreated specimens and GGBFS treated specimens at different relative densities showed that the GGBFS treated specimens have a greater liquefaction resistance in all cases.
- Investigations on effect of curing time on cyclic strength of the GGBFS treated specimens showed that the specimens after 28 days and 14 day curing time have a greater N_L values in comparison with 7 days treated specimens. The results showed that an improvement in the range of $18.3\% \leq IMP \leq 22.6\%$,

$27.4\% \leq IMP \leq 41.7\%$, and $34.9\% \leq IMP \leq 52.2\%$ after 7, 14, and 28 days curing period were recorded.

6.3. CHAPTER CONCLUSIONS

The chapter six investigated the effect of two binders (i.e., FA and GGBFS) on the cyclic liquefaction behaviour of sand. The first part of this chapter investigated the effect of fly ash (FA) on cyclic liquefaction behaviour of sand by performing a series of cyclic triaxial tests. The effect of relative density, FA contents, effective confining pressure, and the curing time were investigated, and the results were presented. The tests were conducted on two types of the specimens (i.e., untreated and 2% FA added) to investigate the effect of relative densities (i.e., 20, 40, 60, and 80%) and the results showed that 2% FA added specimens with a relative density of 80% has the greatest liquefaction resistance. In addition, the investigation on effect of FA contents (i.e., 0, 2, 4, and 6%) showed that the specimens with a greater FA content have a higher cyclic liquefaction resistance. The analysis on the effect of effective confining pressure on 2% FA added specimen showed that the specimens at a greater effective confining pressure intended to be liquefied earlier due to suppression of dilatancy of soil. To investigate the effect of curing time, the FA treated specimens were cured for 14 and 28 days and then tested. The results showed that the specimens cured at a greater curing period have a greater liquefaction resistance.

The second part of this chapter investigated the role of ground granular blast furnace slag (GGBFS) on cyclic liquefaction resistance of sand by performing a series of undrained cyclic triaxial tests. The effect of four GGBFS contents (i.e., 0, 3, 5, and 7%), three effective confining stress (i.e., 100, 200, and 400 kPa), three relative densities (i.e., 40%, 60%, and 80%), and three curing periods of 7, 14 and 28 days were investigated, and the results were presented and analysed. In addition, the improvements in liquefaction resistance were quantified and presented in each section. The results showed that increasing the GGBFS contents is effective and improved the

liquefaction resistance of the specimens. The investigations showed that increasing the relative density is more effective in GGBFS treated specimens than untreated specimens to increase the liquefaction strength of the soil. The results showed that the GGBFS treated specimens have a lower liquefaction resistance when tested under a greater effective confining pressure, and when tested after a greater curing period.

Chapter 7

Effect of Binders on Post-cyclic Behaviour

CHAPTER INTRODUCTION

The main failures in geotechnical structures such as embankments, dams, and slopes happen up to 24 hours after an actual seismic event. Therefore, strength analysis of the soil after a seismic event such as earthquake is of great importance. Beside of the seismic characteristics, the soil characteristics such as relative density, and the external loads are crucial parameters to analyse the post-cyclic behaviour of the soil. Investigation of the effect of two ground improvement additives (i.e., FA and GGBFS) on post-cyclic behaviour of sand is the topic of investigations in this chapter.

The chapter seven is consisted of two parts. In the first part, the effect of FA on post-cyclic strength characteristics of sand has been investigated, and in the second part the effect of GGBFS on post-cyclic strength characteristics of sand has been investigated. The results of the first part published by Keramatikerman et al. (2018b).

Part 1

Effect of FA on Post-cyclic Behaviour of Sand

7.1. Effect of FA on Post-cyclic Behaviour of Sand

7.1.1. Abstract

The main failures in geotechnical structures like slopes and embankments usually happen only a few hours after an earthquake event, hence investigation of the strength characteristics of soil after a seismic event is of great importance. The effect of fine-grained on strength characteristics of soil in post-cyclic phase significantly has been investigated, however the effect of some by-product admixtures such as fly ash (FA) is unknown. This study focused to investigate the effect of FA addition on post-cyclic behaviour of sand by performing a series of undrained post-cyclic monotonic triaxial compression tests. The effect of four FA contents (i.e., 0, 2, 4, and 6% by dry weight), three pre-consolidation relative densities (i.e., 20, 40, and 60%), and three initial mean effective stress (i.e., 50, 70, and 90 kPa) were investigated. To conduct the post-cyclic tests, initially the cyclic tests were performed until a desired pore water pressure ratio (r_u) (i.e., 0.25, 0.50, or 0.75) and then the post-cyclic test initiated. In addition, a series of undrained monotonic triaxial tests were conducted to investigate effect of zero pore water pressure ratio ($r_u=0$). The results showed that increasing the FA contents is effective to increase the ultimate deviatoric strength (q_u) of the specimens. Furthermore, investigations showed that the FA treated specimens have a greater q_u value at a higher relative density and lower initial mean effective stress.

7.1.2. Introduction

7.1.2.1. Post-cyclic Behaviour of Soil

The geo-structures such as slopes and embankments can be damaged during cyclic loadings triggered by a seismic event like earthquake. The damaging and failures can be continued even after an actual seismic event by reduction of shear strength and

stiffness of the soil structure. It has been reported that most failures in earth dams have acquired from just a few hours to up to 24 h after an earthquake event (Wang et al. 2015a; Soroush and Soltani-Jigheh 2009). This phenomenon is known as delayed failure or delayed response and highlights the importance of the post-cyclic behaviour of the soil (Wang et al. 2015a). Previous researches investigated the post-cyclic behaviour of soil (Noorzad and Shakeri 2017; Ishihara et al. 2016; Kargar et al. 2016; Wang et al. 2016: 2015b; Kaya and Erken 2015; Pillai et al. 2014; Tavakoli et al. 2011; Mollamahmutoglu and Yilmaz 2010; Ashour et al. 2009; Zand et al. 2009; Erken and Ulker 2007; Shafiee 2006; Shamoto et al. 1998; Kiku and Tsujino 1996; Chern and Lin 1994). For instance, Rouholamin et al. (2017) investigated effect of initial relative density on post-liquefaction behaviour of the soil by performing a series of cyclic triaxial tests on four types of soil after their liquefaction state. They highlighted the importance of three parameters of the initial shear modulus, critical state shear modulus, and post-dilation shear strain as dependent parameters in initial relative density and in forming stress path behaviour ($q-p'$) of sand in post-liquefaction phase. In another study, Hazirbaba and Omarow (2015) investigated the settlement behaviour of sand after post-cyclic loading by performing a series of strain-controlled undrained cyclic triaxial tests. They also investigated the effect of excess pore water pressure, triggered shear strain, confining pressure, loading cycles, and relative density on settlement of the soil in post-cyclic phase. They indicated that the settlement of the soil in post-liquefaction phase is mainly correlated with excess pore water pressure and increasing the excess pore water pressure increase the settlement behaviour of the soil. They also indicated that increasing the confining pressure in the range of 100 to 400 kPa reduced the excess pore water pressure build-up. In one study, Noorzad and Shakeri (2017) investigated the effect of silt contents on post liquefaction

behaviour of the sand. They indicated that the ultimate deviatoric strength of the soil is changed by increasing the silt contents. For example, the deviatoric strength of the soil reduced by increasing the silt content of the sand by 15% and increased by increasing the silt content by 30%.

In laboratory, the post-cyclic phase is simulated using a cyclic triaxial device by monotonically applying a loading stress after a targeted number of cyclic loadings or a specified pore water pressure ratio. Fig. 7.1 schematically compares the stress-strain ($q-p'$) phase in monotonic ($r_u = 0$), post-cyclic ($r_u = 0.5$), and post-liquefaction ($r_u = 1$) tests.

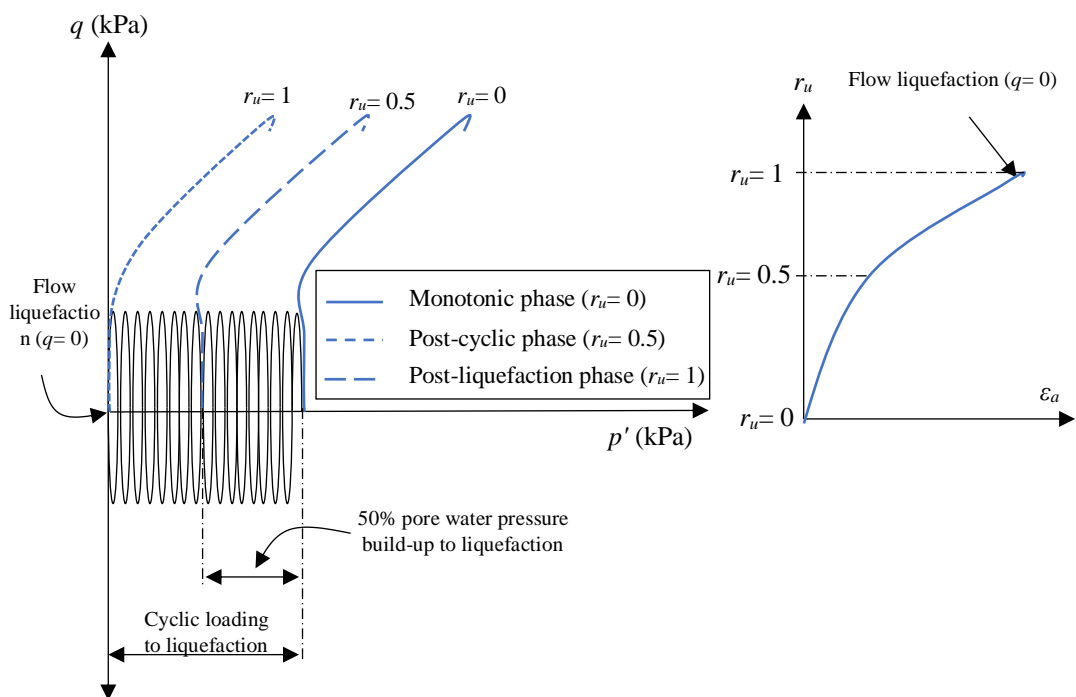


Fig. 7.1. Schematic overview for stress-strain ($q-p'$) and pore water pressure ratio ($r_u-\epsilon_a$) phases in monotonic and two post-cyclic tests

7.1.2.2. Ground Improvement

Application of soil stabilisation agents is a well-accepted approach in ground improvement. However, Portland cement (PC) and lime are two effective agents to increase shear strength characteristics of the soil, their application is accompanying with environmental risks and application of more environmental friendly agents have been encouraged ([Keramatikerman et al. 2016](#)). Fly ash (FA) is a fine and grey by-product materials which is generated from fired coal in power stations. It has a well-round shape particle and has pozzolanic characteristics which encourage the practitioners to use it in ground improvement projects. Previous studies investigated the effect of fly ash in ground improvement ([Keramatikerman et al. 2017b](#); [Horpibulsuk et al. 2011; 2009](#); [Prabakar et al. 2004](#) amongst others). For example, Keramatikerman et al. ([2016](#)) investigated the effect of fly ash on liquefaction strength of the soil and indicated that application of fly ash is effective to increase the cyclic strength of the soil.

In aforementioned literature, the importance of the post-cyclic phase in stability of the geo-structures after a seismic event highlighted. Furthermore, it was determined that application of some environmental friendly agents such as fly ash is effective to improve the cyclic strength of the soil, however, its behaviour after cyclic loadings (i.e., post-cyclic phase) is known. Hence, this study aims to investigate the effect of fly ash on post-cyclic behaviour of the soil. This study is in continue of the effect of Fly ash on liquefaction behaviour of soil at Curtin University ([Keramatikerman et al. 2017b](#)).

7.1.3. Materials and Methods

7.1.3.1. Materials Used

A local sand commercially known as Baldivis sand was supplied from south of Perth, Western Australia. The sieve analysis conducted on the used sand based on ASTM C136 (ASTM 2014b) and the results were presented in Fig. 7.2. The sieve analysis showed that this soil has a uniformity coefficient (C_u) and a coefficient of curvature (C_c) of 2.5 and 1.19 respectively. This sand is a poorly graded soil (SP) based on the Unified Soil Classification System (USCS) [(ASTM D2487, (ASTM 2011a)], and has a specific gravity (G_s) of 2.67. The X-ray powder diffraction (XRD) analysis showed that the quartz (Q) is the main constituent of the used sand. Furthermore, the scanning electron microscopy (SEM) image analysis on used sand revealed that this soil has an angular morphology [see Fig. 7.3]. The used fly ash (FA) was sourced from a local supplier in Perth, Western Australia (Flyash Australia 2016). The XRD analysis showed that quartz (Q), Mullite (Mu), and hematite (H) are the main constituent minerals of the used FA (Keramatikerman et al. 2017b). In addition, the specific gravity of used FA was 3.1. The scanning electron microscopy (SEM) image of used fly ash showed that the used fly ash consists of spherical particles. Fig. 7.4 shows the SEM analysis of used fly ash.

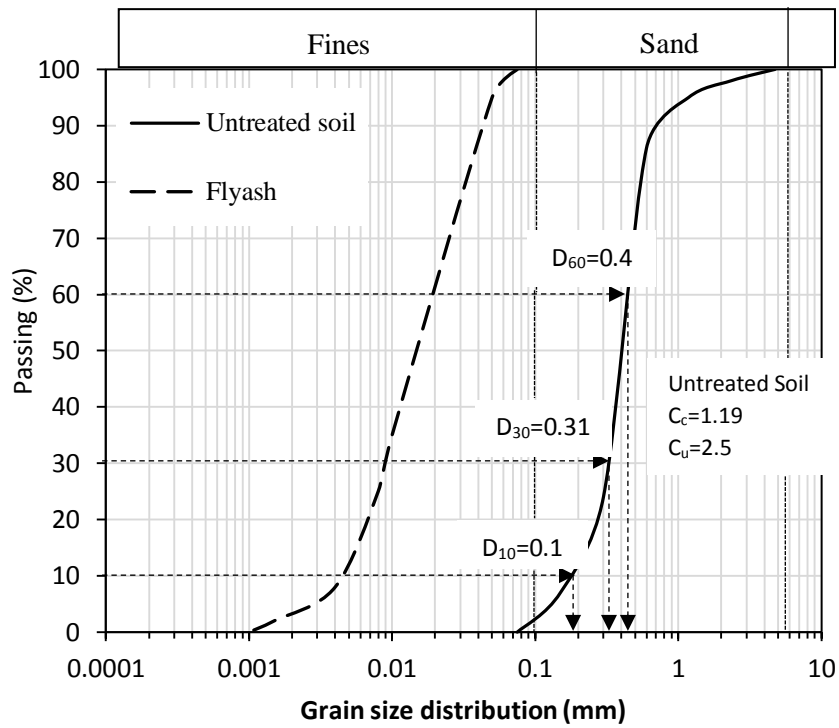


Fig. 7.2. Particle size distribution of used materials

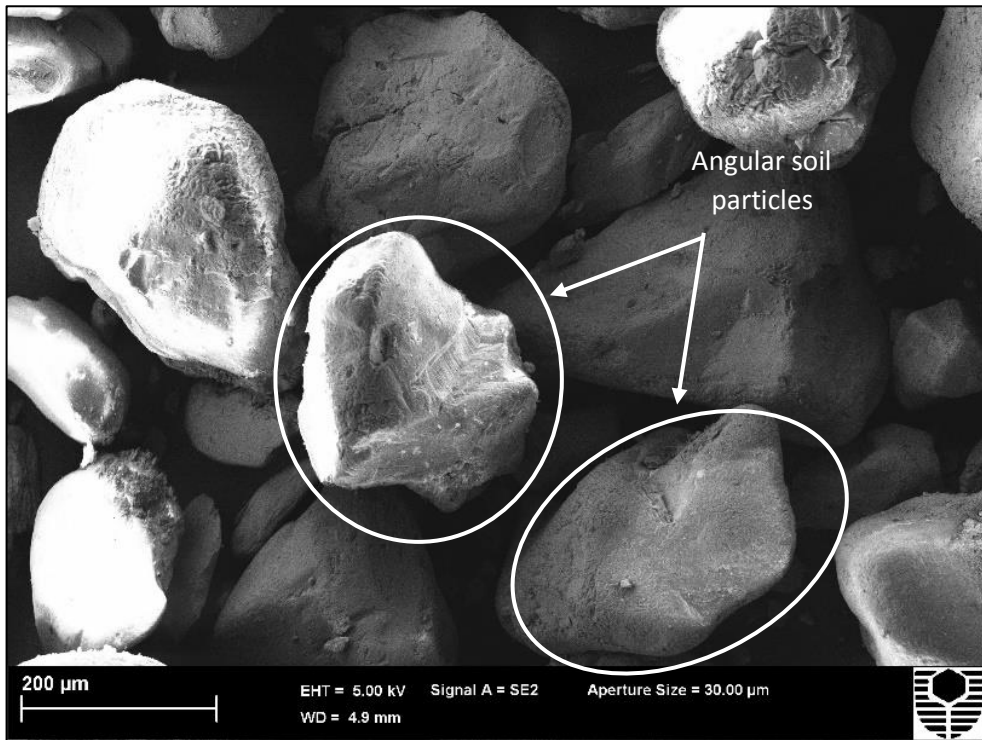


Fig. 7.3. Scanning electron microscopy (SEM) image of used sand

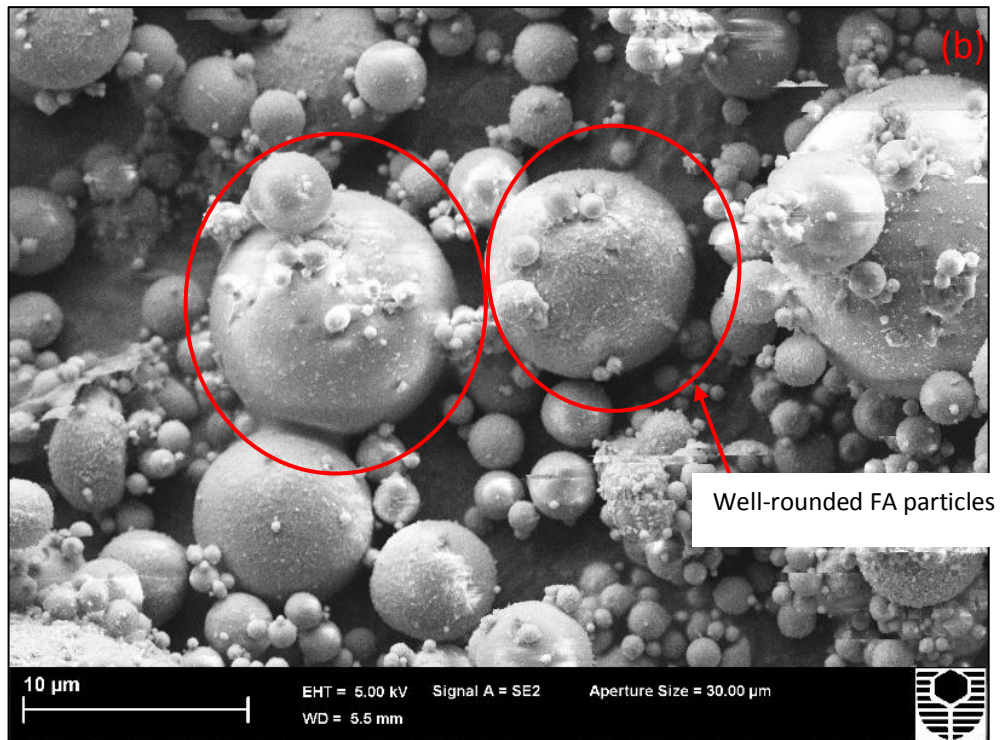


Fig. 7.4. Scanning electron microscopy (SEM) image of used fly ash (FA)

7.1.3.2. Specimen Preparation

The specimen preparation has a crucial role in a triaxial testing since application of different techniques lead to different results. The wet tamping method is a widely accepted technique to prepare the triaxial specimens. This method provides an appropriate level of integrity and homogeneity for sandy specimens. This method also helps the user to have a better control on the density and void ratio of the specimens (Ladd 1978). The wet tamping method was employed in this study to prepare the specimens.

To prepare the specimens, initially the desired amount of soil and FA (i.e., 0, 2, 4, and 6% by dry weight) was mixed with water based on the optimum moisture content of each mixture acquired from compaction tests and thoroughly stirred. After that, the mixture was placed into a cylindrical split mould while a membrane pulled inside of the mould. The membrane was tightened inside of the mould wall with an applied low

vacuum throughout the sample preparation phase. Each mixture was compacted in five layers and compacted until the desired height obtained (i.e., 125-mm) based on the maximum dry density (MDD) values acquired from the compaction tests. A filter paper and porous stone with a diameter of 65-mm was placed on bottom and on top of each sample for ease of saturation before and after sample preparation respectively. The specimens were prepared with initial relative densities (D_r) of 20, 40, and 60%.

7.1.3.3. Testing Procedure

Upon completion of the sample preparation, each specimen was put inside of the triaxial chamber and then the triaxial cell was mounted on the cell base of the triaxial device. The saturation phase was completed when the coefficient of Skempton (i.e., B -value), which is computed by dividing the pore water pressure by the cell pressure (i.e., $\Delta u/\Delta\sigma_3$) is equal or greater than 0.95. When the saturation phase completed, the specimens isotropically were consolidated under the desired initial mean effective stress (p_o') of 50, 70 or 90 kPa. The post-consolidation relative density (D_{rp}) of the specimens were computed by measuring the volumetric strain after completion of consolidation phase. To perform the post-cyclic tests, initially the stress-controlled cyclic triaxial compression tests were conducted with sinusoidal stresses, and a cyclic stress ratio (CSR) of 0.2 at a frequency of 1 Hz. The cyclic tests were in accordance with ASTM D5311 (ASTM 2013) and continued until the pore water pressure ratio (r_u) reached 0.25, 0.50, or 0.75 before sample failure. Furthermore, a series of undrained monotonic triaxial tests were conducted in accordance with ASTM D7181 (ASTM 2011e) to investigate the effect of zero pore water pressure ratio (i.e., $r_u = 0$) on specimens. The pore water pressure ratio is computed by dividing the excess pore water pressure which is triggered by deviatoric stresses by initial mean effective stress

(i.e., $r_u = u/p_0'$) is an appropriate benchmark to evaluate the post-cyclic behaviour of the specimens rather than other parameters such as shear strain since the pore water pressure dramatically increases in a short range of shear strain which provide more complexity for the results. Upon completion of the cyclic stage, the post-cyclic testing phase was initiated by monotonically loading of the specimens with a shear strain rate of 0.1 mm/min until an axial strain of 25%. Fig. 7.5 shows the typical effective stress paths recorded in cyclic loading stage for untreated specimens with an initial relative density of 20% under 50 kPa initial mean effective stress at pore pressure ratios of 0.25, 0.50, and 0.75. As shown, at a greater r_u the specimens have a greater loading cycle number and are close to flow liquefaction state. Table 7.1 shows the test program followed in this study to conduct the tests.

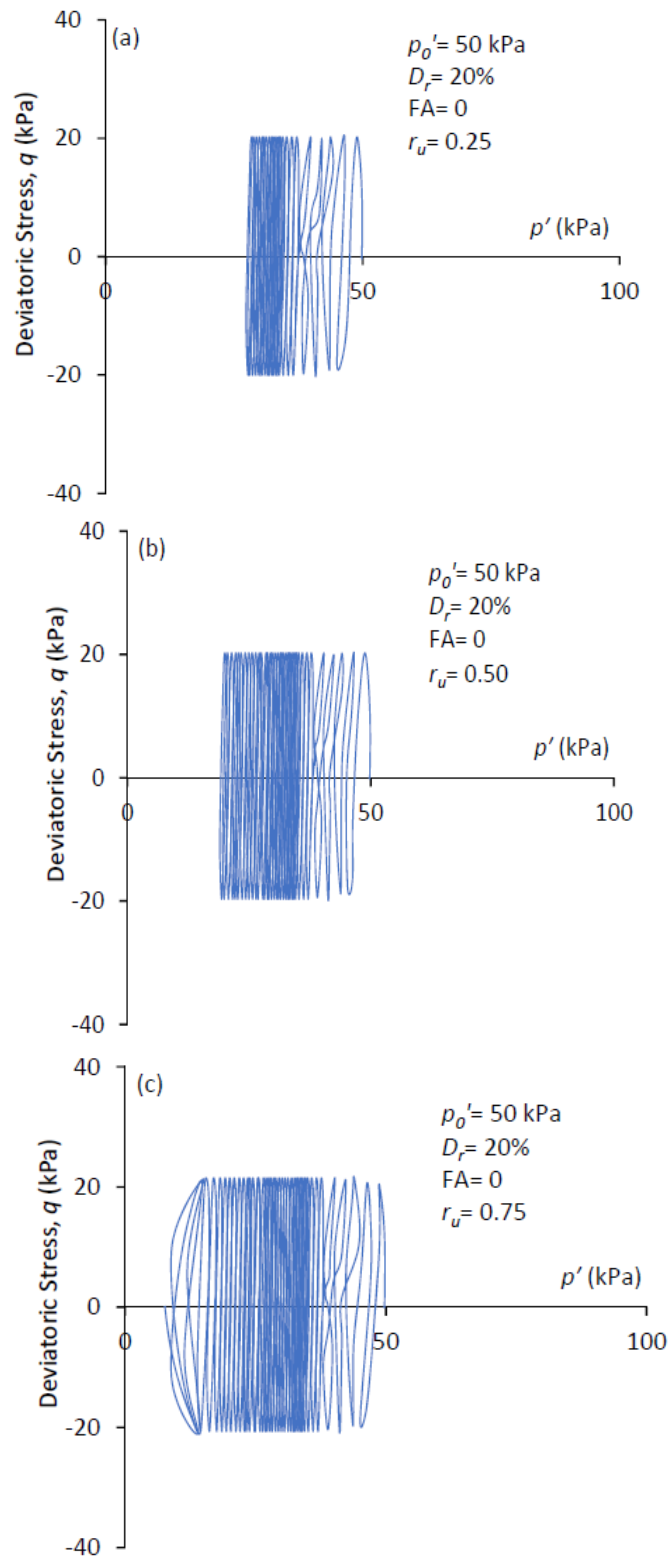


Fig. 7.5. Typical effective stress paths (q - p') recorded in cyclic stage and before initiation of the post-cyclic phase for (a) $r_u = 0.25$; (b) $r_u = 0.50$; and (c) $r_u = 0.75$

Table 7.1. Experimental program and key results for tests

Test No.	Test type	Test ID	FA content (%)	$p_{o'}$ (kPa)	CSR	D_r	D_{rp}	r_u
1	Static	SS1	-	50	-	20	21.6	-
2	Post cyclic	PS1	-	50	0.2	20	21.6	0.25
3	Post cyclic	PS2	-	50	0.2	20	21.6	0.50
4	Post cyclic	PS3	-	50	0.2	20	21.6	0.75
5	Static	SSF1	2	50	-	20	21.6	-
6	Post cyclic	PS4	2	50	0.2	20	21.6	0.25
7	Post cyclic	PS5	2	50	0.2	20	21.6	0.50
8	Post cyclic	PS6	2	50	0.2	20	21.6	0.75
9	Static	SSF2	4	50	-	20	21.6	-
10	Post cyclic	PS7	4	50	0.2	20	21.6	0.25
11	Post cyclic	PS8	4	50	0.2	20	21.6	0.50
12	Post cyclic	PS9	4	50	0.2	20	21.6	0.75
13	Static	SSF3	6	50	-	20	21.6	-
14	Post cyclic	PS10	6	50	0.2	20	21.6	0.25
15	Post cyclic	PS11	6	50	0.2	20	21.6	0.50
16	Post cyclic	PS12	6	50	0.2	20	21.6	0.75
17	Static	SSF4	-	50	-	40	42.1	-
18	Post cyclic	PS13	-	50	0.2	40	42.1	0.25
19	Post cyclic	PS14	-	50	0.2	40	42.1	0.50
20	Post cyclic	PS15	-	50	0.2	40	42.1	0.75
21	Static	SSF5	-	50	-	60	62.3	-
22	Post cyclic	PS16	-	50	0.2	60	62.3	0.25
23	Post cyclic	PS17	-	50	0.2	60	62.3	0.50
24	Post cyclic	PS18	-	50	0.2	60	62.3	0.75
25	Static	SSF6	2	50	-	40	42.1	-
26	Post cyclic	PS19	2	50	0.2	40	42.1	0.25
27	Post cyclic	PS20	2	50	0.2	40	42.1	0.50
28	Post cyclic	PS21	2	50	0.2	40	42.1	0.75
29	Static	SSF7	2	50	-	60	62.3	-
30	Post cyclic	PS22	2	50	0.2	60	62.3	0.25
31	Post cyclic	PS23	2	50	0.2	60	62.3	0.50
32	Post cyclic	PS24	2	50	0.2	60	62.3	0.75
33	Static	SSF8	2	70	-	20	21.6	-
34	Post cyclic	PS25	2	70	0.2	20	21.6	0.25
35	Post cyclic	PS26	2	70	0.2	20	21.6	0.50
36	Post cyclic	PS27	2	70	0.2	20	21.6	0.75
37	Static	SSF9	2	90	-	20	21.6	-
38	Post cyclic	PS28	2	90	0.2	20	21.6	0.25
39	Post cyclic	PS29	2	90	0.2	20	21.6	0.50
40	Post cyclic	PS30	2	90	0.2	20	21.6	0.75

7.1.4. Results and Discussion

7.1.4.1. Typical Monotonic Triaxial Tests

Fig. 7.6 shows the typical results of undrained monotonic triaxial compression tests conducted on untreated soil and FA treated specimens with a pre-consolidation relative density (D_r) of 20% under 50 kPa initial mean effective stress (p'_0). It is seen from the figure that the untreated soil (i.e., SS1) has a contractive behaviour until around 4% axial strain then its stress path changes to strain-hardening until the end of the test. The variation of the excess pore water pressure versus axial strain ($u-\varepsilon_a$) for SS1 specimen also shows that the pore water pressure dramatically increases until around 4% axial strain and then it shows a constant trend until the end of the test. The results show that the addition of FA into the specimens changed the stress-strain behaviour of the soil. For instance, while the untreated soil has a strong strain-softening behaviour, addition of FA caused the FA added specimens (i.e., SSF1, SSF2, and SSF3) to have a weak strain-softening behaviour. Furthermore, increasing the FA contents of the specimens improved the ultimate deviatoric stress (q_u) of the specimens. The pore water pressure build-up also shows a decreasing trend by increasing FA contents. In fact, the FA particles fill the microscopic pores amongst sand particles and prevent generation of the pore water pressure. This may be the main reason for increasing the ultimate deviatoric strength for FA treated specimens.

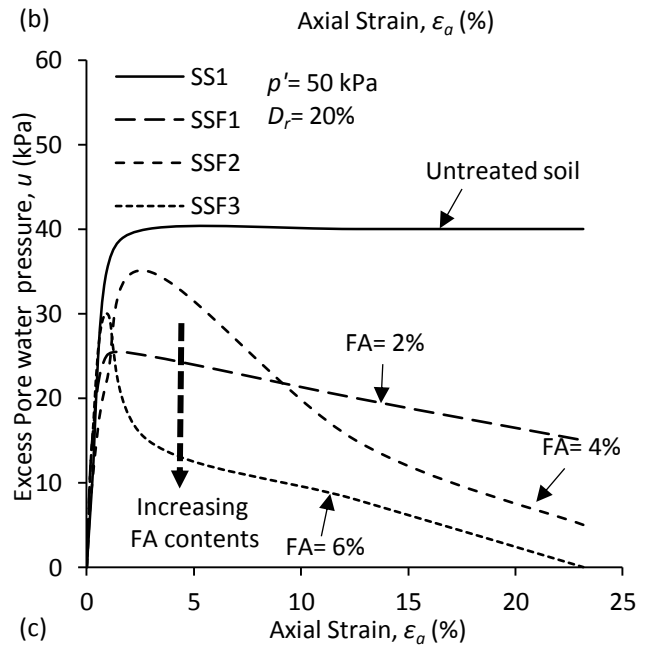
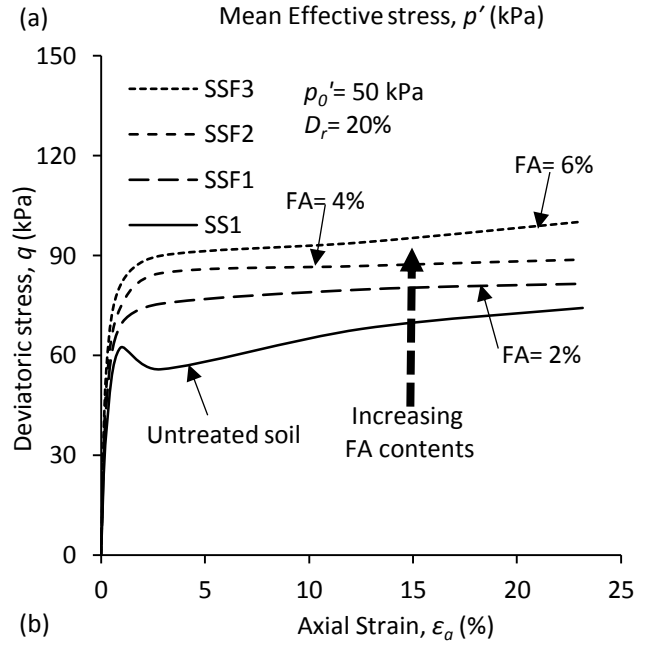
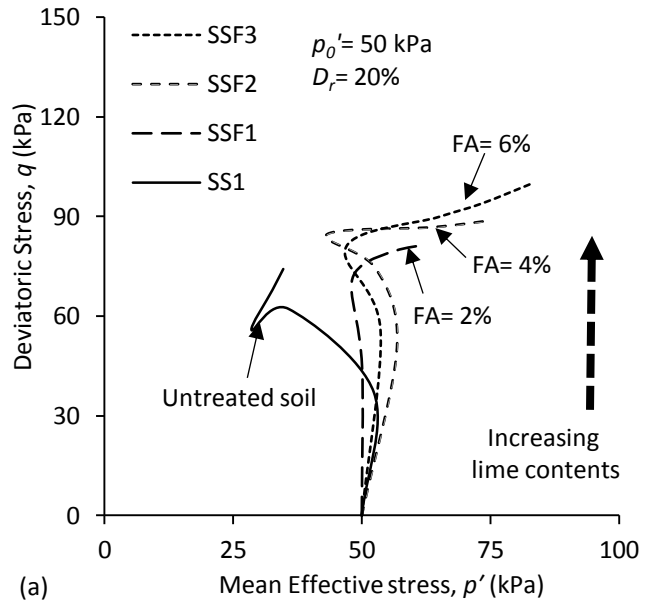


Fig. 7.6. Typical undrained shear response for untreated soil and FA treated specimens with an initial relative density of 20% under 50 kPa initial mean effective stress acquired from monotonic triaxial tests (a) stress path ($q-p'$); (b) stress-strain relation; and (c) excess pore water pressure versus axial strain.

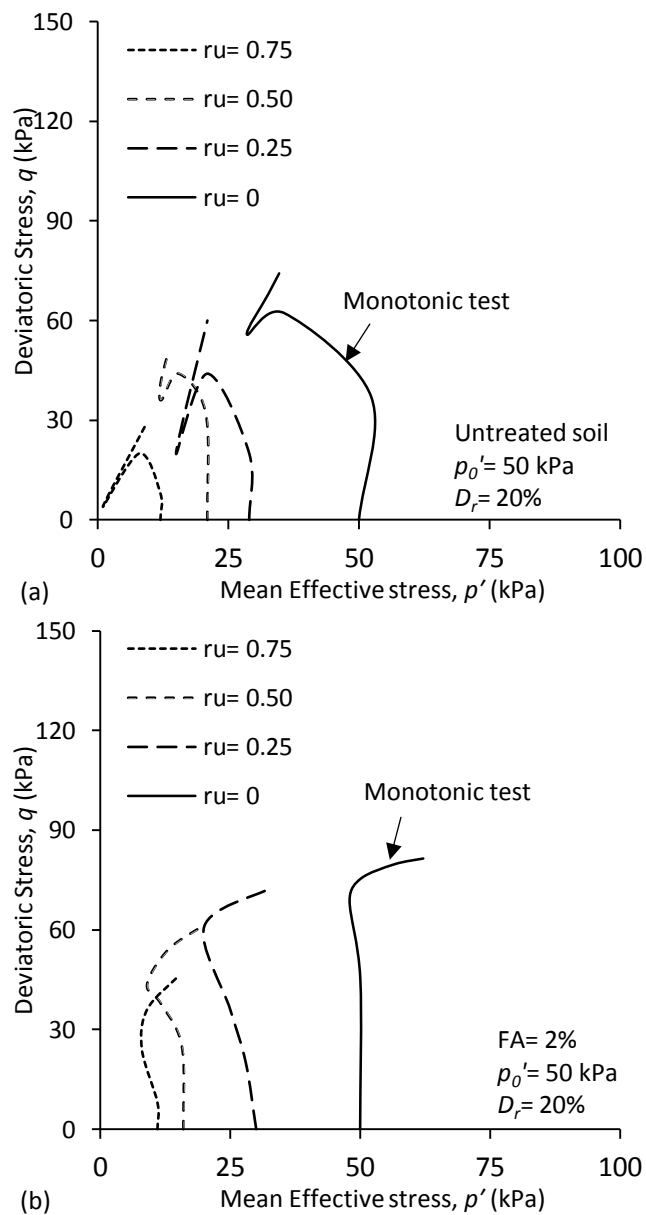
7.1.4.2. Post-cyclic Triaxial Tests

7.1.4.2.1. Effect of FA contents

Fig. 7.7 shows the stress-strain ($q-p'$) results for post-cyclic monotonic triaxial tests performed on untreated and FA treated specimens when specimens prepared with a pre-consolidation relative density of 20% under an initial mean effective stress of 50 kPa when the pore water pressure ratio reached 0.25, 0.50, and 0.75 after cyclic tests. Furthermore, the results of undrained monotonic triaxial tests ($r_u = 0$) have been presented as a benchmark for untreated and FA treated specimens. It is seen from the figure that increasing the FA contents of the specimens increased the ultimate deviatoric stress of the specimens. For instance, the untreated soil has the lowest value of ultimate deviatoric stress and 6% FA treated specimens have the greatest value of ultimate deviatoric stress. In addition, it is seen from the figure that the specimens at a greater pore water pressure ratio has a lower value of ultimate deviatoric stress (q_u). This behaviour can be attributed to the effect of a higher number of cyclic loadings applied on the specimens at a greater r_u that causes a more sliding behaviour for the soil particles and an increase for the pore water pressure and finally liquefaction state for the specimen at pore water pressure ratio equal to one. This may be the main reason for a greater value of ultimate deviatoric stress for tested specimens at $r_u = 0$ (i.e., triaxial monotonic tests) since no cyclic loadings have been applied on the specimens and they have a more stable structure. As shown, the applied initial cyclic loading have negative impacts on ultimate deviatoric stress of the specimens and reduce it. This

effect is more apparent in untreated soil and less obvious for FA treated specimens indicating effectiveness of FA in post-cyclic phase.

Fig. 7.8 shows variations of the normalised ultimate deviatoric stress ($q_u/q_{u(Mon)}$) as a summary for the effect of FA contents on ultimate deviatoric stress of the specimens in post-cyclic phase at different pore pressure ratio. This figure clearly shows that increasing the pore pressure ratio reduced the ultimate deviatoric stress and addition of FA was effective to reduce this increment.



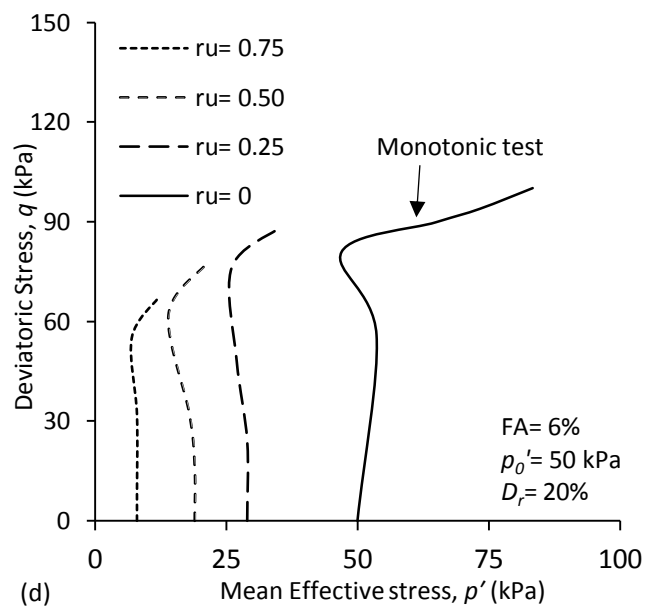
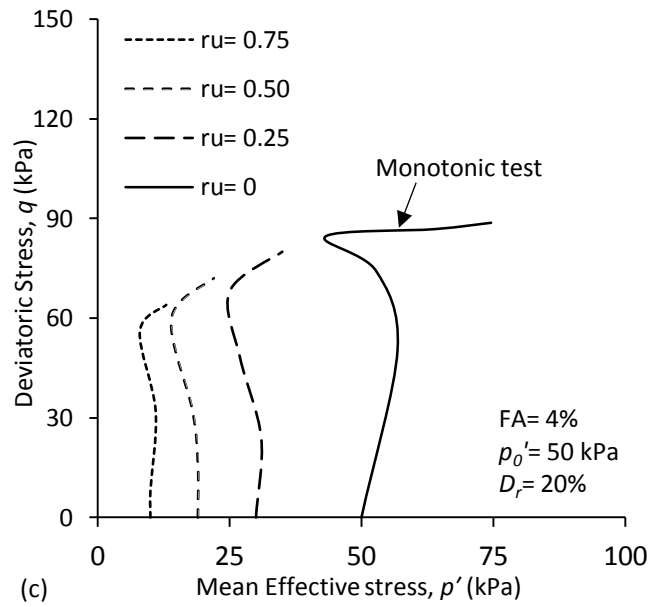


Fig. 7.7. Effect of FA contents on stress path ($q-p'$) in post-cyclic tests (a) untreated soil; (b) FA=2%; (c) FA=4%; and (d) FA=6%.

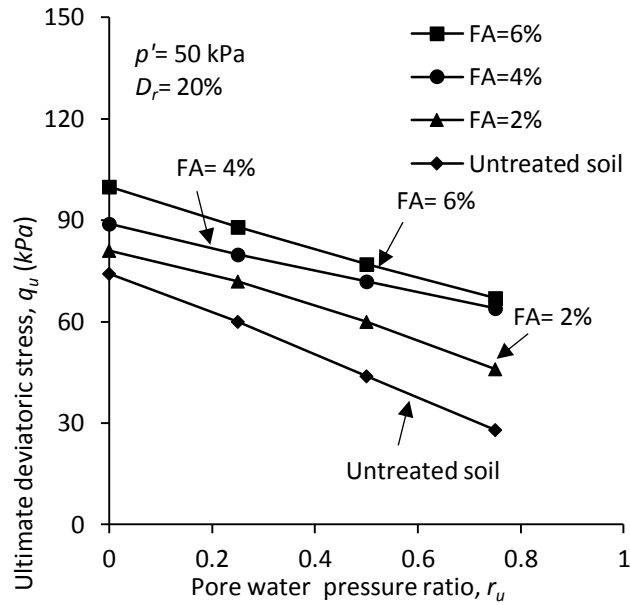
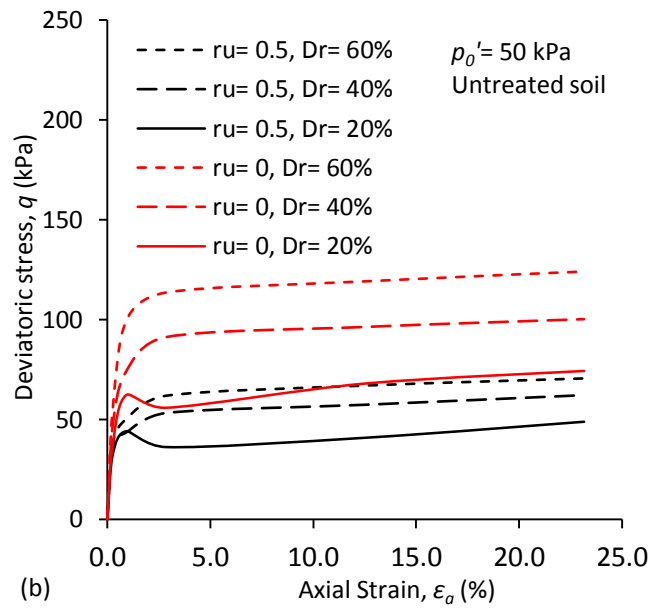
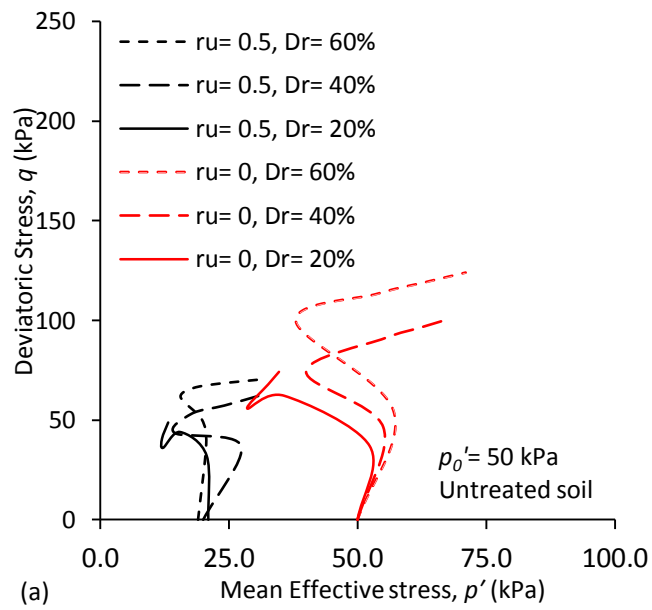


Fig. 7.8. Variations of the ultimate deviatoric stress acquired from post-cyclic tests for untreated and FA treated specimens

7.1.4.2.2. Effect of Relative Density

Fig. 7.9 shows the typical results for undrained monotonic post-cyclic triaxial tests conducted on untreated soil and 2% FA treated specimens at pre-consolidation relative densities of 20, 40, and 60% under 50 kPa initial mean effective stress and pore water pressure ratios of zero and 0.5. It is seen from the figure that both untreated soil specimens tested at $r_u = 0$ and 5 show a limited-liquefaction behaviour at a pre-consolidation relative density of 20% and increasing the pre-consolidation relative density from 20% to 40 and 60% changed their behaviour into the non-flow. The results show that increasing the relative density in FA treated specimens even increased more the ultimate deviatoric stress of the specimens and the increase in ultimate deviatoric stress of FA treated soil is more apparent than the untreated soil by increasing the relative density. Fig. 7.10 shows a summary for the variations of the ultimate deviatoric stress in post-cyclic phase for untreated soil and 2% FA treated specimens at pre-consolidation relative densities of 20, 40, and 60%. This figure

clearly shows that densification of FA treated specimens is more effective and provide a greater value for ultimate deviatoric stress.



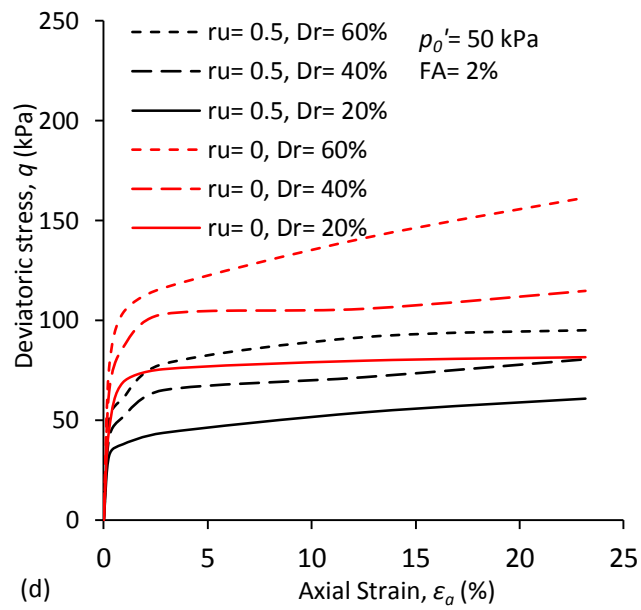
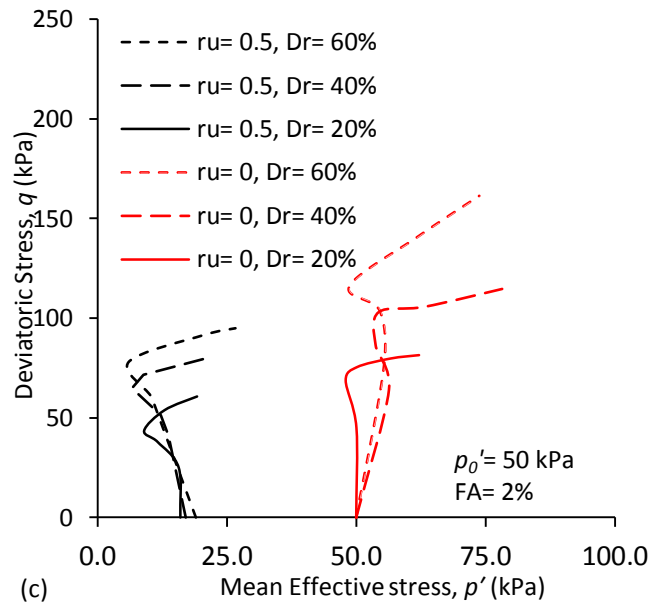


Fig. 7.9. Typical stress path (q - p') acquired from post-cyclic tests on (a) untreated soil; (b) FA=2%; (c) FA=4%; and (d) FA=6%.

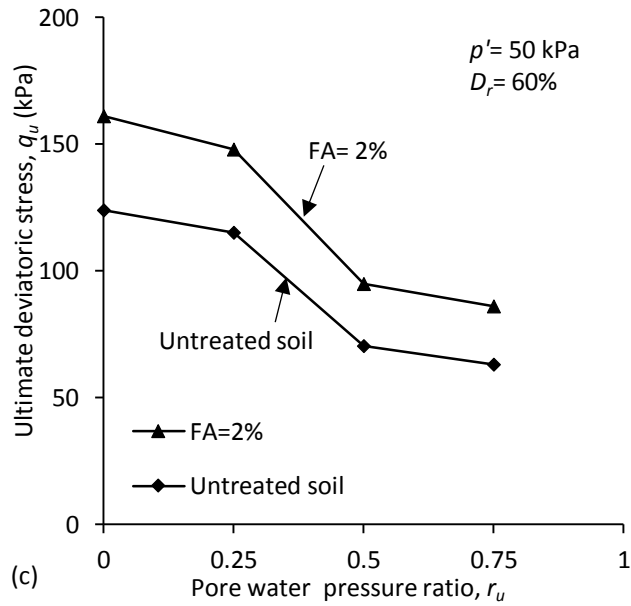
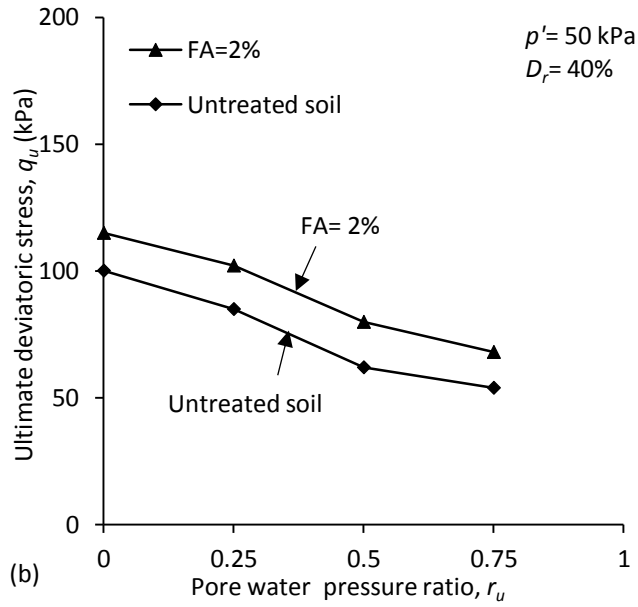
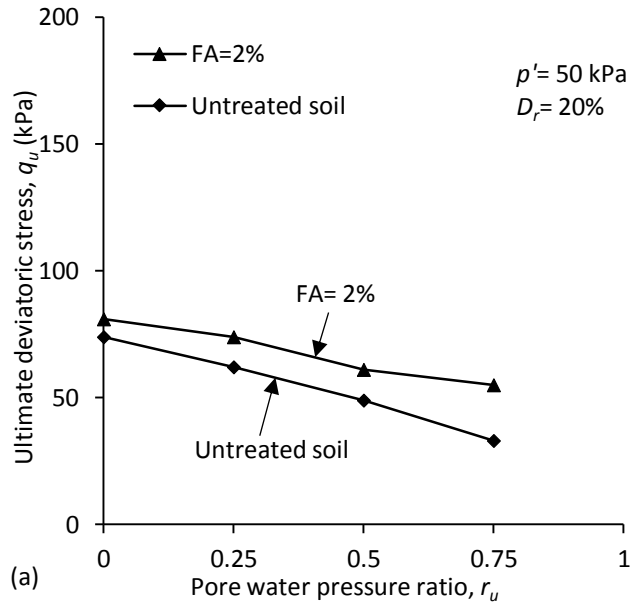


Fig. 7.10. Effect of relative density in variations of ultimate deviatoric stress in post-cyclic phase for untreated and 2% FA treated specimens for (a) $D_r = 20\%$; (b) $D_r = 40\%$; and (c) $D_r = 60\%$.

7.1.4.2.3. Effect of Initial Mean Effective Stress

Fig. 7.11 shows a summary for undrained monotonic and post cyclic triaxial tests conducted on 2% FA treated specimens at a pre-consolidation relative density of 20% under effective confining pressures of 50, 70, and 90 kPa. It is seen from the figure that increasing the initial mean effective stress reduced the ultimate deviatoric stress at all tested pore water pressure ratios. For instance, the ultimate deviatoric stress at a pore water pressure ratio of zero (monotonic test) is 81, 73, and 64 when the tests conducted under an effective confining pressure of 50, 70, and 90 kPa. Increasing the pore water pressure ratio to 0.25 cause an ultimate deviatoric stress of 74, 65, and 57 kPa for the effective confining pressure of 50, 70, and 90 kPa. Similarly, the specimens have an ultimate deviatoric stress in the range of $44 \leq q_u \leq 61$ kPa and $41 \leq q_u \leq 55$ kPa when the tests conducted under 90 to 50 kPa effective confining pressure and at pore water pressure ratios of 0.50 and 0.75 respectively. The recorded behaviour is due to the soil dilatancy and consistent with critical state of soil behaviour and is consistent with reported results by Seed and Harder (1990).

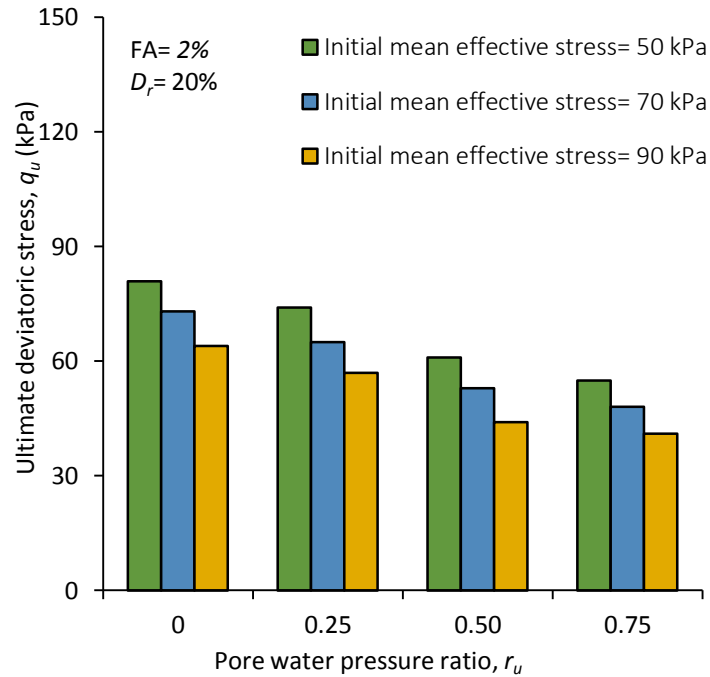


Fig. 7.11. Effect of initial mean effective stress in variations of ultimate deviatoric stress acquired from monotonic and post-cyclic tests for 2% FA treated specimens.

7.1.5. Conclusions

This study investigated the effect of fly ash (FA) addition on post-cyclic behaviour of the soil by performing a series of undrained monotonic triaxial and post cyclic monotonic tests. The effect of four different FA contents (i.e., 0, 2, 4, and 6% by dry weight), three pre-consolidation relative densities (i.e., 20, 40, and 60%), and three effective confining pressures (i.e., 50, 70, and 90 kPa) on post-cyclic behaviour of the soil were investigated. To conduct the post-cyclic tests initially the cyclic loads applied on the specimens until they reached the desired pore water pressure ratios of 0.25, 0.50, and 0.75. Furthermore, the results for pore water pressure ratio of zero was acquired from the monotonic triaxial tests. The following conclusions can be drawn from the results.

- Investigation of effect of FA contents on post-cyclic behaviour of the soil showed that increasing FA contents increased the ultimate deviatoric stress of the specimens in all tested pore water pressure ratios after cyclic loadings.
- The results showed that the ultimate deviatoric stress of the specimens in the post-cyclic phase reduced when the post-cyclic tests initiated at a greater pore water pressure ratio after cyclic loadings. This behaviour was attributed to greater cycle numbers that applied on the specimens and provided a more metastable soil structure.
- The investigation of effect of relative density showed that increasing the pre-consolidation relative density from 20% to 40 and 60% of the specimens increased the ultimate deviatoric stress. This increase was less prone in untreated soil and more apparent in FA treated specimens.
- The Investigations showed that increasing the initial mean effective stress from 50 kPa to 70 and 90 kPa reduced the ultimate deviatoric stress of FA treated specimens. This behaviour was attributed to dilatancy of soil and consistent with critical state of soil and literature.

Part 2

Effect of GGBFS on Post-cyclic Behaviour of Sand

7.2. Effect of GGBFS on Post-Cyclic Behaviour of Sand

7.2.1. Abstract

Although during an actual seismic event some soil failures occur with geo-structures, the main damage can occur up to 24 hours after the actual event. This phenomenon is known as “delayed failure” or “delayed response” and highlights the importance of the post-cyclic behaviour of soil. This shows that the efforts to mitigate the destructive effects of post-cyclic loadings should be as great as efforts to reduce the catastrophic effects in the cyclic stage. This study aims to investigate the effect of ground granulated blast furnace slag (GGBFS) on the post-cyclic behaviour of soil by performing a series of post-cyclic undrained monotonic triaxial compression tests. The effect of four GGBFS contents (i.e., 0, 3, 5, and 7), and three initial mean effective stresses of 100, 200, and 400 kPa on the post-cyclic behaviour of the soil were investigated and the results were presented. To conduct the post-cyclic tests, initially cyclic loadings were applied on the specimens with initial relative densities of 40 and/or 60% until the pore water pressure ratio reached a desired level (i.e., 0.25, 0.50, or 0.75), then the post-cyclic tests were initiated. The results showed that the addition of GGBFS is effective to increase the ultimate deviatoric strength (q_u) of the specimens in the post-cyclic phase. Furthermore, investigation of the effect of initial mean effective stress (p') showed that the GGBFS treated specimens under a greater p' had lower values of ultimate deviatoric stress. Finally, the investigations showed that the densification of the GGBFS treated specimens is more effective to improve the ultimate deviatoric strength of the specimens than untreated soil.

7.2.2. Introduction

The pore water pressure build-up happens in saturated granular sand during an earthquake event which causes a reduction in the strength of the soil. If the generation of pore water pressure continues, by the seismic loadings, the pore water pressure ratio reaches one ($r_u = 1$), and the sand will become liquefied. This disastrous phenomenon is known as liquefaction. The possibility of soil failure after a seismic event is high and this possibility is even higher when the soil is liquefied. Previous studies have been conducted to investigate different aspects of the post-cyclic and post-liquefaction of soil (Ishihara et al. 2016; Wang et al. 2016; 2015a; 2015b; Kaya and Erken 2015; Pillai et al. 2014; Tavakoli et al. 2011; Ashour et al. 2009; Zand et al. 2009; Erken and Ulker 2007; Shafiee 2006; Shamoto et al. 1998; Kiku and Tsujino 1996; Chern and Lin 1994). Besides the properties of the seismic event, the soil's characteristics have a crucial role during post-liquefaction or the post-cyclic stage. For instance, Noorzad and Shakeri (2017) investigated the effect of non-plastic fine-grained soil on the ultimate deviatoric strength (q_u) of sand in the post-cyclic stage. They indicated that the addition of 15% silt reduce the ultimate deviatoric strength. They also indicated that the addition of 30% silt into the specimens can increase the ultimate deviatoric strength of the specimens when the silt motions change the particle contacts amongst coarser grains, otherwise it decreases its strength. Rouholamin et al. (2017) highlighted the importance of the initial relative density on the post-liquefaction behaviour of soil. They indicated that when a liquefied soil is sheared monotonically, stiffness recovery is a factor in initial relative density. They also determined three post-liquefaction parameters which were functions of the initial relative density and provided a correlation between them. In another study, Mollamahmutoglu and Yilmaz (2010) investigated the pre-cyclic and post-cyclic characteristics of colloidal silica grouted

sand by performing a series of cyclic loading tests on specimens at different cyclic stress and suspension ratios and indicated that the stabilised soil has an appropriate resistance against cyclic deformation. Kargar et al. (2016) investigated post-cyclic behaviour of carbonate sand at different effective confining stresses. They investigated the effect of post-cyclic loading on particle breakage by performing grading analysis after the tests. They indicated that particle breakage occurred even when the tests were conducted under the lowest effective confining pressure, however, they could not find a correlation between post-cyclic behaviour and particle breakage. It has been indicated that the cyclic stress ratio (CSR), consolidation type, and the residual cyclic strain are effective parameters in forming post-cyclic strength of sand. In another study, Soroush and Soltani-Jigheh (2009) investigated the effect of coarse contents (sand and/or gravel), number of cycles, effective confining pressure, and cyclic strain amplitude on the pre and post-cyclic behaviour of a mixed clay soil. They indicated that increasing the coarse contents of the soil promotes the generation of the pore water pressure ratio. The post-cyclic phase is simulated using a cyclic triaxial device in the laboratory. Fig. 7.12 shows a schematic overview of the monotonic, post-cyclic, and post-liquefaction phases in a stress path plane.

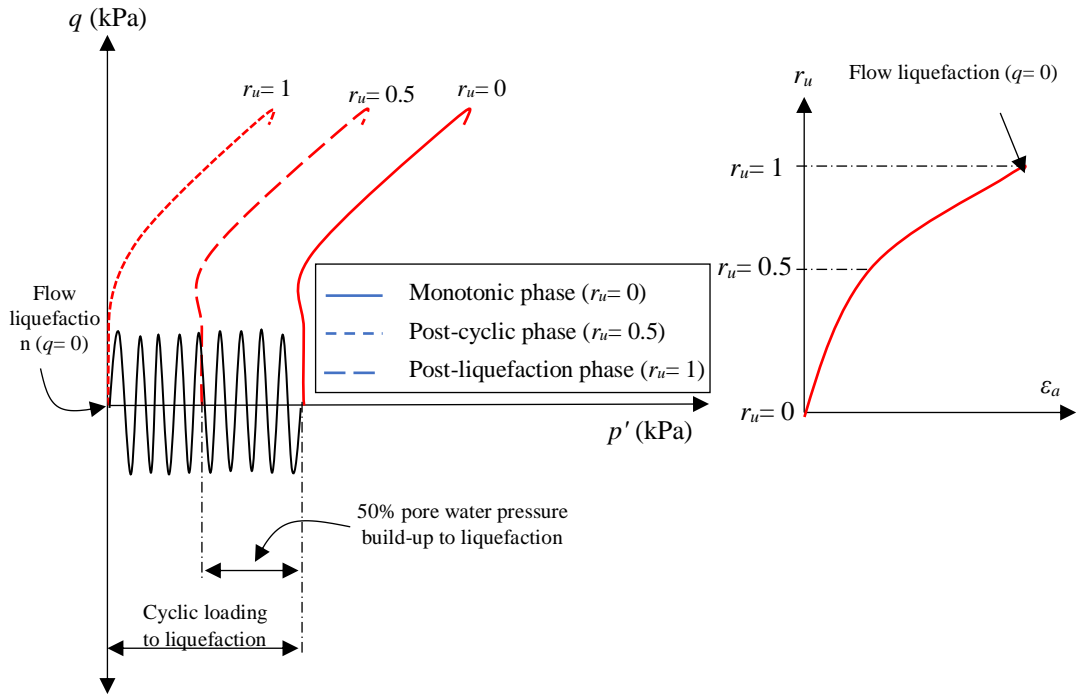


Fig. 7.12. Schematic overview for stress-strain (q - p') and pore water pressure ratio (r_u - ϵ_a) phases in a monotonic and two post-cyclic tests

In recent years, the application of non-environmentally friendly admixtures, such as lime and Portland cement (PC), have been discouraged and the application of more environmentally friendly admixtures like GGBFS have been promoted by many practitioners (Keramatikerman et al 2016; Higgins 2007 amongst others). The granular blast furnace slag (GGBFS) is an abundant by-product material that is generated from the steel industry and has pozzolanic and hydration reactions similar to PC. The production of this material is not only more cost-effective and energy saving but also reduces the carbon footprint in the environment (Higgins 2007). Previous studies on monotonic liquefaction resistance of the sand showed that this material is effective to improve liquefaction resistance of the soil (Sabbar et al. 2017).

The importance of the post-cyclic phases in a seismic event has been investigated in aforementioned literatures. Furthermore, it was determined that the application of some environmental friendly agents such as GGBFS is effective to improve the mechanical characteristics of the soil, however, its behaviour after cyclic loadings (i.e., post-cyclic phase) is unknown. Hence, this study aims to investigate the effect of GGBFS on the post-cyclic behaviour of the soil.

7.2.3. Materials Used

The Baldvis sand was sourced from a local supplier in Perth, Western Australia. Fig. 7.13 shows the results of the sieve analysis [(ASTM C136, (ASTM 2014b)] on the used sand. This sand has a uniformity coefficient (C_u) of 2.5 and a coefficient of curvature of 1.19 according to the sieve analysis. The used sand is categorised as a poorly graded soil (SP) based on the Unified Soil Classification System (USCS) [(ASTM D2487, (ASTM 2011a)]. Furthermore, its specific gravity (G_s) is 2.67. Quartz (Q) is the main mineral of the used sand based on the X-ray powder diffraction (XRD) analysis. Fig. 7.14 shows a scanning electron microscopy (SEM) image from the used sand. The used GGBFS was sourced from BGC Cement, a local supplier in Perth, Western Australia. The used GGBFS has a specific gravity in the range of 2.8 - 3.1 and a melting point of 1350 °C. Table 7.2 shows its mineral constituents. Fig. 7.15 shows the SEM analysis of the used GGBFS.

Table 7.2. Chemical composition of the used GGBFS (BGC Cement 2013).

GGBFS composition	Formula	Percentage
Calcium oxide	CaO	30–50%
Silica, amorphous	SiO ₂	35–40%
Aluminium oxide	Al ₂ O ₃	5–15%
Sulphur	S	5%

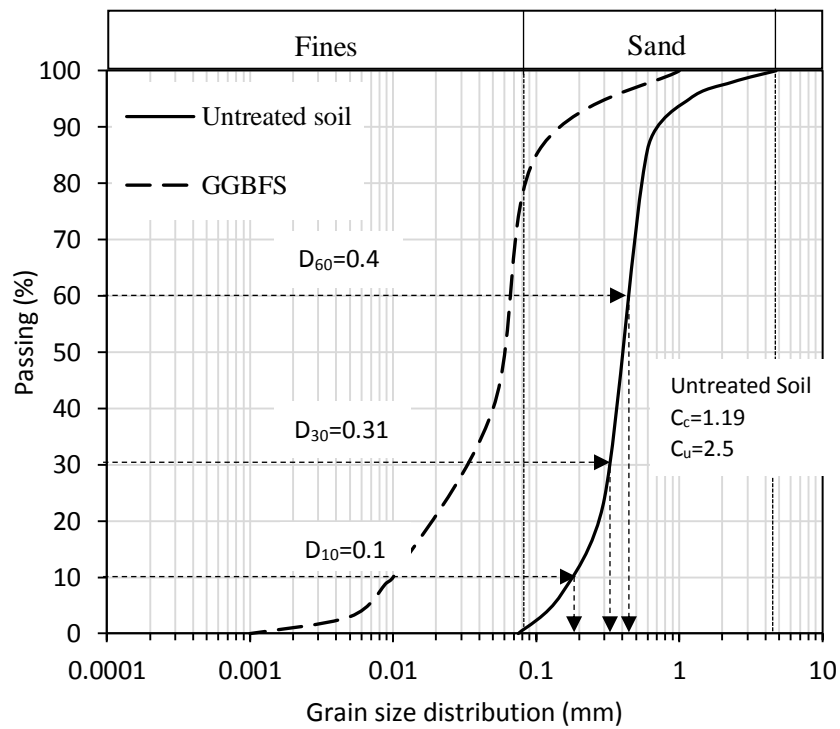


Fig. 7.13. Particle size distribution of used materials

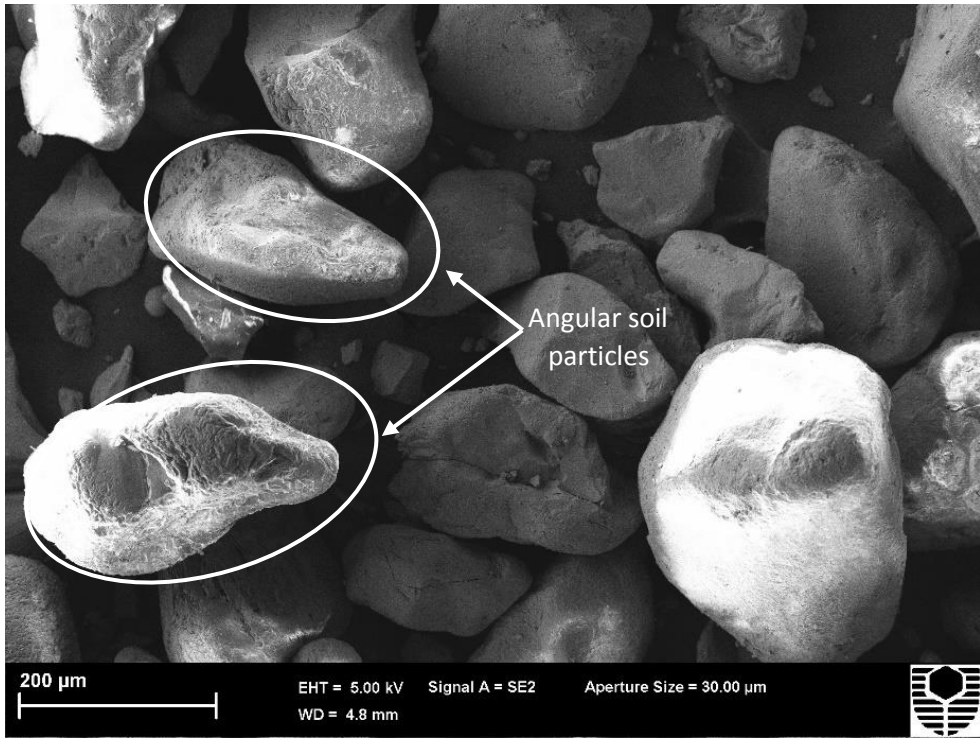


Fig. 7.14. Scanning electron microscopy (SEM) image of used sand

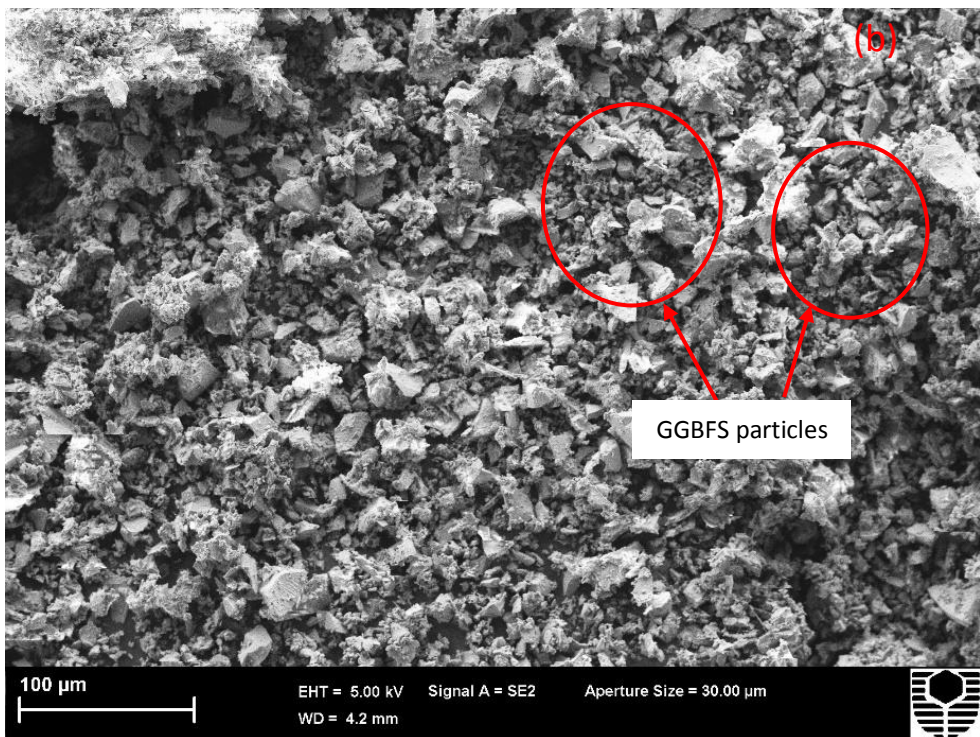


Fig. 7.15. Scanning electron microscopy (SEM) image of used GGBFS

7.2.4. Sample Preparations and Testing Setup

In this study the wet tamping method, a widely used sample preparation technique for a sandy soil in triaxial testing, was employed since the homogeneity and the integrity of the sample is in a satisfactory condition, and as this method also provides better control of the void ratio of the specimens (Ladd 1978). The GGBFS was mixed with sand in four percentages of 0, 3, 5, and 7% (by dry weight of the soil) and thoroughly mixed. Then, water was added into the mixture according to the optimum moisture content acquired from compaction tests and completely stirred until a uniform mixture was achieved. The mixtures were placed into a cylindrical split mould. A membrane was pulled off and tightened and a low vacuum was applied inside of the split mould during the sample preparation stage. The mixtures were compacted in five layers until a height of 125-mm was obtained. In addition, the samples have a diameter of 65-mm which provided an aspect ratio of 2 for the specimens. The specimens were prepared with an initial relative density (D_r) of 40% or 60%.

After sample preparation, the testing was initiated with saturation of the specimens. The saturating of the specimens was continued until the coefficient of Skempton (i.e., B -value) was equal or greater than 0.95. This coefficient is computed using Eq. (7.2.1).

$$B_{value} = \frac{\Delta u}{\Delta \sigma_3} \quad (7.2.1)$$

Where, Δu = pore water pressure (kPa), and $\Delta \sigma_3$ = cell pressure (kPa). After that the specimens were isotropically consolidated under the initial mean effective stresses (p_0') of 100, 200, or 400 kPa. The post-consolidation relative densities of the specimens were measured upon completion of the consolidation phase by evaluating the volumetric strain. After that, the specimens underwent a series of cyclic loadings until the desired pore water pressure ratios (r_u) of 0.25, 0.50, and 0.75 were acquired. The

stress-controlled sinusoidal cyclic loadings [ASTM D5311 (ASTM 2013)] with a cyclic stress ratio (CSR) of 0.2 and a frequency of 1 Hz was applied on the specimens. Furthermore, the pore water pressure ratio is computed using Eq. (7.2.2).

$$r_u = \frac{u}{p'_0} \quad (7.2.2)$$

Where, u = excess pore water pressure. The pore water pressure ratio (r_u) is an accurate benchmark to evaluate the post-cyclic behaviour of the specimens in compare with other parameters such as shear strain since the pore water pressure dramatically increases in a short range of shear strain which provide more complexity for the results. After completion of the cyclic loading stage, the post-cyclic stage was initiated by monotonically shearing the specimens with a strain rate of 0.1 mm/min. Fig. 7.16 shows the typical loading stage for an untreated specimen after finalising the cyclic loading stage and reaching the pore water pressure ratios of 0.25, 0.50, and 0.75. Table 7.3 also shows the test program followed in this study to conduct the tests.

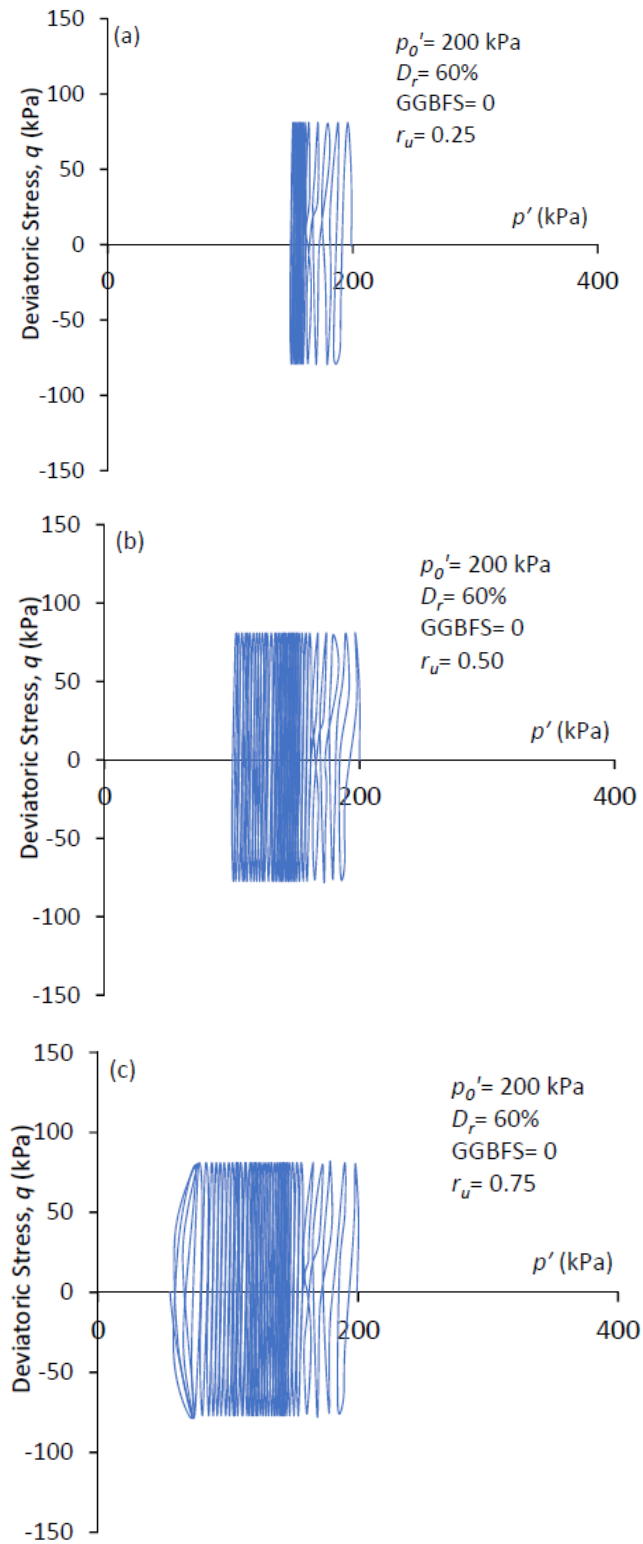


Fig. 7.16. Typical effective stress paths (q - p') recorded in cyclic stage and before initiation of the post-cyclic phase for (a) $r_u = 0.25$; (b) $r_u = 0.50$; and (c) $r_u = 0.75$

Table 7.3. Experimental program and key results for tests

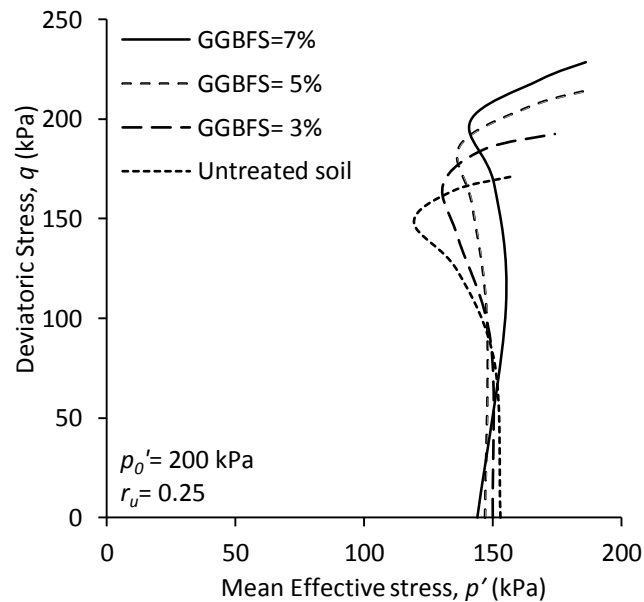
Test No.	Test ID	GGBFS content (%)	p_0' (kPa)	D_r	D_{rp}	r_u
1	CS1	-	200	60	62.5	0.25
2	CS2	-	200	60	62.5	0.50
3	CS3	-	200	60	62.5	0.75
4	CG1	3	200	60	62.5	0.25
5	CG2	3	200	60	62.5	0.50
6	CG3	3	200	60	62.5	0.75
7	CG4	5	200	60	62.5	0.25
8	CG5	5	200	60	62.5	0.50
9	CG6	5	200	60	62.5	0.75
10	CG7	7	200	60	62.5	0.25
11	CG8	7	200	60	62.5	0.50
12	CG9	7	200	60	62.5	0.75
13	CG10	5	100	60	62.5	0.25
14	CG11	5	100	60	62.5	0.50
15	CG12	5	100	60	62.5	0.75
16	CG13	5	400	60	62.5	0.25
17	CG14	5	400	60	62.5	0.50
18	CG15	5	400	60	62.5	0.75
19	CG16	-	200	40	43.6	0.25
20	CG17	-	200	40	43.6	0.50
21	CG18	-	200	40	43.6	0.75
22	CG19	5	200	40	43.6	0.25
23	CG20	5	200	40	43.6	0.50
24	CG21	5	200	40	43.6	0.75

7.2.5. Results and Discussion

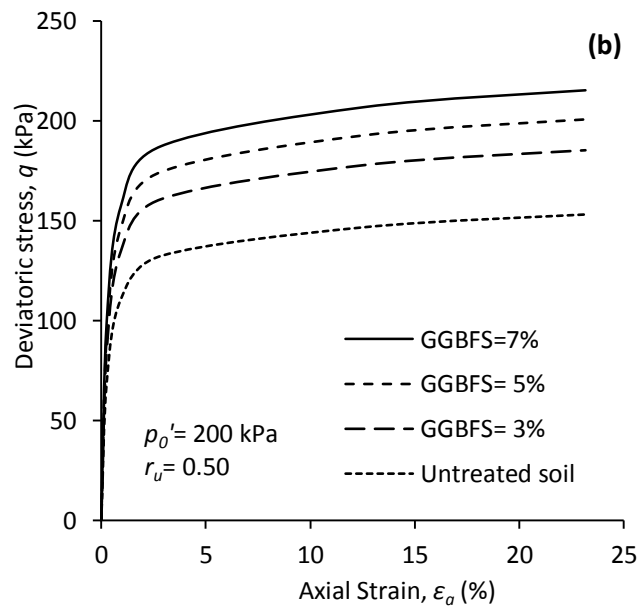
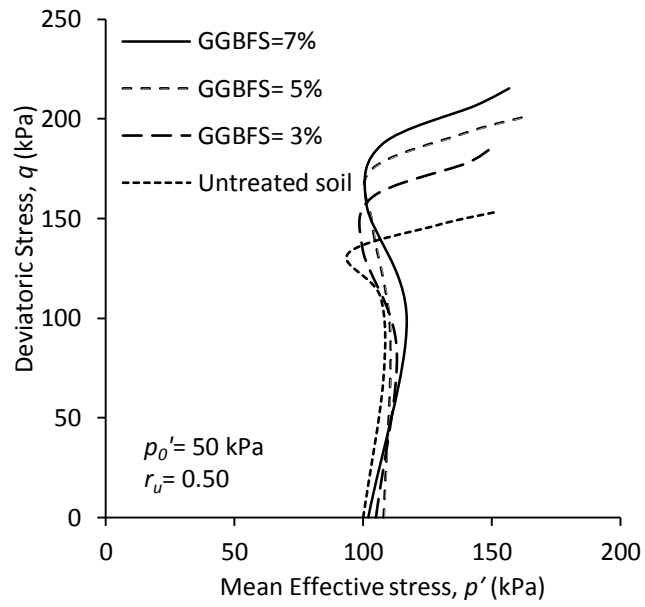
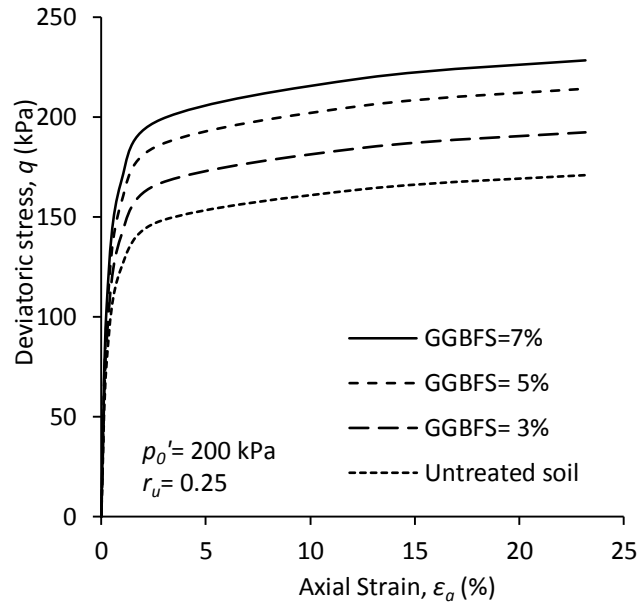
7.2.5.1. Effect of GGBFS Contents on Post-Cyclic

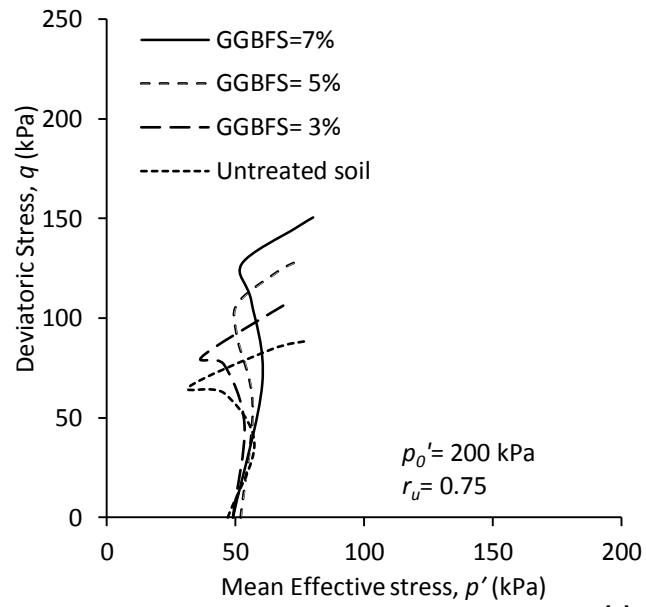
Fig. 7.17 shows variations of the deviatoric stress versus mean effective stress ($q-p'$), and deviatoric stress with axial strain ($q-\varepsilon_a$) in post-cyclic phase for untreated soil and GGBFS treated specimens after pore water pressure ratios of 0.25, 0.50, and 0.75. It is seen from the figure the untreated soil has the lowest amount of ultimate deviatoric stress (q_u) and addition of 3, 5, and 7% GGBFS increased the ultimate deviatoric stress of the specimens in all cases. For example, at a pore water pressure ratio of 0.25, the untreated soil has an ultimate deviatoric stress of 171 kPa while addition of GGBFS caused an increase for ultimate deviatoric stress in the range of $192 \leq q_u \leq 228$ kPa.

Similarly, when the post-cyclic tests initiated after a pore water pressure ratio of 0.50 and 0.75 an ultimate deviatoric stress of 153 and 89 kPa was acquired for the untreated soil respectively. Whereas, the addition of GGBFS caused an ultimate deviatoric stress of $185 \leq q_u \leq 215$ kPa and $108 \leq q_u \leq 151$ kPa when the post-cyclic phase were conducted after pore water pressure ratios of 0.50 and 0.75 respectively. Fig. 7.18 shows a summary of the acquired ultimate deviatoric strength for tested specimens. In fact, increasing the GGBFS particle fills the microscopic pores amongst coarser soil particles and prevent the pore water pressure build-up triggered by cyclic loadings. This may be the main reason for increasing the post-cyclic resistance of the GGBFS treated soil. The results also show that at a greater pore water pressure ratio the specimens have a lower value of ultimate deviatoric strength. This behaviour can be attributed to the greater cycle numbers that apply on the specimens at a greater pore water pressure and provide a more metastable structure for the specimens.



(a)





(c)

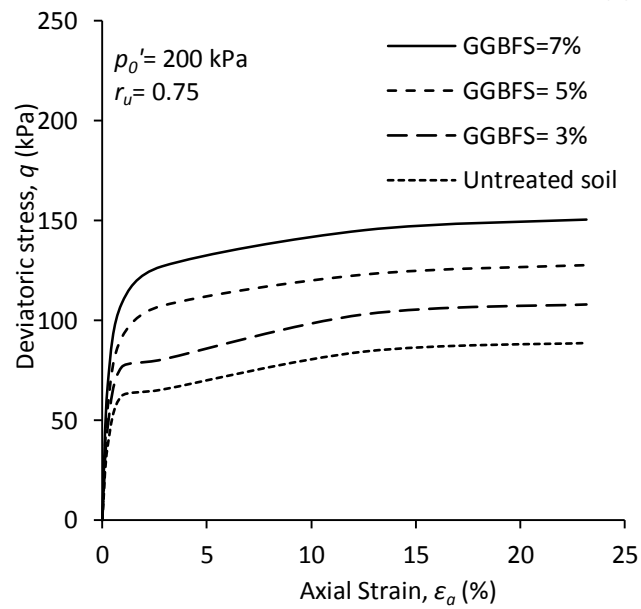


Fig. 7.17. Effect of GGBFS contents on shearing response of sand in post-cyclic phase

(a) $r_u = 0.25$; (b) $r_u = 0.50$; and (c) $r_u = 0.75$.

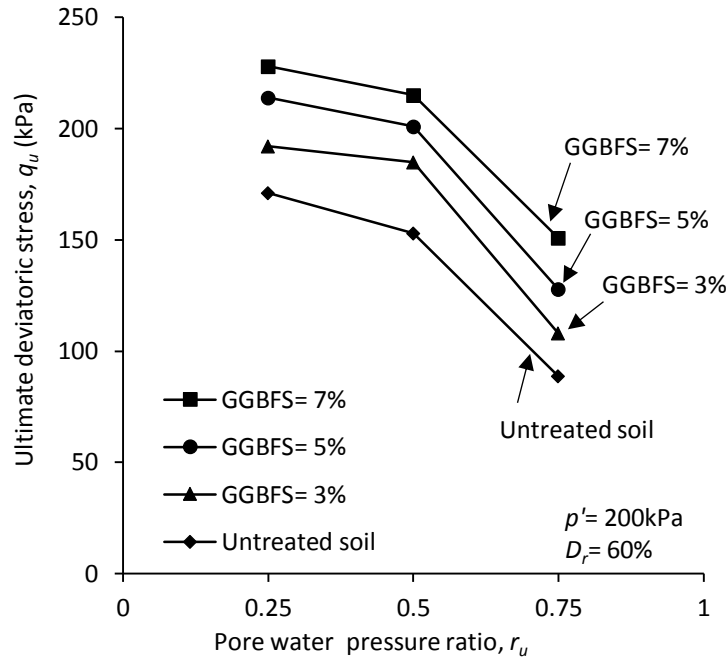
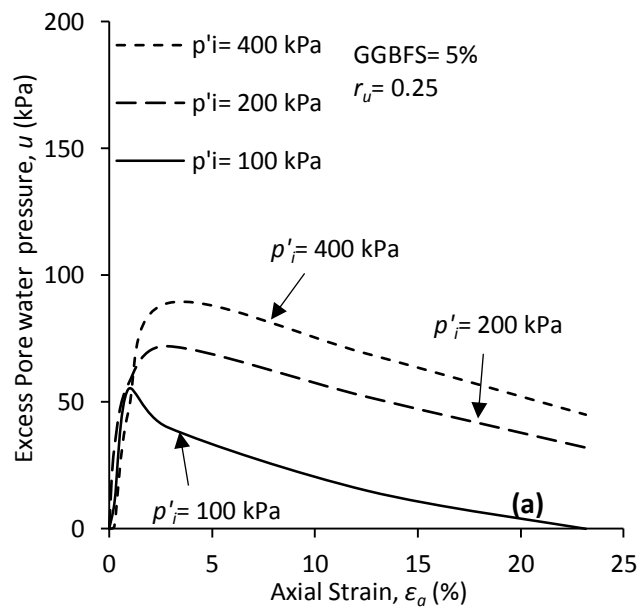


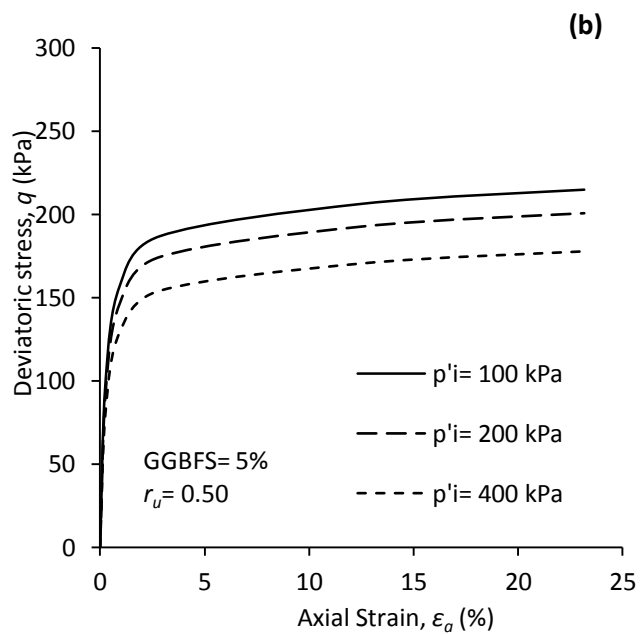
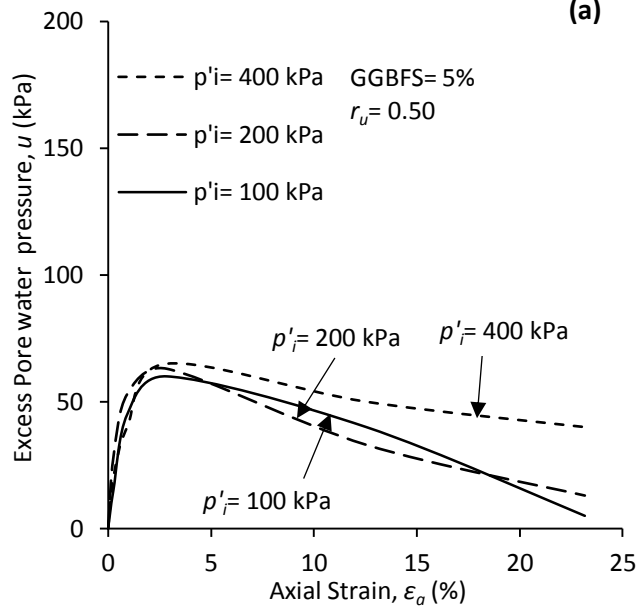
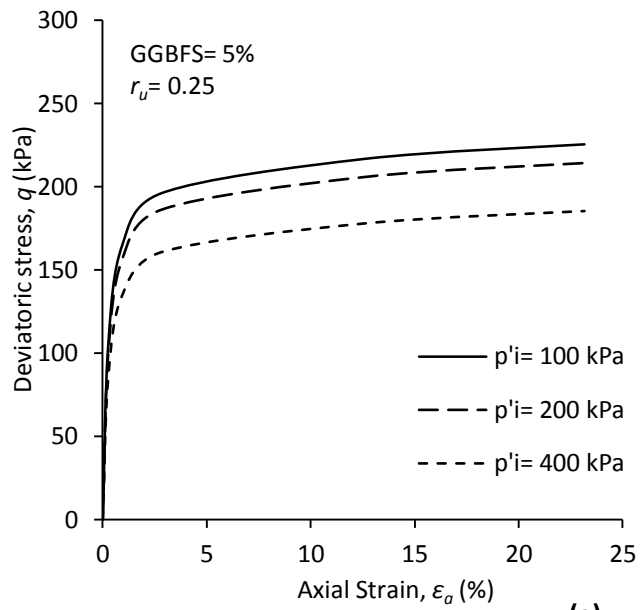
Fig. 7.18. The ultimate deviatoric stress acquired from post-cyclic tests for untreated and GGBFS treated specimens

7.2.5.2. Effect of Initial Mean Effective Stress

Fig. 7.19 shows the variations of deviatoric stress versus axial strain ($q-\epsilon_a$), and excess pore water pressure versus axial strain ($u-\epsilon_a$) acquired from the post-cyclic phase for specimens treated with 5% GGBFS when tested under initial mean effective stresses of 100, 200, and 400 kPa and pore water pressure ratios of 0.25, 0.50, and 0.75. It is seen from the figure that increasing the initial mean effective stress caused a reduction in ultimate deviatoric strength. For instance, for a pore water pressure ratio of 0.25, the test conducted under 100 kPa had an ultimate deviatoric stress of 225 kPa, whereas this value reduced to 214 and 185 kPa when the tests were conducted under 200 and 400 kPa respectively. Similarly, in the case of a pore water pressure ratio of 0.50, the conducted test, under an initial mean effective stress of 100 kPa, had an ultimate deviatoric stress of 215 kPa, and conducting the tests under initial mean effective stresses of 200 and 400 kPa caused an ultimate deviatoric stress of 201 and 178 kPa

respectively. Similar results were acquired in the case of 0.75 pore water pressure ratio. For instance, the specimen tested under 100 kPa had an ultimate deviatoric stress of 146 kPa and conducting the tests under 200 and 400 kPa initial mean effective stress cause 128 and 113 kPa ultimate deviatoric stress values respectively. Fig. 7.20 shows a summary of the acquired ultimate deviatoric stress values at different initial mean effective stresses. Furthermore, the results acquired for the effects of pore water pressure ratio show that the specimens tested under a greater initial mean effective stress have a lower excess pore water pressure. The recorded relation for the ultimate deviatoric stress and initial mean effective stress can be attributed to the soil dilatancy and is consistent with the critical state of soil (Seed and Harder 1990).





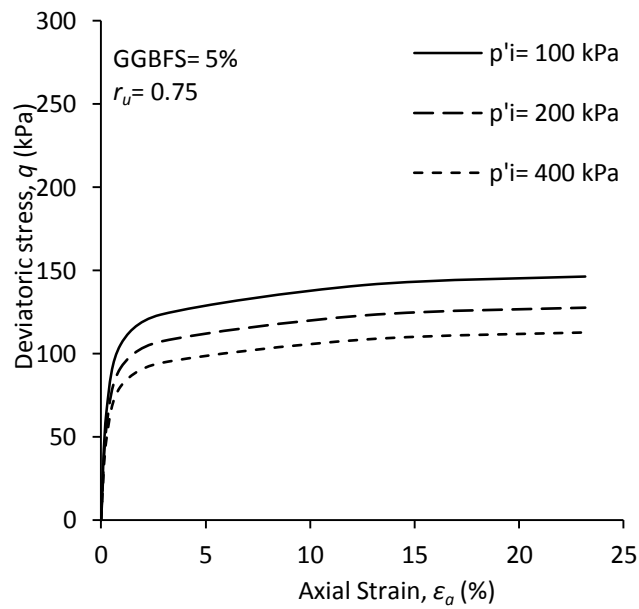
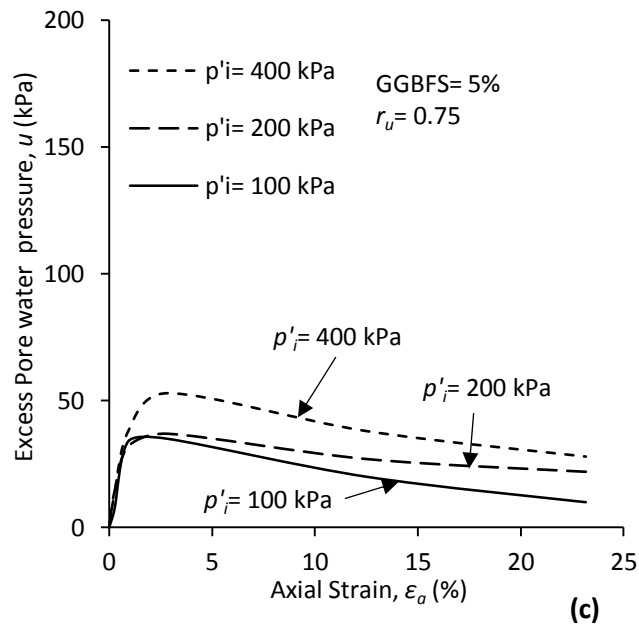


Fig. 7.19. Effect of initial mean effective stress on shearing response of GGBFS treated specimens in post-cyclic phase (a) $r_u=0.25$; (b) $r_u=0.50$; and (c) $r_u=0.75$.

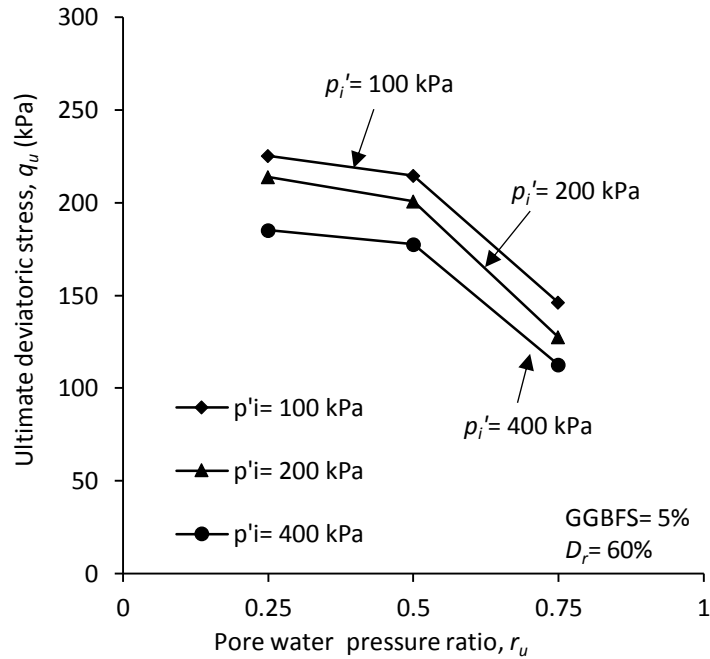
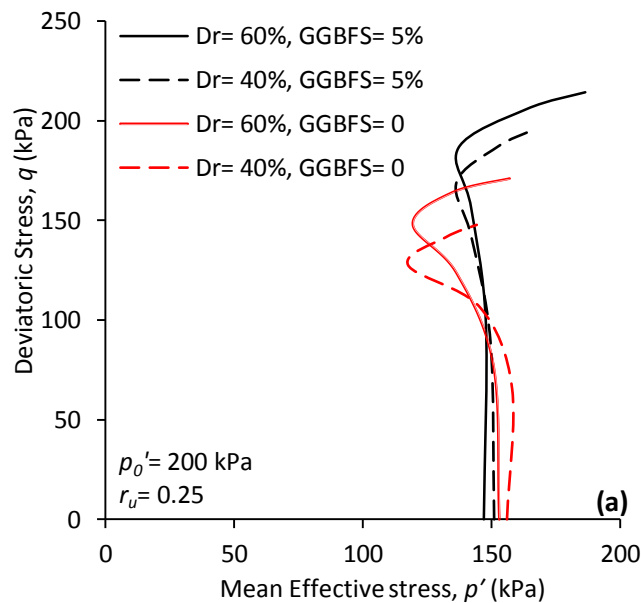


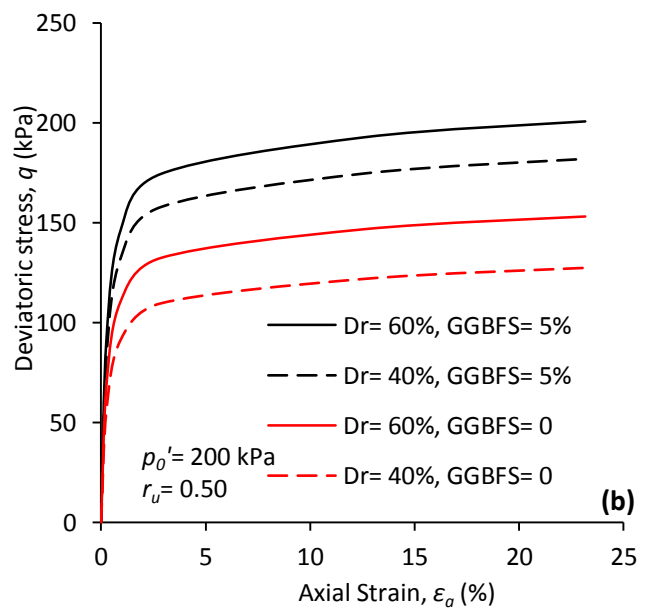
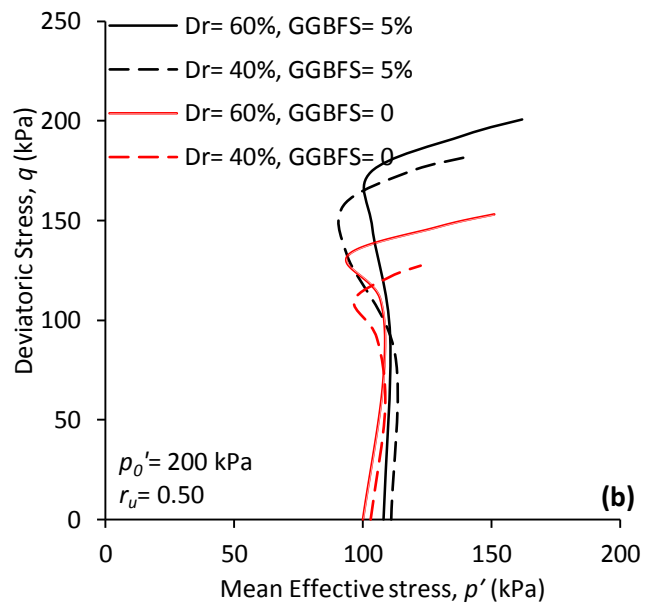
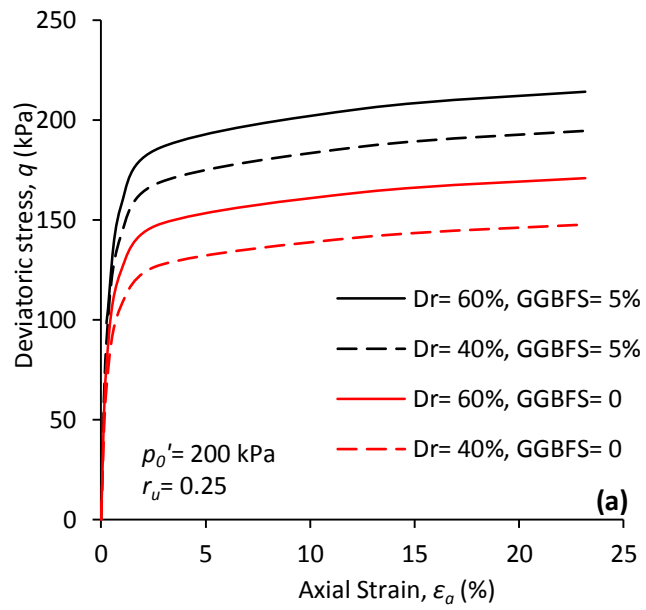
Fig. 7.20. The ultimate deviatoric stress acquired from post-cyclic tests for GGBFS treated specimens tested at different initial mean effective stress

7.2.5.3. Effect of Initial Relative Density

Fig. 7.21 shows the variations of deviatoric stress versus initial mean effective stress ($q-p'$), and deviatoric stress with axial strain ($q-\epsilon_a$) for untreated and 5% GGBFS treated specimens at pore water pressure ratios of 0.25, 0.50, and 0.75 when the samples are prepared with an initial relative density of 40% and 60% under 200 kPa initial mean effective stress. It is seen from the figure that increasing the initial relative density improved the ultimate deviatoric strength of the specimens. For instance, for untreated specimens prepared at 40% initial relative density, ultimate deviatoric stress of 148, 127, and 59 kPa were recorded when the tests were conducted after pore water pressure ratios of 0.25, 0.50, and 0.75 respectively. Increasing the initial relative density to 60% caused an ultimate deviatoric strength of 171, 153, and 89 kPa respectively. It is seen from the figure that the effect of densification is greater in GGBFS treated specimens. For instance, when the GGBFS treated specimens were

prepared with 40% initial relative density they had an ultimate deviatoric strength of 195, 182, and 110 kPa when the tests were conducted at pore water ratios of 0.25, 0.50, and 0.75 respectively. Increasing the initial relative density to 60% caused ultimate deviatoric strengths of 214, 20, and 128 kPa when the tests were conducted after pore water pressure ratios of 0.25, 0.50, and 0.75 respectively. Fig. 7.22 shows a summary of the ultimate deviatoric strength values for specimens at 40% and 60% relative densities. A greater value of ultimate deviatoric stress in densified GGBFS treated specimens can be attributed to a reduction in pores and voids in the densified specimens that dissipate the generation of pore water pressure. The added GGBFS also fills the remained microspores amongst soil particles and reduces the chance of pore water pressure build-up.





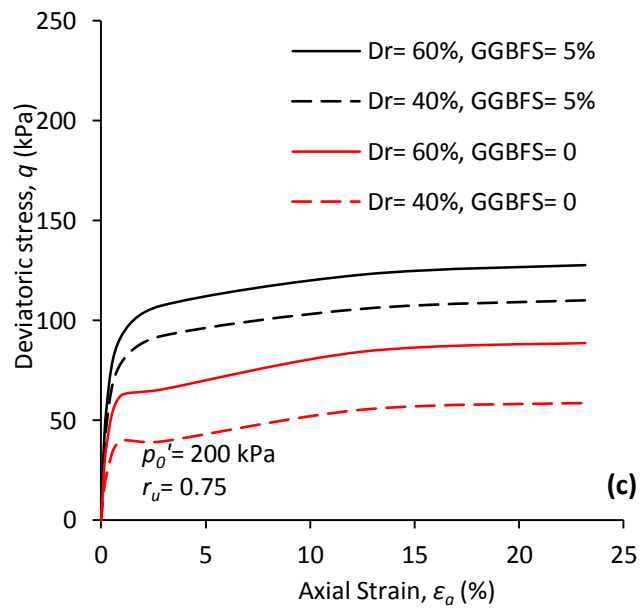
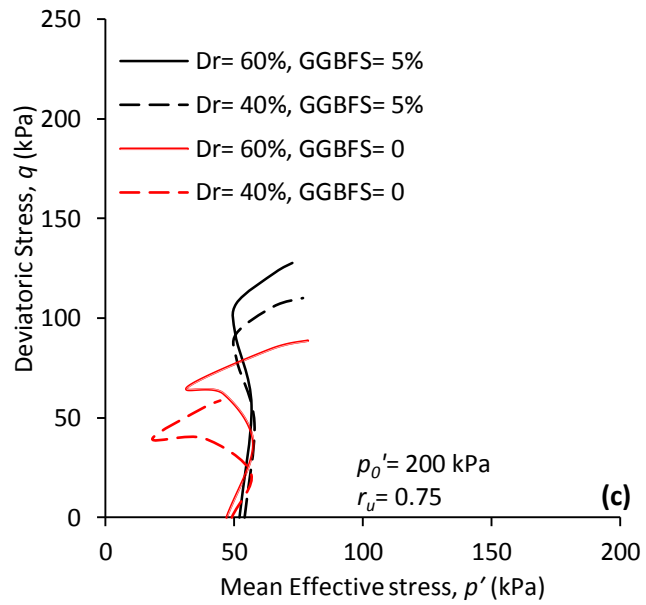


Fig. 7.21. Effect of initial relative density on shearing response of the untreated and 5% GGBFS treated specimens in post-cyclic phase (a) $r_u=0.25$; (b) $r_u=0.50$; and (c) $r_u=0.75$.

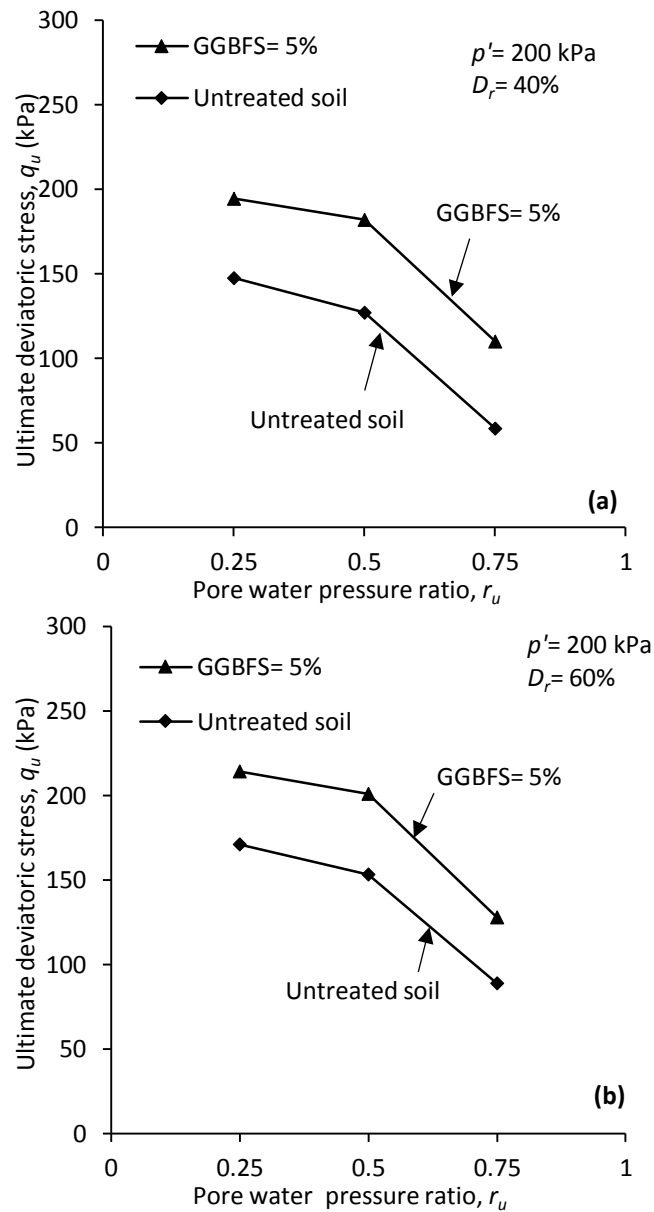


Fig. 7.22. Summary of the ultimate deviatoric stresses for untreated and 5% GGBFS treated specimens in post-cyclic phase for (a) $D_r = 40\%$; and (b) $D_r = 60\%$

7.2.6. Conclusions

Analysis of the improvement of soil behaviour after a seismic event is of great importance since the main geo-structure failures occur up to 24 hours after a seismic event. Ground granulated blast furnace slag (GGBFS) is an environmentally friendly by-product admixture, which is abundant and has hydration and pozzolanic characteristics similar to Portland cement (PC) and lime. This study investigated the

effect of GGBFS on the post-cyclic behaviour of soil by performing a series of undrained post-cyclic monotonic triaxial compression tests. The effect of four GGBFS contents (0, 3, 5, and 7% by dry weight), and three initial mean effective stresses (i.e., 100, 200, and 400 kPa), were investigated. To conduct the post-cyclic tests, the cyclic loadings were applied on the specimens with initial relative densities of 40% or 60% until pore water pressure ratios of 0.25, 0.50, or 0.75, then the specimens were monotonically sheared. The following conclusions can be drawn from the results.

- Investigations of the effect of GGBFS contents on the post-cyclic behaviour of the soil showed that increasing the GGBFS contents improved the ultimate deviatoric strength of the soil. This behaviour was attributed to dissipation of pore water pressure in GGBFS treated specimens due to the presence of the GGBFS and filling of the micro pores.
- The post-cyclic test results showed that the ultimate deviatoric strength for untreated soil and GGBFS treated specimens at a greater pore water pressure ratio is lower than the specimens tested at a lower pore water pressure ratio. This behaviour was attributed to the greater number of cyclic loadings applied on the specimens at a greater pore water pressure ratio which generate a less stable structure for the specimens.
- The results showed that increasing the initial mean effective stress in GGBFS treated specimens reduced the ultimate deviatoric strength. This behaviour was attributed to the soil dilatancy which is consistent with the critical state of soil and literature.
- The results showed that the densification of the GGBFS treated specimens causes the generation of a greater ultimate deviatoric strength than the

untreated soil. This behaviour was attributed to an increase in interlocking forces and filling of the voids which dissipate the generation of pore water pressure. The GGBFS fills the remaining micro pores and makes the generation of pore water pressure even harder.

7.3. CHAPTER CONCLUSIONS

This chapter investigated the effect of two environmentally-friendly binders (i.e., FA and GGBFS) on post-cyclic behaviour of sand by performing a series of undrained post-cyclic monotonic triaxial compression tests. To conduct the post-cyclic tests initially the cyclic loads applied on the specimens until they reached the desired pore water pressure ratios of 0.25, 0.50, and 0.75. Furthermore, the results for pore water pressure ratio of zero in part one was acquired from the monotonic triaxial tests.

In the first part, the effect of four different FA contents (i.e., 0, 2, 4, and 6% by dry weight), three pre-consolidation relative densities (i.e., 20, 40, and 60%), and three effective confining pressures (i.e., 50, 70, and 90 kPa) on post-cyclic behaviour of the soil were investigated and the results were analysed and presented. Investigations showed that increasing the FA contents increased the ultimate deviatoric stress of the specimens in all tested pore water pressure ratios after cyclic loadings. The analysis showed that the ultimate deviatoric stress of the specimens in the post-cyclic phase reduced when the post-cyclic tests initiated at a greater pore water pressure ratio after cyclic loadings. This behaviour was attributed to greater cycle numbers that applied on the specimens and provided a more metastable soil structure. In the next stage, investigation on effect of relative density showed that increasing the pre-consolidation relative density from 20 to 40 and 60% of the specimens increased the ultimate deviatoric stress. This increase was less prone in untreated soil and more apparent in FA treated specimens. Finally, the investigations in the first part of the chapter seven showed that increasing the initial mean effective stress from 50 kPa to 70 and 90 kPa reduced the ultimate deviatoric stress of FA treated specimens. This behaviour was attributed to suppression of dilatancy of soil.

The second part of the chapter seven investigated the effect of GGBFS on the post-cyclic behaviour of soil by performing a series of undrained post-cyclic monotonic triaxial compression tests. The effect of four GGBFS contents (0, 3, 5, and 7% by dry weight), and three initial mean effective stresses (i.e., 100, 200, and 400 kPa) on the specimens with initial relative densities of 40% or 60% were investigated. The investigations showed that increasing the GGBFS contents improved the ultimate deviatoric strength of the soil. This behaviour was attributed to dissipation of pore water pressure in GGBFS treated specimens due to the presence of the GGBFS and filling of the micro pores. The results showed that the ultimate deviatoric strength for untreated soil and GGBFS treated specimens at a greater pore water pressure ratio is lower than the specimens tested at a lower pore water pressure ratio. This behaviour was attributed to the greater number of cyclic loadings applied on the specimens at a greater pore water pressure ratio which generate a less stable structure for the specimens. The investigations on the effect of initial mean effective stress in GGBFS treated specimens showed that the specimens have a greater ultimate deviatoric stress under a lower initial mean effective stress due to the suppression of dilatancy. Furthermore, the results showed that the densification of the GGBFS treated specimen causes the generation of a greater ultimate deviatoric strength than the untreated soil due to increase in interlocking forces which reduced the generation of pore water pressure.

Chapter 8

Constitutive Modelling Analysis

CHAPTER INTRODUCTION

This chapter provides a constitutive analysis based on the critical state of soil on the sand (base material) parameters and sand-FA mixtures in two parts. This constitutive analysis provides relations, which approximate the soil response to the particle characteristics and the FA based on the framework introduced in critical state of soil mechanics (CSSM).

Before performing the analysis on the sand-FA mixtures, it is important to investigate the effective parameters in forming behaviour of the base soil. The particle shape is one of the key parameters, which forms the soil response under external stimuli. Hence, the first part of this chapter investigates the role of particle shape in forming the soil response. The correlations have been presented based on the roundness (R), sphericity (S), and regularity (ρ) for three types of the natural, crushed and mixed soils.

The second part investigates the effect of FA on critical state of soil. The critical state locus of the untreated sand and sand-FA mixtures have been approximated in different planes and the correlations have been presented.

The results of the first part of this chapter have been published by the journal of Keramatikerman and Chegenizadeh (2017c) and the results of the second part of this chapter are under preparation to submit for a high quality journal.

Part 1

Effect of Particle Shape on Monotonic Liquefaction

8.1. Effect of Particle Shape on Monotonic Liquefaction

8.1.1. Abstract

This study investigates the effect of particle shape on monotonic liquefaction of the soil by performing a series of static triaxial compression tests. The tests conducted on three types of natural sand (NS), crushed sand (CS), and mixed sand (MS) (i.e., 50% natural sand + 50% crushed sand by dry weight of the soil) with different particle shape descriptors consist of roundness (R), sphericity (S), and regularity (ρ). The shearing responses showed that the CS and MS specimens showed a dilative response whereas the natural sand had a strain-softening contractive behaviour. Furthermore, the interpreted results based on a framework of the critical state of the soil mechanic (CSSM) showed that in $e-p'$ plane, the specimen with a higher amount of crushed particles have a greater strength due to a higher packing characteristics. The investigations on critical state locus on $q-p'$ plane showed that by increasing the roundness, sphericity and regularity of the specimens the critical friction angle (ϕ_{cs}) decreased. In addition, studies on flow liquefaction in undrained instability state (UIS) showed that by increasing the particle shape descriptor values, the specimens are more pronounced to be liquefied.

8.1.2. Introduction

The soil shape and size can vary due to chemical and mechanical interactions, their source of mineralogy, transportation, and depositional environment (Cho et al, 2006). Roundness (R), sphericity (S), and regularity (ρ) have been known as main particle descriptors (Krumbein and Sloss, 1963; Cho et al, 2006). Previous studies conducted to investigate the effect of particle shape in a triaxial behaviour of the soil. For instance, Yang and Wei (2012) performed a series of experimental tests to investigate the effect

of fine particle shape on collapsibility of the sand. They tested two types of fine shapes consist of glass bead and crushed silt. They indicated that addition of crushed silt to sand caused an increase of critical state friction angle and addition of well-rounded fine to sand reduced this parameter. They also studied the effect of fine particle shape on flow liquefaction of the soil and indicated that the soil containing round fine particle are more prone to be liquefied than the soil with crushed fine particles. Later, Wei and Yang (2014) in a complementary study proved that the observed behaviour of the tested soil containing fine particles was due to particle shape. In another study, Borhani and Fakharian (2016) investigated the effect of particle shape on dilative response of the soil. They indicated that the sand with more angular particle shape has a more dilative tendency. It was also concluded that internal friction angle of the soil is more dependent on particle shape than the peak strength.

Altuhafi et al. (2016) examined the effect of particle shape on the mechanical behaviour of a compiled database of 25 natural sands. They highlighted that the particle shape is an effective parameter on the critical state intercept in plane of void ratio (e) versus logarithm mean effective stress (p') since the shape has an effect on packing characteristics rather than on gradient in a low-pressure range. It was also indicated that parameters such as minor particle damages and particle rearrangement have an effect on gradient. They indicated that the particle shape has a low effect on the location of the critical state line at higher stresses since the particle strength is the governing parameter. They introduced a universal parameter known as shape-angularity group indicator (SAGI), which was a combination of shape individual parameters such as sphericity (S), convexity (C_x), and aspect ratio (AR). It was summarised that the new parameter has a better correlation with packing and angularity characteristics than each individual parameter. They also confirmed that this

new parameter has no clear relation to critical state internal friction angle since it is highly affected by the convexity of the soil particles (Altuhami et al. 2016).

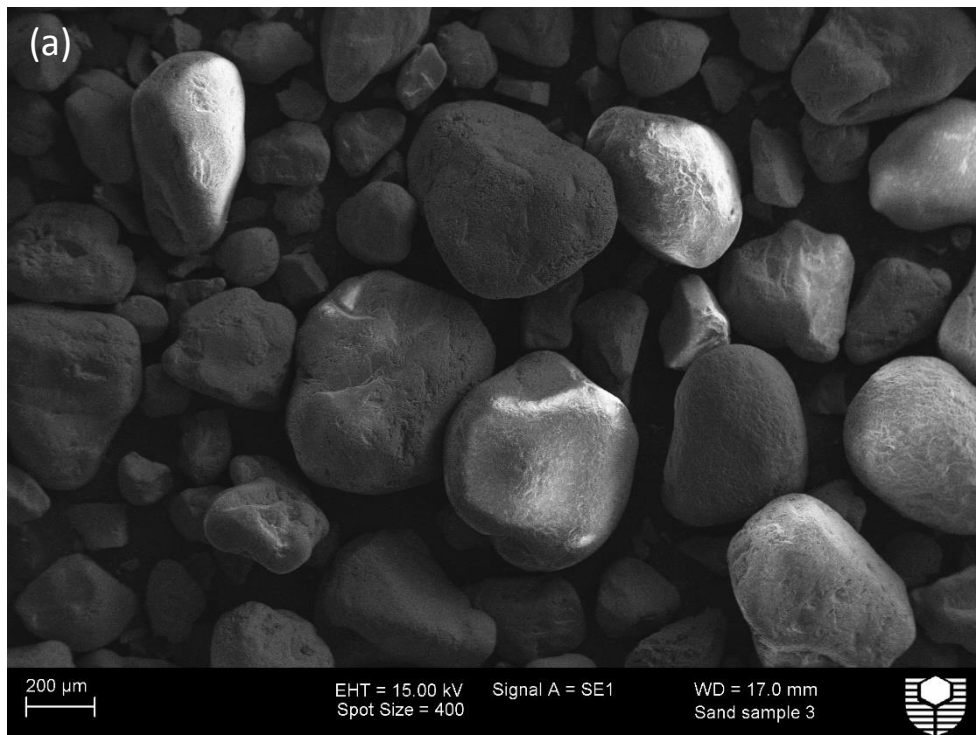
Yang and Luo (2015) investigated the relation between particle shape and the critical state of soil mechanics by performing a comprehensive laboratory study. They combined two types of circular and crushed glass beads with a uniform type of soil in different percentages and conducted a series of drained and undrained triaxial compression tests, and analysed the results based on the critical state of soil mechanics (CSSM). It was concluded that soil combined with circular glass beads is more prone to an instability state than the other mixture (i.e., crushed glass beads). They also proposed a new particle descriptor index which is known as the overall regularity. This newly suggested particle descriptor is the average of three previously indicated indices. They conducted their analysis on this index as well as on the other three indices.

In an older study, Rousé et al. (2008) investigated the effect of roundness on the void ratio of a compiled series of sand and glass beads. They indicated that roundness is an effective parameter in an experimental study which had a good correlation with void ratio range parameter (i.e., $\Delta e = e_{max} - e_{min}$) rather than maximum and minimum void ratios (i.e., e_{max} and e_{min}).

This study aims to investigate the effect of particle shape on liquefaction characteristics of the natural and crushed sand based on particle descriptors.

8.1.3. Test Materials and Methods

Three types of soil with different particle shapes were tested in this study. The natural sand (NS) was obtained from Baldivis, a suburb located in Perth, Western Australia. The second sand was prepared by manually crushing of the natural sand, and the third sample was prepared by mixing of the natural and crushed sand (CS) in the ratio of 1:1; this sample was called mixed sand (MS). Fig. 8.1 shows the scanning electron micrograph (SEM) images of the tested samples. The particle size analysis and physical characteristics of each sample are summarised in Fig. 8.2 and Table 8.1 respectively. The X-ray powder diffraction (XRD) analysis showed that the used sand contain mainly quartz.



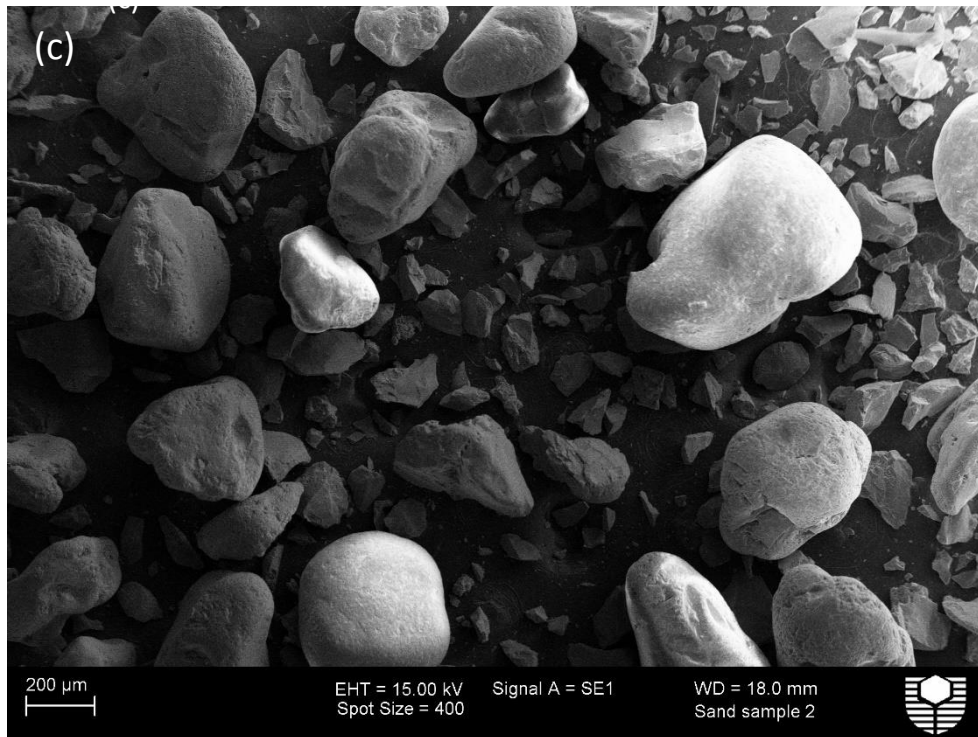
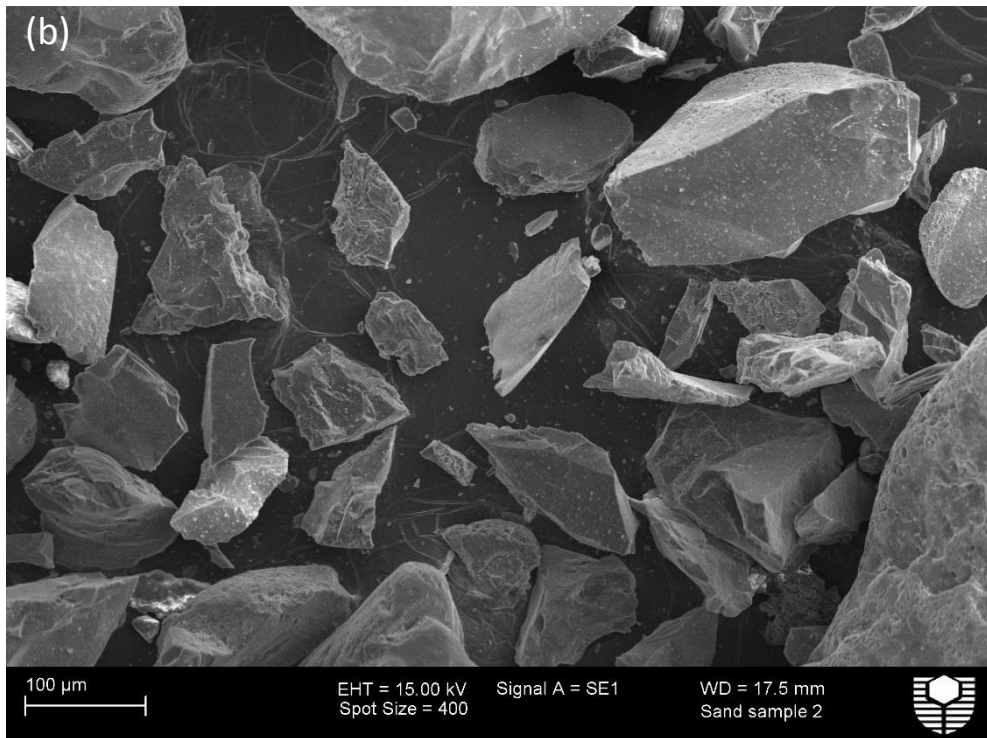


Fig. 8.1. Scanning electron microscopic (SEM) images for (a) natural sand; (b) crushed sand; (c) mixed sand

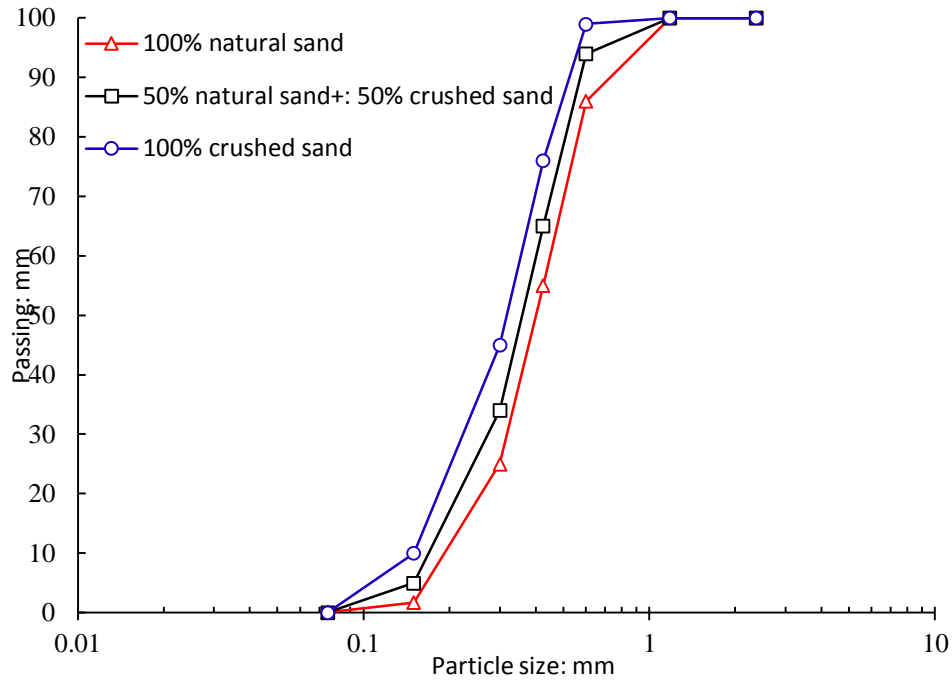


Fig. 8.2. Particle size distribution for tested sands

Table 8.1. Properties of the tested sands in this study

Sand type	Crushed (%)	Particle shape characteristics						Particle shape descriptor			Compaction test	
		C _c	C _u	D ₅₀	Sand (%)	USCS	G _s	R	S	ρ	MDD	OMC
NS	0	1.02	2.35	0.41	100	SP	2.72	0.82	0.91	0.87	1.65	9.3
CS	100	1.15	2.35	0.36	100	SP	2.72	0.33	0.42	0.38	1.67	9.3
MS	50	0.87	2.47	0.31	100	SP	2.72	0.58	0.60	0.59	1.66	9.2

Note: $C_c = d_{30}^2 / (d_{60} + d_{10})$; $C_u = d_{60} / d_{10}$; D_{50} , mean grain size; G_s , specific gravity; R, roundness; S, sphericity; ρ , regularity; MDD, maximum dry density; OMC, optimum moisture content; USCS, unified soil classification system

The particle shape descriptors were quantified visually using scanning electron microscope images according to Krumbein and Sloss (1963) empirical chart. For each soil, 40 grains were randomly selected and the mean values of sphericity (S), and roundness (R) were measured carefully. The sphericity is a ratio of the radius of the largest surrounded circle in the particle to the smallest circle to the particle. The roundness was measured as the proportion of the average radius of the soil grain

features to the radius of the largest circle in the soil particle. The regularity is quantified as the mean of roundness and sphericity. The regularity (ρ) factor was computed based on proposed equation by Cho et al. (2006). This parameter is a factor of roundness and sphericity. Fig. 8.3 shows a typical procedure to calculate sand grain shape descriptors.

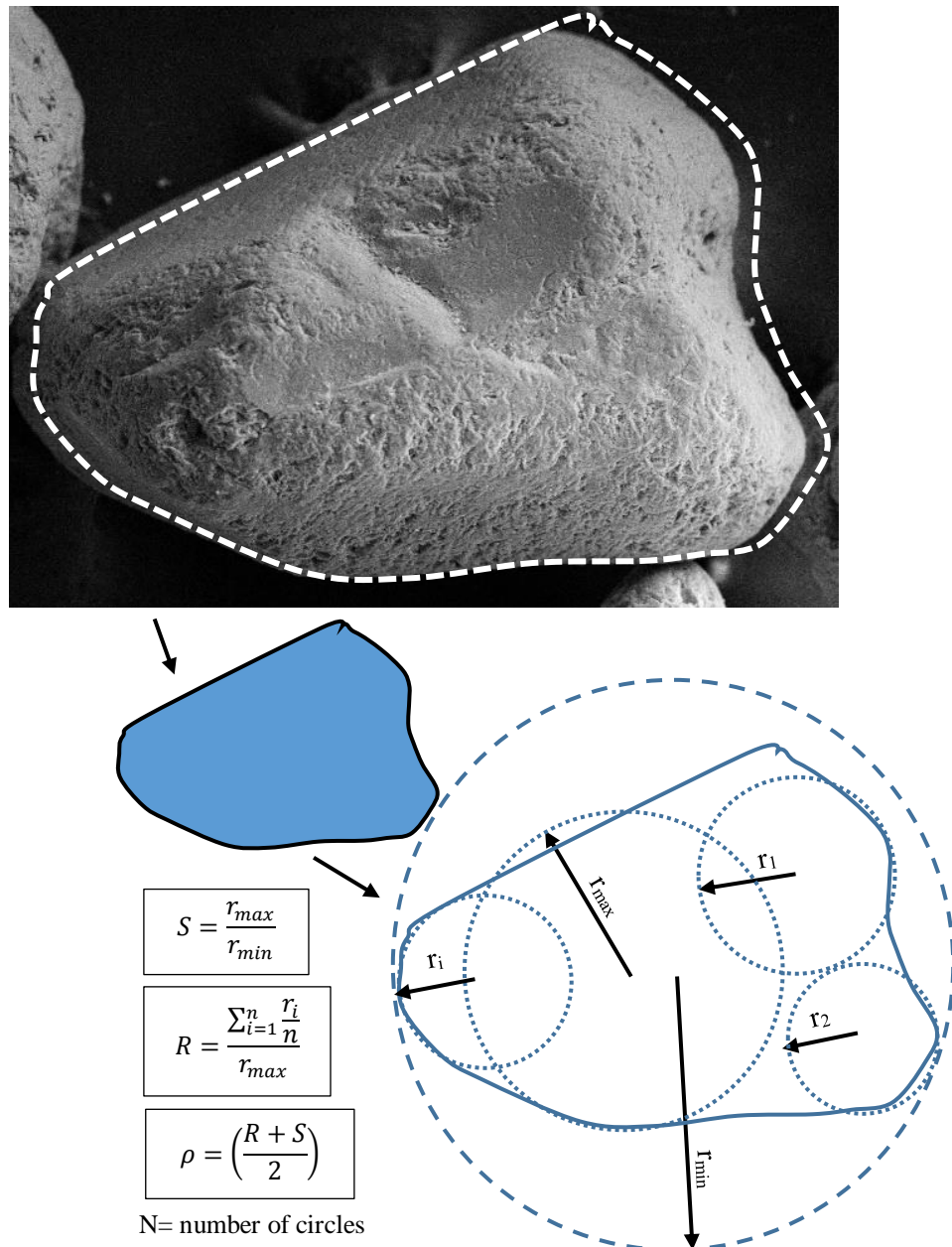


Fig. 8.3. Procedure for calculation of particle shape descriptors (Principles from Krumbein and Sloss, 1963; Cho et al, 2006).

The particle shape characterisations can be performed manually or by using an automated image analyser (Smart 2008). In the manual method, a series of sand particles are randomly selected, and the mean value of the shape parameters are determined based on the chart using the images acquired from a conventional optical device (Krumbein and Sloss 1963). In an automated image analyser, a series of binary images are captured from a steady flow of particles through the vertical shaft of the machine, and the parameters are computed automatically (Yang and Luo 2015). Although, the manual method is a cost-effective approach and has been used in previous studies (Payan et al. 2016; Rousé et al. 2008), application of automated methods, like the laser scanning technique, are encouraged for future works as in this method, the soil particles undergo a three dimensional characterisation in a timely manner, which causes the generation of more accurate results (Yang and Luo 2015; Smart 2008).

The undrained monotonic triaxial compression tests (UC) were performed in accordance with ASTM D7181 (ASTM 2011e) using an automated Bishop and Wesley triaxial machine (Bishop and Wesley 1975). The prepared specimens had 70 mm diameter and 140 mm height (i.e., aspect ratio of 2). The under-compaction method by moist-tamping the soil was applied to prepare the specimens to avoid segregation (Ladd 1978). To prepare the specimens, the desired amount of soil was mixed with water based on its optimum moisture content (OMC) and thoroughly stirred. Then, the soil compacted in the cylindrical, steel split mould into five layers until the desired height was achieved. When the sample preparation completed, specimens were saturated by injecting de-aired water from the bottom of the specimen. The saturation stage was completed when a B -value of at least 0.96 was achieved. After saturation, the specimens were isotopically consolidated to the targeted initial

mean effective stress (p'_0). The post-consolidation void ratio of samples were recorded based on initial void ratio (e_0) and its volumetric strain when the consolidation phase completed. The post-consolidation void ratio (e) values were double-checked using different technique by measuring the final water content at the end of the tests.

8.1.4. Results and Discussion

8.1.4.1. Stress-strain Relation

Fig. 8.4 shows the typical shear responses of the NS, MS, and CS in deviatoric stress versus mean effective stress ($q-p'$) and deviatoric stress versus axial strain ($q-\varepsilon_a$) planes for an initial mean effective stress of 500 kPa at the same post-consolidation void ratio (e). As can be seen, an increase in the contribution of the crushed particles in the soil system caused dramatic changes in shearing response of the specimens. For instance, the NS specimen containing rounded particles showed a contractive strain-softening response, whereas the MS and CS specimens with 50% and 100% crushed grains showed a strong dilative response. The deviatoric stress in natural sand after reaching the peak of 450 kPa at 1.9% axial strain showed a decreasing trend until 280 kPa at 30% axial strain. Conversely, the MS specimen containing 50% crushed, reached the peak deviatoric strength of 502 kPa immediately after 1.8% strain. The strength of this specimen reached the maximum amount of 751 kPa after 30% axial strain. Similar to MS specimen, the CS specimen containing 100% crushed sand particles showed a strong dilative response. The recorded peak deviatoric stress was 593 kPa after 2% axial strain. The deviatoric stress specimen reached 965 kPa after 30% axial strain. The observed variation in the shearing responses of the tested specimens highlights the effect of particle shape. Table 8.2 shows a summary of the recorded shearing responses for three tested soils.

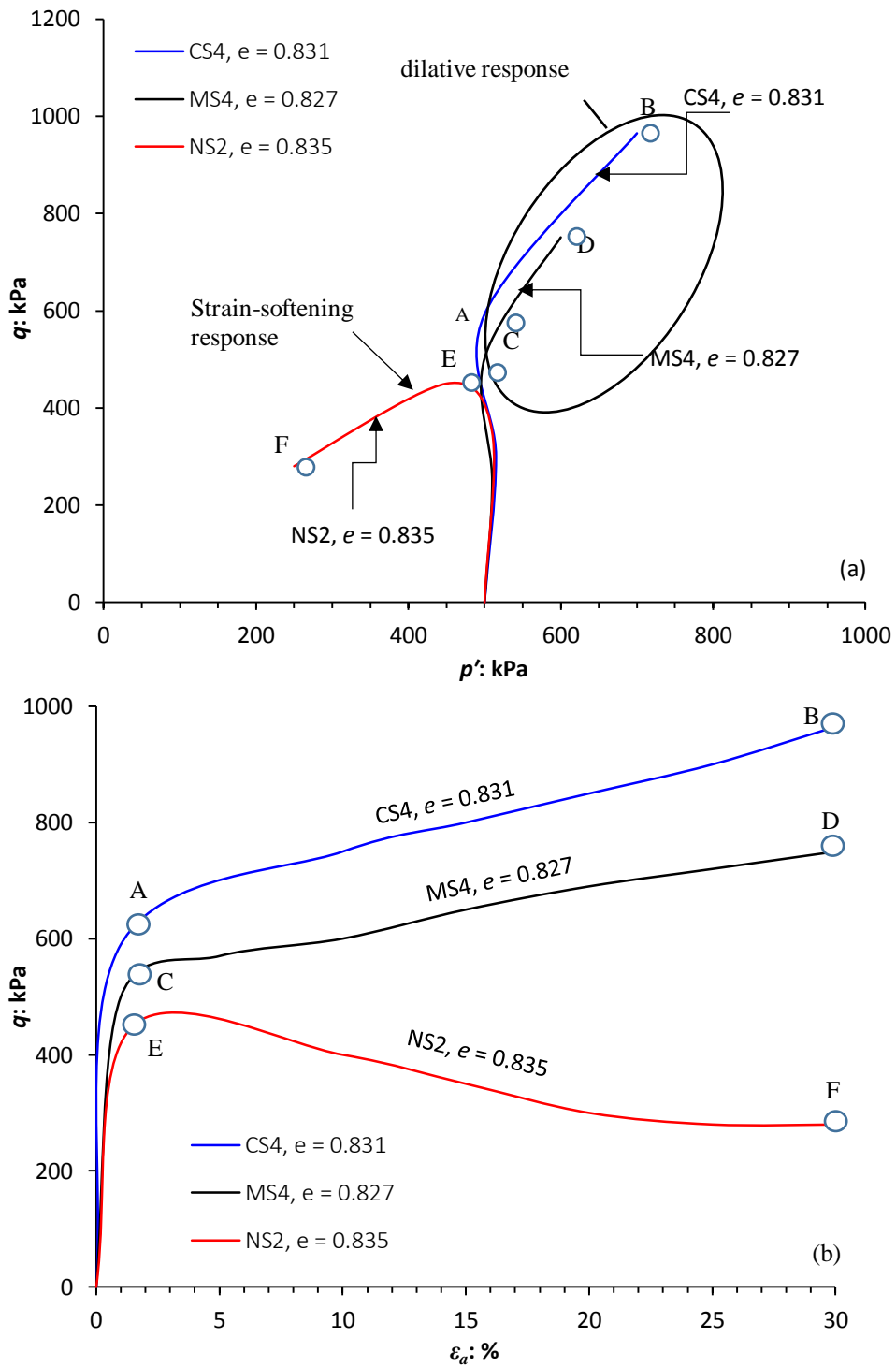


Fig. 8.4. Undrained shear behaviour of NS, MS, and CS specimens under 500 kPa initial mean effective stress (a) stress path (q - p'); (b) stress-strain relation.

Table 8.2. Experimental program conducted in this study and recorded results

Test ID	e_0	e	$P'_0: kPa$	Critical state (CS)	
				$P': kPa$	$q: kPa$
CS1	0.902	0.881	500	156	914
CS2	0.881	0.862	500	351	135
CS3	0.868	0.845	500	592	732
CS4	0.853	0.831	500	700	965
CS5	0.843	0.825	500	1102	1134
MS1	0.896	0.875	500	110	634
MS2	0.871	0.853	500	281	224
MS3	0.859	0.837	500	521	447
MS4	0.848	0.827	500	600	750
MS5	0.829	0.807	500	1000	875
NS1	0.878	0.856	500	50	71
NS2	0.854	0.835	500	250	280
NS3	0.836	0.818	500	460	463
NS4	0.816	0.795	500	690	580
NS5	0.795	0.771	500	950	934

Note: e_0 , initial void ratio; e , post-consolidation void ratio; P'_0 , initial mean effective confining pressure; P' , mean effective confining pressure; q , deviatoric stress.

8.1.4.2. Critical State Locus in e - p' Plane

The critical state locus in compression space is presented by Eq. (8.1.1)

$$e = \Gamma - \lambda_c \log p' \quad (8.1.1)$$

Where e = void ratio; Γ = void ratio intercept at $p'= 1$ kPa; λ_c = slope of the straight line; and p' = mean effective stress. Although, Eq. (8.1.1) is a simple form of a linear relation to represent the CSL in compression space, previous studies (e.g. [Yang and Luo 2015](#); [Yang and Wei 2012](#)) highlighted that the CSL in a semi log graph is curved rather than linear. Therefore, Eq. (8.1.1) is not appropriate for representing the CSL or analysing the subsequent mechanical responses in compression space. Li and Wang ([1998](#)) introduced a more accurate representation of the CSL in compression space, known as power law function. Eq. (8.1.2) shows this representation.

$$e = e_{\Gamma} - \lambda_c \left(\frac{p'}{p_a} \right)^n \quad (8.1.2)$$

Where e_{Γ} = void ratio intercept at $p=0$; p_a = atmospheric pressure (=101 kPa); and n = an optimised ratio for sand (=0.6). Fig. 8.5 shows the critical state lines of the NS, MS and CS specimens in compression space (i.e., e - p' plane) presented based on power law function. As can be seen, by increasing the contribution of crushed particles in the soil structure, the critical state locus dropped down. This behaviour indicates that the critical state locus in CS and NS is greater than the NS specimens. For instance, the crushed sand specimen with a post-consolidation void ratio in the range of $0.825 \leq e \leq 0.881$ has a power law function in the range of $1.30 \leq (p'/p_a)^n \leq 4.19$. The post-consolidation void ratio value range decreased to $0.807 \leq e \leq 0.875$ and $0.771 \leq e \leq 0.856$ for MS and NS specimens by reduction of the power law function values in the range of $1.05 \leq (p'/p_a)^n \leq 3.96$ and $0.66 \leq (p'/p_a)^n \leq 3.84$. The recorded behaviour for tested specimens was consistent with results presented by Been et al. (1991). Fig. 8.6 shows the computed critical state locus slopes (λ_{cs}) in e - p' plane versus particle shape descriptors consisting of roundness, sphericity, and regularity. It is seen from the figure that, increasing the particle shape descriptors caused an increase in computed critical slopes (λ_{cs}). Cho et al. (1998) reported no correlation between critical state slope (λ_{cs}) in e - p' plane and the particle descriptors since the tests were conducted in a wide range of soils with different particle size distributions (PSD), and CSL was presented with linear lines in e - $\log p'$ space rather than curved lines (Yang and Luo 2015). Fig. 8.7 also shows variations of the computed void ratio intercept (e_{Γ}) in e - p' plane versus particle shape descriptors. As can be seen, the void ratio intercept decreased by increasing the particle descriptors values. The observed behaviour was attributed to

the packing response of the specimens and is in good agreement with reported results by Yang and Luo (2015), Yang and Wei (2012), and Cho et al. (2006).

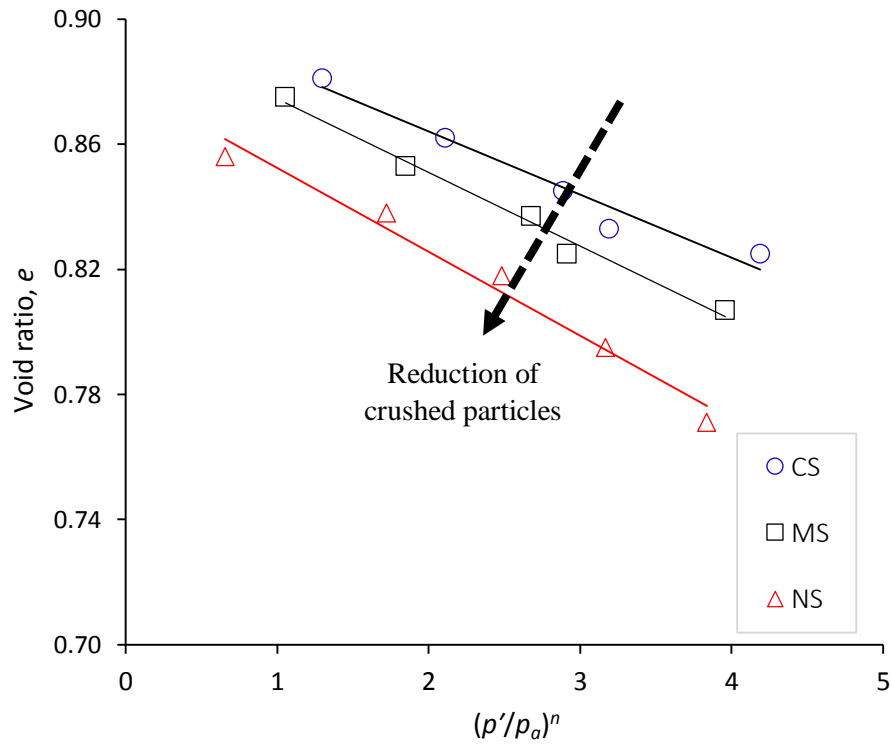
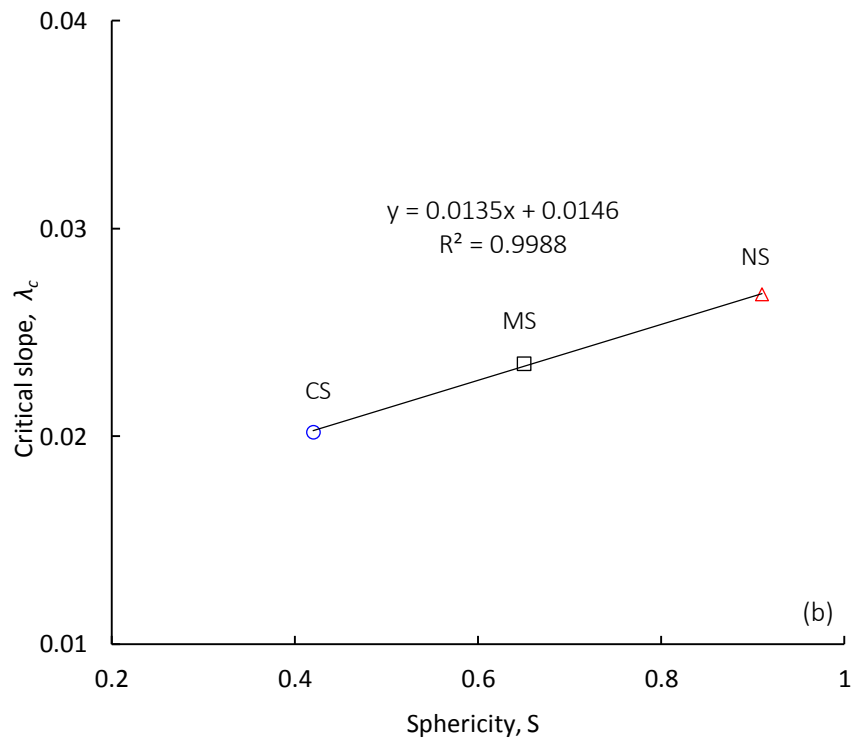
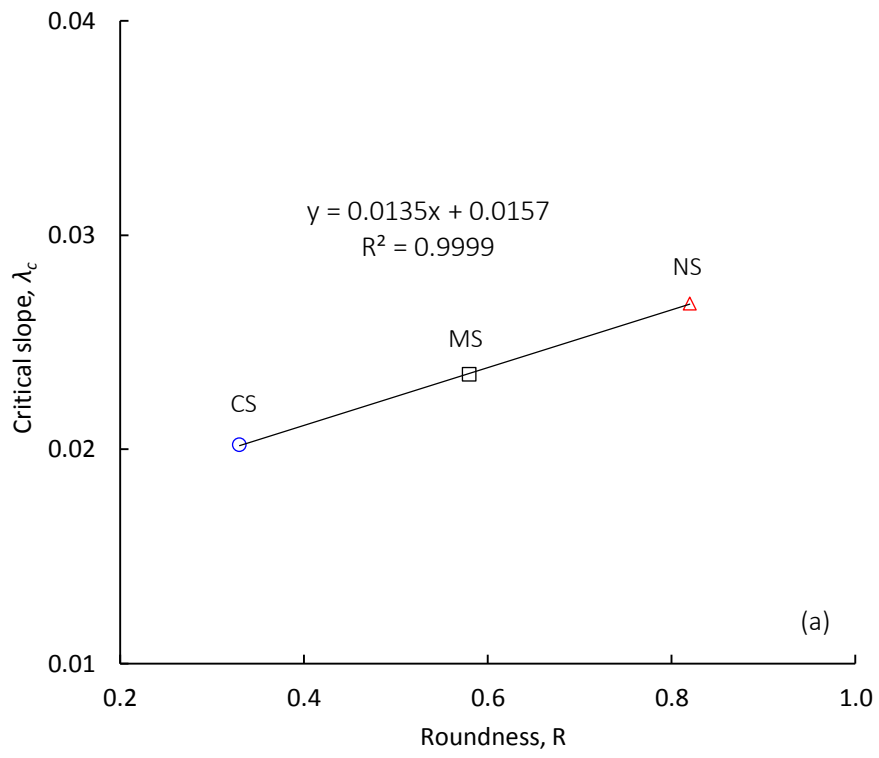


Fig. 8.5. Critical state locus in $e-p'$ plane for CS, MS, and NS specimens.



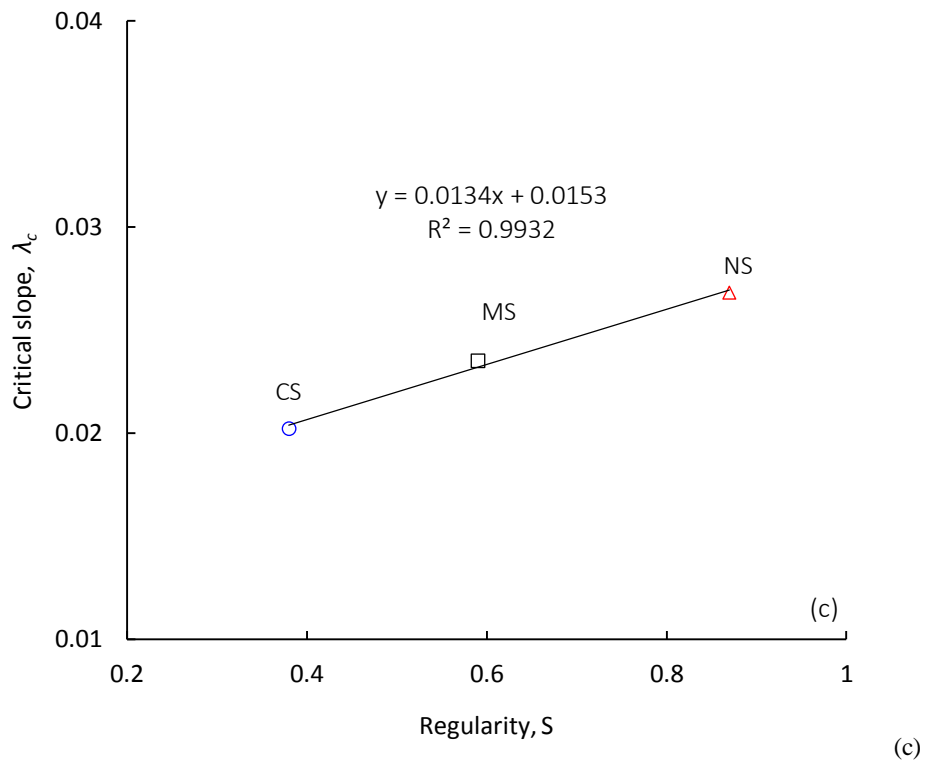
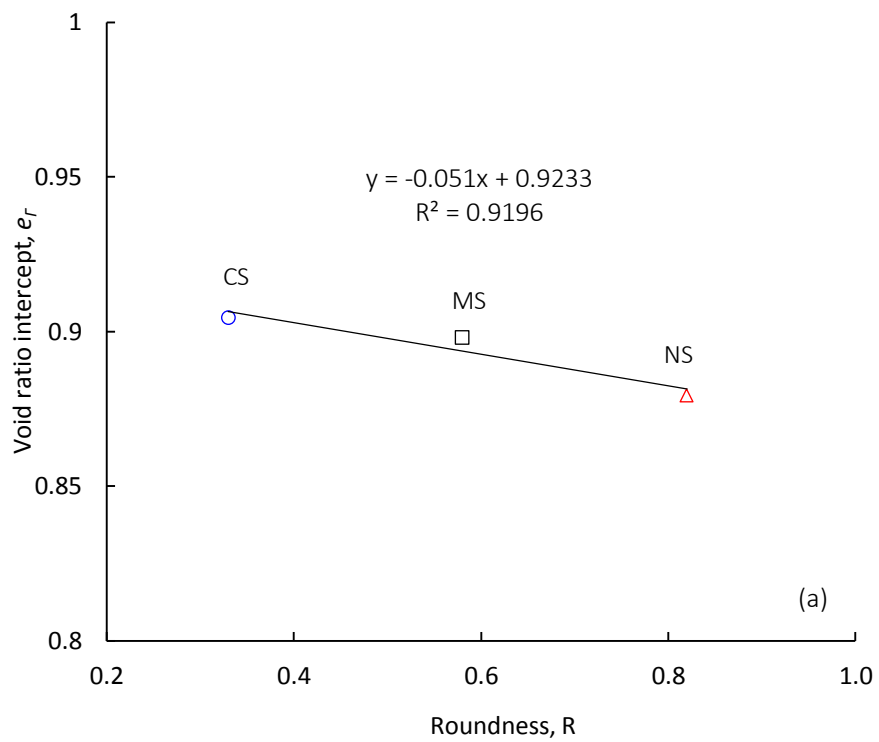


Fig. 8.6. Slope of critical state locus (λ_{cs}) in $e-p'$ plane versus (a) roundness; (b) sphericity; and (c) regularity.



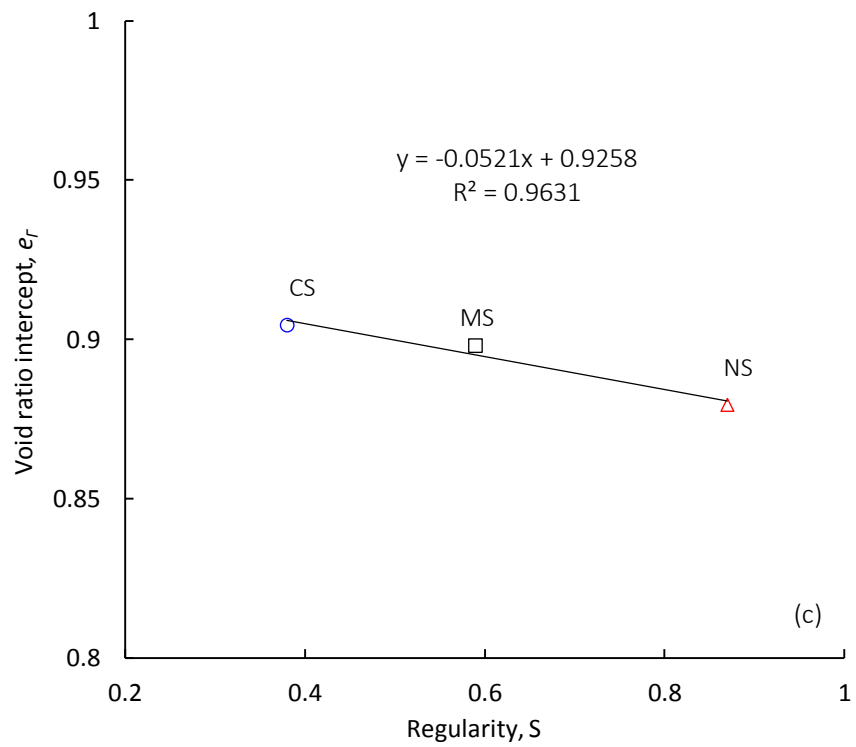
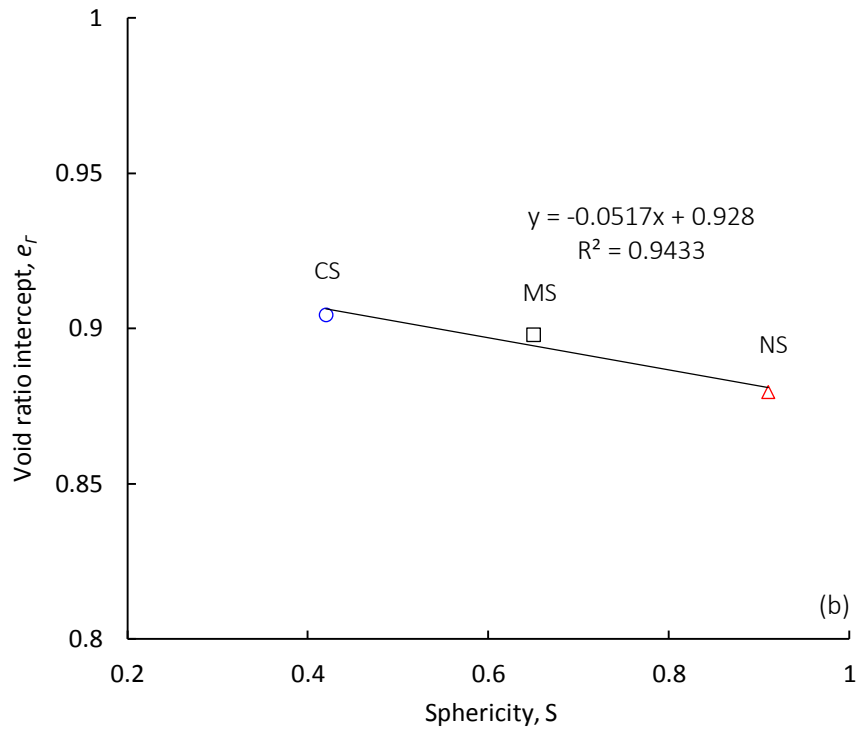


Fig. 8.7. Critical state locus intercept (e_r) in $e-p'$ plane versus (a) roundness; (b) sphericity; and (c) regularity.

8.1.4.3. Critical State Locus in q - p' Plane

Fig. 8.8 shows the critical state locus of the CS, MS, and NS in q - p' plane. The critical state slope of the tested soils was determined based on the following equation:

$$q = M_{cs}p' \quad (8.1.3)$$

Where M_{cs} = effective stress ratio at critical state which corresponds to the critical state friction angle. As can be seen, the critical state friction angle (ϕ_{cs}) acquired from critical state line increased by increasing the crushed particles in the soil system. For instance, the critical friction angle of NS was 28.30° , this value increased to 31.61° and 34.06° for MS and CS respectively. Furthermore, the effective stress ratios at critical state (M_{cs}) increased by increasing the crushed particles contribution in the soil structure. For instance, an effective stress ratio at critical state of 1.13, 1.27, and 1.38 was recorded when the soil system contained 0, 50, and 100% crushed particles, respectively. Similar results were reported in the literature when the crushed glass beads content of the soil increased (Yang and Luo 2015). For instance, combinations of Fujian sand with 20% and 40% glass beads (increasing R , S , and ρ of the soil system) caused a M_{cs} value of 1.13 and 1.08, whereas combinations of the same soil with 20% and 40% crushed glass beads (reduction of R , S , and ρ of the soil system) caused a M_{cs} value of 1.26 and 1.34 respectively (Yang and Luo 2015). In fact, in both cases, increasing the contribution of natural particles in the soil system caused a clockwise rotation for the critical state line (CSL) in the q - p' plane, and increasing the contribution of crushed particle caused an anti-clockwise rotation for the CSL. The reported results in this section clearly highlight the relation between particle shape and critical state line in the q - p' plane. In addition, variations of the critical state friction angle (ϕ_{cs}) with particle shape descriptors (i.e., R , S , and ρ) for the tested soils were

shown in Fig. 8.9. A well-fitted correlation (i.e., $R^2 > 0.99$) in all three cases is evidence for the effect of particle descriptors on CSL. The figure shows that the critical state frictional angle (ϕ_{cs}) decreased by increasing the roundness, sphericity, and regularity. Furthermore, the linear equations (i.e., $\phi_{cs} = 38 - 12R$, $\phi_{cs} = 39 - 12S$, and $\phi_{cs} = 40 - 14\rho$ for variations of ϕ_{cs} - R , ϕ_{cs} - S , and ϕ_{cs} - ρ respectively) showed a good correlation with reported relation for variation of the critical state friction angle with roundness (i.e., $\phi_{cs} = 42 - 17R$) by Cho et al. (2006). The results acquired in this section also are in good agreement with results presented by Yang and Wei (2012).

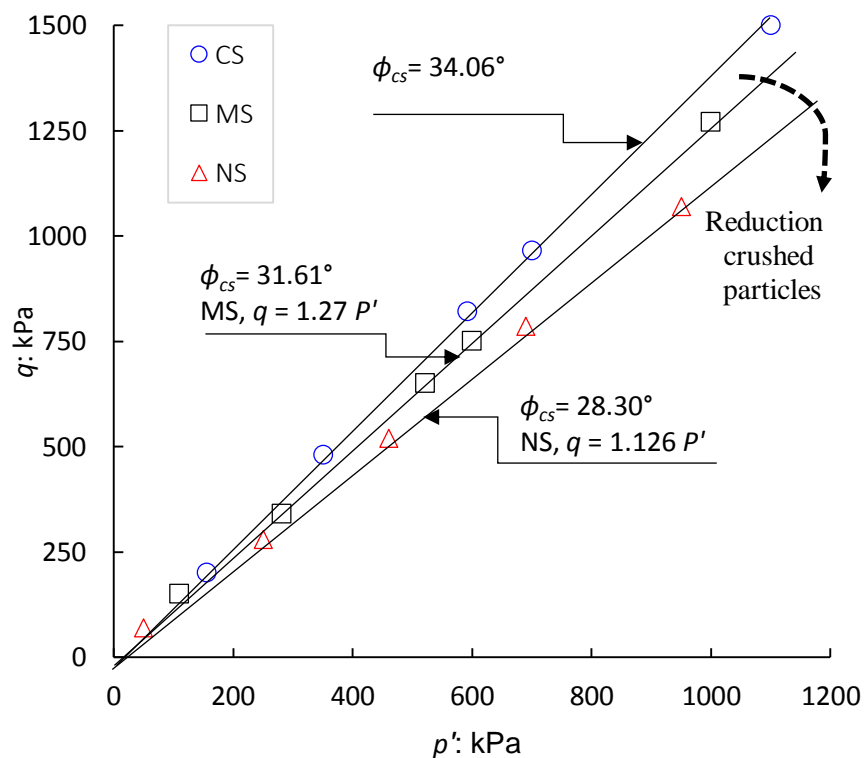
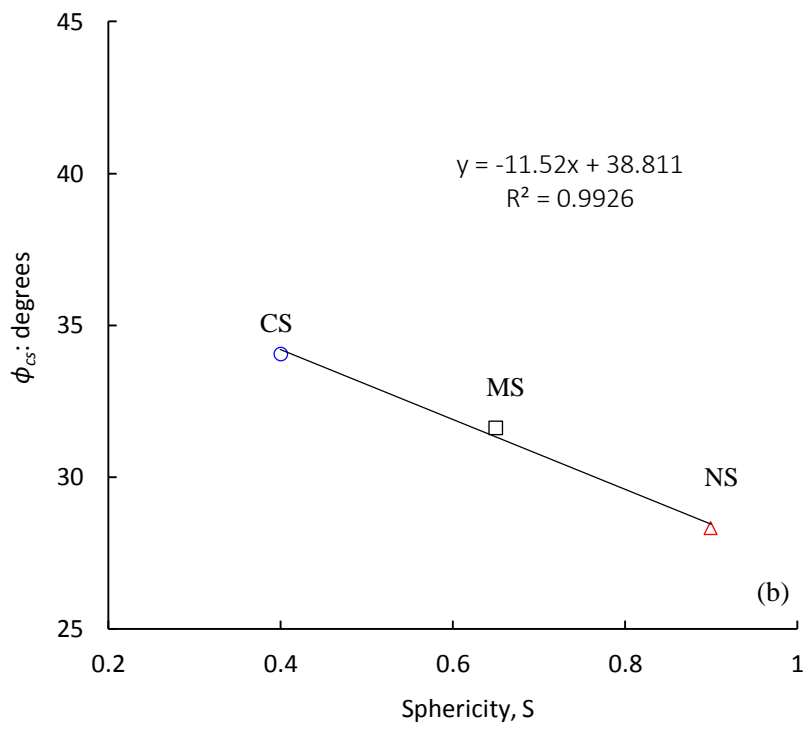
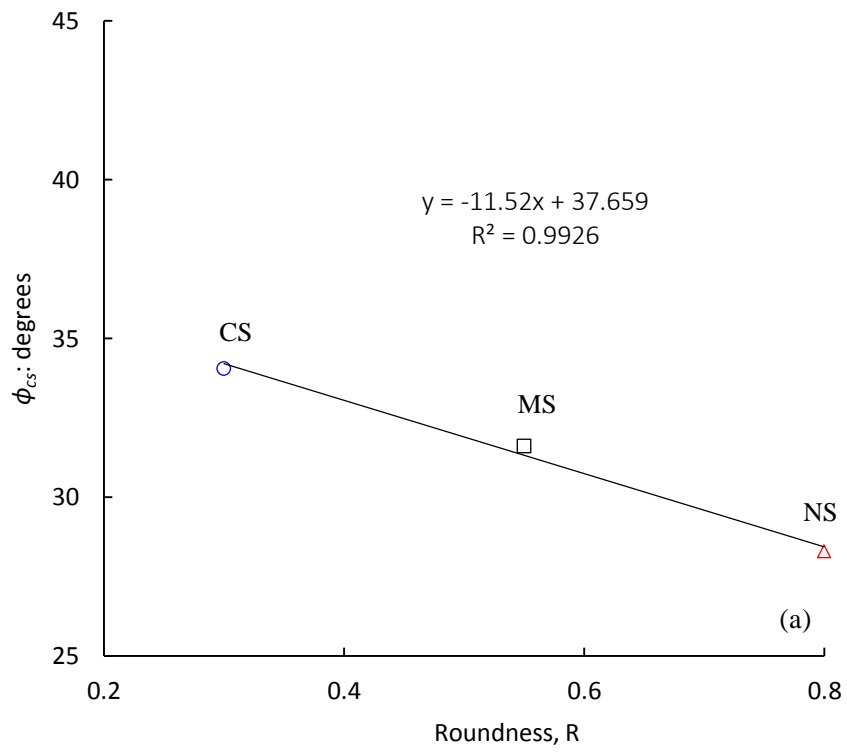


Fig. 8.8. Critical state locus in q - p' plane for CS, MS, and NS specimens.



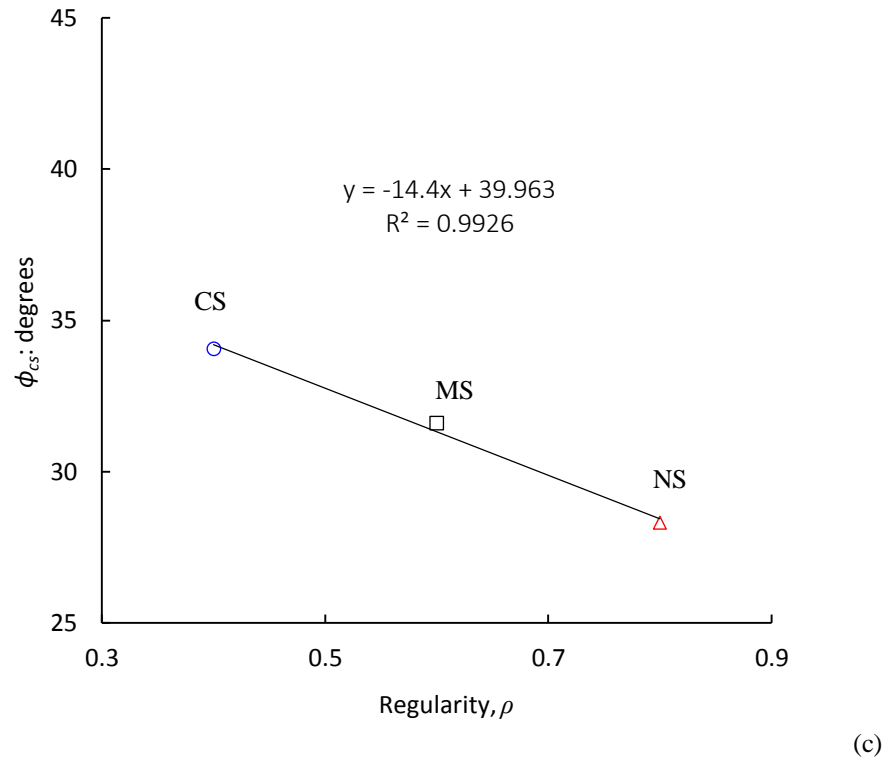


Fig. 8.9. Variation of the Critical state slope in q - p' plane versus (a) roundness; (b) sphericity; and (c) regularity

8.1.4.4. Liquefaction Inception

The liquefaction inception of the specimens was characterised by critical stress ratio (q/p') at the undrained instability state using flow liquefaction line (Kramer, 1996). Fig. 8.10 shows variation of the critical stress ratios versus post-consolidation void ratios for natural, mixed, and crushed soil particles under 500 kPa effective confining pressure. The acquired well-fitted correlations (i.e., $R^2 \geq 0.96$) for variation of q/p' - e highlights the role of particle descriptors in liquefaction inception of the tested soils. It is seen from the figure that increasing the contribution of crushed particles in the soil system caused the acquired straight lines to be shifted to the right. For instance, a critical stress ratio in the range of $0.95 \leq q/p' \leq 1.27$, $0.75 \leq q/p' \leq 1.1$, and $0.98 \leq q/p' \leq 1.03$ corresponding to the post-consolidation void ratio in the range of $0.85 \leq e \leq$

0.918, $0.853 \leq e \leq 0.92$, and $0.793 \leq e \leq 0.873$ was recorded for natural mixed and crushed soil particles respectively. This trend implies that the flow liquefaction triggered at a lower value of stress ratio for soils with a greater amount of rounded particles (Yang and Wei 2012). Furthermore, full or partial replacement of the crushed soil particles (i.e., 100% or 50%) with natural soil particles caused a greater inclination for the soil with higher crushed particles, which indicates a greater resistance to onset liquefaction. The variation of the critical stress ratio with post-consolidation void ratio (e) at instability state can be quantified using the following equations;

NS:

$$q/p' = 1.502 - 0.593e \quad (8.1.4)$$

MS:

$$q/p' = 5.472 - 5.124e \quad (8.1.5)$$

CS:

$$q/p' = 5.325 - 4.766e \quad (8.1.6)$$

The recorded behaviour indicates that the liquefaction inception is more pronounced in a specimen containing more rounded particles. In terms of liquefaction resistance, Wei and Yang (2014) indicated that the specimens mixed with higher percentages of rounded glass beads have a lower stable structure than the same specimens containing the same amount of crushed glass beads. Yang and Wei (2012) also reported that the soil mixed with rounded fine particles has a less stable structure than the soil mixed with crushed fine particles.

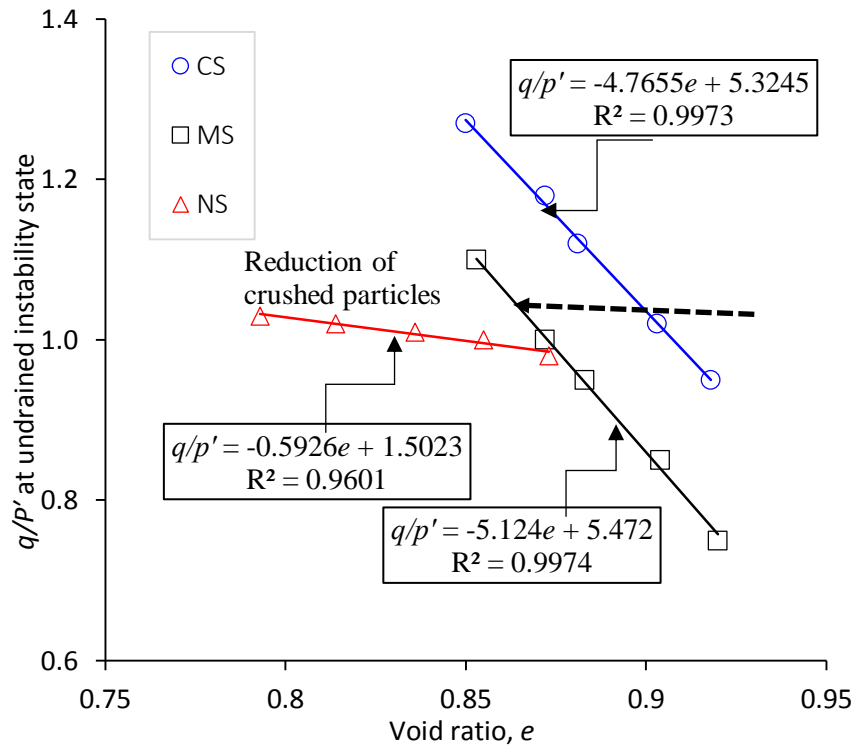


Fig. 8.10. Variation of the stress ratio (q/p') versus void ratio for CS, MS, and NS.

8.1.5. Conclusions

This study investigated the effect of particle shape on monotonic liquefaction of the sand by performing a series of the static triaxial compression tests. The tests conducted on three types of natural sand (NS), crushed sand (CS), and mixed sand (MS) (i.e. 50% natural sand + 50% crushed sand). The following conclusions can be drawn from the results.

- The CS and MS specimens had a strong dilative shearing response while the NS showed a contrastive strain-softening behaviour.
- The interpreted results in $e-p'$ plane based on critical stress state framework showed that by increasing the values of soil shape descriptors (i.e., roundness, sphericity and regularity), the acquired curves dropped, and the strength decreased.

- Investigation on critical state locus in $q-p'$ plane showed that the tested specimens have a critical friction angle of 28.30° , 31.61° , and 34.06° for NS, MS, and CS. The results in this section indicate that by increasing the particle shape descriptors values of the specimens the critical friction angle increased.
- Investigations on undrained instability state of the specimens on the variation of the critical stress ratio (q/p') versus post-consolidation void ratio showed that by decreasing the crushed grains contributions, the soil tended to be liquefied earlier.
- In this study, 15 triaxial compression tests were conducted on three types of soils (i.e., NS, CS, and MS), which caused the generation of three points with a high value of R^2 in particle descriptor graphs. It is recommended that more tests be conducted in future studies to have a clear understanding about the effects of particle descriptors on the critical state of soil.

Part 2

Constitutive Modelling of Sand-FA Mixture

8.2. Constitutive Modelling of Sand-FA Mixture

8.2.1. Abstract

This technical note briefly analyses the effect of fly ash (FA) on critical state parameters and instability state of the soil by performing a series of undrained monotonic triaxial compression tests. Four FA contents consisting of 0%, 2%, 4%, and 6% (by dry weight of the soils) were selected and the results were analysed based on the critical state of soil mechanics (CSSM). The analysis showed that increasing the FA contents caused an increase for the critical state locus in void ratio versus logarithm mean effective stress plane ($e-\log p'$). The computed critical parameters in $e-\log p'$ space such as critical slope (λ_{cs}) and intercept (Γ_{cs}) showed a reduction by increasing the FA contents. The analysis on deviator stress versus mean effective stress plane ($q-p'$) showed that the critical state friction angle (ϕ_{cs}) and its constant parameter (M_{cs}) increased by addition of FA. Analysis on liquefaction inception in undrained instability state (UIS) showed that the specimens containing FA have a strain-hardening behaviour without brittleness (i.e., brittleness index, $I_B=0$), which was effective to mitigate the flow liquefaction.

8.2.2. Introduction

Application of fly ash (FA) in ground improvement area has been reported by previous researchers in the literature ([Keramatikerman et al 2017b](#); [Horpibulsuk et al. 2011](#); [Prabakar et al. 2004](#) amongst other). Fly ash is a pozzolanic material remains in electrical power plants after burning. This by-product is effective to improve the mechanical behaviour of the soil such as swelling, controlling the volume change, and increasing the compressibility ([Horpibulsuk et al. 2009](#)). Fly ash increases the reactive

surfaces of the soil grains and causes an increase in production of hydration and pozzolanic reactions amongst soil particles. These characteristics show that the fly ash has a good potential for replacement for Portland cement (PC) (Horpibulsuk et al. 2009).

Geotechnical soil investigation reports mainly consist of shear strength parameters and rarely reports on critical state parameters of the soil (Dev et al. 2013). Studying critical state parameters helps to understand the fundamental behaviour of the soil in different stress conditions based on natural characteristics of the soil. The introduced parameters such as critical state slope (λ_{cs}), intercept (Γ_{cs}), and constant slope factor (M_c) are known as the critical parameters of the soil which can be determined from triaxial compression tests (Schofield and Wroth 1968). The positions of the critical state parameters were shown in Fig. 8.11.

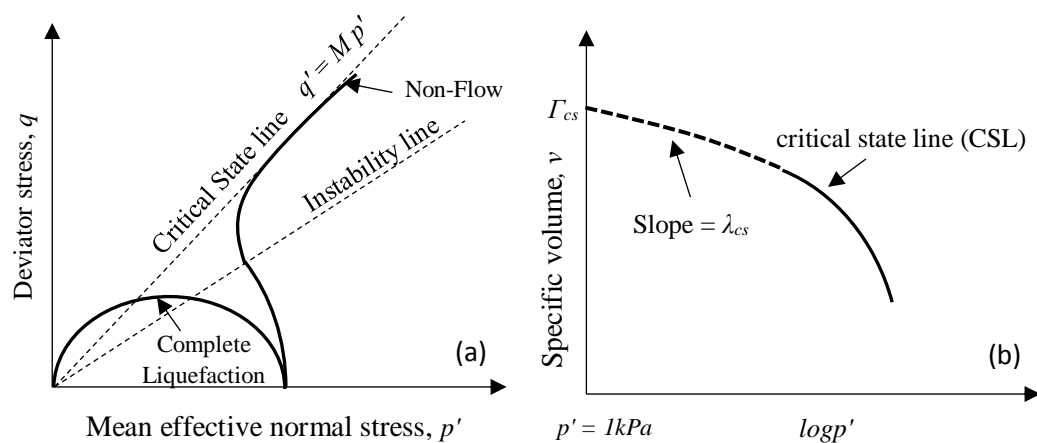


Fig. 8.11. Typical critical state parameters of the soil in a monotonic triaxial test in (a) q - p' plane; (b) v - $\log p'$ plane.

In undrained triaxial condition, a peak deviator stress occurs at a small shear strain. This peak is followed with a large strain at low effective confining pressure and a low strength. In the final state of shear failure, the soil flows under constant stress and

constant volume, which is recognised as flow liquefaction [see Fig. 8.11(a)]. In fact, flow liquefaction failure can be determined by an abrupt failure in deviator stress and a prompt expansion in deformation, which is the most destructive part of the liquefaction (Vaid and Chern 1985; Yang 2002). In theory, flow liquefaction is defined for a strain-softening behaviour in q - p' plane, and it is the line that cross the origin point and the peak point of the deviator stress, which is in the undrained instability state as shown in Fig. 1(a) (Yang and Wei 2012). This line is used to characterise the onset instability of the soil. In the CSSM framework, Yang (2002) indicated that the instability line is not unique and is a parameter of initial state as presented in Eq. (8.2.1).

$$\left(\frac{q'}{p'}\right)_{UIS} = \frac{M_{cs}}{B} \exp(A\psi) \quad (8.2.1)$$

Where ψ = the state parameter defined by Been and Jefferies (1985), which is difference between the current void ratio and the critical void ratio (e_{cs}) at the current mean effective stress (i.e., $e - e_{cs}$); and A and B = calibrating parameters. If sand specimens are sheared from the same stress level, Eq. (8.2.1) can be given in the alternative form in Eq. (8.2.2) as indicated by Yang and Wei (2012);

$$\left(\frac{q'}{p'}\right)_{UIS} = \frac{M_{cs}}{B \exp(Ae_{cs})} \exp(Ae) \quad (8.2.2)$$

To quantify the strength loss for the strain-softening behaviour a better parameter, which is named as brittleness index (I_B), is introduced as Eq. (8.2.3), by Bishop (1967);

$$I_B = \frac{q_{u(yield)} - q_{min}}{q_{u(yield)}} \quad (8.2.3)$$

Where $q_{u(yield)}$ = deviatoric stress at the UIS state; q_{min} = minimum deviatoric stress at the critical state. The I_B characterises the degree of collapsibility, which varies from one, for complete liquefaction, to zero, for a completely dilative response.

This study aims to conduct an analysis on critical state parameters and flow liquefaction of the FA treated specimens in triaxial testing condition.

8.2.3. Materials Used

The sand was sourced from Baldivis, a suburb located in south of Perth, Western Australia. To investigate mineral constituents and physical characteristics of the used materials, X-ray powder diffraction (XRD) test and sieve analysis [ASTM D4221 (ASTM 2011b)] conducted. The XRD tests results showed that the quartz is the main constituent of the used sand. Furthermore, silicon dioxide, aluminium oxide, and ferric oxide are the main constituent of the used FA (Flyash Australia 2016). The sieve analysis showed that the used sand has a uniformity coefficient of (C_u) and a coefficient of curvature (C_c) of 2.5 and 1.19 respectively. The used sand is a poorly graded soil (SP) based on the Unified Soil Classification System (USCS) [(ASTM D2487, (ASTM 2011a)]. The PSD analysis of the used materials was shown in Fig. 8.12. The specific gravity (G_s) of the sand used and FA was 2.67 and 3.1 respectively.

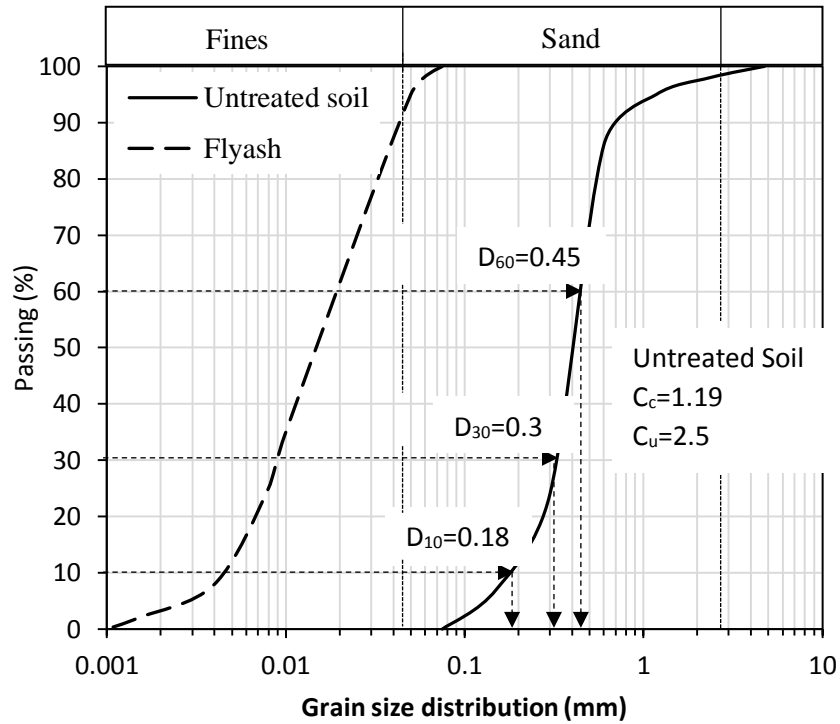


Fig. 8.12. Particle size distribution of the used materials

8.2.4. Specimen Preparation and Triaxial Tests

An automated Bishop-Wesley triaxial machine (Bishop and Wesley 1975) used to conduct a series of undrained monotonic triaxial compression tests in accordance with ASTM D7181 (ASTM 2011e). The specimens with 62.5 mm diameter and 125 mm height (i.e., aspect ratio of 2) were prepared by moist tamping the specimens, which is proposed as the under compaction method by Ladd (1978). Initially, desired amount of FA was mixed with soil and mixed completely, then water added according to the optimum moisture content (OMC) of each mixture acquired from standard proctor tests. Each mixture was compacted in five layers into a cylindrical split mould until the desired height was obtained based on the maximum dry density (MDD). After preparation, the mould was wrapped and were placed in a moist and temperature controlled room to be cured for 3 days. Upon completion of the curing time, the triaxial testing procedure started and water injected through the sample until a *B*-value of at

least 0.99 was achieved, and saturation stage completed. Then, the specimens isotropically were consolidated until the initial mean effective stress of 500 kPa. The post-consolidation void ratio (e_p) of each specimen was recorded based on the pre-consolidation void ratio (e_o) and the occurred volumetric strain during consolidation stage. Table 8.3 shows the test program followed to conduct the tests and the key results.

Table 8.3. Experimental program conducted in this study and recorded results

Test ID	FA content (%)	e_o	e_p	OMC (%)	MDD (kN/m ³)	p' (kPa)	B -value	Critical state (CS)	
								q (kPa)	p' (kPa)
S1	-	0.629	0.591	9.3	16.5	500	0.95	0	0
S2	-	0.619	0.587	9.3	16.5	500	0.95	458	387
S3	-	0.613	0.581	9.3	16.5	500	0.95	687	587
S4	-	0.607	0.575	9.3	16.5	500	0.95	1020	876
SF1	2	0.632	0.598	10.7	16.3	500	0.95	1021	790
SF2	2	0.621	0.595	10.7	16.3	500	0.95	1191	914
SF3	2	0.614	0.591	10.7	16.3	500	0.95	1452	1110
SF4	2	0.615	0.588	10.7	16.3	500	0.95	1732	1325
SF5	4	0.639	0.61	12.5	16.1	500	0.95	1174	840
SF6	4	0.625	0.608	12.5	16.1	500	0.95	1389	997
SF7	4	0.616	0.605	12.5	16.1	500	0.95	1742	1245
SF8	4	0.617	0.601	12.5	16.1	500	0.95	2021	1456
SF9	6	0.646	0.618	14.8	16.01	500	0.95	1480	990
SF10	6	0.630	0.616	14.8	16.01	500	0.95	1702	1150
SF11	6	0.624	0.613	14.8	16.01	500	0.95	2050	1378
SF12	6	0.618	0.611	14.8	16.01	500	0.95	2319	1568

8.2.5. Triaxial Test Results

8.2.5.1. Typical Stress-strain Relation

Deviator stress (q) and mean effective normal stress (p') in triaxial tests were computed using Eq. (8.2.4) and (8.2.5) respectively.

$$q = \sigma'_1 - \sigma'_3 \quad (8.2.4)$$

$$p' = \frac{(\sigma'_1 + 2\sigma'_3)}{3} \quad (8.2.5)$$

Where σ'_1 = effective major principal stress; and σ'_3 = effective minor principal stress. Typical stress-strain behaviour for untreated and FA treated specimens was shown in Fig. 8.13. A contractive strain-softening behaviour can be seen from shearing response (q - p') graph for untreated specimen. The untreated specimen reached the maximum deviator stress (q) of 417 kPa at axial strain of 1.3% and showed a complete liquefaction when reached 18% axial strain. In contrast, the specimens containing FA showed a dilative response. For example, the specimen containing 2% FA (i.e., SF1) had a peak deviator stress of 507 kPa at 1.2% axial strain and reached 1021 kPa deviator stress at 25% axial strain. Similarly, the specimens containing 4% and 6% FA (i.e., SF5 and SF9) showed a dilative response. They reached the maximum deviator stress of 573 and 627 kPa at axial strain of 1.1% and 1.3%. The deviator stress in SF5 and SF9 increased to 1174 and 1480 kPa at 25% of axial strain. The acquired results in this section indicate that increasing the FA contents caused a change in shearing response of the soil from contractive strain-softening to dilative. Also, the results showed that in FA treated specimens increasing the duration of the testing until 25% of axial strain caused an increase for deviator stress, whereas, the deviator stress reached zero by increasing the duration of the test.

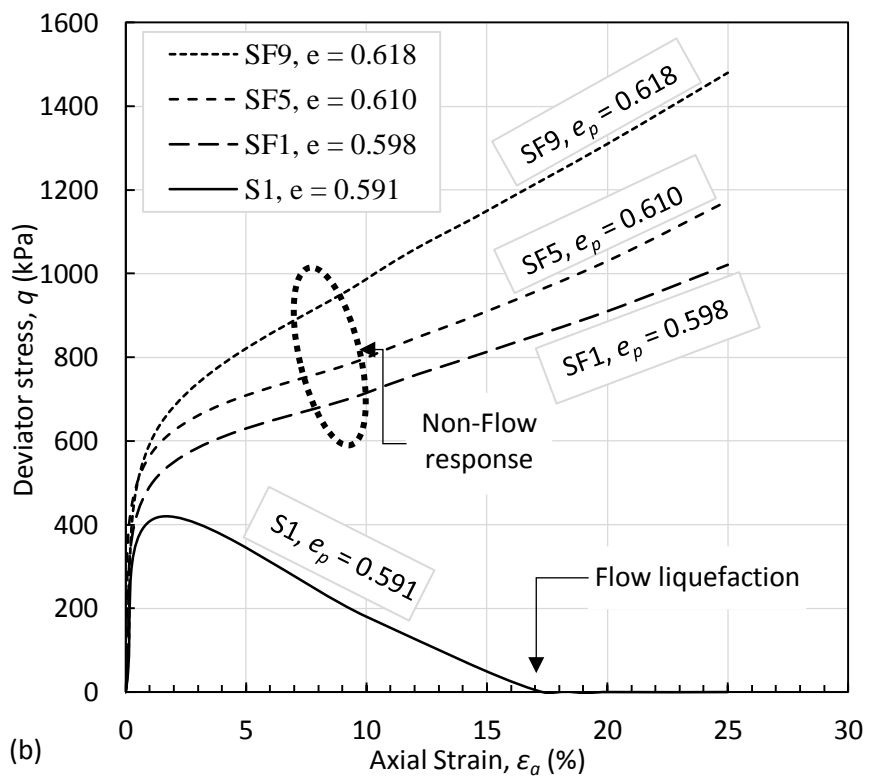
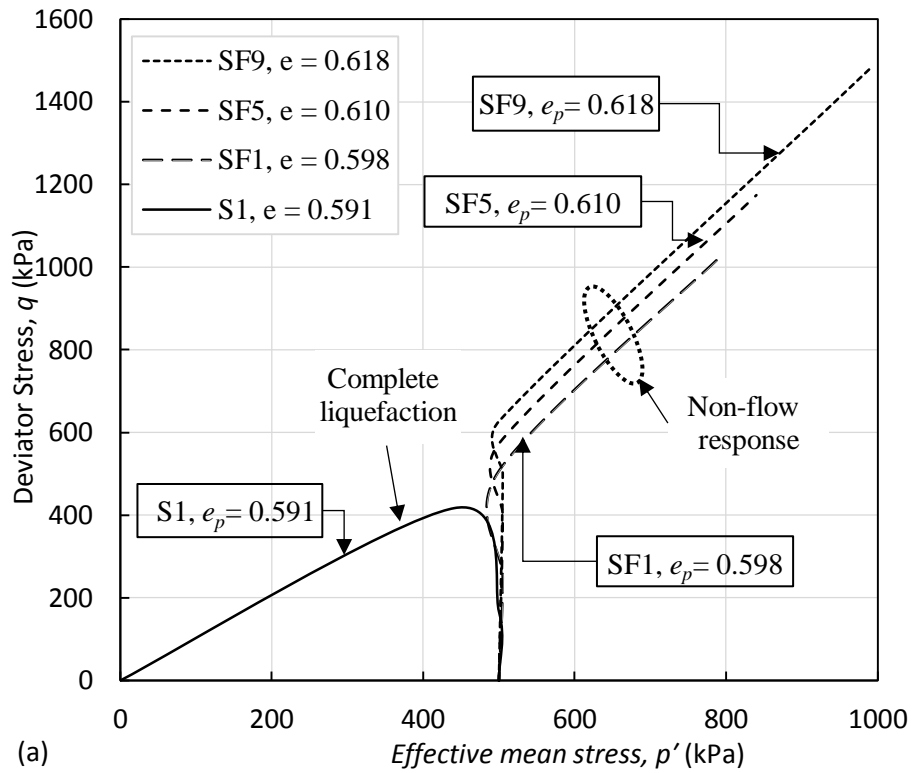


Fig. 8.13. Undrained shear behaviour of untreated and FA treated specimens under 500 kPa initial mean effective stress (a) stress path (q - p'); (b) stress-strain relation.

8.2.5.2. Critical State Locus in e_p - $\log p'$ Plane

To compute the critical state parameters of the soils Eq. (8.2.6) were introduced by Schofield and Wroth (1968);

$$\Gamma_{cs} = v + \lambda_{cs} \ln p' \quad (8.2.6)$$

Where Γ_{cs} = value for v when $p' = 1$ kPa on the critical state line; v = specific volume, which is equal to void ratio (e) plus 1.0; λ_{cs} = slope line in the space of specific volume versus logarithm of the mean effective stress; and p' = mean effective normal stress in triaxial condition. The shearing responses of the untreated and FA treated specimens were analysed in e - $\log p'$ plane, and the acquired critical state locus have been compared. The variations of the post-consolidation void ratio values versus logarithm initial effective stress (p') was shown in Fig. 8.14. It is seen from the figure that by increasing the FA contents, the locus has an upward tendency. For instance, the untreated specimens have a post-consolidation void ratio (e_p) in the range of $0.575 \leq e_p \leq 0.587$ and mean effective stress in the range of $387 \leq p' \leq 876$ kPa. Whereas, the post-consolidation void ratio for 2% FA treated specimens increased to $0.588 \leq e_p \leq 0.598$ at mean effective stress in the range of $840 \leq p' \leq 1456$ kPa. For 4% and 6% FA treated specimens, the void ratio range values even increased more and were in the range of $0.601 \leq e_p \leq 0.61$ and $0.611 \leq e_p \leq 0.618$ respectively. Similarly, mean effective stress increased to the range of $840 \leq p' \leq 1456$ and $990 \leq p' \leq 1568$ kPa respectively. Based on the acquired critical state locus in e_p - $\log p'$ plane, the critical state slope (λ_{cs}) and intercept (Γ_{cs}) were computed and were presented based on the FA contents in Fig. 14. As shown, by increasing the FA contents of the soil structure the slope and intercept of the critical state locus. These reductions were in the

range of $8.33 \times 10^{-5} \leq \lambda_{cs} \leq 8.91 \times 10^{-5}$ and $0.617 \leq \Gamma_{cs} \leq 0.661$ for critical state slope and intercept respectively.

Figs. 8.15(a) and (b) show the computed critical state slope (λ_{cs}) and intercept (Γ_{cs}) acquired from the e_p - $\log p'$ plane. As can be seen, by increasing the FA contents of the soil matrix the slope and intercept of the critical state locus decreased. These reductions were in the range of $1.21 \times 10^{-5} \leq \lambda_{cs} \leq 2.45 \times 10^{-5}$ and $0.596 \leq \Gamma_{cs} \leq 0.63$ for critical state slope and intercept respectively.

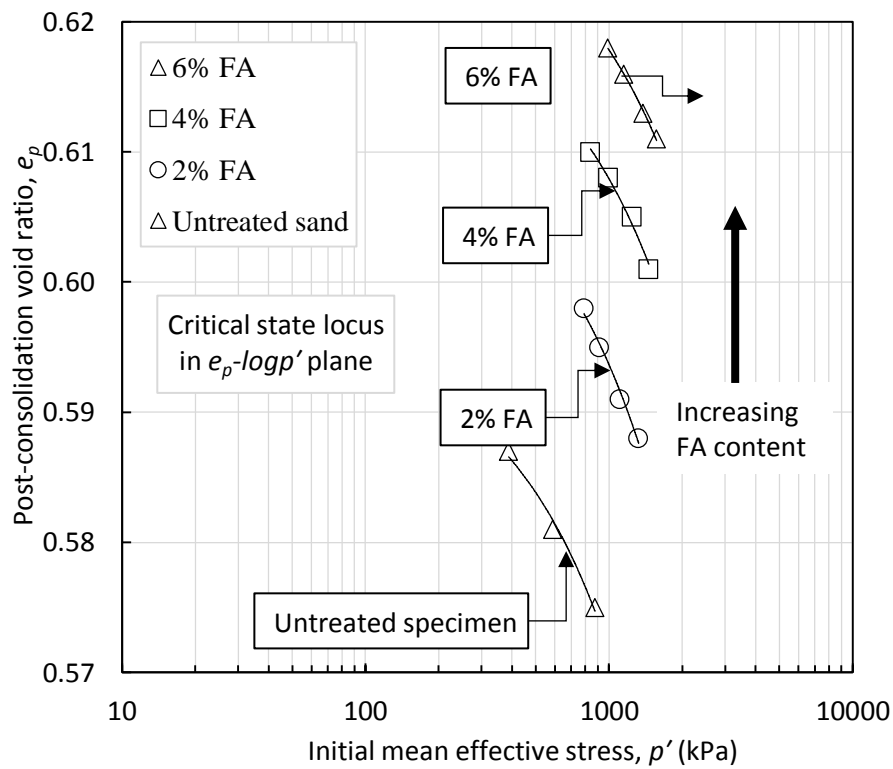


Fig. 14. Critical state locus in e - $\log p'$ plane for untreated and FA treated soil

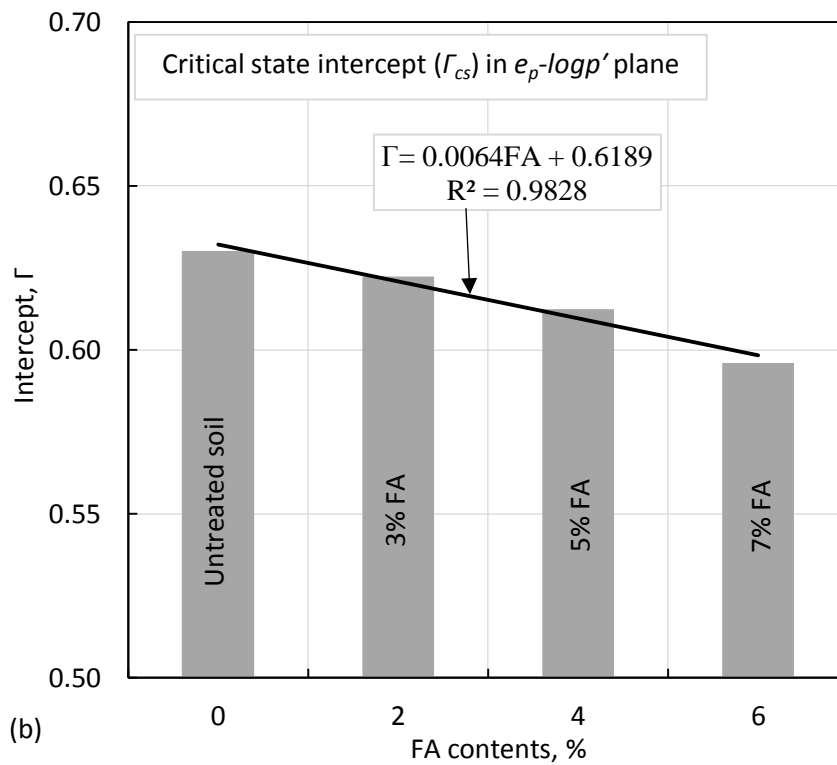
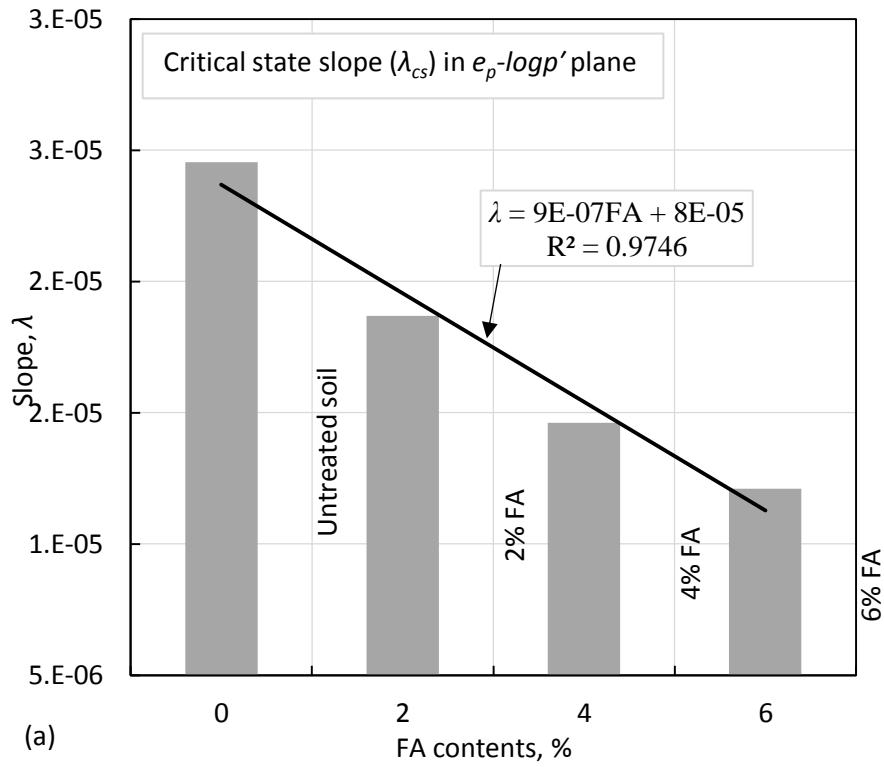


Fig. 8.15. Effect of FA contents on (a) critical state slope (λ_{cs}) in e_p - $\log p'$ plane; (b) critical state intercept (Γ_{cs}) in e_p - $\log p'$ plane.

8.2.5.3. Critical State Locus in q - p' Plane

The critical state parameters in $q - p'$ plane can be computed using Eq. (8.2.7) (Schofield and Wroth 1968);

$$q = M_{cs} p' \quad (8.2.7)$$

Where q = deviatoric stress in triaxial condition; p' = mean effective normal stress in triaxial condition; M_{cs} = factor for internal friction of the critical state line in the $q - p'$ plane and computed using Eq. (8.2.8);

$$M = \frac{(6 \sin \phi_{cs})}{3 - \sin \phi_{cs}} \quad (8.2.8)$$

Where ϕ_{cs} = critical frictional angle of the soil. The acquired shearing behaviours and critical state locus were analysed and compared on the q - p' plane for untreated and FA treated specimens and the results were presented in Fig. 8.16. As can be seen, increasing the FA contents of the specimens increased the critical friction angle (ϕ_{cs}). For instance, the untreated specimen had a critical friction angle of 29.18° , whereas, this value for 2%, 4%, and 6% FA treated specimens increased to 32.46° , 34.31° , and 35.76° respectively. Fig. 8.17 shows the variation of the critical friction angle with FA contents. Table 8.4 shows the characteristics of the untreated and FA treated specimens in q - p' plane. The M_{cs} showed an increase by increasing the FA contents. For instance, the untreated specimen has a critical state constant value of 1.164, whereas, addition of 2%, 4%, and 6%, caused an increase to 1.307, 1.388, and 1.452 respectively.

Table 8.4. Effect of FA on critical frictional angle and slope factor

Specimen	FA content (%)	M_{cs}	ϕ_{cs} (degree)
Untreated specimen	-	1.164	29.18
2FA	2	1.307	32.46
4FA	4	1.388	34.31
6FA	6	1.452	35.76

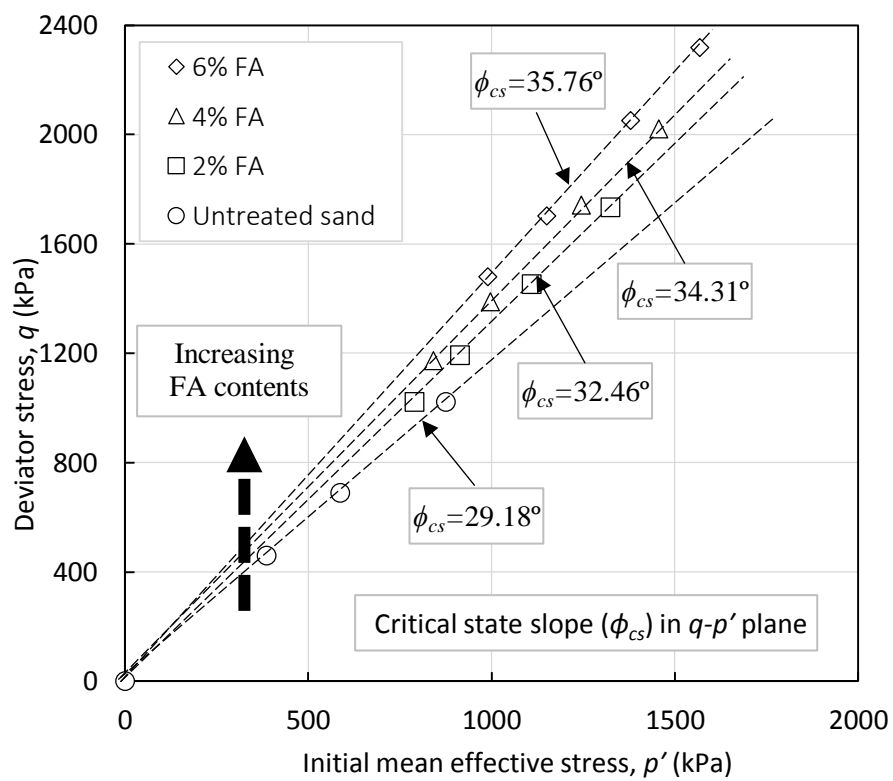


Fig. 8.16. Critical state locus in q - p' plane for untreated and FA treated specimens

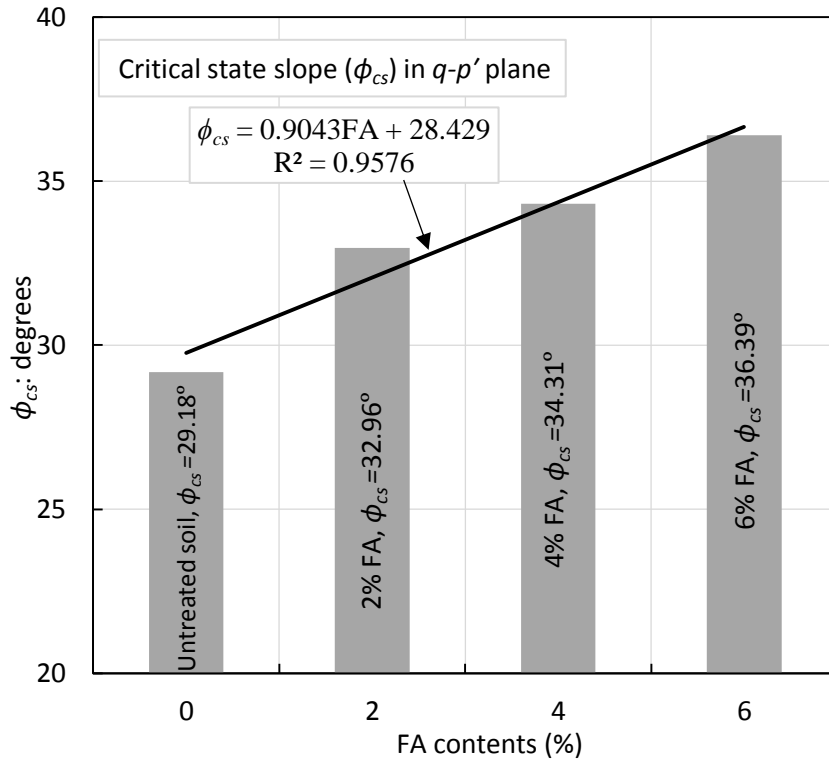


Fig. 8.17. Variation of the critical state frictional angle (ϕ_{cs}) versus FA contents

8.2.5.4. Flow Liquefaction

The liquefaction inception of the soil is known by the critical stress ratio (q/p') at the undrained instability state using flow liquefaction line (Kramer 1996). Fig. 8.18 shows the variation in the critical stress ratio versus post-consolidation void ratio under 500 kPa initial mean effective stress. As can be seen, by increasing the FA contents in the specimens the acquired locus is inclined to the right. This behaviour indicates that the liquefaction inception is less pronounced in a specimen containing a greater amount of FA. Fig. 8.19 shows the typical brittleness index (I_B) for untreated and FA treated specimens. In general, the I_B has a range value between zero to one. A brittleness index equal to one highlights a very brittle behaviour associated with a low deviator stress (q_{min}), whereas for a brittleness index equal to zero indicates a non-brittle or strain-hardening behaviour without any reduction in deviatoric stress (q) during undrained

shearing (Sadrekarimi 2014). As shown in Fig. 8.11, the untreated specimen shows a brittle or strain-softening behaviour and its undrained post-liquefaction deviator stress reached zero (q_{min}) whereas, in FA treated specimens a strain-hardening behaviour was recorded after peak deviator stress for undrained post-consolidation strength and the liquefaction did not happen.

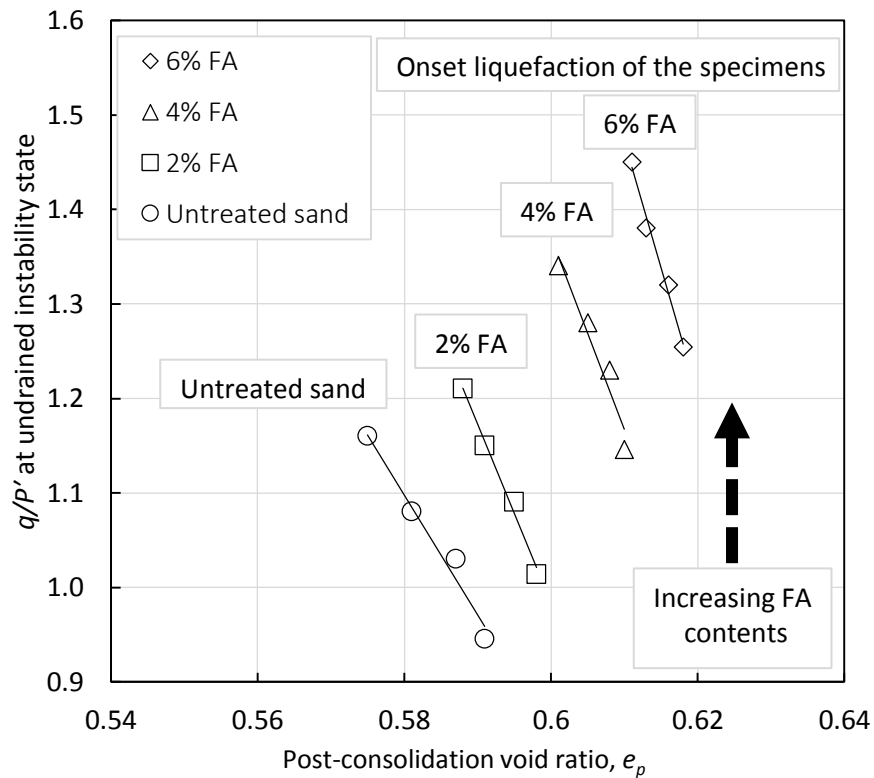


Fig. 8.18. Variation of the stress ratio (q/p') versus void ratio for untreated and FA treated specimens

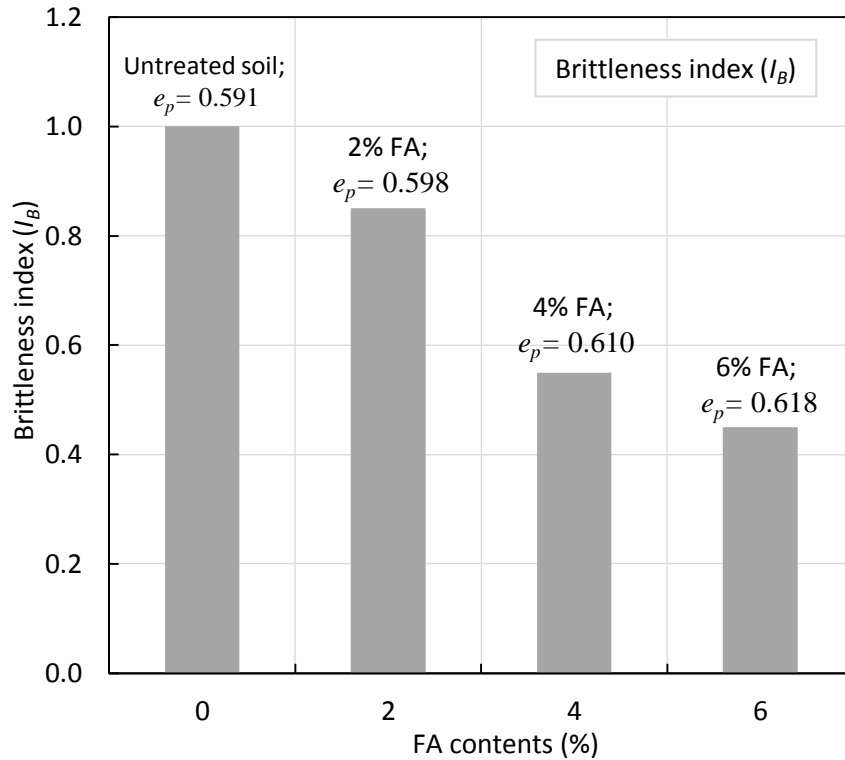


Fig. 8.19. Typical brittleness index (I_B) for untreated and FA treated specimens.

8.2.6. Conclusions

This study conducted a brief analysis on the critical state parameters and flow liquefaction of the fly ash (FA) treated soil by performing a series of monotonic triaxial compression tests. The results showed that increasing the FA contents caused an increase for the locus in e_p - $\log p'$ plane, and a reduction in critical state slope (λ_{cs}) and intercept (Γ_{cs}). The analysis on critical state locus in q - p' space showed that increasing the FA contents increased the critical friction angle (ϕ_{cs}) and factor of slope (M_{cs}). The analysis on flow liquefaction of the FA treated specimens at instability state showed that the FA treated specimens have a lower tendency for liquefaction when contribution of the FA increased in the specimens. Investigation on brittleness index (I_B) of the specimens showed that the specimens containing FA have a strain-hardening behaviour, and a low value of brittleness, whereas, the untreated specimen have a

strain-softening response and a very brittle behaviour which led to a I_B value of one, indicating complete liquefaction.

8.3. CHAPTER CONCLUSIONS

The constitutive modelling of the treated soils helps to approximate the soil response under external stimuli using acquired correlations. In this chapter, a series of investigations were conducted based on the critical state of the soil mechanics (CSSM) to investigate the soil behaviour when treated with fly ash (FA) and ground granulated blast furnace slag (GGBFS). Furthermore, the investigations conducted on the role of particle shape to understand their effect in forming the soil response. Three types of soils consisting of natural sand (NS), crushed sand (CS) and mixed sand (MS) (50% crushed + 50% natural) were used and the results were analysed. The analysis on $e-p'$ plane showed that by increasing the values of soil shape descriptors (i.e., roundness, sphericity and regularity), the acquired curves dropped, and the strength decreased and the critical friction angle of 28.30° , 31.61° , and 34.06° for NS, MS, and CS. The results in this section indicate that by increasing the particle shape descriptors values of the specimens the critical friction angle increased.

Analysis on the critical state parameters of the fly ash (FA) treated soil showed that increasing the FA contents caused an increase for the locus in $e_p\text{-log}p'$ plane, and a reduction in critical state slope (λ_{cs}) and intercept (Γ_{cs}). The analysis on critical state locus in $q-p'$ space showed that increasing the FA contents increased the critical friction angle (ϕ_{cs}) and factor of slope (M_{cs}). The analysis on flow liquefaction of the FA treated specimens at instability state showed that the FA treated specimens have a lower tendency for liquefaction when contribution of the FA increased in the specimens.

The investigation of the effect of GGBFS on $e\text{-log}p'$ plane based on the critical state of soil mechanics (CSSM) framework showed that by increasing the GGBFS contribution in the soil structure, the acquired curves increased. Investigation on

critical state locus in $q-p'$ plane showed that the tested specimens have a critical friction angle of 28.81° , 30.77° , 32.36° , and 35.34 for untreated, 3%, 5%, and 7% GGBFS treated specimens. The results in this section show that by increasing the GGBFS contents of the specimens the critical friction angle (λ_{cs}) and intercept (Γ_{cs}) are increased.

Chapter 9

Conclusions and Recommendations

9. Conclusions

This study investigated the effect of ground granular blast furnace slag (GGBFS) and fly ash (FA) on liquefaction behaviour of the sand by performing a comprehensive series of experimental investigations. The GGBFS is an abundant environmental-friendly by-product, which is remained from steel manufacturing process. This chemical additive has a hydration and pozzolanic characteristics similar to the Portland cement (PC) and lime, which encourage the practitioners to apply that in their ground improvement projects. The FA is also an environmental-friendly chemical additive, which is remained from electricity power station. Similarly, this additive has a hydration and pozzolanic characteristics to the traditional chemical agents.

In the first stage of the study, a comprehensive series of preliminary experimental analysis conducted on three types of the ground improvement additives (i.e., reinforcement, traditional, and environmentally friendly additives) to evaluate their performance and to select the most effective materials, and to follow the main part of the experimental studies based on the selected material. Since the chemical additives can have a full hydration and pozzolanic reactions in clayey soils, the preliminary experimental analysis conducted on two types of clayey soils.

There are a wide range of studies investigated the effect of reinforcement materials such as fibre to improve the mechanical behaviour of the soil, however, less studies investigated the effect of the sawdust and the recycled tyre on improvement of the mechanical behaviour of the soil. Hence, two recent materials were considered as the representative materials for reinforcement techniques to investigate the 1-D consolidation and the hydraulic conductivity of the soil. The results showed that the recycled tyre is not effective to reduce the compressibility and hydraulic conductivity of the soil and the sawdust is relatively effective.

The second series of preliminary experimental analysis conducted on lime as the representative for the traditional binders by performing a series of volumetric shrinkage, unconfined compressive strength (UCS), and the ring shear tests. The results showed that however, the addition of lime is effective to improve the mechanical properties of the soil, its application accompanies with some deficiencies such as cracking and fully or partially replacement of that with GGBFS is effective to address this issue. The GGBFS was selected as the representative for the environmental-friendly admixtures by performing a series of direct shear tests on GGBFS added soil. The analysis showed that the application of GGBFS is effective to increase the shear strength of the soil.

According to the acquired results from preliminary experimental results the GGBFS was selected to continue the main part of the experimental analysis. Furthermore, fly ash (FA) was selected as another environmental-friendly chemical additive to conduct the liquefaction analysis for confirmation of the results. In the next stage of analysis, a series of monotonic, cyclic, and post-cyclic experimental tests conducted to investigate the effect of the recent environmental friendly agents on liquefaction behaviour of the soil. The following section provide a summary of the acquired results.

9.1. Monotonic behaviour

The effect of FA on the monotonic liquefaction of sand were investigated by performing a series of undrained monotonic triaxial compression tests in one part in Chapter 5. The analysis conducted to investigate the effect of FA contents, initial relative density, initial mean effective stress, and curing time. No study performed to investigate the effect of GGBFS on monotonic liquefaction of sand since this study already has been conducted by Sabbar et al. (2017). In this chapter the effect of four

FA contents (i.e., 0, 2, 4, and 6%), three initial mean effective stresses (i.e., 50, 70, and 90%), and three initial relative densities (i.e., 20, 40, and 60%) were investigated. Furthermore, the effect of two curing periods of 14 and 28 days were evaluated on selected specimens.

The investigation of the effect of FA contents showed that while the control specimen has an ultimate deviatoric stress of 74 kPa, addition of FA caused ultimate deviatoric stress values of 81, 89, and 100 kPa when 2%, 4%, and 6% FA added into specimens respectively. This behavior was attributed to the filled existing micro pores amongst soil particles by FA which reduced the pore water pressure build-up.

The investigation of the effect of initial mean effective stress showed that the FA added specimens tested under a greater initial mean effective stress have a lower ultimate deviatoric strength value. For instance, an ultimate deviatoric stress of 81, 75, and 64 kPa was recorded when the tests conducted under 50, 70, and 90 kPa initial mean effective stress respectively. This was attributed to the suppression of dilatancy and consistent with critical state of soil.

The results showed that the densification is more effective in FA added specimens as these specimens showed a greater q_u value in all relative densities than the untreated soil. For instance, an ultimate deviatoric strength of 81, 115, and 161 kPa when the 2% FA treated specimens tested with an initial relative density of 20, 40, and 60% respectively.

The investigation of the effect of curing time on FA added specimens showed that the specimens with a greater curing period have a greater ultimate deviatoric strength. For instance, while 2% FA treated specimen showed an ultimate deviatoric strength of 81

kPa. Curing the specimens for 14 and 28 days caused an ultimate deviatoric strength of 96 and 108 kPa respectively.

9.2. Cyclic Behaviour

The effect of FA and GGBFS on cyclic liquefaction strength of sand were investigated by performing a series of stress-controlled undrained cyclic triaxial tests in two parts in Chapter 6. In the first part, the effect of FA contents, initial relative density, effective confining pressure, and curing time on cyclic liquefaction resistance of the soil has been investigated and the results have been analysed. In the second part, the effect of different parameters such as GGBFS contents, initial relative density, effective confining pressure, and curing time on cyclic liquefaction strength of the soil have been investigated and the results were presented and analysed.

9.2.1. Effect of FA on Cyclic Liquefaction

A series of cyclic triaxial tests have been performed to investigate the effect of fly ash (FA) on the liquefaction strength of sand. The effect of relative density, FA content, effective confining pressure and curing time have been compared and presented. To investigate the effect of relative density, two types of specimens, including untreated soil and sand mixed with 2% FA with 0.2 CSR under 50 kPa effective confining pressure with relative density of 20%, 40%, 60% and 80%, have been tested. The results suggested that specimens of sand mixed with 2% FA with 80% relative density have the most resistance for liquefaction in comparison with other relative densities. In continuing to determine the effect of FA content, a series of cyclic triaxial tests for the specimens mixed with 4% and 6% FA were conducted under 50, 70 and 90 kPa

effective confining pressure with 20% relative density and 0.2 CSR. The results suggested that specimens with a higher FA content have a lower tendency to be liquefied. In the last stage of the study, effect of the effective confining pressure and curing time was studied. The results showed that the specimens of sand mixed with 2% FA liquefied earlier under higher effective confining pressures. Furthermore, to investigate the effect of curing time, two specimens with 2% FA content were cured for 14 and 28 days and tested under 50 kPa effective confining pressure and 20% relative density. The results were then compared with an instantly tested specimen in a cyclic stress ratio (CSR) versus number to liquefaction (N_L) graph. Results showed that an increase in curing time led to an increase in liquefaction resistance.

9.2.2. Effect of GGBFS on Cyclic Liquefaction

The investigations on effect of GGBFS on cyclic liquefaction strength of soil showed that the addition of 3, 5, and 7% GGBFS in the specimens caused an increase for the liquefaction resistance and improved in the range of $9.7\% \leq IMP \leq 16.5\%$, $18.3\% \leq IMP \leq 22.6\%$, and $22.9\% \leq IMP \leq 38.3\%$ respectively. In addition, the investigations showed that the effective confining pressure has an opposite behaviour with liquefaction resistance of the GGBFS treated soil, and the specimens under greater effective confining pressures showed a lower value of the cyclic strength. The analysis showed that increasing the relative density of the GGBFS treated specimens, increased the liquefaction resistance of the specimens. A comparison between N_L values of untreated specimens and GGBFS treated specimens at different relative densities showed that the GGBFS treated specimens have a greater liquefaction resistance in all cases. For instance, the specimens treated with 5% GGBFS liquefied at the cycle numbers of 221, 207, and 189 at the relative density of 40%, 60%, and 80%, whereas

the untreated specimens have N_L values of 204, 187, and 175 at the same relative densities.

Finally, the investigations on the effect of curing time on cyclic strength of the GGBFS treated specimens showed that the specimens after 28 days and 14 day curing time have a greater N_L values in comparison with 7 days treated specimens. The results showed that an improvement in the range of $18.3\% \leq IMP \leq 22.6\%$, $27.4\% \leq IMP \leq 41.7\%$, and $34.9\% \leq IMP \leq 52.2\%$ after 7, 14, and 28 days curing period were recorded.

9.3. Post-cyclic Behaviour

The main failures in geotechnical structures such as embankments, dams, and slopes happen up to 24 hours after an actual seismic event. Therefore, strength analysis of the soil after a seismic event such as earthquake is of great importance. Beside of the seismic characteristics, the soil characteristics such as relative density, and the external loads are crucial parameters to analyse the post-cyclic behaviour of the soil. Chapter 7 investigated the effect of FA and GGBFS on post-cyclic behaviour of sand in two parts.

9.3.1. Effect of FA on Post-cyclic Behaviour

The effect of FA on post-cyclic strength of sand investigated by performing a series of undrained post cyclic monotonic triaxial compression tests. The effect of four different FA contents (i.e., 0, 2, 4, and 6% on the basis of dry mass), three initial relative densities (i.e., 20, 40, and 60%), and three effective confining pressures (i.e., 50, 70, and 90 kPa) on post-cyclic behaviour of the soil were investigated. The cyclic loads applied on the specimens until they reached the desired pore water pressure ratios of 0.25, 0.50, and 0.75.

The investigation of the effect of FA contents on post-cyclic behaviour of the soil showed that increasing FA contents increased the ultimate deviatoric stress of the specimens in all tested pore water pressure ratios after cyclic loadings. As an example, while untreated sand has an ultimate deviatoric stress value of 74, 60, 44, and 28 kPa at pore water pressure ratios of 0, 0.25, 0.50, and 0.75, treatment of the specimens with 2% FA caused ultimate deviatoric stress values of 81, 72, 60, and 46 kPa at the same pore water pressure ratios.

In continue, the results showed that the ultimate deviatoric stress of the specimens in the post-cyclic phase reduced when the post-cyclic tests initiated at a greater pore water pressure ratio after cyclic loadings. This behaviour was attributed to greater cycle numbers that applied on the specimens and provided a more metastable soil structure.

The investigation of the effect of relative density showed that increasing the pre-consolidation relative density from 20% to 40 and 60% of the specimens increased the ultimate deviatoric stress. This increase was less prone in untreated soil and more apparent in FA treated specimens. For instance, the ultimate deviatoric stress value of

2% FA treated specimen at 20% relative density was 81, 74, 61, and 55 kPa at 0, 0.25, 0.50, and 0.75 pore water pressure ratios, while increasing the relative density to 40% caused an ultimate deviatoric stress value of 115, 102, 80, and 68 kPa at the same pore water pressure ratios.

The Investigations showed that increasing the initial mean effective stress from 50 kPa to 70 and 90 kPa reduced the ultimate deviatoric stress of FA treated specimens. For instance, the ultimate deviatoric stress at a pore water pressure ratio of zero was 81, 73, and 64 when the tests conducted under an effective confining pressure of 50, 70, and 90 kPa. Increasing the pore water pressure ratio to 0.25 causes an ultimate deviatoric stress of 74, 65, and 57 kPa for the effective confining pressure of 50, 70, and 90 kPa. This behaviour was attributed to suppression of dilatancy of soil which is consistent with critical state of soil and literature.

9.3.2. Effect of GGBFS on Post-cyclic Behaviour

The effect of GGBFS on the post-cyclic behaviour of soil investigated by performing a series of undrained post-cyclic monotonic triaxial compression tests. The effect of four GGBFS contents (0, 3, 5, and 7% on the basis of dry mass), and three initial mean effective stresses (i.e., 100, 200, and 400 kPa), were investigated. To conduct the post-cyclic tests, the cyclic loadings were applied on the specimens with initial relative densities of 40% or 60% until pore water pressure ratios of 0.25, 0.50, or 0.75, then the specimens were monotonically sheared.

The investigations of the effect of GGBFS contents on the post-cyclic behaviour of the soil showed that increasing the GGBFS contents improved the ultimate deviatoric strength of the soil. For example, at a pore water pressure ratio of 0.25, the untreated soil had an ultimate deviatoric stress of 171 kPa while addition of GGBFS (i.e., 3%-

7%) caused an increase for ultimate deviatoric stress in the range of $192 \leq q_u \leq 228$ kPa. In a similar trend, when the tests conducted after a pore water pressure ratio of 0.50 and 0.75 an ultimate deviatoric stress of 153 and 89 kPa was recorded for the untreated soil respectively. Whereas, the addition of GGBFS caused an ultimate deviatoric stress of $185 \leq q_u \leq 215$ kPa and $108 \leq q_u \leq 151$ kPa after pore water pressure ratios of 0.50 and 0.75 respectively. This behaviour was attributed to dissipation of pore water pressure in GGBFS treated specimens due to the presence of the GGBFS and filling of the micro pores. The post-cyclic test results also showed that the ultimate deviatoric strength for untreated soil and GGBFS treated specimens at a greater pore water pressure ratio is lower than the specimens tested at a lower pore water pressure ratio. This behaviour was attributed to the greater number of cyclic loadings applied on the specimens at a greater pore water pressure ratio which generate a less stable structure for the specimens.

The results showed that increasing the initial mean effective stress in GGBFS treated specimens reduced the ultimate deviatoric strength. This behaviour was attributed to the soil suppression of dilatancy which is consistent with the critical state of soil and literature. As an example, for a pore water pressure ratio of 0.25, the test conducted under 100 kPa had an ultimate deviatoric stress of 225 kPa, whereas this value reduced to 214 and 185 kPa when the tests were conducted under 200 and 400 kPa respectively.

The results showed that the densification of the GGBFS treated specimens caused the generation of a greater ultimate deviatoric strength than the untreated soil. As an example, for untreated specimens prepared at 40% initial relative density, ultimate deviatoric stress of 148, 127, and 59 kPa were recorded when the tests were conducted after pore water pressure ratios of 0.25, 0.50, and 0.75 respectively, and the initial relative density to 60% caused an ultimate deviatoric strength of 171, 153, and 89 kPa.

This behaviour was attributed to an increase in interlocking forces and filling of the voids which dissipate the generation of pore water pressure. The GGBFS fills the remaining micro pores and makes the generation of pore water pressure even harder.

9.4. Constitutive Modelling

The constitutive analysis based on the critical state of soil mechanics (CSSM) conducted on base soil and sand-FA mixture by performing a series of undrained monotonic triaxial compression tests in two parts in Chapter 8. The constitutive analysis provided relations, which approximate the soil response to the particle characteristics and the FA based on the framework introduced in critical state of soil mechanics (CSSM). In the first part, the correlations were presented based on the roundness (R), sphericity (S), and regularity (ρ) for three types of the natural, crushed and mixed soils. In the second part, the critical state locus of the untreated sand and sand-FA mixtures were approximated in different planes and the correlations presented.

9.4.1. Effect of Particle Shape on Monotonic Behaviour

Part one investigated the effect of particle shape on monotonic liquefaction of the sand by performing a series of the static triaxial compression tests. The tests conducted on three types of natural sand (NS), crushed sand (CS), and mixed sand (MS) (i.e. 50% natural sand + 50% crushed sand). The results showed that the CS and MS specimens had a strong dilative shearing response while the NS showed a contrastive strain-softening behaviour.

The interpreted results in $e-p'$ plane based on critical stress state framework showed that by increasing the values of soil shape descriptors (i.e., roundness, sphericity and regularity), the acquired curves dropped and the strength decreased. Investigation on critical state locus in $q-p'$ plane showed that the tested specimens have a critical friction angle of 28.30° , 31.61° , and 34.06° for NS, MS, and CS. The results in this section indicated that by increasing the particle shape descriptors values of the specimens the critical friction angle increased.

Investigations on undrained instability state of the specimens on the variation of the critical stress ratio (q/p') versus post-consolidation void ratio showed that by decreasing the crushed grains contributions, the soil intended to be liquefied earlier. For instance, a critical stress ratio in the range of $0.95 \leq q/p' \leq 1.27$, $0.75 \leq q/p' \leq 1.1$, and $0.98 \leq q/p' \leq 1.03$ corresponding to the post-consolidation void ratio in the range of $0.85 \leq e \leq 0.918$, $0.853 \leq e \leq 0.92$, and $0.793 \leq e \leq 0.873$ was recorded for natural mixed and crushed soil particles respectively.

However, in this study, 15 triaxial compression tests were conducted on three types of soils (i.e., NS, CS, and MS), which caused the generation of three points with a high value of R^2 in particle descriptor graphs. It is recommended that more tests be conducted in future studies to have a clear understanding about the effects of particle descriptors on the critical state of soil.

9.4.2. Effect of FA on Monotonic Behaviour

Part 2 conducted a series of analysis on the critical state parameters and flow liquefaction of the FA added soil by performing a series of monotonic triaxial compression tests. The results showed that increasing the FA contents caused an increase for the locus in e_p - $\log p'$ plane, and a reduction in critical state slope (λ_{cs}) and intercept (Γ_{cs}). As an example, the untreated specimens have a post-consolidation void ratio (e_p) in the range of $0.575 \leq e_p \leq 0.587$ and mean effective stress in the range of $387 \leq p' \leq 876$ kPa. Whereas, the post-consolidation void ratio for 2% FA treated specimens increased to $0.588 \leq e_p \leq 0.598$ at mean effective stress in the range of $840 \leq p' \leq 1456$ kPa. For 4% and 6% FA treated specimens, the void ratio range values even increased more and were in the range of $0.601 \leq e_p \leq 0.61$ and $0.611 \leq e_p \leq 0.618$ respectively.

The analysis on critical state locus in q - p' space showed that increasing the FA contents increased the critical friction angle (ϕ_{cs}) and factor of slope (M_{cs}). For instance, the untreated specimen had a critical friction angle of 29.18° , whereas, this value for 2%, 4%, and 6% FA treated specimens increased to 32.46° , 34.31° , and 35.76° respectively.

The analysis on flow liquefaction of the FA treated specimens at instability state showed that the FA treated specimens have a lower tendency for liquefaction when contribution of the FA increased in the specimens. Investigation on brittleness index (I_B) of the specimens showed that the specimens containing FA have a strain-hardening behaviour, and a low value of brittleness, whereas, the untreated specimen have a strain-softening response and a very brittle behaviour which led to a I_B value of one, indicating complete liquefaction.

9.5. Recommendations for Future Studies

In this study, a series of experimental analysis conducted to investigate the effect of FA and GGBFS on monotonic, cyclic, and post-cyclic behaviour of sand. The analysis conducted on different parameters such as additive contents, initial relative density, effective confining pressure, and curing time. The results indicated that the FA and GGBFS are effective to improve the strength characteristics of sand against liquefaction. The FA and GGBFS are abundant, cost-effective, by-products additives, which are remained from electrical plant and steel manufacturing process respectively. Furthermore, application of these materials causes less carbon foot print in the environment. Hence, their application in improvement of the soil strength against liquefaction and seismic events are highly recommended. In addition, following recommendations are suggested for the future studies;

- Along with the technology advancements in the world, new by-product materials are producing. It is suggested that this new technology and by-product materials to be identified and effect of newly produced materials to be tested and reported;
- This study was focused from a technical point of view to investigate effect of by-product materials in improvement of the soil behaviour. It is suggested that a study to be conducted to investigate from a cost effectiveness point of view;
- Testing the effect of by-product materials on soil liquefaction behaviour using physical models and advanced experimental instruments such as centrifuge modelling and shaking tables is recommended as a continuation to this study;

- The effect of different sample preparation methods as a critical function in forming liquefaction soil behaviour is recommended to be investigated as a continuation for this study

References

- Adalier, K., and Elgamal, A. (2004). "Mitigation of liquefaction and associated ground deformations by stone columns." *Engineering Geology*, 72(3), 275-291.
- Aldaef, A. A. and Rayhani, M. T. (2014). "Hydraulic performance of Compacted Clay Liners (CCLs) under combined temperature and leachate exposures." *Waste management*, 34(12), 2548-2560.
- Aldood, A., M. Bouasker, and M. Al-Mukhtar, *Impact of wetting–drying cycles on the microstructure and mechanical properties of lime-stabilized gypseous soils*. *Engineering Geology*, 2014a. 174: p. 11-21.
- Al-Malack, M. H., Abdullah, G. M., Al-Amoudi, O. S. B., and Bukhari, A. A. (2016). "Stabilization of indigenous Saudi Arabian soils using fuel oil flyash." *Journal of King Saud University-Engineering Sciences*, 28(2), 165-173.
- Al-Mukhtar, M., Khattab, S., and Alcover, J.F. (2012). "Microstructure and geotechnical properties of lime-treated expansive clayey soil." *Engineering Geology* 139: 17-27.
- Altuhafi, F. N., Coop, M. R. and Georgiannou, V. N. (2016). "Effect of Particle Shape on the Mechanical Behavior of Natural Sands." *Journal of Geotechnical and Geoenvironmental Engineering*, 142(12), p.04016071.
- Anayi, J., Boyce, J., and Rogers, C. (1989). "Modified Bromhead ring shear apparatus." *Geotechnical Testing Journal* 12(2): 171-173, <http://dx.doi.org/10.1520/GTJ10694J>. ISSN 0149-6115.
- Arabi, M. and Wild, S. (1989). "Property changes induced in clay soils when using lime stabilization." *Proceedings of the Institution of Civil Engineers, Municipal Engineer* 6(2): 85–99.

- Asghari, E., Toll, D. G. and Haeri, S. M. (2003). "Triaxial behaviour of a cemented gravely sand, Tehran alluvium." *Geotechnical & Geological Engineering*, 21(1), pp.1-28.
- Ashour, M., Norris, G., and Nguyen, T. (2009). "Assessment of the undrained response of sands under limited and complete liquefaction." *Journal of geotechnical and geoenvironmental engineering*, 135(11), 1772-1776.
- Askarani, K. and Pakbaz, M. (2016). "Drained Shear Strength of Over-Consolidated Compacted Soil-Cement." *Journal of Materials in Civil Engineering*, [10.1061/\(ASCE\)MT.1943-5533.0001510](https://doi.org/10.1061/(ASCE)MT.1943-5533.0001510), 04015207.
- ASTM (1999). "Standard test method for torsional ring shear test to determine drained residual shear strength of cohesive soils." *ASTM D6467*, West Conshohocken, PA.
- ASTM (2007). "Standard method for compressive strength of molded soil-cement cylinders." ASTM, *ASTM D1633*. West Conshohocken, PA.
- ASTM (2011d). "Standard Test Method for Direct Shear Test of Soils Under Consolidated Drained Conditions, *ASTM D3080*, West Conshohocken, PA.
- ASTM (2012a). "Standard Test Methods for Laboratory Compaction Characteristics of Soil Using Standard Effort (12 400 ft-lbf/ft³ (600 kN-m/m³)), *ASTM D698*, West Conshohocken, PA.
- ASTM (2015b). "Standard Test Method for Measurement of Hydraulic Conductivity of Porous Material Using a Rigid-Wall, Compaction-Mold Permeameter," *ASTM D5856*, West Conshohocken, PA.

- ASTM. (2010). “Standard Test Methods for Liquid Limit, Plastic Limit, and Plasticity Index of Soils.” *ASTM D4318*, West Conshohocken, PA.
- ASTM. (2011a). “Standard practice for classification of soils for engineering purposes (unified soil classification system).” *ASTM D2487*, West Conshohocken, PA.
- ASTM. (2011b). “Standard Test Method for Dispersive Characteristics of Clay Soil by Double Hydrometer.” *ASTM D4221*, West Conshohocken, PA.
- ASTM. (2011c). “Standard test methods for one-dimensional consolidation properties of soils using incremental loading.” *ASTM D2435*, West Conshohocken, PA.
- ASTM. (2011e). “Standard test method for consolidated drained triaxial compression test for soils.” *ASTM D7181*, West Conshohocken, PA.
- ASTM. (2012b). “Standard Test Methods for Laboratory Compaction Characteristics of Soil Using Modified Effort (56,000 ft-lbf/ft³ (2,700 kN-m/m³)).” *ASTM D1557*, West Conshohocken, PA.
- ASTM. (2013). “Standard Test Method for Load Controlled Cyclic Triaxial Strength of Soil” *ASTM D5311*, West Conshohocken, PA.
- ASTM. (2014a). “Standard Test Methods for Specific Gravity of Soil Solids by Water Pycnometer”, *ASTM D854*, West Conshohocken, PA.
- ASTM. (2014b). “Standard Test Method for Sieve Analysis of Fine and Coarse Aggregates.” *ASTM C136*, West Conshohocken, PA.
- ASTM. (2015a). “Standard Test Method for Slump of Hydraulic-Cement Concrete.” *ASTM C143*, West Conshohocken, PA.

- Australasian (iron & steel) Slag Association, ASA. (2017). “Ground Granulated Blast Furnace Slag (GGBFS)”. <http://www.asa-inc.org.au/products/ground-granulated-blast-furnace-slag> (Accessed 11/03/2017)
- Azam, A.M., D.A. Cameron, and M. M. Rahman. (2014). “Permanent Strain of Unsaturated Unbound Granular Materials from Construction and Demolition Waste.” *Journal of Materials in Civil Engineering* 27 (3): 04014125.
- Baez, J. I. and Martin, G. R., (1995). “Permeability and shear wave velocity of vibro-replacement stone columns.” Soil Improvement for Earthquake Hazard Mitigation. ASCE Geotechnical Special Publication, vol. 49, pp. 66–81. New York, NY.
- Baumann, V., and Bauer, G. E. A. (1974). The performance of foundations on various soils stabilized by the vibro-compaction method. *Canadian Geotechnical Journal*, 11(4), 509-530.
- Been, K. and Jefferies, M. G. (1985). “A state parameter for sands.” *Geotechnique* 35, No. 2, 99–102, <http://dx.doi.org/10.1680/geot.1985.35.2.99>.
- Been, K., Jefferies, M. G. and Hachey, J. (1991). “Critical state of sands.” *Geotechnique*, 41(3), pp.365-381.
- Bell, F. G. (1996). “Lime stabilization of clay minerals and soils.” *Eng. Geol.* 42 (4), 223–237. [http://dx.doi.org/10.1016/0013-7952\(96\)00028-2](http://dx.doi.org/10.1016/0013-7952(96)00028-2).
- BGC Cement (2013a). “Material safety datasheet for GGBFS”
- BGC Cement. (2013b). “Safety Data Sheet for Portland and Blended Cement”

- Bhalla, G., Kumar, A. and Bansal, A. (2010). "Performance of scrap tire shreds as a potential leachate collection medium." *Geotechnical and Geological Engineering*, 28(5), pp.661-669.
- Bishop, A. W. (1967). "Progressive failure: with special reference to the mechanism causing it." Proceedings of the geotechnical conference, Oslo, Vol. 2, pp. 142–150.
- Bishop, A. W. and Wesley, L. D. (1975). "A hydraulic triaxial apparatus for controlled stress path testing." *Geotechnique* 25, No. 4, 657–670.
- Bohnhoff, G. and Shackelford, C. (2013). "Consolidation Behavior of Polymerized Bentonite-Amended Backfills." *J. Geotech. Geoenviron. Eng.*, 10.1061/(ASCE)GT.1943-5606.0001079, 04013055.
- Boominathan, A. and Hari, S., (2002). "Liquefaction strength of fly ash reinforced with randomly distributed fibers." *Soil Dynamics and Earthquake Engineering*, 22(9), pp.1027-1033.
- Borhani, A. and Fakharian, K. (2016). "Effect of Particle Shape on Dilative Behavior and Stress Path Characteristics of Chamkhaleh Sand in Undrained Triaxial Tests." *International Journal of Civil Engineering*, 14(4), pp.197-208.
- Boulanger, R. W., and Hayden, R. F. (1995). "Aspects of compaction grouting of liquefiable soil." *Journal of geotechnical engineering*, 121(12), 844-855.
- Boulanger, R., Idriss, I., Stewart, D., Hashash, Y., Schmidt, B. (1998). "Drainage capacity of stone columns or gravel drains for mitigating liquefaction." Proc., Geotech. Earthquake Eng. and Soil Dynamics III. ASCE Geotech. Special Publ. No. 75, vol. 1, pp. 678– 690.

- Bravo, M., and de Brito, J. (2012). "Concrete made with used tyre aggregate: durability-related performance." *Journal of Cleaner Production*, 25, 42-50.
- Brooks, R.M. (2009). "Soil stabilization with fly ash and rice husk ash." *International Journal of Research and Reviews in Applied Sciences*, 1(3), pp.209-217.
- Cai, Y., Shi, B., N.g., C. W., and Tang, C. S. (2006). "Effect of polypropylene fibre and lime admixture on engineering properties of clayey soil." *Engineering Geology* 87(3): 230-240.
- Caijun, S. and Day R. L. (1993). "Chemical activation of blended cements made with lime and natural pozzolans." *Cement and Concrete Research* 23(6): 1389–1396.
- Celauro, B., Bevilacqua, A., Bosco, D. L., and Celauro, C. (2012). "Design procedures for soil-lime stabilization for road and railway embankments. Part 1-review of design methods." *Procedia-Social and Behavioral Sciences*, 53, 754-763.
- Civil Engineering World Blogspot, (2018). Access from <https://civil-engg-world.blogspot.com/2012/02/what-are-class-f-fly-ash-and-class-c.html> (access date 27/10/2018)
- Chand, S., Paul, B., and Kumar, M. (2017). "Short-term leaching study of heavy metals from LD slag of important steel industries in Eastern India." *Journal of Material Cycles and Waste Management*, 19(2), 851-862.
- Chegenizadeh, A. (2012). *Experimental approach to investigate reinforced clay*. (Doctoral dissertation, Curtin University).

- Chegenizadeh, A., M. Keramatikerman, S. Panizza, and H. Nikraz. (2017). "Effect of powdered recycled tire on sulfate resistance of cemented clay." *Journal of Materials in Civil Engineering* 29 (10).
- Chegenizadeh, A., M. Keramatikerman, and Nikraz, H., (2018a). "Liquefaction resistance of fibre reinforced low-plasticity silt." *Soil Dynamics and Earthquake Engineering*, 104, pp.372-377.
- Chegenizadeh, A., M., Keramatikerman, G., Dalla Santa, and H. Nikraz. (2018b). "Influence of Recycled Tyre Amendment on Mechanical Behaviour of Cut-off Walls." *Journal of Cleaner Production*. 177: 507-515.
- Chern, J. C., and Lin, C. C. (1994). "Post-cyclic consolidation behavior of loose sands." *ASCE Geotechnical Special Publication*. P. 40.
- Cho, G. C., Dodds, J. and Santamarina, J. C. (2006). "Particle shape effects on packing density, stiffness, and strength: natural and crushed sands." *Journal of geotechnical and geoenvironmental engineering*, 132(5), pp.591-602.
- Chow, Y. K., Yong, D. M., Yong, K. Y. and Lee, S. L. (1992). "Dynamic compaction analysis." *Journal of Geotechnical engineering*, 118(8), pp.1141-1157.
- Clare, K.E. and Cruchley, A. F. (1957). "Laboratory experiments in the stabilization of clays with hydrated lime." *Geotechnique* 7: 97-111.
- Clough, G. W., Iwabuchi, J., Rad, N. S., & Kuppusamy, T. (1989). "Influence of cementation on liquefaction of sands." *Journal of Geotechnical Engineering*, 115(8), 1102-1117.
- Cockburn Cement. (2012). "Materials Safety Data Sheet for Hydrated Lime."

- Cokca, E. (2001). "Use of Class C Fly Ashes for the Stabilization – of an Expansive Soil " *Journal of Geotechnical and Geoenvironmental Engineering* 127: 568-573.
- Cokca, E., and Yilmaz, Z. (2004). "Use of rubber and bentonite added fly ash as a liner material." *Waste management*, 24(2), 153-164.
- Croft, J. B. (1964). "The pozzolanic reactivities of some New South Wales fly-ashes and their application to soil stabilization." Proceedings of the ARBB Australia, Australian Road Research Board (ARRB), Australia, vol. 2, part 2, paper 120, pp. 1114–1167.
- Daniel, D., Anderson, D., and Boynton, S. (1985). "Fixed-Wall Versus Flexible-Wall Permeameters," *Hydraulic Barriers in Soil and Rock* ASTM International, West Conshohocken, PA, 874, 107-126.
- Dermatas, D., & Meng, X. (2003). "Utilization of fly ash for stabilization/solidification of heavy metal contaminated soils." *Engineering geology*, 70(3), 377-394.
- Dev, K. L., Pillai, R. J. and Robinson, R. G. (2013). "Estimation of Critical State Parameters from One-dimensional Consolidation and Triaxial Compression Tests." *Indian geotechnical journal*, 43(3), pp.229-237.
- Du, Y. J., Fan, R. D., Liu, S. Y., Reddy, K. R. and Jin, F. (2015). "Workability, compressibility and hydraulic conductivity of zeolite-amended clayey soil/calcium-bentonite backfills for slurry-trench cutoff walls." *Engineering Geology*, 195, pp.258-268.
- Eades, J. L. and Grim, R. E. (1960). "Reaction of hydrated lime with pure clay minerals in soil stabilization." *Highway Research Board Bulletin*, (262).

- Edil, T. B., Park, J. K. and Kim, J. Y. (2004). "Effectiveness of scrap tire chips as sorptive drainage material." *Journal of Environmental Engineering*, 130(7), pp.824-831.
- El Takch, A., Sadrekarimi, A., and El Naggar, H. (2016). "Cyclic resistance and liquefaction behavior of silt and sandy silt soils." *Soil Dynamics and Earthquake Engineering*, 83, 98-109.
- Elgamal, A., Yang, Z., Parra, E. and Ragheb, A. (2003). "Modeling of cyclic mobility in saturated cohesionless soils." *International Journal of Plasticity*, 19(6), pp.883-905.
- Environmental Protection Agency (EPA). (2004). "40 CFR Part 63 National Emission Standards for Hazardous Air Pollutants for Lime Manufacturing Plants;" Final Rule. January 5, 2004. Available from: <https://www3.epa.gov/airtoxics/lime/fr05ja04.pdf>
- Erken, A., and Ulker, B. C. (2007). "Effect of cyclic loading on monotonic shear strength of fine-grained soils." *Engineering Geology*, 89(3), 243-257.
- European commission. (2013). "Best Available Techniques (BAT) Reference Document for the Production of Cement, Lime and Magnesium Oxide." Industrial Emissions Directive 2010/75/EU (Integrated Pollution Prevention and Control. Joint research Centre Institute for Prospective Technological Studies Sustainable Production and Consumption Unit European IPPC Bureau. Available from http://eippcb.jrc.ec.europa.eu/reference/BREF/clm_bref_0510.pdf
- Fatahi, B., Engelbert, D., Mujic, S., and Khabbaz, H. (2012a). "Assessment of surcharging on strength and stiffness of cement treated clays." In: Johnsen,

L.F., Bruce, D.A., Byle, M.J. (eds.) *Proceedings of the fourth international conference on grouting and deep mixing*. ASCE, USA, 272-280.

Fatahi, B., Khabbaz, H. and Fatahi, B. (2012b). "Mechanical characteristics of soft clay treated with fibre and cement." *Geosynthetics International*, 19, No. 3, 252–262.

Fatahi, B., Le, T.M., Fatahi, B., and Khabbaz, H. (2013). "Shrinkage properties of soft clay treated with cement and geofibers." *Geotechnical and Geological Engineering* 31(5): 1421-1435.

Feng, S. J., Du, F. L., Shi, Z. M., Shui, W. H., and Tan, K. (2015). "Field study on the reinforcement of collapsible loess using dynamic compaction." *Engineering Geology*, 185, 105-115.

Flyash Australia. (2016). "Material Safety Data Sheet (MSDS) for Flyash Class F." [Accessed 01.11.15 and 14.05.16].

Flyash Australia. (2017). <http://www.flyashaustralia.com.au/whatisflyash.aspx>. [Accessed 03.11.2017].

Fogarasi, S. and Cormos, C. C. (2017). "Assessment of coal and sawdust co-firing power generation under oxy-combustion conditions with carbon capture and storage." *Journal of Cleaner Production*, 142, pp.3527-3535.

Fogarasi, S. and Cormos, C.C., (2015). "Technico-economic assessment of coal and sawdust co-firing power generation with CO₂ capture." *Journal of Cleaner Production*, 103, pp.140-148.

- Fourie, A. B., Blight, G. E., & Papageorgiou, G. (2001). Static liquefaction as a possible explanation for the Merriespruit tailings dam failure. *Canadian Geotechnical Journal*, 38(4), 707-719.
- Frost Matthew W., Paul R. Fleming, and Christopher D. F. Rogers. 2004. "Cyclic Triaxial Tests on Clay Subgrades for Analytical Pavement Design." *Journal of Transportation Engineering* 130 (3): 378-386. doi: doi:10.1061/(ASCE)0733-947X(2004)130:3(378).
- Gallagher, P. M., and Mitchell, J. K. (2002). "Influence of colloidal silica grout on liquefaction potential and cyclic undrained behavior of loose sand." *Soil Dynamics and Earthquake Engineering*, 22(9), 1017-1026.
- GDS. (2013). "What is Triaxial Testing? Part 1 of 3" Published on the GDS website www.gdsinstruments.com, [accessed 03/11/2017] http://www.gdsinstruments.com/__assets__/pagepdf/000037/Part%201%20Introduction%20to%20triaxial%20testing.pdf
- Gennadii, B., and Ilya, I. (2013). "Soil Property Improvement Using Slag Binder" International Conference on Case Histories in Geotechnical Engineering. Paper 32. http://scholarsmine.mst.edu/icchge/7icchge/session_06/32
- Ghazavi, M. (2004). "Shear strength characteristics of sand-mixed with granular rubber." *Geotechnical & Geological Engineering*, 22(3), pp.401-416.
- Goodarzi, A.R., and M Salimi. (2015). "Stabilization Treatment of a Dispersive Clayey Soil Using Granulated Blast Furnace Slag and Basic Oxygen Furnace Slag." *Applied Clay Science* 108: 61-69.

- Gouvenot D. (1998). "State of the art in European grouting." Proceedings of the the ICE - Ground Improvement 1998;2(2):51–67.
- Gratchev, I. B., Sassa, K., Osipov, V. I., and Sokolov, V. N. (2006). "The liquefaction of clayey soils under cyclic loading." *Engineering Geology*. 86 (1), 70-84.
- Gray, D. H. (1970) "Role of woody vegetation in reinforcing soils and stabilizing slopes" *Proc., Symp. on Soil Reinforcement and Stabilizing Techniques*, pp. 253-306.
- Haeri, S. M., Noorzad, R. and Oskoorouchi, A. M. (2000). "Effect of geotextile reinforcement on the mechanical behavior of sand." *Geotextiles and Geomembranes*, 18(6), pp.385-402.
- Hamidi, A. and Hooresfand, M. (2013). "Effect of fiber reinforcement on triaxial shear behavior of cement treated sand." *Geotextiles and Geomembranes*, 36, pp.1-9.
- Haque, M. A., (2016). "Assessment of nickel leaching phenomena from landfill waste mixed paving block for eco-friendly field application." *Journal of Cleaner Production*, 139, pp.99-112.
- Harris, A.J. and Watson, P.D.J. (1997). "Optimal procedure for the ring shear test." *Ground Engineering*, 30(6)3.
- Hashemi, M. A., T. J. Massart, S. Salager, G. Herrier, and B. François. (2015). "Pore Scale Characterization of Lime-Treated Sand–Bentonite Mixtures." *Applied Clay Science* 111: 50-60. doi: <http://dx.doi.org/10.1016/j.clay.2015.04.001>.

- Hazarika, H., Hyodo, M., and Yasuhara, K. (2010). "Investigation of tire chips–sand mixtures as preventive measure against liquefaction." *Geo-Shanghai International Conference, 2010*, Shanghai, China.
- Hazirbaba, K., and Omarow, M. (2015). "Post-cyclic loading settlement of saturated clean sand." *Soil Dynamics and Earthquake Engineering*, 77, 337-347.
- Hesami, S., Hikouei, I. S., and Emadi, S. A. A. (2016). "Mechanical behavior of self-compacting concrete pavements incorporating recycled tire rubber crumb and reinforced with polypropylene fiber." *Journal of Cleaner Production*, 133, 228-234.
- Higgins, D. (2007). "Briefing: GGBS and sustainability" *Proceedings of the Institution of Civil Engineers Construction Materials* 160. CM3. Pp. 99-101.
- Higgins, D.D. (1998). What's new in ggbs? *Concrete Magazine*, May.
- Hong, C., Shackelford, C., and Malusis, M. (2012). "Consolidation and Hydraulic Conductivity of Zeolite-Amended Soil-Bentonite Backfills." *J. Geotech. Geoenviron. Eng.*, 10.1061/(ASCE)GT.1943-5606.0000566, 15-25.
- Hong, Y., Yang, Z., Orense, R. P., and Lu, Y. (2015). "Investigation of Sand-Tire Mixtures as Liquefaction Remedial Measure." *Proceedings of the Tenth Pacific Conference on Earthquake Engineering Building an Earthquake-Resilient Pacific*. November 2015, Sydney, Australia
- Horpibulsuk, S., Phetchuay, C. and Chinkulkijniwat, A. (2011). "Soil stabilization by calcium carbide residue and fly ash." *Journal of materials in civil engineering*, 24(2), pp.184-193.

- Horpibulsuk, S., Rachan, R., and Raksachon, Y. (2009). "Role of fly ash on strength and microstructure development in blended cement stabilized silty clay." *Soils and Foundation* 49(1), 85–98.
- Hyder (2012). "Study into Domestic and International Fate of End-of-life Tyres". <http://www.tyrestewardship.org.au/static/uploads/files/hyder-end-life-tyres-wfdtpqukoyut.pdf> (accessed 03/11/2017)
- Ibraim, E., Diambra, A., Wood, D. M. and Russell, A. R. (2010). "Static liquefaction of fibre reinforced sand under monotonic loading." *Geotextiles and Geomembranes*, 28(4), pp.374-385.
- Ishihara, K., Harada, K., Lee, W. F., Chan, C. C., and Safiullah, A. M. M. (2016). "Post-liquefaction settlement analyses based on the volume change characteristics of undisturbed and reconstituted samples." *Soils and Foundations*, 56(3), 533-546.
- Ishihara, K., Yamazaki, F. (1980). "Cyclic simple shear tests on saturated sand in multi-directional loading." *Soils and Foundations* 20 (1), 49– 59.
- Ishii H, Higaki K, Horikoshi K. (2011). "New liquefaction countermeasure method HDD for ground beneath existing structures." In: Proceedings of the fifth international conference on advances in Earthquake Geotechnical Engineering, 5th ICEGE. Santiago, Chile; 2011 paper N. NLCIS.
- Jafari, M., and Esna-ashari, M. (2012). "Effect of waste tire cord reinforcement on unconfined compressive strength of lime stabilized clayey soil under freeze–thaw condition." *Cold Regions Science and Technology*, 82, 21-29.

- Jakka, R. S., Datta, M., and Ramana, G. V. (2010). "Liquefaction behaviour of loose and compacted pond ash." *Soil Dynamics and Earthquake Engineering*, 30(7), 580-590.
- James, R., Kamruzzaman, A. H. M., Haque, A., Wilkinson, A. (2008). "Behaviour of lime-slag treated clay." *Proceedings of the Institution of Civil Engineers-Ground Improvement*, 161 (4), 207–216.
- Jegandan, S., Liska, M., Osman, A. A. and Al-Tabbaa, A. (2010). "Sustainable binders for soil stabilisation." *Proceedings of the Institution of Civil Engineers-Ground Improvement*, 163(1), pp.53-61.
- Kamruzzaman, A.H., Chew, S. H. and Lee, F. H., (2009). "Structuration and destructuration behavior of cement-treated Singapore marine clay." *Journal of geotechnical and geoenvironmental engineering*, 135(4), pp.573-589.
- Kaneko, T., Orense, R. P., Hyodo, M. and Yoshimoto, N. (2012). "Seismic response characteristics of saturated sand deposits mixed with tire chips." *Journal of Geotechnical and Geoenvironmental Engineering*, 139(4), pp.633-643.
- Kang, J. and Shackelford, C. (2010). "Consolidation of a Geosynthetic Clay Liner under Isotropic States of Stress." *J. Geotech. Geoenviron. Eng.*, 10.1061/(ASCE)GT.1943-5606.0000181, 253-259.
- Kaniraj, S. R., and Havanagi, V. G. (1999). "Compressive strength of cement stabilized fly ash-soil mixtures." *Cement and Concrete Research*, 29(5), 673-677.

- Kargar, S. H. R., Salehzadeh, H., and Shahnazari, H. (2016). "Post-cyclic behavior of carbonate sand of the northern coast of the Persian Gulf." *Marine Georesources & Geotechnology*, 34(2), 169-180.
- Karim, M. E. and Alam, M. J., (2014). "Effect of non-plastic silt content on the liquefaction behavior of sand–silt mixture." *Soil Dynamics and Earthquake Engineering*, 65, pp.142-150.
- Kashani, A., Ngo, T. D., Mendis, P., Black, J. R., and Hajimohammadi, A. (2017). "A sustainable application of recycled tyre crumbs as insulator in lightweight cellular concrete." *Journal of Cleaner Production*, 149, 925-935.
- Kaya, Z., and Erken, A. (2015). "Cyclic and post-cyclic monotonic behavior of Adapazari soils." *Soil Dynamics and Earthquake Engineering*, 77, 83-96.
- Keller, G. R. (2016). "Application of geosynthetics on low-volume roads." *Transportation Geotechnics*. 8, 119–131
- Keramatikerman, M., and A. Chegenizadeh. (2015). "A Review of Soil Stabilization Techniques." World Academy of Science, Engineering and Technology (WASET), 17th International Conference on Civil and Geological Engineering ICCGE 2015, Chicago, USA, October 08-09, 2015.
- Keramatikerman, M., Chegenizadeh, A. and Nikraz, H. (2016). "Effect of GGBFS and lime binders on the engineering properties of clay". *Applied Clay Science*, 132, pp.722-730.
- Keramatikerman, M., Chegenizadeh, A., and Nikraz, H. (2017a). "An investigation into effect of sawdust treatment on permeability and compressibility of soil-bentonite slurry cut-off wall." *Journal of Cleaner Production*, 162(6), 1-6.

- Keramatikerman, M., Chegenizadeh, A. and Nikraz, H. (2017b). "Experimental study on effect of fly ash on liquefaction resistance of sand." *Soil Dynamics and Earthquake Engineering*, 93, pp.1-6.
- Keramatikerman, M., and A. Chegenizadeh. (2017c). "Effect of Particle Shape on Monotonic Liquefaction: Natural and Crushed Sand." *Experimental Mechanics* 57 (8): 1341-1348.
- Keramatikerman, M., A. Chegenizadeh, and H. Nikraz. (2018a). "Shear Strength Characteristics of Over-consolidated Clay Treated with GGBFS." *Australian Geomechanics Journal (AGJ)* 53 (2): pp. 141-149.
- Keramatikerman, M., Chegenizadeh, A., & Nikraz, H. (2018b). "Effect of Flyash on Post-Cyclic Behavior of Sand." *Journal of Earthquake Engineering*, 1-13.
- Kestler, M. A. (2009). "Stabilization Selection Guide for Aggregate-and Native-surfaced Low-volume Roads." US Department of Agriculture, Forest Service, National Technology & Development Program.
- Khemissa, M. and Mahamedi, A. (2014). Cement and lime mixture stabilization of an expansive overconsolidated clay. *Applied Clay Science*,95, pp.104-110.
- Kiku H, Tsujino S. (1996) "Post liquefaction characteristic of sand." In: Proceedings of the 11th world conference on earthquake engineering, Acapulco; 1088p.
- Kim, J., Park, J., and Edil, T. (1997). "Sorption of Organic Compounds in the Aqueous Phase onto Tire Rubber." *J. Environ. Eng.*, 10.1061/(ASCE)0733-9372(1997)123:9(827), 827-835.
- Kitazume, M. and Terashi, M. 2013. *The deep mixing method*. CRC Press. Leiden. The Netherland.

- Kolias, S., V. Kasselouri-Rigopoulou, and A. Karahalios. (2005). "Stabilisation of Clayey Soils with High Calcium Fly Ash and Cement." *Cement and Concrete Composites* 27 (2): 301-313. doi: <http://dx.doi.org/10.1016/j.cemconcomp.2004.02.019>
- Kramer, S. L. (1996). "Geotechnical earthquake engineering." Englewood Cliffs, NJ, USA: Prentice Hall.
- Krumbein, W. C., and Sloss, L. L. (1963). "*Stratigraphy and sedimentation*", 2nd Ed., Freeman and Company, San Francisco.
- Ladd, R. S. (1978). "Preparing Test Specimens Using Undercompaction," *Geotechnical Testing Journal*, 1 (1), pp. 16-23.
- Lambe, T. W., (1958). "The structure of compacted clay." *Journal of the Soil Mechanics and Foundations Division, ASCE*, 84(SM2), pp.1-34.
- Lee A. R. (1974). "Blastfurnace and Steel Slag." Edward Arnold Publishers Ltd, London, UK.
- Lee, F.H., Lee, Y., Chew, S.H. and Yong, K.Y. (2005). "Strength and modulus of marine clay-cement mixes." *Journal of geotechnical and geoenvironmental engineering*, 131(2), pp.178-186.
- Liao, H. J., Huang, C. C., & Chao, B. S. (2003). "Liquefaction resistance of a colloid silica grouted sand." In *Grouting and ground treatment* (pp. 1305-1313).
- Li, X. S. and Wang, Y. (1998). "Linear representation of steady-state line for sand." *Journal of Geotechnical and Geoenvironmental Engineering*, 124(12), pp.1215-1217.

- Lian, F., Huang, F., Chen, W., Xing, B. and Zhu, L. (2011). "Sorption of a polar and polar organic contaminants by waste tire rubber and its chars in single-and bi-solute systems." *Environmental pollution*, 159(4), pp.850-857.
- Lian, F., Song, Z., Liu, Z., Zhu, L. and Xing, B. (2013). "Mechanistic understanding of tetracycline sorption on waste tire powder and its chars as affected by Cu²⁺ and pH." *Environmental pollution*, 178, pp.264-270.
- Liu, J., Wang, G., Kamai, T., Zhang, F., Yang, J., and Shi, B. (2011). "Static liquefaction behavior of saturated fiber-reinforced sand in undrained ring-shear tests." *Geotextiles and Geomembranes*, 29(5), 462-471.
- Lorenzo, G.A., Bergado, D. T. (2004). "Fundamental parameters of cement-admixed clay: new approach." *J Geotechnical Geoenvironmental Engineering* 130(10): 1-9.
- Maher, M. H. and Ho, Y. C. (1993). "Behavior of FiberReinforced Cemented Sand Under Static and Cyclic Loads", *Geotechnical Testing Journal*, GTJODJ, Vol. 16, No. 3, September 1993, pp. 330-338.
- Maher, M. H., Ro, K. S., & Welsh, J. P. (1994). "Cyclic undrained behavior and liquefaction potential of sand treated with chemical grouts and microfine cement (MC-500)." *Geotechnical Testing Journal*, 17(2), 159-170.
- Maheshwari, B.K., Singh, H.P. and Saran, S. (2012). "Effects of reinforcement on liquefaction resistance of solani sand." *Journal of Geotechnical and Geoenvironmental Engineering*, 138(7), pp.831-840.
- Makusa, G. (2012) "Soil stabilization methods and materials in engineering practice", in *State of the Art Report, Luleå University of Technology, Luleå*. 2012.

- Malasavage, Nicholas E, Santhi Jagupilla, Dennis G Grubb, Mahmoud Wazne, and William P Coon. 2012. "Geotechnical Performance of Dredged Material—Steel Slag Fines Blends: Laboratory and Field Evaluation." *Journal of Geotechnical and Geoenvironmental Engineering*.
- Maleki, M., A. Ezzatkhah, M. Bayat, and M. Mousivand. 2011. "Effect of Physical Parameters on Static Undrained Resistance of Sandy Soil with Low Silt Content." *Soil Dynamics and Earthquake Engineering* 31 (10): 1324-1331. doi: <http://dx.doi.org/10.1016/j.soildyn.2011.05.003>.
- Malusis, M., Barben, E., and Evans, J. (2009). "Hydraulic Conductivity and Compressibility of Soil-Bentonite Backfill Amended with Activated Carbon." *J. Geotech. Geoenviron. Eng.*, 10.1061/(ASCE)GT.1943-5606.0000041, 664-672.
- Mardani-Aghabaglou, A., Kalıpcılar, İ., Sezer, G. İ., Sezer, A., & Altun, S. (2015). "Freeze–thaw resistance and chloride-ion penetration of cement-stabilized clay exposed to sulfate attack." *Applied Clay Science*, 115, 179-188.
- Mashiri, M. S., Vinod, J. S., and Sheikh, M. N. (2016). "Liquefaction Potential and Dynamic Properties of Sand-Tyre Chip (STCh) Mixtures," *Geotechnical Testing Journal*, 39(1), pp. 69-79.
- Meehan, C., Brandon, T., and Duncan, J. (2007). "Measuring drained residual strengths in the Bromhead ring shear." *Geotechnical Testing Journal* 30(6): 1-8, 2007. <http://dx.doi.org/10.1520/GTJ101017>. ISSN 0149-6115.
- Mesri, G., and Abdel-Ghaffar, M. E. M. (1993). "Cohesion intercept in effective stress-stability analysis." *J. Geotech. Eng.*, 10.1061/(ASCE) 0733-9410(1993)119:8(1229), 1229–1249.

- Mollamahmutoglu, M., and Yilmaz, Y. (2010). "Pre-and post-cyclic loading strength of silica-grouted sand." *Proceedings of the Institution of Civil Engineers-Geotechnical Engineering*, 163(6), 343-348.
- Monkul, M. M., Gültekin, C., Gülver, M., Akın, Ö., & Eseller-Bayat, E. (2015). "Estimation of liquefaction potential from dry and saturated sandy soils under drained constant volume cyclic simple shear loading." *Soil Dynamics and Earthquake Engineering*, 75, 27-36.
- Mott, H. V., and Weber, W. J. (1992). "Sorption of low molecular weight organic contaminants by fly ash: Considerations for the enhancement of cutoff barrier performance." *Environ. Sci. Technol.*, 26(6), 1234–1242.
- Nabavi-Pelesaraei, A., Bayat, R., Hosseinzadeh-Bandbafha, H., Afrasyabi, H. and Chau, K.W. (2017). "Modeling of energy consumption and environmental life cycle assessment for incineration and landfill systems of municipal solid waste management-A case study in Tehran Metropolis of Iran." *Journal of Cleaner Production*, 148, pp.427-440.
- Naeini, S. A., and N. Gholampoor. (2014). "Cyclic Behaviour of Dry Silty Sand Reinforced with a Geotextile." *Geotextiles and Geomembranes* 42 (6): 611-619. doi: <http://dx.doi.org/10.1016/j.geotexmem.2014.10.003>.
- Neaz Sheikh, M., Mashiri, M. S., Vinod, J. S. and Tsang, H. H. (2012). "Shear and compressibility behavior of sand–tire crumb mixtures." *Journal of Materials in Civil Engineering*, 25(10), pp.1366-1374.
- Nelson J. and Miller, D. J. (1997). *Expansive soils: problems and practice in foundation and pavement engineering*. John Wiley & Sons. New York.

- Nidzam, R. M. and Kinuthia, J. M. (2010). "Sustainable soil stabilisation with blast furnace slag—a review." *Proceedings of the Institution of Civil Engineers-Construction Materials*, 163(3), pp.157-165.
- Noorzad, R., and P. Fardad Amini. (2014). "Liquefaction Resistance of Babolsar Sand Reinforced with Randomly Distributed Fibers under Cyclic Loading." *Soil Dynamics and Earthquake Engineering* 66: 281-292. doi: <http://dx.doi.org/10.1016/j.soildyn.2014.07.011>.
- Noorzad, R., and Shakeri, M. (2017). "Effect of silt on post-cyclic shear strength of sand." *Soil Dynamics and Earthquake Engineering*, 97, 133-142.
- Obuzor, G.N., Kinuthia, J.M., and Robinson, R.B. 2012. Soil stabilisation with lime-activated-GGBS—A mitigation to flooding effects on road structural layers/embankments constructed on floodplains. *Engineering Geology* 151: 112-119.
- O'Connor, J. and Orr, T. (2016). "Using IBPs to improve the geotechnical properties of soil." *Proceedings of the Institution of Civil Engineers-Ground Improvement*, 169(4), pp.286-296.
- Oishi, H., Tanaka, Y. (1993). "Densification of surrounding soils due to gravel drain construction." Proc., 4th U.S.–Japan Workshop on Earthquake Resistant Design of Lifeline Facilities and Countermeasures against Soil Liquefaction, Buffalo, NY.
- Olson, R. E. (1986). "State of the art: Consolidation testing." *Consolidation of soils: testing and evaluation*, ASTM STP 892, R. N. Yong and F. C. Townsend, eds., ASTM, West Conshohoken, Pa., 7–70.

- Ono, Y., Ito, K., Nakajima, Y., Oishi, H. (1991). "Efficient installation of gravel drains." Proc., 2nd Int. Conference on Recent Advances in Geotechnical Earthquake Engineering and Soil Dynamics, St. Louis, Missouri. Paper No. 3.24.
- Oti, J.E., Kinuthia, J.M., and Robinson, R.B. 2014. The development of unfired clay building material using brick dust waste and Mercia mudstone clay. *Applied Clay Science 102*: 148-154.
- Park, J. K., Edil, T. B., Kim, J. Y., Huh, M., Lee, S. H., and Lee, J. J. (2003). Suitability of shredded tyres as a substitute for a landfill leachate collection medium. *Waste management & research, 21(3)*, 278-289.
- Park, J. K., Kim, J. Y., Madsen, C. D., & Edil, T. B. (1997). Retardation of volatile organic compound movement by a soil-bentonite slurry cutoff wall amended with ground tires. *Water Environment Research, 69(5)*, 1022-1031.
- Payan, M., Khoshghalb, A., Senetakis, K., & Khalili, N. (2016). "Effect of particle shape and validity of Gmax models for sand: A critical review and a new expression." *Computers and Geotechnics, 72*, 28-41.
- Pelisser, F., Zavarise, N., Longo, T. A., and Bernardin, A. M. (2011). "Concrete made with recycled tire rubber: effect of alkaline activation and silica fume addition." *Journal of Cleaner Production, 19(6)*, 757-763.
- Petry, T. M. and Little, D. N. (2002). Review of stabilization of clays and expansive soils in pavements and lightly loaded structures-history, practice, and future. *Journal of Materials in Civil Engineering, 14(6)*, pp.447-460.

- Phetchuay, C., Horpibulsuk, S., Arulrajah, A., Suksiripattanapong, C. and Udomchai, A. (2016). "Strength development in soft marine clay stabilized by fly ash and calcium carbide residue based geopolymer." *Applied Clay Science*, 127, pp.134-142.
- Philip, L. K. (2001). "An investigation into contaminant transport processes through single-phase cement–bentonite slurry walls." *Engineering geology*, 60(1), pp.209-221.
- Pillai, R. J., Nazeeh, K. M., and Robinson, R. G. (2014). "Post-cyclic behaviour of clayey soil." *Indian Geotechnical Journal*, 44(1), 39-48.
- Plant, R., Wilmot, K. and Ege, C. (2014) "Contaminated Soil Wastes in Australia." [Prepared for the Australian Department of the Environment]. Institute for Sustainable Futures, University of Technology, Sydney (Online report, access date: 02/05/2016).
- Porcino, D., Marcianò, V. and Granata, R. (2015). "Cyclic liquefaction behaviour of a moderately cemented grouted sand under repeated loading." *Soil Dynamics and Earthquake Engineering*, 79, pp.36-46.
- Prabakar, J., Dendorkar, N. and Morchhale, R. K., (2004). "Influence of fly ash on strength behavior of typical soils." *Construction and Building Materials*, 18(4), pp.263-267.
- Prakasha, K., and V. Chandrasekaran. (2005). "Behavior of Marine Sand-Clay Mixtures under Static and Cyclic Triaxial Shear." *Journal of Geotechnical and Geoenvironmental Engineering* 131 (2): 213-222. doi: doi:10.1061/(ASCE)1090-0241(2005)131:2(213).

- Prusinski, J., Bhattacharja, S. (1999). "Effectiveness of Portland cement and lime in stabilizing clay soils." *Transportation Research Record: Journal of the Transportation Research Board* 1652, 215–227.
- Puppala, A. J., Wattanasanticharoen, E. and Punthutaecha, K. (2003). "Experimental evaluations of stabilisation methods for sulphate-rich expansive soils." *Proceedings of the Institution of Civil Engineers-Ground Improvement*, 7(1), pp.25-35.
- Puppala, A.J., Katha, B., and Hoyos, L. R. (2004). "Volumetric shrinkage strain measurements in expansive soils using digital imaging technology." *ASTM Geotechnical Testing Journal* 27(6): 547-556.
- Puppala, Anand J., Thammanoon Manosuthikij, and Bhaskar C.S. Chittoori. (2013). "Swell and shrinkage characterizations of unsaturated expansive clays from Texas." *Engineering Geology* 164: 187-194.
- Purwana, Yusep Muslih. (2013). *Experimental study on unsaturated direct shear and California bearing ratio tests with suction monitoring on sand-kaolin clay mixtures*. Ph.D. Department of Civil Engineering, School of Civil and Mechanical Engineering, Curtin University.
- Rao, G. V. and Dutta, R. K. (2006). "Compressibility and strength behaviour of sand–tyre chip mixtures." *Geotechnical & Geological Engineering*, 24(3), pp.711-724.
- Ressi, A. and Cavalli, N. (1985). "Bentonite slurry trenches." *Engineering Geology*, 21(3-4), pp.333-339.

- Rong, L., Zhang, C., Jin, D. and Dai, Z. (2017). "Assessment of the potential utilization of municipal solid waste from a closed irregular landfill." *Journal of Cleaner Production*, 142, pp.413-419.
- Rouholamin, M., Bhattacharya, S., and Orense, R. P. (2017). "Effect of initial relative density on the post-liquefaction behaviour of sand." *Soil Dynamics and Earthquake Engineering*, 97, 25-36.
- Rousé, P. C., Fannin, R. J., and Shuttle, D. A. (2008). "Influence of roundness on the void ratio and strength of uniform sand." *Géotechnique*, 58(3), 227-231.
- Rubber Manufacturers Association. (2002). "U.S. scrap tire markets 2001." Washington, D.C.
- Sabbar, A. S., Chegenizadeh, A., and Nikraz, H. (2017). "Static liquefaction of very loose sand–slag–bentonite mixtures." *Soils and Foundations*, 57(3), pp.341-356.
- Sabry, M. A., Abdel-Ghani, Kh. I., and El Nahas, A. M. (1996). "Strength characteristics of soil-lime columns sections." In: Yonekura, R. et al. (eds.), *Proceedings of International Conference on Ground Improvement Geosystems*, Tokyo, vol. 1. Balkema, 447-452.
- Sadrekarami, A., (2014). "Static liquefaction-triggering analysis considering soil dilatancy." *Soils and Foundations*, 54(5), pp.955-966.
- Sağlam, Selman, and B. Sadık Bakır. 2014. "Cyclic Response of Saturated Silts." *Soil Dynamics and Earthquake Engineering* 61–62: 164-175. doi: <http://dx.doi.org/10.1016/j.soildyn.2014.02.011>.

- Saito, A., Taghawa, K., Tamura, T., Oishi, H., Nagayama, H., Shimaoka, H. (1987).
 “A countermeasure for sand liquefaction: gravel drain method.” Nippon
 Kokan Technical Report, Overseas No. 51, Japan.
- Saxena, S. K., Reddy, K. R., & Avramidis, A. S. (1988). “Liquefaction resistance of
 artificially cemented sand.” *Journal of Geotechnical Engineering*, 114(12),
 1395-1413.
- Saxena, S. K., Reddy, K. R., & Avramidis, A. S. (1988). “Liquefaction resistance of
 artificially cemented sand.” *Journal of Geotechnical Engineering*, 114(12),
 1395-1413.
- Schnaid, F., Prietto, P. D. and Consoli, N. C., (2001). “Characterization of cemented
 sand in triaxial compression.” *Journal of Geotechnical and
 Geoenvironmental Engineering*, 127(10), pp.857-868.
- Schofield AN, Wroth CP (1968). “Critical state soil mechanics.” McGraw-Hill
 Publications, London
- Scrap Tire News. (2017). “Crumb rubber Manufacturing Technologies”
<http://www.scraptirenews.com/crumb.php#prettyPhoto>, (accessed
 03/11/2017)
- Seed R. B. and Harder L. F. (1990). “SPT-based analysis of cyclic pore pressure
 generation and undrained residual strength.” In: Bolton H, Seed
 Memorial Symposium Proceedings, vol. 2, pp. 351–376; 1990
- Seed, H. B., Booker, J. R. (1977). “Stabilization of potentially liquefiable sand deposits
 using gravel drains.” *ASCE Journal of Geotechnical Engineering Division*
 103 (7), 757– 768.

- Shafiee, A. (2006). "Cyclic resistance, pre and post-Liquefaction behavior of dry pluviated silty sands." *Journal of Seismology and Earthquake Engineering*, 8(3), 163.
- Shamoto, Y., Zhang, J. M., and Tokimatsu, K. (1998). "New charts for predicting large residual post-liquefaction ground deformation." *Soil dynamics and earthquake engineering*, 17(7), 427-438.
- Sharma, A.K. and Sivapullaiah, P.V. (2016). "Strength development in fly ash and slag mixtures with lime." *Proceedings of the Institution of Civil Engineers-Ground Improvement*, pp.1-12.
- Shukla, A., Zhang, Y. H., Dubey, P., Margrave, J. L. and Shukla, S. S. (2002). "The role of sawdust in the removal of unwanted materials from water." *Journal of Hazardous Materials*, 95(1), 137-152.
- Sibelco Australia. (2011). Material safety data sheet for Clay Prestige NY.
- Singh, S. P., Chowdhury, S., & Mishra, P. N. (2015). "An Experimental Investigation on Strength Characteristics of Alkali Activated Fly Ash." *Procedia Earth and Planetary Science*, 11, 402-409.
- Sivapullaiah, P.V., Sridharan, A., and Bhaskar Raju, K.V. 2000. Role of amount and type of clay in the lime stabilization of soils. *Proceedings of the Institution of Civil Engineers-Ground Improvement* 4(1): 37-45.
- Skempton, A. W. (1970). "First-Time Slides in Over-Consolidated Clays." *Géotechnique*, 20(3), pp. 320-324.

- Smart, P. (2008). "Discussion of Influence of roundness on the void ratio and strength of uniform sand" by P. C. Rousé, R. J. Fannin, and D. A. Shuttle. *Géotechnique*, 58(8), 681-681.
- Sonu, C. J., Ito, K., Oishi, H. (1993). "Harry Seed, liquefaction and gravel drain." *Civil Engineering ASCE* 63 (12), 58– 60.
- Soroush, A., and Soltani-Jigheh, H. (2009). "Pre-and post-cyclic behavior of mixed clayey soils." *Canadian Geotechnical Journal*, 46(2), 115-128.
- Stark, T., Choi, H., and McCone, S. (2005). "Drained Shear Strength Parameters for Analysis of Landslides." *J. Geotech. Geoenviron. Eng.*, [10.1061/\(ASCE\)1090-0241\(2005\)131:5\(575\)](https://doi.org/10.1061/(ASCE)1090-0241(2005)131:5(575)), 575-588.
- SUEZ. (2016). "Tyres." (http://www.sita.com.au/community-education/site_522_tours-education/recycling-tips/tyres/) (Jan. 10, 2016).
- Tasong, W.A., Wild, S., Tilley, R.J.D. (1999). "Mechanisms by which Ground Granulated Blastfurnace Slag prevents sulphate attack of lime-stabilised kaolinite." *Cement and Concrete Research*, 29. Elsevier Science Ltd., pp. 975–982.
- Tavakoli, H. R., Shafiee, A., and Jafari, M. K. (2011). "Post-Cyclic Undrained Behavior of Compacted Composite Clay Subjected to Various Cyclic Loading Paths." *Geotechnical and Geological Engineering*, 29(6), 1085.
- Terzaghi, K., Peck, R. B., and Mesri, G. (1996). "Soil mechanics in engineering practice.", 3rd Ed., Wiley, New York.

- Togrol, E., and Güler, E. (1984). "Effect of repeated loading on the strength of clay." *International Journal of Soil Dynamics and Earthquake Engineering*, 3(4), 184-190.
- Tokimatsu, K. and Yoshimi, Y. (1980). "Effects of vertical drains on the bearing capacity of saturated sand during earthquakes." Proc., International Conference on Engineering for Protection from Natural Disasters, Bangkok, Thailand, 643- 655.
- Towhata, I. (2008). "Mitigation of liquefaction-induced damage." In *Geotechnical Earthquake Engineering* (pp. 588-642). Springer Berlin Heidelberg.
- Turner, A. and Rice, L. (2010). "Toxicity of tire wear particle leachate to the marine macroalga, *Ulva lactuca*." *Environmental Pollution*, 158(12), pp.3650-3654.
- Uchimura, T., Chi, N., Nirmalan, S., Sato, T., Meidani, M. and Towhata, I. (2007). "Shaking table tests on effect of tire chips and sand mixture in increasing liquefaction resistance and mitigating uplift of pipe." In *Proceedings, international workshop on scrap tire derived geomaterials—opportunities and challenges, Yokosuka, Japan* (pp. 179-186).
- Vaid, Y. P. and Chern, J. C. (1985). "Cyclic and monotonic undrained response of sands." In *Advances in the art of testing soils under cyclic loading conditions, proceedings of the ASCE convention, Detroit* (ed. V. Khosla), pp. 120–147. New York, NY, USA: ASCE.
- Vakili, M. V., Chegenizadeh, A., Nikraz, H., Keramatikerman, M. (2016). "Investigation on shear strength of stabilised clay using cement, sodium silicate and slag." *Appl. Clay Sci.* 124, 243–251.

- Vashisth, P., Wayne Lee, K., and Wright, R. M. (1998). "Assessment of water pollutants from asphalt pavement containing recycled rubber in Rhode Island. Environmental and social effects of transportation." *Transportation Research Record 1626*, Transportation Research Board, Washington, D.C.
- Vercueil, D., Billet, P. and Cordary, D. (1997). "Study of the liquefaction resistance of a saturated sand reinforced with geosynthetics." *Soil Dynamics and Earthquake Engineering*, 16(7-8), pp.417-425.
- Waldron, L. J. (1977). "Shear resistance of root-permeated homogeneous and stratified soil." *Soil Society. Of American Journal*41 (5), pp. 843–849.
- Wang, J., Liu, F. Y., Wang, P., and Cai, Y. Q. (2016). "Particle size effects on coarse soil-geogrid interface response in cyclic and post-cyclic direct shear tests." *Geotextiles and Geomembranes*, 44(6), 854-861.
- Wang, S., Luna, R., & Onyejekwe, S. (2015a). "Postliquefaction behavior of low-plasticity silt at various degrees of reconsolidation." *Soil Dynamics and Earthquake Engineering*, 75, 259-264.
- Wang, S., Luna, R., & Zhao, H. (2015b). "Cyclic and post-cyclic shear behavior of low-plasticity silt with varying clay content." *Soil Dynamics and Earthquake Engineering*, 75, 112-120.
- Wang, Y., Chen, Y., Xie, H., Zhang, C. and Zhan, L., (2016). "Lead adsorption and transport in loess-amended soil-bentonite cut-off wall." *Engineering Geology*, 215, pp.69-80.

- Wei, L. M. and Yang, J. (2014). "On the role of grain shape in static liquefaction of sand–fines mixtures." *Geotechnique* 64, No. 9, 740–745
[<http://dx.doi.org/10.1680/geot.14.T.013>]
- Wild, S., Kinuthia, J.M., Jones, G. I., Higgins, D. D. (1998). "Effects of partial substitution of lime with ground granulated blast furnace slag (GGBS) on the strength properties of lime stabilised sulphate-bearing clay soils." *Engineering Geology*. 51 (1), 37–53
- Wu, T. H., Beal, P. E., Lan, C. (1988) "In situ shear test of soil-root system." *Journal of Geotech Engineering ASCE* 114 (12), pp. 1376-1394.
- Yang, J. (2002). "Non-uniqueness of flow liquefaction line for loose sand." *Geotechnique*, 52, No. 10, 757–760, <http://dx.doi.org/10.1680/geot.2002.52.10.757>.
- Yang, J. and Luo, X. D. (2015). "Exploring the relationship between critical state and particle shape for granular materials." *Journal of the Mechanics and Physics of Solids*, 84, pp.196-213.
- Yang, J. and Wei, L. M. (2012). "Collapse of loose sand with the addition of fines: the role of particle shape." *Geotechnique* 62, No. 12, 1111–1125, <http://dx.doi.org/10.1680/geot.11.P.062>.
- Yang, J., Wei, L. M. and Dai, B. B. (2015). "State variables for silty sands: Global void ratio or skeleton void ratio?" *Soils and Foundations*, 55(1), pp.99-111.
- Ye, B., Lu, J., and Ye, G. (2015). "Pre-shear effect on liquefaction resistance of a Fujian sand." *Soil Dynamics and Earthquake Engineering*, 77, 15-23.

- Yencho Nathan A. ffros, Brian C. Dudley, Pedro J. Amaya, William E. Wolfe, and Tarunjit Butalia. 2013. "Liquefaction Potential of Impounded of Class F Fly Ash." In *2013 World of Coal Ash (WOCA Conference)*, Lexington, KY, April 22-25, 2013.
- Yeo, S., Shackelford, C., and Evans, J. (2005). "Consolidation and Hydraulic Conductivity of Nine Model Soil-Bentonite Backfills." *J. Geotech. Geoenviron. Eng.*, 10.1061/(ASCE)1090-0241(2005)131:10(1189), 1189-1198.
- Yi, Y., Gu, L., and Liu, S. (2015). "Microstructural and mechanical properties of marine soft clay stabilized by lime-activated ground granulated blastfurnace slag." *Applied Clay Science*, 103, 71-76.
- Yi, Y., Liska, M. and Al-Tabbaa, A. (2013). "Properties of two model soils stabilized with different blends and contents of GGBS, MgO, lime, and PC." *Journal of Materials in Civil Engineering*, 26(2), pp.267-274.
- Youwai, S. and Bergado, D. T. (2003). "Strength and deformation characteristics of shredded rubber tire sand mixtures." *Canadian Geotechnical Journal*, 40(2), pp.254-264.
- Zand, B., Tu, W., Amaya, P. J., Wolfe, W. E., and Butalia, T. S. (2009). "An experimental investigation on liquefaction potential and post-liquefaction shear strength of impounded fly ash." *Fuel*, 88(7), 1160-1166.

Every reasonable effort has been made to acknowledge the owners of copyright material.

I would be pleased to hear from any copyright owner who has been omitted or incorrectly acknowledged.

Appendixes

Permissions

Mahdi Keramatikerman

From: Tanya Kouzmin <tanyaok@gmx.com>
Sent: Wednesday, 28 March 2018 7:43 AM
To: Mahdi Keramatikerman
Subject: RE: FW: FW: Your paper on shear strength characteristics of oc clay with BGGFS

Hi Mahdi,
Yes , all good. You have permission to use the paper in your thesis provided that you cite the reference to Australian Geomechanics.
Regards

Tanya Kouzmin
Editor, Australian Geomechanics

On 26 Mar 2018 23:28, Mahdi Keramatikerman <mahdi.keramatikerman@postgrad.curtin.edu.au> wrote:

Hi Tanya,

Do you have any news for me? I am going to submit my thesis soon.

Looking forward to hear from you.

Thanks,

Mahdi

From: TANYA KOUZMIN [mailto:tanyaok@gmx.com]
Sent: Monday, 19 March 2018 4:07 PM
To: Mahdi Keramatikerman <mahdi.keramatikerman@postgrad.curtin.edu.au>
Subject: Re: FW: FW: Your paper on shear strength characteristics of oc clay with BGGFS

Hi Mahdi,

Are you going to use the entire content of the paper in your thesis?

I am sorry, I am new to the editor role and will have to find out about this. I will get back to you within a week.

Regards

Tanya

Sent: Saturday, March 17, 2018 at 9:17 AM
From: "Mahdi Keramatikerman" <mahdi.keramatikerman@postgrad.curtin.edu.au>
To: "TANYA KOUZMIN" <tanyaok@gmx.com>
Subject: FW: FW: Your paper on shear strength characteristics of oc clay with BGGFS

Hi Tanya,

Could you please let me know how I can have permission for my accepted paper with AGS?

Kind Regards,

Mahdi

From: Mahdi Keramatikerman
Sent: Thursday, 1 March 2018 9:22 PM
To: "TANYA KOUZMIN" <tanyaok@gmx.com>
Subject: RE: FW: Your paper on shear strength characteristics of oc clay with BGGFS

Dear Tanya,

Can you please let me know how I can obtain the permission from AGS to use the accepted paper in my thesis?

Kind Regards,

Mahdi

From: TANYA KOUZMIN [<mailto:tanyaok@gmx.com>]
Sent: Monday, 26 February 2018 10:01 AM
To: Mahdi Keramatikerman <mahdi.keramatikerman@postgrad.curtin.edu.au>
Subject: Re: FW: Your paper on shear strength characteristics of oc clay with BGGFS

Dear Mahdi,

Congratulations! Your revised paper on shear strength characteristics of OC clay with BGGFS, has been accepted for publication in *Australian Geomechanics*.

It will likely be published in the June 2018 edition.

**ELSEVIER LICENSE
TERMS AND CONDITIONS**

Oct 15, 2017

This Agreement between Curtin University -- Mahdi Keramatikerman ("You") and Elsevier ("Elsevier") consists of your license details and the terms and conditions provided by Elsevier and Copyright Clearance Center.

License Number	4198280036008
License date	Sep 29, 2017
Licensed Content Publisher	Elsevier
Licensed Content Publication	Applied Clay Science
Licensed Content Title	Effect of GGBFS and lime binders on the engineering properties of clay
Licensed Content Author	Mahdi Keramatikerman,Amin Chegenizadeh,Hamid Nikraz
Licensed Content Date	Nov 1, 2016
Licensed Content Volume	132
Licensed Content Issue	n/a
Licensed Content Pages	9
Start Page	722
End Page	730
Type of Use	reuse in a thesis/dissertation
Portion	full article
Format	both print and electronic
Are you the author of this Elsevier article?	Yes
Will you be translating?	No
Title of your thesis/dissertation	Cyclic Behaviour of clayey Sand
Expected completion date	Apr 2018
Estimated size (number of pages)	200
Requestor Location	Curtin University 40 Mitchell St. Bentley, 6102 Australia Attn: Mahdi
Total	0.00 AUD
Terms and Conditions	

INTRODUCTION

1. The publisher for this copyrighted material is Elsevier. By clicking "accept" in connection with completing this licensing transaction, you agree that the following terms and conditions apply to this transaction (along with the Billing and Payment terms and conditions established by Copyright Clearance Center, Inc. ("CCC"), at the time that you opened your Rightslink account and that are available at any time at <http://myaccount.copyright.com>).

GENERAL TERMS

2. Elsevier hereby grants you permission to reproduce the aforementioned material subject to the terms and conditions indicated.

<https://s100.copyright.com/CustomAdmin/PLF.jsp?ref=ccf68e2b-8f47-4383-ba72-b4ba891a899d>

1/5

**SPRINGER LICENSE
TERMS AND CONDITIONS**

Oct 15, 2017

This Agreement between Curtin University -- Mahdi Keramatikerman ("You") and Springer ("Springer") consists of your license details and the terms and conditions provided by Springer and Copyright Clearance Center.

License Number	4206490658880
License date	Oct 12, 2017
Licensed Content Publisher	Springer
Licensed Content Publication	Experimental Mechanics
Licensed Content Title	Effect of Particle Shape on Monotonic Liquefaction: Natural and Crushed Sand
Licensed Content Author	M. Keramatikerman, A. Chegenizadeh
Licensed Content Date	Jan 1, 2017
Licensed Content Volume	57
Licensed Content Issue	8
Type of Use	Thesis/Dissertation
Portion	Full text
Number of copies	1
Author of this Springer article	Yes and you are the sole author of the new work
Order reference number	
Title of your thesis / dissertation	Cyclic Behaviour of dayey Sand
Expected completion date	Apr 2018
Estimated size(pages)	200
Requestor Location	Curtin University 40 Mitchell St. Bentley, 6102 Australia Attn: Mahdi
Billing Type	Invoice
Billing Address	Curtin University 40 Mitchell St. Bentley, Australia 6102 Attn: Mahdi
Total	0.00 USD
Terms and Conditions	

Introduction

The publisher for this copyrighted material is Springer. By clicking "accept" in connection with completing this licensing transaction, you agree that the following terms and conditions apply to this transaction (along with the Billing and Payment terms and conditions established by Copyright Clearance Center, Inc. ("CCC"), at the time that you opened your Rightslink account and that are available at any time at <http://myaccount.copyright.com>).

<https://s100.copyright.com/CustomAdmin/PLF.jsp?u=12de93b5-4179-4ed4-b54d-e2fcbcc2b69f>

Mahdi Keramatikerman

From: Permissions Helpdesk <permissionshelpdesk@elsevier.com>
Sent: Wednesday, 4 October 2017 12:29 AM
To: Mahdi Keramatikerman
Subject: RE: request for a permission to use my published papers in my thesis

Dear Mahdi,

As an Elsevier journal author, you retain the right to include the article in a thesis or dissertation (provided that this is not to be published commercially) whether in full or in part, subject to proper acknowledgment; see <https://www.elsevier.com/about/our-business/policies/copyright/personal-use> for more information. As this is a retained right, no written permission from Elsevier is necessary.

If I may be of further assistance, please let me know.

Best of luck with your thesis and best regards,
Laura

Laura Stingelin
Permissions Helpdesk Associate
ELSEVIER | Global E-Operations Books
+1 215-239-3867 office
lstingelin@elsevier.com
Contact the Permissions Helpdesk
+1 800-523-4069 x3808 | permissionshelpdesk@elsevier.com

From: Mahdi Keramatikerman [mailto:mahdi.keramatikerman@postgrad.curtin.edu.au]
Sent: Friday, September 29, 2017 11:16 AM
To: Permissions Helpdesk <permissionshelpdesk@elsevier.com>
Subject: request for a permission to use my published papers in my thesis

***** External email: use caution *****

Dear Sir/Madam,

I am a PhD candidate who has a couple of publications in Elsevier. Currently, I am at the stage of thesis writing and require to use my published materials in my thesis. Just wondering how should I get a permission to use my published materials with Elsevier in my thesis.

Best,
Mahdi

Mahdi Keramatikerman

From: waset.org web site <noreply@waset.org>
Sent: Monday, 13 November 2017 7:08 AM
To: Mahdi Keramatikerman
Subject: Your Question

Dear Mr. Mahdi Keramatikerman,

Thanks for the inquiry! We kindly grant you the requested permission to use your published paper in your dissertation.

If you have any questions, please do not hesitate to contact us at <http://waset.org/profile/messages>.

Best regards,

Waset Team
International Science Council
Tel:++15756350018
www.waset.org

11/25/2018

Mail - mahdi.keramatikerman@postgrad.curtin.edu.au

Copyright.com Order Confirmation


no-reply@copyright.com

Mon 11/26/2018 9:43 AM

To: Mahdi Keramatikerman <mahdi.keramatikerman@postgrad.curtin.edu.au>;

Do Not Reply Directly to This Email

To ensure that you continue to receive our emails,
please add copyright@marketing.copyright.com to your [address book](#).

Thank You for Your Order with Copyright Clearance Center	
Dear Mahdi Keramatikerman,	
Thank you for placing your order with Copyright Clearance Center .	
Order Summary: Order Date: 11/25/2018 Confirmation Number: 11768116 Items in order: 1 Order Total: \$ 0.00	
To view or print your order details or terms and conditions, click the following link and log in: Order link	
Need additional permissions? Go here .	
How was your experience? Click here to give us feedback .	
If you need assistance, please visit our online help (www.copyright.com/help).	
Please do not reply to this message. This e-mail address is not monitored for responses.	
Toll Free: +1.866.238.3416 Local: +1.978.848.2800 info@copyright.com www.copyright.com	

<https://outlook.office.com/owa/?realm=student.curtin.edu.au>

1/2

11/25/2018

Mail - mahdi.keramatikerman@postgrad.curtin.edu.au

Please visit [Copyright Clearance Center](#) for more information.

This email was sent by Copyright Clearance Center
222 Rosewood Drive, Danvers, MA 01923 USA

To view the privacy policy, please [go here](#).

This message (including attachments) is confidential, unless marked otherwise. It is intended for the addressee(s) only. If you are not an intended recipient, please delete it without further distribution and reply to the sender that you have received the message in error.

Get Permission / Find Title

Go


[Advanced Search Options](#)

Note: Copyright.com supplies permissions but not the copyrighted content itself.

1
PAYMENT2
REVIEW3
CONFIRMATION

Step 3: Order Confirmation

[Start new search >](#)[View your Order History >](#)

 [Print order information:](#) includes order confirmation, terms and conditions, and citation information ([What's this?](#))

Thank you for your order! A confirmation for your order will be sent to your account email address. If you have questions about your order, you can call us 24 hrs/day, M-F at +1.855.239.3415 Toll Free, or write to us at info@copyright.com. This is not an invoice.

Confirmation Number: 11768116
Order Date: 11/25/2018

If you paid by credit card, your order will be finalized and your card will be charged within 24 hours. If you choose to be invoiced, you can change or cancel your order until the invoice is generated.

Payment Information

Mahdi Keramatikerman
Curtin University
mahdi.keramatikerman@postgrad.curtin.edu.au
+61 (4)78088973
Payment Method: n/a

Order Details

Canadian geotechnical journal : Revue canadienne de géotechnique

Order detail ID: 71680941
Order License Id: 4476201119863
ISSN: 0008-3674
Publication Type: Journal
Volume:
Issue:
Start page:
Publisher: Canadian Science Publishing

Permission Status:  **Granted**

Permission type: Republish or display content
Type of use: Republish in a thesis/dissertation

[View details](#)

Note: This item will be invoiced or charged separately through CCC's [RightsLink](#) service. [More info](#)

\$ 0.00

Total order items: 1

This is not an invoice.

Order Total: 0.00 USD